Use of Pump-down Tests to Infer Hydraulic Resistance of Wastewater Forcemains

by

Ronald Bailey Strong

Submitted in partial fulfillment of the requirements

for the degree of Master of Applied Science

at

Dalhousie University

Halifax, Nova Scotia

November 2022

Table of Contents

List of Tables

List of Figures

Abstract

Forcemains are an integral part of sewerage systems. However, they deteriorate, occlude, and become faulty with time. Owners of small lift-stations often cannot afford sophisticated supervisory control and data acquisition systems and are therefore left utilizing naïve pump-down tests to infer the hydraulic resistance of a forcemain. These hydraulic resistance inferences were expected to be erroneous. The aim of this study was to investigate when a naïve interpretation of hydraulic resistance will lead to erroneous inferences.

A model was created to simulate unsteady conditions, including flow establishment. Four lift-station sites were investigated with naïve pump-down test results and compared to a more detailed model output. It was found that inferences of hydraulic resistance were often over-estimated using naïve pump-down tests. When conducting a naïve interpretation of hydraulic resistance, the loss in diameter for the forcemain and the pump curve migration due to impeller deterioration is sometimes overlooked. However, the apparent hydraulic resistance is sensitive to these characteristics. Even when duplicate systems were investigated, inferred hydraulic resistance differed, and the differences were not insignificant.

Monte Carlo simulations of 767,761 hypothetical lift-station set-ups were investigated to determine the generalizability of the error in the inference of hydraulic resistance. The erroneous inference of hydraulic resistance was quantified for each simulation and investigated. The roughness utilized in the Monte Carlo simulations were imposed at the start of the simulation. After a given simulation was completed, a naïve interpretation of hydraulic resistance was conducted utilizing simulation results. After stratifying the resulting simulation dataset outcomes by error, a classification tree was created, and the probability density functions were investigated. The classification tree was designed to ensure the severe category was optimally accurate, while other categories were less accurate to ensure interpretability. The root split for the classification tree determined that the most severe erroneous inferences were pumping times below 156 seconds. The second most important parameter investigated was a naïve interpretation of relative roughness. Both the time spent pumping and a naïve interpretation of hydraulic resistance account for over 94.2% of the relative parameter importance for the classification tree. The classification tree can be utilized to investigate when a more detailed approach is needed for inferring hydraulic resistance.

The probability densities of the simulated results indicated that numerous parameters are indicative of an erroneous outcome of hydraulic resistance. Prominent parameters that were predictors of being in the moderate or severe error category include: the ratio of the duration of time spent establishing flow to the time spent pumping is greater than 0.34, the ratio of the volume in the forcemain to the volume of the wet-well is greater than 46, the ratio of the average flow rate to the maximum flow rate was less than 0.83, or the friction factor determined naively is between 0.017 and 0.028.

List of Abbreviations and Symbols Used

Dimensions and Fundamental Quantities

L = Length

T = Time

M = Mass

F = Force

E = Energy

rev = Revolutions

$ = Currency

= Changing units depending on the purpose

Imperial Based

A = Area associated with the internal cross-sectional area of the wet-well (L^2)

A_p = Internal area of the forcemain (L^2)

ALK = Total alkalinity $\left(\frac{M}{L^3}\right)$

a = Empirical coefficient associated with the characteristic curve of the pump $(-)$

b = Empirical exponent associated with the characteristic curve of the pump $(-)$

c = Empirical constant associated with the characteristic curve of the pump $(-)$

Ca^{2+} = Free calcium $(-)$

$CaCO_3$ = Calcium carbonate $(-)$

C_e = Installation costs ($)

C_d = Decommissioning costs ($)

C_{dt} = Down time costs ($)

C_{env} = Environmental costs ($)

C_{HW} = Hazen-Williams coefficient $(-)$

C_{ic} = Initial costs ($)

C_m = Operational costs ($)

C_o = Energy costs ($)

D_{p_0} = Inside diameter associated with the forcemain at time of installation or commissioning (L)

D_p = Inside diameter associated with the forcemain (L)

d_w = Liquid level in the wet-well as measured from a datum (i.e. bottom of the wet-well) (L)

e = Error tolerance $(-)$

$E_{\Lambda_{percent}}$ = Error associated with any variable "Λ" expressed as a percentage $(-)$

$E_{\Lambda_{scalar}}$ = Error associated with any variable "Λ" expressed as a scalar $(-)$

$E[Entity]$ = Expected value of Entity $(\#)$

E_j = Error categories $(-)$

f = Friction factor in Darcy-Weisbach equation $(-)$

F = Feature/Parameter importance $(-)$

g = Gravitational constant $\left(\frac{L}{T^2}\right)$

G_r = Growth rate of absolute roughness $\left(\frac{L}{T}\right)$

H = Dynamic head (L)

h_a = Acceleration head (L)

H_{avg} = Average dynamic total head (L)

h_f = Losses in the system due to friction (L)

h_L = Losses associated with pipe friction and minor losses (L)

h_m = Losses in the system due to minor losses (L)

H_o = Head associated with pump at the operating point (L)

H_0 = Dynamic head provided by the pump at commissioning (L)

H_{max} = Head associated with maximum flowrate (L)

H_p = Dynamic head provided by the pump (L)

h_{sd} = Static head on the discharge side of the pump (L)

h_{ss} = Static head on the suction side of the pump (L)

$h_{ss_{avg}}$ = Average geometric static head associated with wet-well (L)

H_{SI} = Shut-in head (L)

H_{ST} = Total static head (L)

$H_{ST_{max}}$ = Highest static head (L)

$H_{ST_{min}}$ = Lowest static head (L)

I_{st} = Stroheckers relation Index $(-)$

K = Minor loss coefficient

L = Length of the forcemain (L)

LI = Langelier Index

LCC = Life cycle costs associated with pumps ($)

M = Bandwidth associated with kernel density estimation $(-)$

n = Number of simulations $(-)$

N_j = Observation count associated with "j" $(-)$

p = Pressure $\left(\frac{F}{L^2}\right)$

pH = Potential hydrogen $(-)$

pH_s = pH of saturation of $CaCO_3$ $(-)$

$\widehat{Pr}$ = Predicted probability $(-)$

$\Pr(Entity)$ = Probability of entity $(-)$

P_s = Power supplied to the system $\left(\frac{FL}{T}\right)$

$Q = \frac{dV}{dt}$ = Rate of removal of wastewater from the wet-well $\left(\frac{L^3}{T}\right)$

Q_{in} = Flowrate associated with the inflow into the wet-well $\left(\frac{L^3}{T}\right)$

$Q_{well} = Q - Q_{in}$ = Net flowrate associated with the wet-well $\left(\frac{L^3}{T}\right)$

Q_{max} = Maximum flow through the forcemain for a simulation $\left(\frac{L^3}{T}\right)$

Re = Reynolds number $(-)$

S_f = Slope of the energy gradient $\left(\frac{L}{L}\right)$

S_t = Encrustation thickness (L)

t = Time (T)

t_{naive} = Total time spent pumping (as naively determined) (T)

T = Temperature associated with the fluid $(°C)$

t_a = Time spent establishing flow from the start of pumping (T)

TDS = Total dissolved solids $\left(\frac{M}{L^3}\right)$

U = Velocity through the forcemain $\left(\frac{L}{T}\right)$

V = Active (or effective) volume within the wet-well (L^3)

V_{pipe} = Volume of liquid in the pipe (L^3)

x = Specific parameter value associated with X_i $(\#)$

$x\ (version\ 2)$ = General variable $(\#)$

y = General variable $(\#)$

X_i = Random variable $(\#)$

$Z_{\frac{\alpha}{2}}$ = Z score associated with normal distribution at probability $\left(1-\frac{\alpha}{2}\right)$, $(-)$

Greek Based

α = Confidence interval for two-tailed normal distribution $(-)$

β = Weighting coefficients for curve-fitting $(-)$

ϵ = Absolute roughness (L)

ϵ_{naive} = Absolute roughness height inferred from naïve pump-down test (L)

ϵ_0 = Absolute roughness height associated with a newly installed forcemain (L)

ϵ_t = Absolute roughness height associated with forcemain after some period of time t (L)

η = Efficiency of the pump $(-)$

γ = Unit weight of liquid $\left(\frac{ML}{T^2}\right)$

λ_i = Darcy-Weisbach friction factor estimations depending on the state of flow, for unified approach $(-)$

μ = Dynamic viscosity of a fluid $\left(\frac{FT}{L^2}\right)$

ν = Kinematic viscosity of a fluid $\left(\frac{L^2}{T}\right)$

Φ = Constant scalar for inflow estimate (%)

ρ = Fluid density $\left(\frac{M}{L^3}\right)$

τ = Node Index $(-)$

Θ = Age of the pipe $(years)$

θ = Switching function for Brkić-Praks methodology

ω = Classification label

$\xi\{\tau\}$ = Impurity as a function of node index

$\xi\{s,\tau\}$ = Goodness of Split (s) metric for node τ

ζ = Coefficients associated with curve-fitting $(-)$

Multi-Use Subscripts

0 – Parameter with respect to the initial implementation (newly installed)

avg – Average (regarding the forcemain unless otherwise indicated)

BP – Friction losses calculated utilizing Brkić-Praks (2018) methodology

HW – Reference to the Hazen-Williams equation

naïve –With respect to the naïve interpretation of hydraulic resistance or pump-down test

max – With respect to the maximum value achieved

min – With respect to the minimum value achieved

model – Derived with respect to the detailed model

i, j – index indicators

O – associated with the operating point

SJ – Friction losses calculated utilizing the Swamee-Jain methodology

t – With respect to time

Miscellaneous Notation

{} (curly brace) refers to a variable being a function of another variable

$fun\{x\}$ = Function of "x" notation

Acronyms

BEP – Best Efficiency Point

BP – Brkić-Praks methodology for determining the Darcy-Weisbach friction factor

EGL – Energy Grade Line

HGL – Hydraulic Grade Line

HW – The Hazen-Williams methodology for inferring friction losses

IC - Initial Commissioning

PP – Prolonged Period

OAT – One at a Time

PDT – Partially-developed turbulent

SCADA – Supervisory Control and Data Acquisition

SJ – Swamee-Jain methodology for inferring Darcy-Weisbach friction factor

Glossary

Terminology	Brief Description
Forcemain	A pressurized main is utilized to lift liquid from a lower energy to a higher energy.
Wet-well	A concrete well or underground chamber that fills with sewage until the pump is powered on. Utilized in the design of lift-stations.
Lift-station (Pumping station)	A point in the sewage system in which energy is added to move the sewage from lower energy to a higher energy location.
Submersible pump	Typical pump utilized in smaller lift-stations. The pump and motor turning it are submerged within the sewage.
SCADA	Supervisory control and data acquisition. This is the electrical equipment used in larger stations where accurate knowledge of the conditions of the system is required.
Sewerage system	The infrastructure that conveys sewage or surface runoff using sewers, including forcemains.
Sewage	Wastewater and excrement that is conveyed in sewers.
Dynamic head	The sum of the static head, pressure head difference, kinetic head difference, friction losses, and minor losses. An accelerative head is also present if unsteadiness is present.
Absolute roughness	The measure of internal roughness of a conduit, as used in the Moody Diagram. Absolute roughness is usually denoted by ϵ.
Relative roughness	The ratio of absolute roughness to the internal diameter of the pipe.
Characteristic curve	A curve that relates dynamic head to flow rate for a given pump.

Terminology	Brief Description
System curve	The curve relates the head required by a system (such as a forcemain) to the flow through the system.
Operating point	The point of intersection between a characteristic curve and a system curve.
Flow establishment	The portion of time during pumping in which the flow rate is accelerating. The flow is considered established (steady) at the point when this acceleration ceases.
Naïve pump-down test	A field test done to determine the average flow rate of a system by timing how long the active volume takes to completely empty.
Naïve interpretation of hydraulic resistance	A method of inferring the hydraulic resistance of a forcemain. The method utilizes the naïve pump-down test information along with forcemain and lift-station characteristics. Additional simplifying assumptions are made regarding variables not known directly due to the unsteady nature the system.

1.0 Introduction and Background

Wastewater lift-stations are intricate and complex systems within the greater sewerage system of a typical city. These lift-stations use pumps to raise sewage from a lower energy to a higher energy. A typical lift-station is depicted in Figure 1.

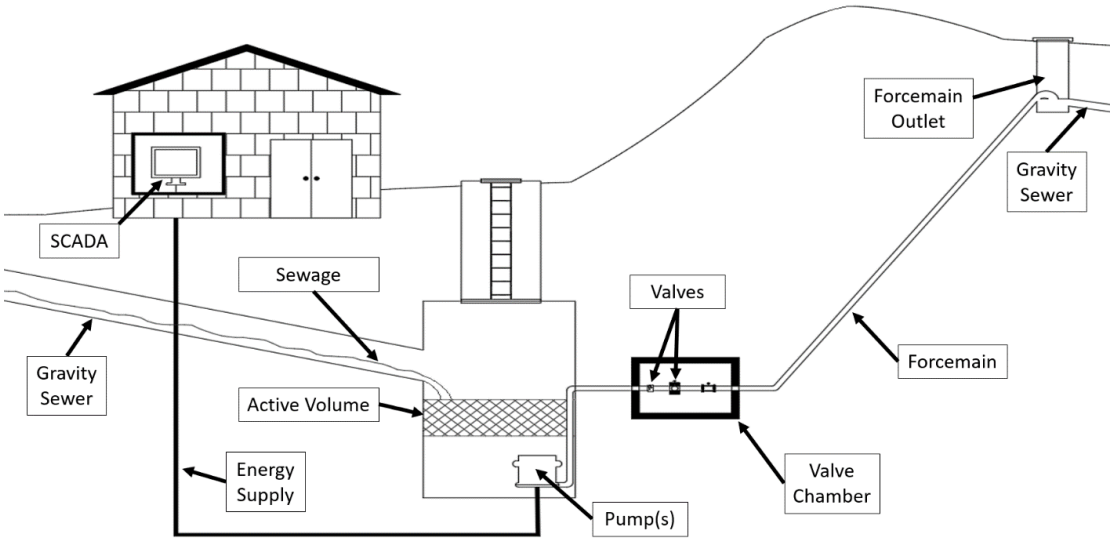

Figure 1: Components of a typical lift-station.

Each component presented in Figure 1 plays a vital role in the system. The supervisory control and data acquisition (SCADA) system controls the operation of the station (see Figure 2). It controls the liquid level within the wet-well. When the liquid level reaches the top of the active volume (also known as the effective volume), the SCADA triggers a pump to turn on. When the liquid level decreases to the bottom of the active volume, the SCADA system turns that pump off. SCADA systems also provide information that is useful for remotely monitoring various other conditions of lift-stations. The more sophisticated SCADA systems collect data on flow rates, wet-well liquid levels, pumping head, and impeller rotation. SCADA systems are housed in lift-stations as depicted in Figure 3.

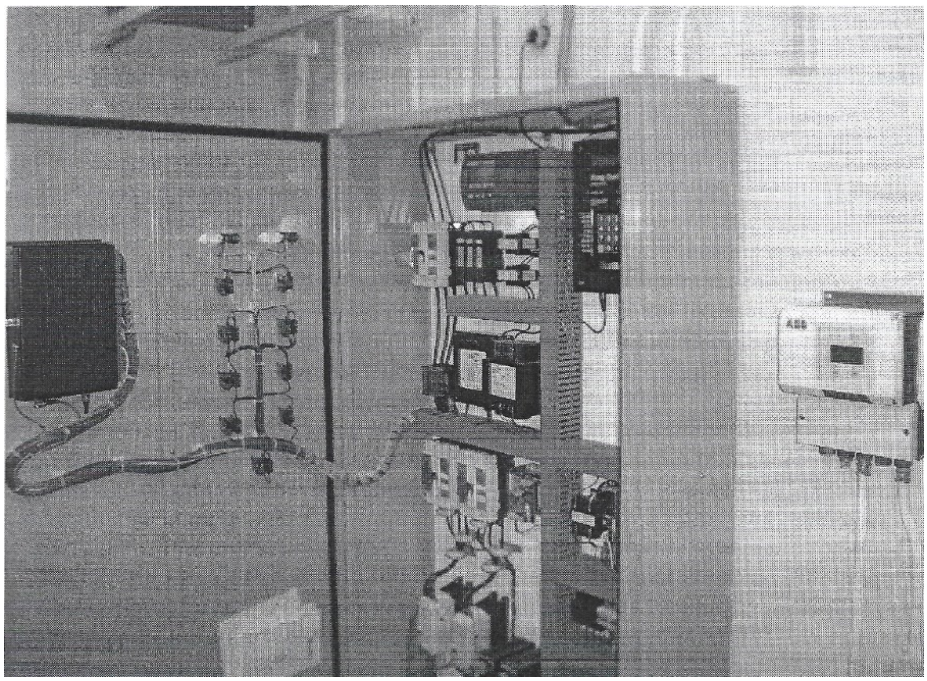

Figure 2: Typical SCADA system in a lift-station (Jean, 2006).

Figure 3: Example of the exterior of a medium-sized lift-station (Jean, 2006).

Small and medium-sized lift-stations usually use a single-speed unit in which the electric motor is coupled to the pump via a short drive shaft (close-coupled units). In such stations, the entire

unit is usually submerged. The binary nature of single-speed (~1800 rpm) close-coupled units means that their on-off sequencing must be related to a volume of fluid that is removed from the wet-well many times per day, known as the active volume (or effective volume). This volume is selected such that, if a unit is to turn on at all, it will need to run for a minimum amount of time. If the active volume is made small, many starts per day will be induced, wearing out the unit. The fact that pumps also require a minimum amount of submergence to avoid ingesting air means that there is both an upper limit and a lower limit on the vertical bounds of the active volume for a given wet-well footprint. The wet-well will therefore have start and stop sensors, such as a float sensor. In large stations, the pumps are installed adjacent to the wet-well in a compartment called the dry well. It is common practice to have at least two pumps installed per lift-station. This provides redundancy in case of pump failure and permits the continuance of operation during the maintenance of a given pump, as happens due to the need to (regularly) replace impellers.

The pump adds energy to the system by converting electrical energy into mechanical energy via a motor to rotate a shaft that has an impeller. The mechanical energy is converted into hydraulic energy via the impeller. The pump needs to overcome the elevational difference between the liquid level in the wet-well and the outlet elevation, as well as the hydraulic losses associated with the fluid moving through conduits and valves. Lift-station pumps can be submersible (Figure 4) or non-submersible (Figure 5). Submersible pumps are fastened to the bottom of the wet-well, submerged in the sewage, and have no intake line. Due to the need to pass solid waste and miscellaneous items moving through a sewerage system, wastewater pumps are designed not to clog. However, this clog prevention often comes at the expense of pump efficiency.

Valves, actuators, and fittings allow for additional control and maintenance of the lift-station. Valves are application-specific, allowing operators to meet the needs of the specific lift-station. Various types of valves, actuators, and fittings are utilized within lift-stations. It is helpful to keep valves and actuators in proximity, allowing for ease of maintenance. Valves, actuators, and fittings are sometimes housed above the well in lift-stations. However, having such components housed separately avoids interaction with the sewage and the associated noxious gases. Separate housing for the valves and actuators is referred to as the valve chamber (see Figure 6). If the SCADA system is sophisticated, it is common to have flow and/or pressure measurement equipment within this chamber.

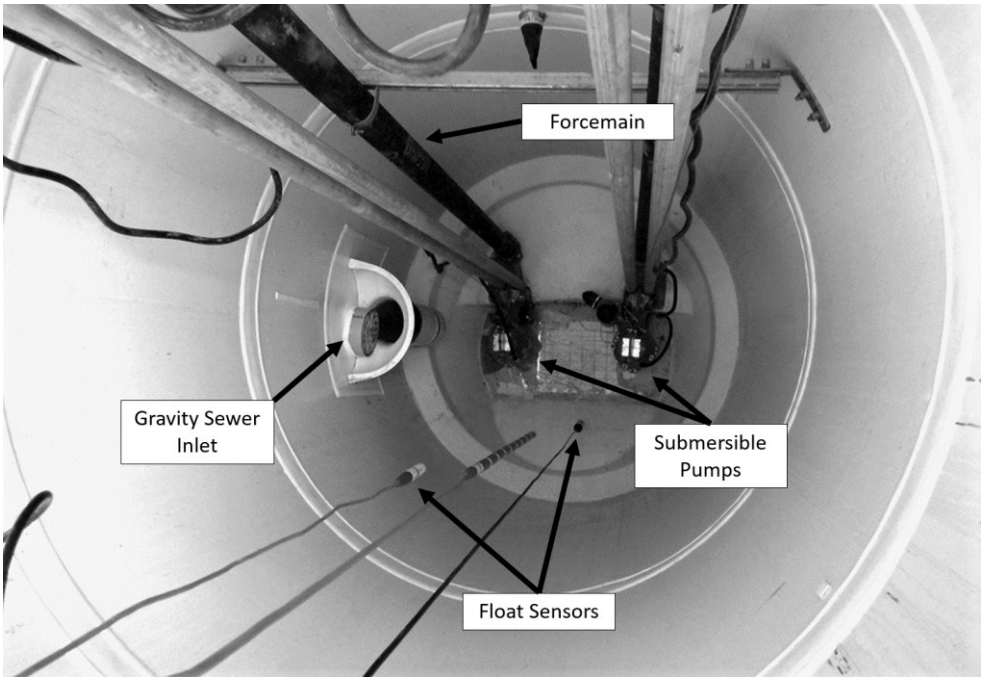

Figure 4: Example of wet-well for a small lift-station (after Romtec Utilities, Inc., undated).

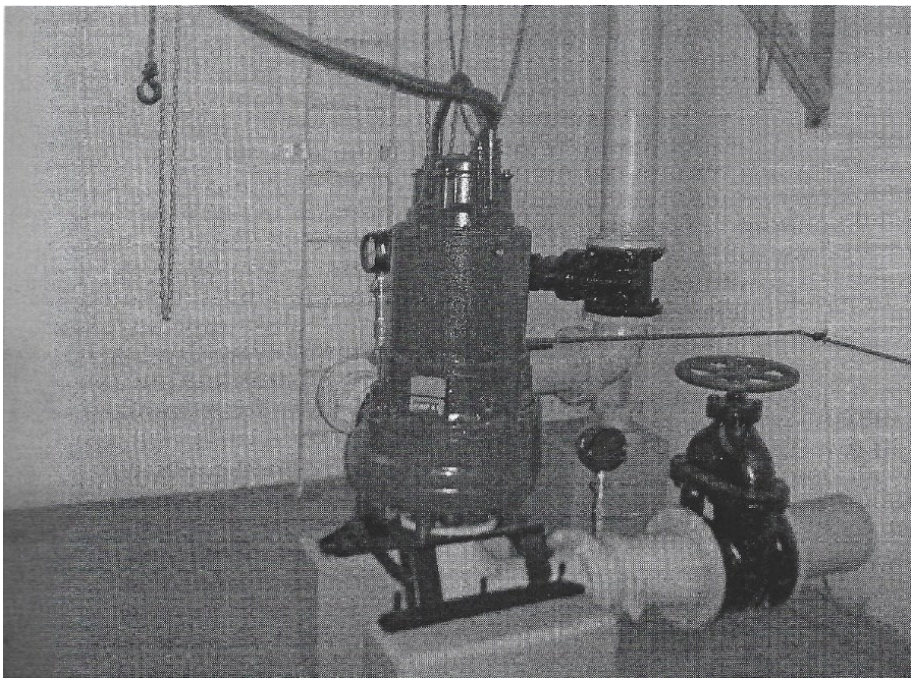

Figure 5: Example of a pump in a dry well (Jean, 2006).

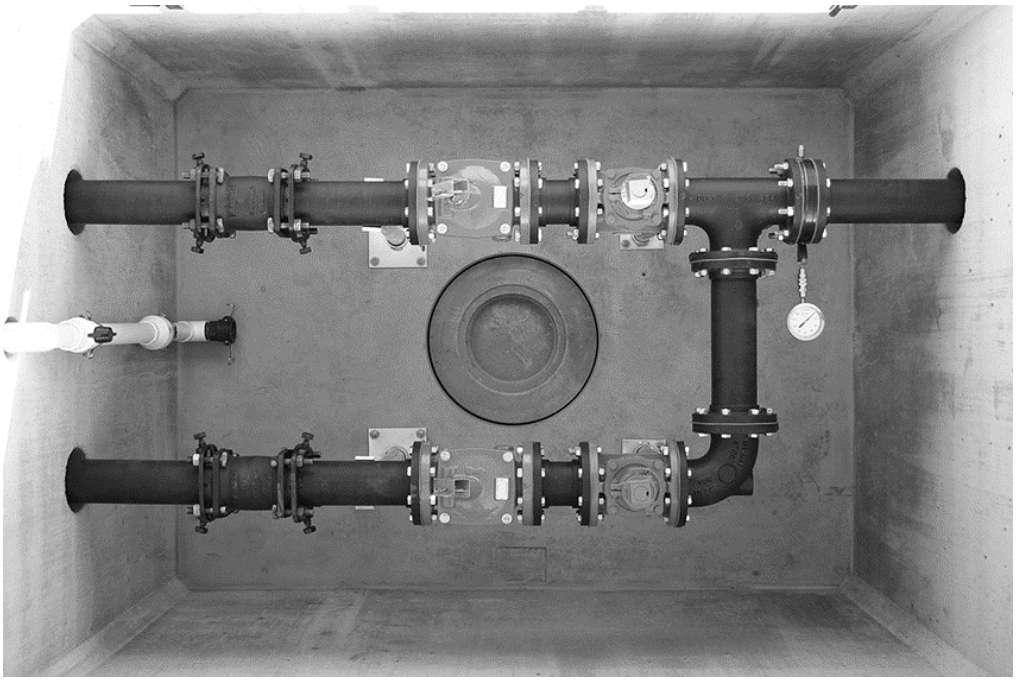

Figure 6: Example of a wastewater valve chamber (Romtec Utilities, Inc., undated).

The forcemain (see Figure 7) is a pressurized pipe connected at one end to the pump and the other end to an outlet location such as a forcemain manhole. The forcemain is usually more robust than a conduit used in a gravity-driven system, due to the higher internal pressure introduced by the pump. Forcemains come in various materials and do not follow a linear path between the wet-well and the outlet point. The need for bends and turns introduces minor head losses. Local high and low points introduce the need for air relief valves and scour valves, though these should be avoided by design.

The outlet of the forcemain usually consists of a free outlet into a special manhole (Figure 8), though a submerged outlet is possible. The manhole is where the transition back to a gravity-driven system occurs. If the manhole is designed to allow the free exit of the liquid pumped through the forcemain, it will need baffles (Halifax Water, 2022). Occasionally, the outlet is another lift-station.

Forcemains are often placed beneath or beside roads/street and are hundreds of meters in length. This will be referred to herein as the forcemain proper, to distinguish it from the often-complex header and valve chamber conduits, fittings, and appurtenances. The latter system features do

contribute to the hydraulic resistance, but it is the hydraulic resistance of the forcemain proper that is of primary interest.

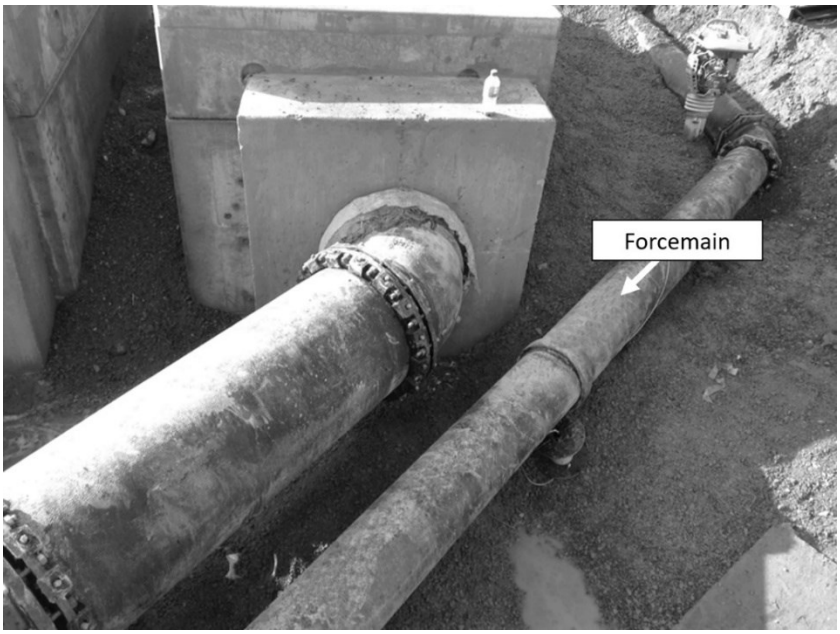

Figure 7: Example of a forcemain (right) - (after Romtec Utilities, Inc., undated).

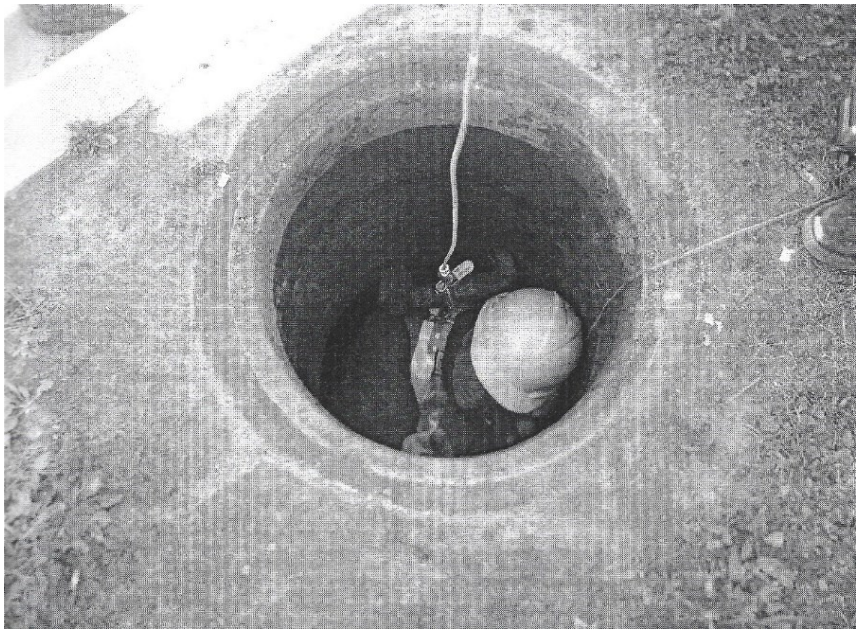

Figure 8: Collecting data regarding pipe diameter at a forcemain outlet manhole (Jean, 2006).

Lift-stations have significant costs, both capital and operating. A study by HR Wallingford (Lauchlan *et al.*, 2005) estimated that the UK capital cost of the pumps and associated pipe networks to be approximately $2.36 billion as a conservative estimate. The operational costs associated with the network were estimated to be $236 million per year in 2005. Lauchlan *et al.* (*ibid*) also note that one of the largest operators of lift-stations within the UK is responsible for about 2500 lift-stations. The average force main length of approximately one kilometre.

Design choices have long-term impacts. Lift-stations are expected to function for long periods of time. The expected service life can be upwards of a century. Pump impellers, on the other hand, only last a few years. Systems are often designed with the new infrastructure in mind but may neglect that system dynamics tend to change over time.

A component in sewerage systems that tends to change its hydraulic properties over time is the forcemain. The properties of the forcemain are influenced by system dynamics and wastewater quality. As a result of the changing hydraulic properties, the cost associated with energy expenditure increases over time. Various concerns associated with forcemains are that they often become rougher, occluded, faulty, or deformed over time. Leaks can induce sinkholes that then cause catastrophic failures. To assess a forcemain thoroughly requires an intensive and occasionally intrusive assessment. The pump is another component that tends to change over time. The pump will degrade, providing less flow for an equivalent head than a newly installed pump. Maintenance, such as degraded impeller (Figure 9) replacements, is performed to avoid such losses in flow output. Maintenance also consists of lubricating and cleaning parts (bearings and seals) and correcting alignments

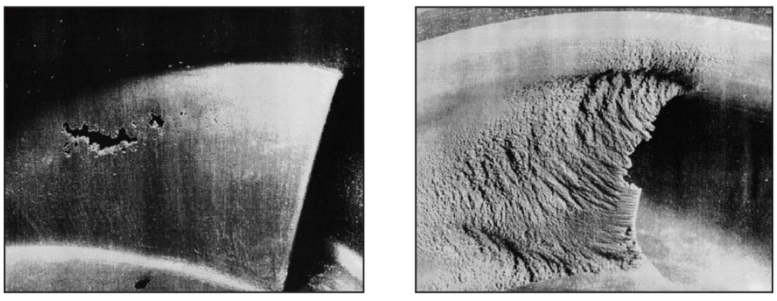

Figure 9: Examples of deteriorated impeller vanes due to cavitation (Xylem, 2015).

The more real-time information one can collect about a station, the better. A more sophisticated SCADA system is preferred over a less sophisticated SCADA system. A major drawback of more sophisticated SCADA systems is cost. It is difficult for operators of small lift-stations to justify using a sophisticated SCADA system. As a result, smaller stations often go without proper data collection to monitor and assess conditions. Industry professionals have proposed methods to estimate the hydraulic characteristics of forcemains without expensive techniques and technologies. One of these methods is the so-called pump-down test. The pump-down test estimates the flow rate associated with the pumping system by utilizing the active volume and time spent pumping (Figure 10). This test will be referred to herein as a naïve pump-down test. The volumetrically determined average flow rate can be utilized to estimate the hydraulic resistance of the forcemain with additional assumptions about the static total head and dynamic head provided by the pump. Hydraulic resistance in this study refers to the resistance encountered by the flow due to friction in a closed conduit. When the roughness of the forcemain is inferred with the naïve pump-down test and additional assumptions, it will be referred to as the naïve interpretation of hydraulic resistance (or of the specific metric being inferred). The naïve pump-down test, the concept of hydraulic resistance, and the naïve interpretation of hydraulic resistance are elaborated on in later sections.

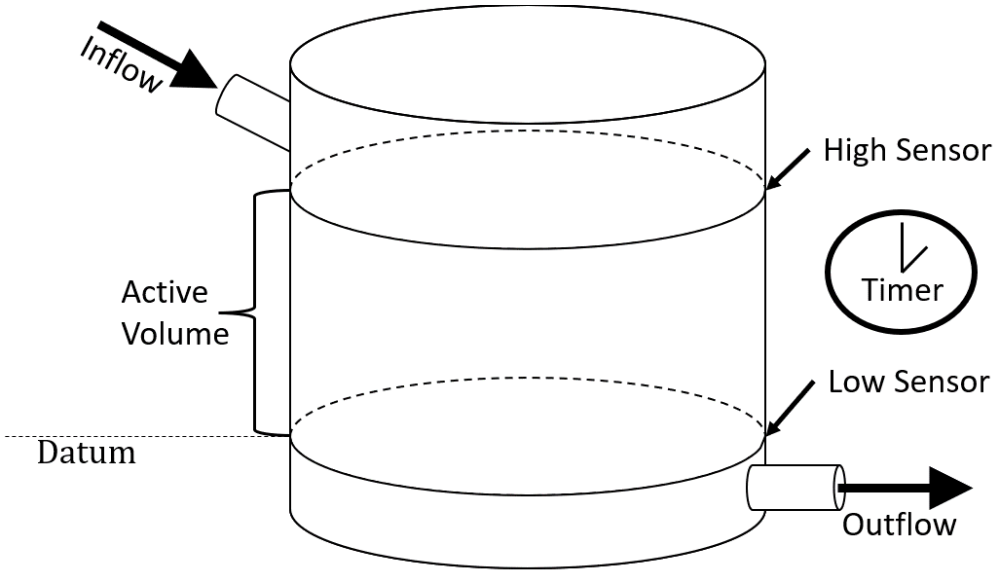

Figure 10: Simple schematic for pump-down test.

As system components age, the time need to pump out the same active volume will increase, implying a lower average flow rate. Therefore, the amount of time spent pumping out this fixed volume can be a good diagnostic in evaluating the dynamics of the system. It was surmised that hydraulic resistance inferences arising from naïve pump-down tests might be misleading or erroneous in certain cases. However, no guidelines or methodology exist in the literature regarding when this might happen.

The research described herein builds on a small study done at Dalhousie University in 2005-2006 (Jean, 2006). Four Halifax lift-stations were considered in the Jean (2006) study. The locations are indicated in Figure 11.

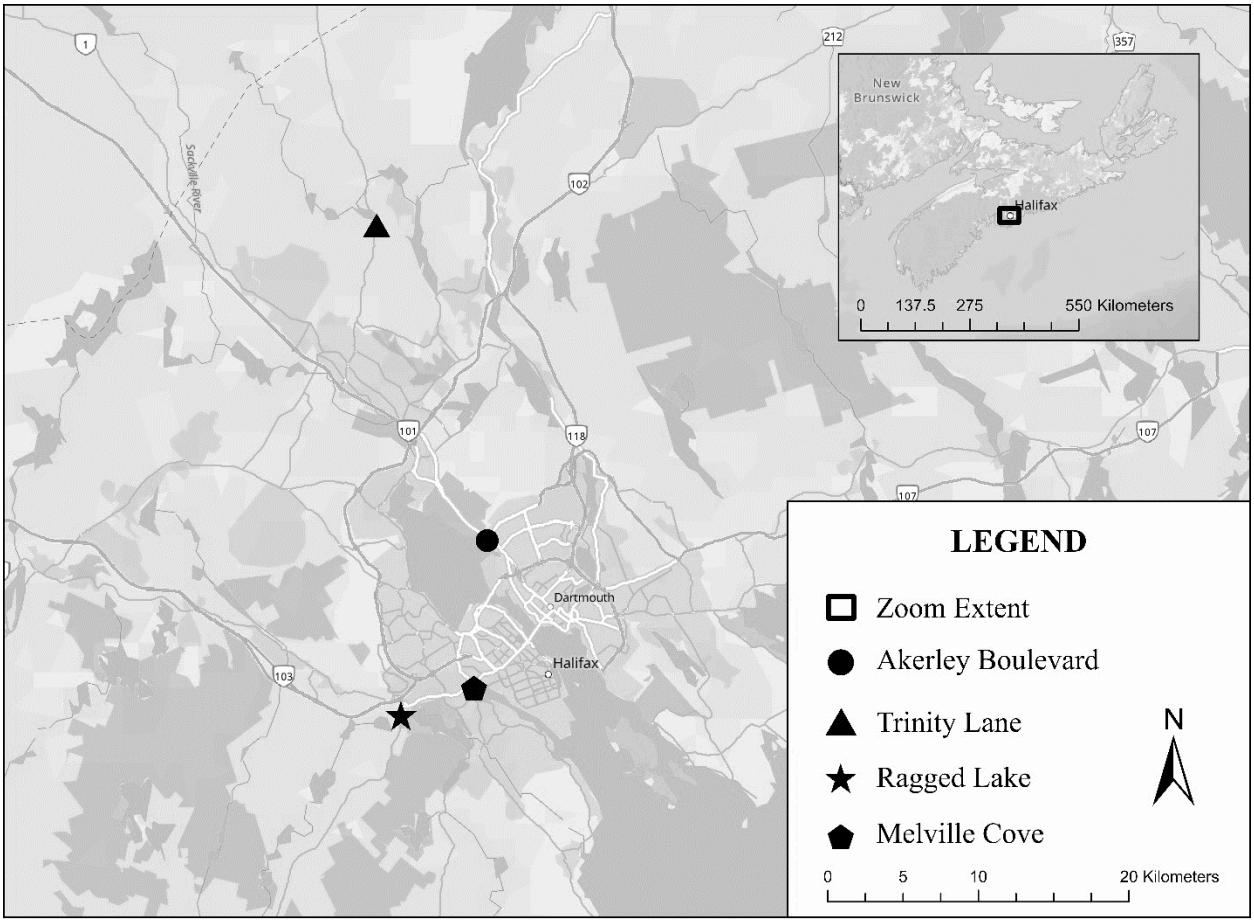

Figure 11: Lift-stations considered for the study (Jean, 2006) within Halifax Regional Municipality, Nova Scotia.

The Trinity Lane lift-station is the youngest station, being less than two years old at the time of testing. This lift-station is also the smallest of the four. Ragged Lake is the second oldest station, being ten years old at the time of testing and having the second longest forcemain in the set. This lift-station is adjacent to a commercial zone. Akerley Boulevard is the third oldest station, 38 years old at the time of testing, but was upgraded and modified approximately 18 years after commissioning. Akerley Boulevard has the longest forcemain within the study. It is located within a commercial area of Dartmouth, Nova Scotia. Melville Cove is the oldest and largest of the stations. However, Melville Cove has the shortest forcemains and the highest elevational difference to overcome. Melville Cove is located on the northwest side of the Northwest Arm, and services a residential area. Trinity Lane, Ragged Lake, and Akerley Boulevard have similar discharge static heads. Trinity Lane has a PVC forcemain, while the others have ductile iron. Trinity Lane and Akerley Boulevard have continuous flow and liquid level monitoring. Ragged Lake and Melville Cove only have continuous liquid level monitoring. The systems investigated had static suction head changes during the test of less than one meter (Jean, 2006).

This research also references the hydraulic research of a study done by HR Wallingford (Lauchlan *et al.*, 2005). The HR Wallingford study conducted field measurements of 23 lift-stations to determine the effects of biofilm (slime) on the hydraulic resistance of the forcemains. The clients were interested in studying only the effects of the biofilm in the main. These tests were conducted with considerable field and in-place equipment. However, not all stations within the HR Wallingford study (2005) had flow meters, in which cases the flow was inferred from the change in the liquid level in the wet-well and knowledge of the geometry of the wet-well.

Hansen (2007) commented that although such pump-down tests are common, they may yield erroneous results. Hansen (*ibid*) pointed out dynamics that are often not considered during such testing. The fluid level decreases during the test and causes the flow rate to also decrease over the test. There is therefore a migration of the operating point associated with the pump. The Darcy-Weisbach friction factor may be expected to change throughout a test due, to flow rate changes. Knowing that system dynamics are real, this study developed a model to investigate such errors, as could emerge from a naïve test. The model utilizes that same information that can be collected naively.

2.0 Objectives

The aim of the study was to investigate naïve interpretations of hydraulic resistance. In particular, the circumstances under which erroneous inferences occur. The study investigated data associated with a naïve interpretation of hydraulic resistance from four real sites as well as hypothetical systems. The aim of the study was achieved by a series of objectives:

1) Identify and compile the governing mechanics, variables and equations that describe the unsteady dynamics of the operating point migration for a pump-down test.
2) Identify approaches to solving the governing equations.
3) Develop methodologies to describe the migration of the operating point through numerical modelling and semi-analytical solutions.
4) Evaluate the naïve interpretation of hydraulic resistance as compared to methodologies obtained from objective three.
5) Determine what information is neglected when a naïve interpretation of hydraulic resistance is conducted that would contribute to an erroneous inference. Where possible, quantify the magnitude of the errors produced by neglected information.
6) Determine indicators of when the naïve interpretation of roughness is erroneous for ideal system dynamics.
7) Compare and contrast results with relevant literature.

3.0 Literature Review

3.1 Effects of Aging on Pressure Conduits

Studies suggest that internal pipe conditions change over time (Abdelmonem *et al.*,2020; Colebrooke and White,1937; Kaur *et al.*, 2018). The characteristics of the pipe material selected significantly affect how internal conditions change over time. Yousefi (2019) pointed out that the three leading causes of the deterioration of service lines with age are corrosion, encrustation, and biofouling. Yousefi (*ibid*) investigated service line head loss due to aging. Forcemains are subject to similar liquids to service lines and would be expected to have some similar deterioration mechanisms. Corrosion depends on the pipe material and the chemical make-up of the conveyed fluid. Encrustation tends to happen concurrently with corrosion. It involves mineral deposits that build up on the interior walls of a pipe. These deposits tend to build up slowly and constrict the flow. Shahzad and James (2002) determined that some forms of encrustation happen due to precipitation of calcium and magnesium carbonates and/or sulfates, iron and manganese compounds (particularly their hydroxides and/or hydrated oxides), and scaling caused by bacterial slimes.

Biofouling, also known as biofilm development, is the accumulation of micro-organism deposits on the inner wall of the pipe. Biofilm is produced by a combination of physical, chemical, and biological processes (Geldreich and LeChevallier, 1999), tending to become established within sediments, tubercles, areas of low liquid flow, dead ends, standpipes, and storage tanks. Biofilms may be disturbed by utilizing different disinfection techniques to prolong the integrity of the pipe (Geldreich and LeChevallier, *ibid*).

Numerous studies have been conducted on sewerage systems deterioration but not with a focus on forcemains (Vladeanu, 2018; Balekelayi and Tesfamariam, 2019). Such studies can provide insights because gravity-driven sewerage and forcemains are exposed to the same liquids. Valeneau (2018) found that the deterioration of gravity sewerage systems had various causes or contributing factors: pipe material, age, burial depth, load transfer, inflow and infiltration rates, and level of maintenance. Balekelayi and Tesfamariam (2019) studied the wastewater system in Calgary and found similar effects. Balekelayi and Tesfamariam (*loc. cit.*) found that the slope of a pipe was not considered in various studies on gravity sewerage systems. However, the slope

affects the velocity of the sewerage, and low velocities promote sediment deposition. Balekelayi and Tesfamariam (*loc. cit.*) suggest that the following list of aspects are of interest when determining deterioration:

- material type,
- age,
- length,
- diameter,
- depth,
- slope,
- number of connections and type (residential or commercial),
- maintenance type performed and frequency,
- root intrusion extent, and
- geospatial location of a pipe.

A study from the University of Guelph (Shahzad and James, 2002) exposed various aspects of these forms of deterioration for a potable water system, which is pressurized like a forcemain. After modelling the water supply network of Walkerton, Ontario (assumed to be over 100 years old), it was found that estimated encrustations on the internal diameter had increased over time. The diameter of a pipe is correlated to encrustation thickness. The larger the internal diameter of the pipe, the more encrustation happened to build up over time. Shahzad and James (*loc. cit.*) also estimated that the increase in pipe age had a linear relationship with absolute roughness. Abdelmonem (2020) suggests that the early stage in the life of a pipe has a parabolic increase in roughness, but this tapers off in later stages. Swamee (2001) suggested that the design of the forcemain diameter should be based upon the "end of design period" roughness. Halifax Water (2022) suggests that forcemains should be in place for at least 75 years. Swamee (2001) also estimates the cost associated with pumping mains, where the physical characteristics change over time, suggesting that allowing for the effects of changing system dynamics can lead to the optimal solution.

Wagner and Steffens (2014) analyzed over 800 kilometres of old forcemain. As of 2010, it was also found that (within the United States) over 60% of forcemains consisted of ferrous materials. The next most common material was concrete, based at 15%. Wagner and Steffens (*ibid*) also

found that 65% to 75% of ferrous forcemain failures were preventable via comprehensive management and maintenance programs. Internal corrosion accounted for 26% of failures. It was also found that about 54% of failures of concrete forcemains were from corrosion or structural deterioration. Wagner and Steffens (*ibid*) built statistical models of the time until forcemain failure and found forcemains are likely to not yield before 25 years since the last inspection and may last up to 120 years. The median life expectancy was about 60 years for ferrous pipes.

Decreasing the scale of the investigation to a small size can provide further insight into the dynamics of the flow through a forcemain. A computational fluid dynamics model was conducted on a meter-long segment of an old pipe by Kaur *et al.* (2018). The authors augmented a cross-section of pipe with a millimetre-scale roughness to the inner surface of the pipe. The rate of pressure drops, and the average velocities were inferred. The software code EPANET2 was then used to infer the roughness of the pipe. Kaur *et al.* (2018) utilized the nominal diameter of the pipe rather than the diameter at each of the numerous cross sections. It was found that the more the pressure drop increased over the length of the pipe, the more significant the difference between the inferred roughness and the actual roughness (used by the model). The difference was attributed to the model not correctly accounting for the diameter changes at each cross-section. Kaur *et al.* (2018) suggested that one should either use nominal diameters and associate the roughness values within the pipes to differing Reynolds numbers or associate the effective diameters in the pipe with reasonable roughness values within the pipes. The author also suggested that the aging process in the pipe incorporates the reduction in pipe diameter and the increase in roughness, rather than being only on a base increase in roughness.

3.2 Temporal Changes in Hydraulic Resistance

Several authors have tried to model the increase in roughness with respect to pipe age within potable water distribution and sewerage systems (Abdelmonem, 2020; Colebrooke and White, 1937; Lamont, 1981; NEWWA, 1935; Mielcarzewics and Pelka, 1997). Abdelmonem (2020) provided estimates of the roughness growth rate in a pipe over time that carries sewage proposed the following formulation and supplementary information in Table 1:

$$\frac{\epsilon_t}{\epsilon_0} = \mathrm{C}_1\left(\frac{\Theta}{50}\right)^2 + \mathrm{C}_2\left(\frac{\Theta}{50}\right) + C_3 \quad (1)$$

Where:

$\Theta =$ Age of the pipe $(years)$,

ϵ_t = Absolute roughness at time of interest (L),

ϵ_0 = Initial roughness of the pipe (L), and

C_i = Weighting Coefficients based on pipe material $(-)$.

Table 1: Abdelmonem (2020) weighting coefficients based on pipe material.

Pipe Material	C_1	C_2	C_3
Cemented mortar-lined cast iron	34.744	3.701	1.4
Cast iron/Ductile iron	43.602	-3.414	0.1
Reinforced concrete	30.134	5.312	1.517
Asbestos cement	14.666	2.755	1.272
PVC	13.655	0	1.336
Steel	168.05	7.564	-1.424

(Based on a study of four-inch pipes)

Colebrooke and White (1937) researched the increase in roughness in water mains. They found that the water quality, the size of the pipe, the pipe material, the lining of the pipe, and the fluid velocity all influenced eventual internal roughness. Growth in roughness height occurred linearly with respect to time and was experimentally found to be between 0.0025 inches per year and 0.08 inches per year. The pH of the water heavily influenced the roughness height growth. It was found that for cast-iron pipes, the following formulation could be utilized:

$$2\ln(G_r) = 3.8 - pH \quad (2)$$

Where:

G_r = growth rate of roughness per year $\left(\frac{feet}{year}\right)$.

Colebrook and White (*loc. cit.*) determined that the smaller the diameter of the pipe, the more rapid its deterioration. Lamont (1981) reported that tuberculation could reduce the carrying capacity of iron mains by 15 to 70% of the original capacity after 30 years of service. This loss of capacity was attributed to the liquid quality and the diameter of the main. It was also found that slime formation reduced hydraulic capacity by as much as 50%, in extreme cases, after just 20 years of service. Sharp and Walski (1988) credited Lamont (1981) with formulating an equation for the increase in tuberculation with respect to the chemical characteristics of the water. Sharp and Walski (*ibid*) state that Lamont (1981) determined the growth rate as follows:

$$G_r = (304.8) * 10^{-(4.08+0.38LI)} \quad for\ LI < 0 \quad (3)$$

Where:

G_r = Growth rate $\left(\frac{mm}{yr}\right)$, and

LI = Langelier Index.

The Langelier Index provides a measure of the chemical stability of water with respect to its degree of $CaCO_3$ saturation (Gebbie, 2000). The Langelier Index relates the pH of the water to the pH at which the water is saturated with calcium carbonate. Water undersaturated with calcium carbonate has a negative LI value and may be corrosive. The Langelier Index can be stated as follows:

$$LI = pH - pH_s \quad (4)$$

Where:

pH_s = pH of saturation of $CaCO_3$ $(-)$.

Colebrook and White (1937) also suggested that roughness height and effective diameter change linearly with time. NEWWA (1935) presented pH and age-based methods for determining roughness changes as follows:

$$G_r = \left(0.0253exp(1.9 - 0.5pH)\right)(1000)\left(\frac{mm}{year}\right) \quad (5)$$

$$\epsilon_t = G_r PipeAge\ (mm) \quad (6)$$

The empirically based Mielcarzewics and Pelka (1997) formulation uses alkalinity, pH, diameter, and age. A means of estimating encrustation thickness was also presented as follows

$$I_{st} = pH - 11.39 + 2\log_{10}(ALK\ as\ CO_2) \quad (7)$$

$$-1.51 \leq I_{st} \leq 0.25$$

$$\epsilon_t = 0.6 + \left(0.119 - 0.000203D_{p_0} - 0.121I_{st}\right)PipeAge \quad (8)$$

$$S_t = 0.0169(PipeAge)^{0.439}\left(D_{p_0}\right)^{0.841} \quad (9)$$

$$S_t = \left(0.088 + 0.00031D_{p_0} + 0.0084I_{st}\right)PipeAge \quad (10)$$

Where:

S_t = Encrustation Thickness (mm),

I_{st} = Strohecker relation Index $(-)$, and

D_{p_0} = Initial diameter of the pipe (mm).

3.3 Pumping Theory for Lift-Stations

Lift-stations utilize pumps to lift a liquid from a point of lower energy to a point of higher energy. The basic fluid mechanics for an incompressible fluid in an un-steady state can be described using the Bernoulli energy equation (Franzini & Finnemore, 1997):

$$h_{ss} + \frac{p_1}{\gamma} + \frac{U_1^2}{2g} + H_p = h_{ds} + \frac{p_2}{\gamma} + \frac{U_2^2}{2g} + h_f + h_m + h_a \qquad (11)$$

Where:

H_p = Head added to the system by the pump (L),

h_{ss}= Static head on the suction side of the pump (L),

p_i = Pressure at point of interest "i" $\left(\frac{F}{L^2}\right)$,

γ = Specific weight of the fluid $\left(\frac{F}{L^3}\right)$,

U_i = Velocity of fluid associated with a point of interest "i" $\left(\frac{L}{T}\right)$,

h_f = Friction losses (L),

h_m = Minor losses (L), and

h_a = Head requirement due to acceleration (L).

The static total head (H_{ST}) is the difference between the static suction head and the static discharge head (see Figure 12, case a). The dynamic total head is the difference between the dynamic suction head and the dynamic discharge head (Figure 12, case b). The typical schematic depicting the energy losses and nomenclature for a steady state system (also without h_a) is depicted in Figure 12, case c. The head in the wet-well changes during a pumping test and thus requires an unsteady analysis of the energy balance. This will be discussed more in-depth in later sections.

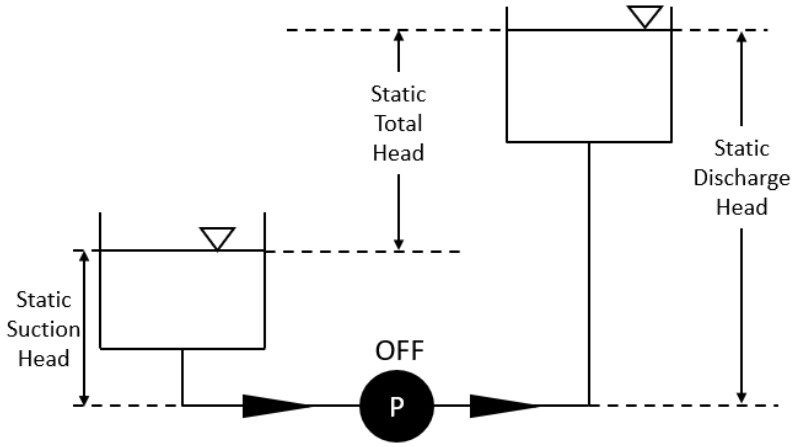

a) depicts the static total head while the pump is offline.

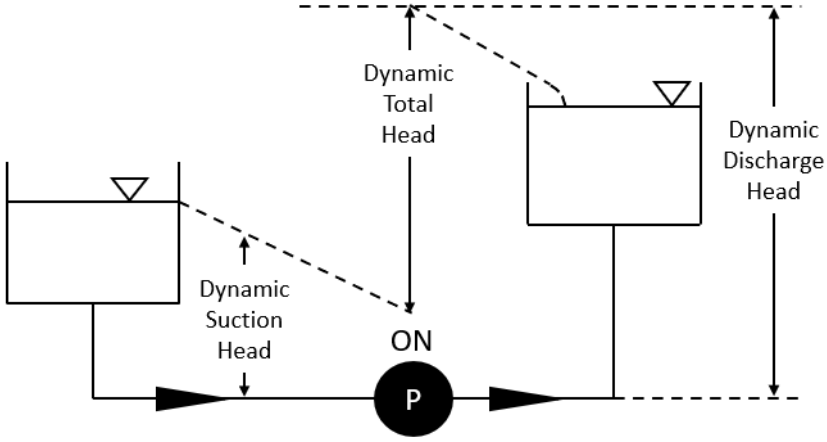

b) depicts the dynamic total head while the pump is online.

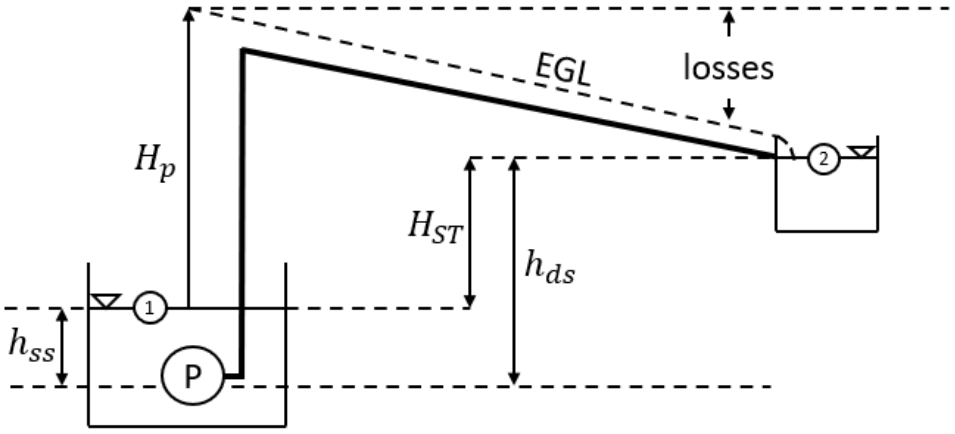

c) depicts the nomenclature and energy losses for a steady-state system (minor losses exist but are not depicted).

Figure 12: Schematics relating to the steady-state energy equation.

3.4 Pumps

Pumps vary widely in their designed characteristics, are highly tailored to their applications, and have defined and distinct categories (Jones *et al.*, 2008). Wastewater pumps impart velocity and pressure to the fluid by passing it through an impeller. The impeller and the volute enclosing it cause the velocity of the fluid to become additional pressure. Most small and medium-sized lift-stations utilize submersible centrifugal pumps. These pumps can have three additional features: non-clogging, vortex-inducing, and grinding. All three are sometimes selected for use in wastewater systems. Figure 13 depicts a pump impeller and volute of the type used for wastewater conveyance by small to medium-sized stations.

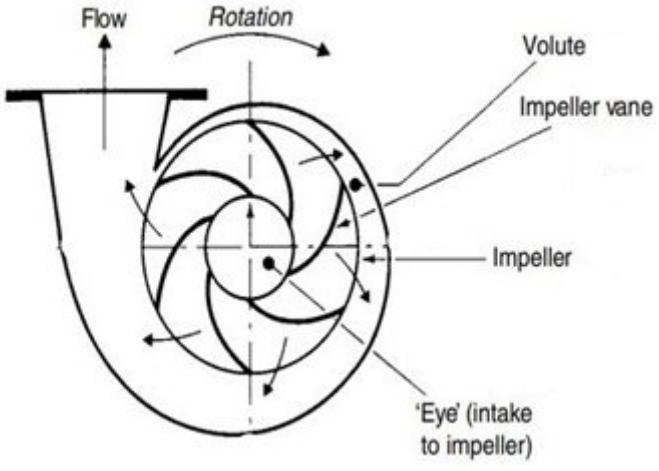

Figure 13: Centrifugal pump volute and impeller schematic (after Butler *et al.*, 2018).

3.4.1 Pump Curves

Manufacturers provide a wide variety of information for their pumps, but the most important is the characteristic curve. Other important information includes the power usage curve, the efficiency curve, and the net positive suction head required (*e.g.*, Figure 14). These curves have flow rates on the abscissa in the technical documentation.

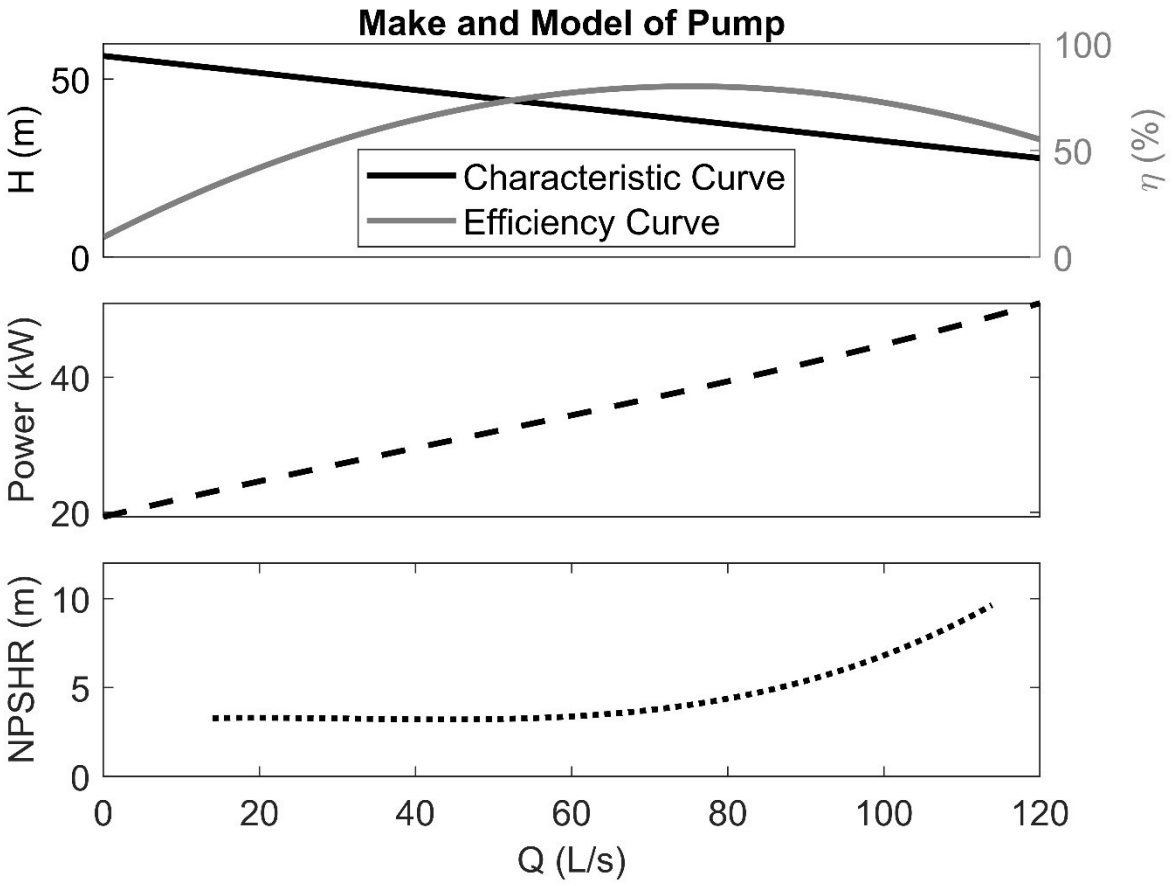

Figure 14: Pumping curves, as might be provided by a manufacturer.

The key characteristic curve of a pump declares how the dynamic head varies with the flow rate. Typically, the head that the pump can provide decreases as the flow rate increases. Such characteristic curves are often characterized using polynomial curves but can be expressed by:

$$H_p = aQ^b + c \tag{12}$$

Where:

H_p = Dynamic head provided by the pump (L),

Q = Flowrate $\left(\frac{L^3}{T}\right)$,

a, b, c = Coefficient, exponent, and constant associated with a characteristic curve $(-)$, and

$c \approx H_{SI}$ = Shut-off head for the pump.

The power curve indicates the power required to produce a flow rate. As the flow rate increases, so does the power requirement. The efficiency curves provide the ratio between the power input to the electric motor and the power output implied by the flow at the head difference that is being overcome. The selection of the pump(s) for a new lift-station determined by whether a pump will be able to operate at or near the best efficiency point (BEP). These curves often follow an inverted parabolic shape. The NPSH-R (net positive suction head required) for the pump must be exceeded by the NPSH-A (net positive suction head available), a quantity also governed by external conditions. Halifax Water (2022) requires that the NPSH-A to NPSH-R ratio be two or greater to exclude the possibility of cavitation.

3.4.2 Economics Aspects of Lift-Stations

Life cycle costs should be an important aspect of the design of wastewater lift-stations. Costs associated with pumping can be summarized as follows (Block and Budris, 2013).

$$LCC = C_{ic} + C_{in} + C_e + C_o + C_m + C_{dt} + C_{env} + C_d \quad (13)$$

Where:
LCC = Life Cycle Cost ($),
C_{ic} = Initial Costs ($),
C_e = Installation Costs ($),
C_o = Energy Costs ($),
C_m = Operational Costs ($),
C_{dt} = Downtime Costs ($),
C_{env} = Environmental Costs ($), and
C_d = Decommissioning Costs ($).

The internal forcemain conditions contribute to the pumping station energy, operational, environmental, and decommissioning costs.

The reliability of a pump is affected by various factors. Block and Budris (2013) provide a summary of the components that contribute to the reliability of a pump over time (see Figure 15).

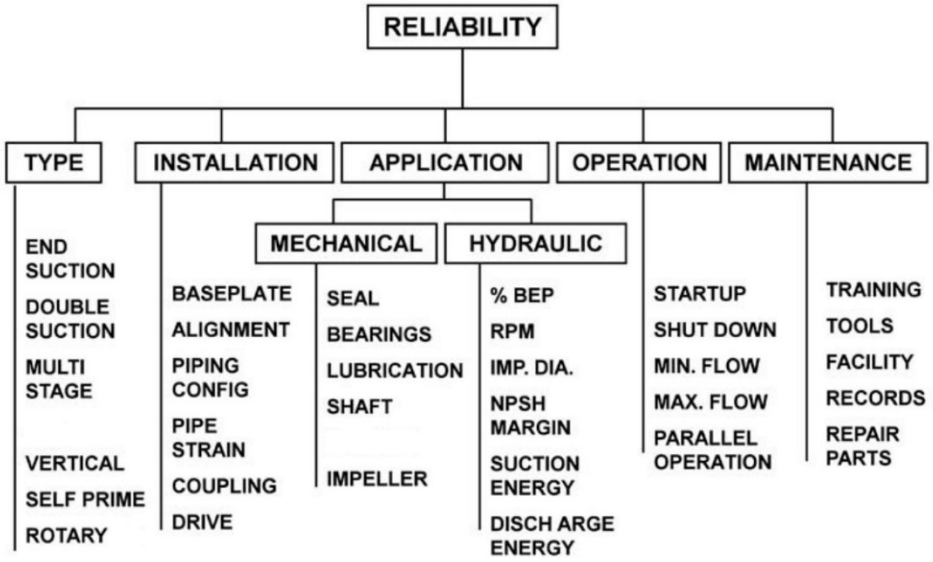

Figure 15: Factors to consider in pump reliability (after Block and Budris, 2013).

Gulich (2020) emphasizes the importance of selecting a pump based on allowable operational ranges. An off-design operational range can be unavoidable. Criteria to consider for defining operating ranges include energy costs, heating of fluid at low flow, type of pump and service, fluid to be pumped and its temperature, power class of the pump, head per stage, the impellor tip speed, risk of cavitation, part load recirculation, vibrational behaviour in the system, stability of the flow-head curve, and power consumption of the motor. The pump should also be optimized for thousands of hours of use in continuous operation without excessive damage/wear.

3.4.3 Starting and Stopping of Pumps

When starting and stopping centrifugal pumps, there are various aspects to consider. When the specific speed of the pump is low, closing the discharge valve while opening the suction valve

may be required before turning it on. A closed valve ensures minimum loading on the pump driver before starting. Due to the discharge pressure making it difficult to open a fully-shut valve, the discharge valve is usually partially open upon start up. Block and Budris (2013) suggest that about one-eighth open should suffice. After the pump has started, the discharge valve is usually opened slowly. When shutting down the pump, it is said to be essential to close the discharge valve first to take the load off the motor.

Starting and stopping protocols could not be obtained for the sites considered but can affect the ability of the engineer to make inferences about internal conditions. Gulich (2020) has pointed out that the starting torque of the pump needs to be greater during the starting process (than the torque at the operating point). Pump similarity laws can be used to obtain the ratio of the torque provided to the speed of the shaft.

Valves can influence the starting and stopping of the pump. When the power consumption for the pump is lower at the shut-off head than the power associated with pumping at the BEP, the pump often starts against a closed valve because its starting torque is low at this point. This is often the case for small to medium-sized pumps. Once the operating speed is achieved, the discharge valve is opened. Most small to medium-sized stations have check valves to stop backflow when the pump is not operating. If the pump start-up begins with the discharge valve open, the check valve will open when the differential pressure across the valve is enough to open it.

3.4.4 Power Requirements

Pump and motor configurations behave in ways governed by the systems set up. Pumps are often rigorously tested in design to determine the energy output of a pump compared to the input. Pump systems cannot perfectly transfer energy from the input to the output; therefore, efficient energy transfer becomes of interest to the system (Karassik *et al.*, 2008). The efficiency of the system can be determined by:

$$\eta = \frac{\gamma H_p Q}{P_s} \tag{14}$$

Where:

η = Total efficiency of the pump $(-)$,

H_p = Total dynamic head (L),

Q = Flowrate provided by the pump $\left(\frac{L^3}{T}\right)$, and

P_s = Power input into the motor $\left(\frac{FL^2}{T^3}\right)$.

The power associated with lifting a liquid is as follows:

$$Water\ Power = \gamma Q H_p \tag{15}$$

Power is the rate of change in energy with time. The following equation can be utilized to determine the energy requirements for pumping:

$$Energy = \int \frac{\gamma H_p\{t\} Q\{t\}}{\eta} dt \tag{16}$$

3.4.5 Pump Monitoring and Degradation

Methods are introduced in the literature to monitor and maintain water/wastewater transport pumping systems. These systems often introduce SCADA to collect information about the system continuously. State-of-the-art SCADA systems often collect the following data (Purvis, undated):

- static and dynamic pressures associated with suction and discharge side,
- flowrate,
- power (input and output),
- wire to water efficiency,
- wastewater temperature, and
- liquid level in the wet-well.

SCADA is utilized to help maintain the longevity of a lift-station. They indicate when the lift-station components begin degrading and should be exchanged for new components. These systems are often costly to implement. Smaller stations cannot feasibly consider SCADA to infer the health of their lift-station and associated degradation over time.

Degradation can happen in different forms and for numerous reasons. Gulich (2020) describes aspects relating to the corrosion of steel components of pumps in freshwater, cooling water, and sewage (see Table 2).

Table 2: Corrosion of pumps (after Gulich, 2020)

Corrosion pathway	Descriptive information
Oxygen content	Corrosive attacks increase with oxygen concentration. However, a minimum amount is needed for protective films.
Temperature	Corrosion is highly correlated to the temperature of the sewage. Increasing temperature from 10 to 30 degrees Celsius can double corrosion rates.
pH	Neutral or weakly alkaline sewage has some corrosion. Acidic sewage is classified as strongly corrosive.
Water hardness	Water hardness influences corrosion and boiler scaling deposits. Hard water is needed for protective calcareous rust scales. Soft water is often aggressive.
Carbon dioxide	Complex with respect to corrosion. Some carbon dioxide is needed to keep carbonates in the solution. Excess of the needed carbon dioxide often leads to corrosion of steel and concrete. More information is provided by Gulich (2020).
Chlorides/Halogens	Increases in chlorine and other halogens increase the softness of water.

(**Table 2**, continued)

Sulfates	Sulfates cause pitting in steel and graphitic corrosion on gray cast iron if in excess, as well as concrete corrosion.
Hydrogen sulfide/Fluorides	Aggressive corrosion of all metals.
Ammonia	Causes stress corrosion cracking in brass and corrosion of copper/copper-nickel alloys.
Flow velocity	At low flow velocities (< 1 m/s), deposits or aeration elements can form. Low velocity allows for the local concentration of corrosive substances. An increased corrosion rate can occur due to accelerated mass transfer, or erosion-corrosion can be induced.
Corrosion inhibitors	Substances such as phosphates, aluminum compounds, and silicon dioxide are often present in natural waters. These compounds can inhibit corrosion and are often added to closed circuit systems.

Another type of pump degradation is abrasion (Gulich, 2020). Abrasion is the loss of physical removal or eroding of material, especially the metal of the impeller. The metal is then entrained in the liquid. Gulich (*ibid*) summarizes the main causes of abrasion (Table 3).

Table 3: Abrasion in pumping sewage (after Gulich, 2020)

Abrasion pathway	**Descriptive information**
Concentration of solids	Metal loss of pump components tend to increase with increased concentration of solids entrained in the liquid. The metal loss of the pump tends to be proportional to the concentration of solids. The relationship may level off at a high concentration of solids due to particles interacting more frequently.
Flow velocity and pattern	Higher kinetic energy tends to contribute to higher abrasion. As kinetic energy is proportional to squared velocity, it can be theoretically stated that abrasion is proportional to velocity to the third power. However, it was found to have a power of 0.9 to 5.
Vortices	Vortices create high velocities near the surface of the pump, causing high kinetic energy near the walls. Corner vortices between vanes, side plates, and incident flow lead to severe abrasion.

(**Table 3**, continued)

Turbulence	Fosters the transport of fluid perpendicular to the flow and allows solids to meet the walls more frequently.
Impingement angle	The angle at which flow moves relative to the pump components significantly impacts abrasion. If the particles hit the wall at 90 degrees, the deterioration will be greater than parallel flow to surface movement.
Grain size, shape, and hardness	The kinetic energy of a particle increases with its mass within the fluid. The harder the grain/particle, the more abrasive. Angular shapes cause more damage than spherical shapes. Angular shapes will also take more construed flow paths.
Corrosion and cavitation	Both contribute to abrasive wear.
Material properties	Abrasion due to a material can be defined by the material hardness ratio and particle solicitation ratio. Abrasive wear diminishes as the hardness of the surface of a material increases. The chemical structure of the material also plays a role. The material is exposed to numerous tiny shocks to its structure. The individual shocks alone do not cause any noticeable damage, but the summation of all the shocks can cause noticeable deterioration.

3.4.6 Pumping Efficiency Studies

A large study of pump efficiencies was conducted by Papa *et al.* (2014). The study included 152 water pumps in the potable water distribution systems of eight Canadian communities. Low voltage (600V) pumps accounted for 57% of the total pumps studied, and medium voltage (2300-4200V) pumps accounted for the other 43%.

The average efficiency at the BEP was 86.4%, which is much higher than the efficiency a wastewater pump would have. The actual efficiencies of the pumps in operation, was about 77%. The pumps were anywhere from 1 to 64 years old, with an average age of 25. The age of the pump and the efficiencies had no noticeable correlation between pump age and degradation after analyzing the collected data. A third party researched the data and suggested that reliability techniques such as the Cox Regression be conducted and stated that further data collection would be needed to ensure the suitability of the model (Eaton *et al.*, 2018).

It was found that the average efficiencies of the pumps were approximately 9.3% lower than claimed at the best efficiency point. It was also found that the average actual operational efficiency was 12.7% lower than the BEP. It should be noted that these pumps were utilized in potable water systems. Sewage causes pump degradation to happen more quickly. Industry professionals suggest that a commercial sewage pump lasts approximately a decade, depending on the type of pump and sewage water quality. Impellers are replaced about every two to three years. There is currently no data-driven literature available for the deterioration of wastewater pumps over time.

3.5 Friction Losses

Darcy and Weisbach (1854) discovered an empirical formulation that can describe the friction head loss due to incompressible fluids through a conduit. The Darcy-Weisbach equation (Darcy, 1854) is still widely utilized and is stated as follows:

$$h_f = f \frac{L}{D_p} \frac{U^2}{2g} \tag{17}$$

Where:

h_f = Head loss due to friction (L),

f = Darcy-Weisbach friction factor (-),

L = Length of pipe (L),

D_p= Internal diameter of the pipe (L),

U = Mean pipe flow velocity $\left(\frac{L}{T}\right)$, and

g =gravitation acceleration $\left(\frac{L}{T^2}\right)$.

The Darcy-Weisbach friction factor depends on the flow state, which is classified by the Reynolds number. Reynolds number can be determined by the ratio of inertial to viscous forces within a fluid. Therefore, the following equation can be used:

$$Re = \frac{\rho U D_H}{\mu} = \frac{U D_H}{\nu} \tag{18}$$

Where:

Re = Reynolds number $(-)$,

U = Average velocity in a conduit having a cross-section related to a geometric shape $\left(\frac{L}{T}\right)$,

D_H = Hydraulic diameter cross-section (L),

μ = Dynamic viscosity of a fluid $\left(\frac{FT}{L^2}\right)$,

ν = Kinematic viscosity of a fluid $\left(\frac{L^2}{T}\right)$, and

ρ = Density of a liquid $\left(\frac{M}{L^3}\right)$.

The three classifications of the state of flow are laminar, transitional, and turbulent flows. The three zones or turbulent regimes have different behaviors with respect to the Darcy-Weisbach friction factor. Laminar flow is determined when the Reynolds value is less than 2000. Within the laminar zone, the Darcy-Weisbach friction factor may be found as (Gupta, 2008):

$$f = \frac{64}{Re} \tag{19}$$

$$0 < Re < 2000$$

The transition between the laminar and turbulent regime (also known as the critical region) happens between a Reynolds number of 2000 to 4000 (Gupta, 2008). There has yet to be an

accurate method for determining the Darcy-Weisbach friction factor in this region. The turbulent regime prevails for Reynolds values greater than 4000 (Gupta, *ibid*). Turbulent flow can be further divided into partially-developed turbulent flow and fully-developed turbulent flow. Partially developed turbulence is a turbulent flow with significant dissipation or stirring (Hsu *et al.*, 2022) and a less efficient energy cascade. Within this zone, the Darcy-Weisbach friction factor decreases with increasing Reynolds Numbers. A fully-developed turbulent flow is classified by flows in which the energy cascade of eddies is as efficient as it can be and for a given relative roughness. Within this zone, the Darcy-Weisbach friction factor is static with respect to the Reynolds Number.

A study by Nikuradse (1932) found relationships between relative roughness in smooth uncoated and artificially roughened pipes and the Darcy-Weisbach friction factors within the turbulent zone. The relative roughness was classified to be the average diameter of the sand grain divided by the internal diameter of the pipe. However, it was later found that the non-uniform sand roughness and commercial pipes did not frequently coincide. This discovery led to an equivalent sand roughness. The study by Nikuradse determined that friction did not play a strong role in the energy loss of conveying liquid within pipes with low relative roughness. The study also found that, viscosity no longer played a role in the determination of the Darcy-Weisbach friction factor for flow in rough pipes. These discoveries lead Prandtl (1935) and von Karman (1930) to establish the boundaries for the Darcy-Weisbach friction factor for turbulent flow in a smooth pipe as described by Gupta (2008), as follows:

$$\frac{1}{\sqrt{f}} = -2\log\left(\frac{2.51}{Re\sqrt{f}}\right) \tag{20}$$

The Darcy-Weisbach friction factor with respect to relative roughness in fully-developed turbulent flow was found as (Gupta, *ibid*):

$$\frac{1}{\sqrt{f}} = -2\log\left(\frac{\varepsilon}{3.7D_p}\right) \quad (21)$$

Where:

$\varepsilon =$ Equivalent sand roughness height of materials surface (L).

Due to most pipe flow falling in the partially turbulent flow region, Colebrook and White (1937 and 1939) created a hybrid of the two Prandtl and von Karman equations. The Colebrook-White equation is an implicit equation with respect to the Darcy-Weisbach friction factor:

$$\frac{1}{\sqrt{f}} = -2\log\left(\frac{\varepsilon}{3.7D_p} + \frac{2.51}{Re\sqrt{f}}\right) \quad (22)$$

$$4000 < Re < 10^8$$

$$0 < \frac{\epsilon}{D_p} < 0.05$$

Utilizing the Colebrook-White and Prandtl-von Karman equations, Moody (1944) created a diagram (Figure 16) to help infer the Darcy-Weisbach friction factor based on the relative roughness and Reynolds number more efficiently. The Moody diagram contains the relationship between the Darcy-Weisbach friction factor, Reynolds number and relative roughness. Also included in the diagram are key regions such as the laminar flow region, transition region (critical region), partially-developed turbulent flow region, rough turbulent flow region, the Darcy-Weisbach friction factor for smooth pipes, and the partially-developed turbulence to complete turbulence (rough turbulence) shift. The Moody diagram is the most common way to graphically describe how the Darcy-Weisbach friction factor behaves, over all three regimes of turbulence, and the nature of the role of relative roughness (if any).

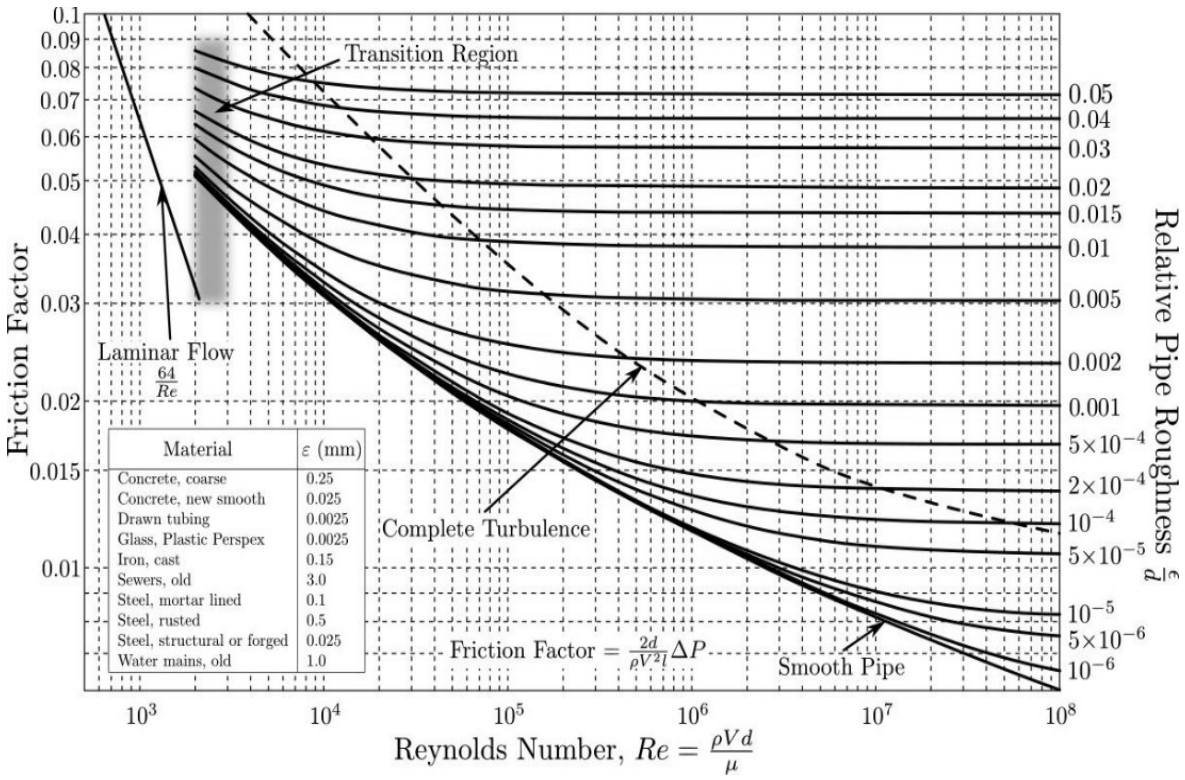

Figure 16: Moody diagram (after Engineers Edge, undated).

Swamee and Jain (1976) found an explicit method for calculating the value of the Darcy-Weisbach friction factor within a tolerance of approximately 1% error for turbulent flows, as follows:

$$f = \frac{0.25}{\log 10\left(\frac{\frac{\varepsilon}{D_p}}{3.7} + \frac{5.74}{Re^{0.9}}\right)^2} \qquad (23)$$

$$5000 < Re < 10^8$$

$$10^{-6} < \frac{\epsilon}{D_p} < 0.01$$

Explicit methods were later reviewed by Brkić (2011), and the Swamee-Jain approximation was found to have an error of 2.04% within the limits of the Colebrook-White equation. In recent

decades other methodologies have been presented to estimate the Darcy-Weisbach friction factor (Brkić, 2011). Figure 17 depicts the error associated with the inference of relative roughness between the Swamee-Jain method and the Colebrook-White method. The contours relate to the percentage error (log-scaled) between the methods, with Colebrook-White considered the correct relative roughness.

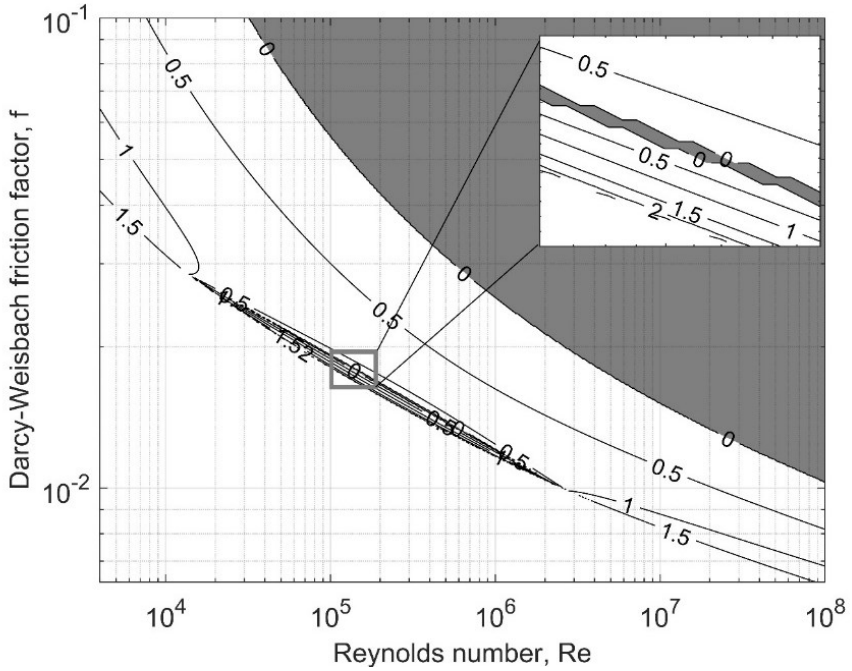

Figure 17: Error in Swamee-Jain versus Colebrook-White in the inference relative roughness. The errors are presented as log-scaled percentage errors in relative roughness for any Darcy-Weisbach friction factor and Reynolds number combination within the limits of Colebrook-White. Colebrook-White is taken to be the correct inference of relative roughness.

Brkić and Praks (2018) proposed an effective unified formulation that combines all flow states based on an artificial neural network fit to the data provided by Nikuradse (1932). The formulation utilizes switching functions to unify all states of flow. The formulation is as follows:

$$f = \lambda_1(1-\theta_1) + \lambda_2(\theta_1 - \theta_3) + \lambda_3\theta_2 \qquad (24)$$

$$\theta_1 = 1 - \frac{1048}{\frac{4.489}{10^{20}} Re^6 \left(0.148Re - \frac{2.306(Re)}{0.003133Re + 9.646}\right) + 1050} \quad (25)$$

$$\theta_2 = 1.012 - \frac{1}{0.02521Re\left(\frac{\epsilon}{Dp}\right) + 2.202} \quad (26)$$

$$\theta_3 = 1 - \frac{1}{0.000389(Re^2)\left(\frac{\epsilon}{D_p}\right)^2 + 0.0000239Re + 1.61} \quad (27)$$

$$\lambda_1 = \frac{64}{Re} \quad (28)$$

$$\lambda_2 = \frac{0.316}{Re^{0.25}} \quad (29)$$

$$\lambda_3 = \frac{0.25}{\left(log10\left(\frac{\epsilon}{3.71Dp}\right)\right)^2} \quad (30)$$

Where:

θ_i =Switching functions $(-)$, and

λ_i = Components that depend on the state of flow $(-)$.

The formulation covers the inflection curves in the transition from laminar to turbulent flow. However, the complexity of this estimation of the Darcy-Weisbach friction factor is greater. Plascencia *et al*. (2020) claim that the formulation has a low error in predicting the Darcy-Weisbach friction factor associated with the head losses determined by the Nikuradse dataset (1932). Figure 18 depicts the error associated with the inference in relative roughness between the Brkić-Praks method and the Colebrook-White method. The contours relate to the percentage error (log-scaled) between the methods, with Colebrook-White considered the correct relative roughness.

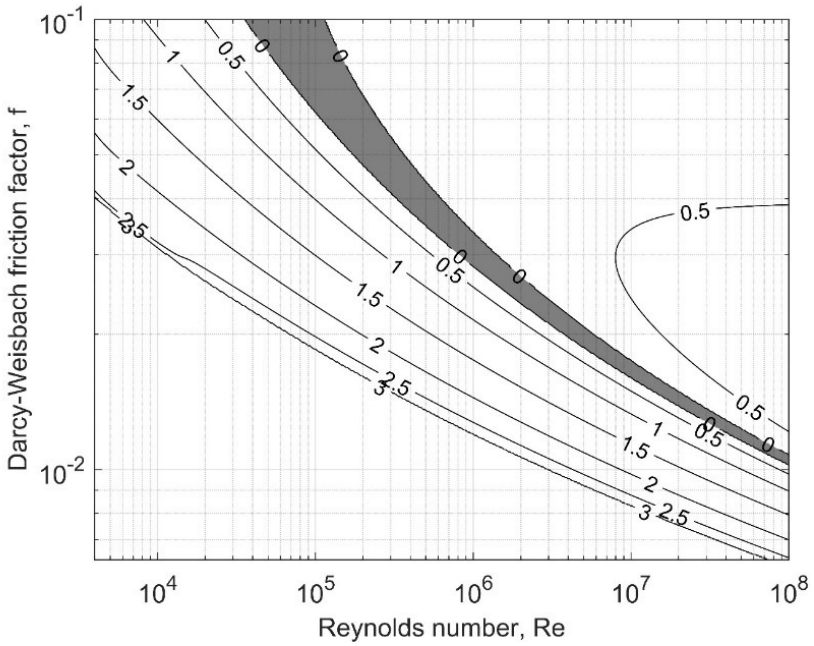

Figure 18: Error in Brkić-Praks versus Colebrook-White in the inference relative roughness. The errors are presented as log-scaled percentage errors in relative roughness for any Darcy-Weisbach friction factor and Reynolds number combination within the limits of Colebrook-White. Colebrook-White is taken to be the correct inference of relative roughness.

Another widely used formulation is the Hazen-Williams equation (Hazen and Williams, 1905). This equation lumps several aspects associated with hydraulic resistance into a single coefficient. A fluid velocity estimate can be determined using the Hazen-Williams coefficient, hydraulic radius, and friction slope. Stephensen (1989) modified the Moody diagram to include Hazen-Williams coefficients, demonstrating how the two methodologies are similar and where there is disagreement (Figure 19).

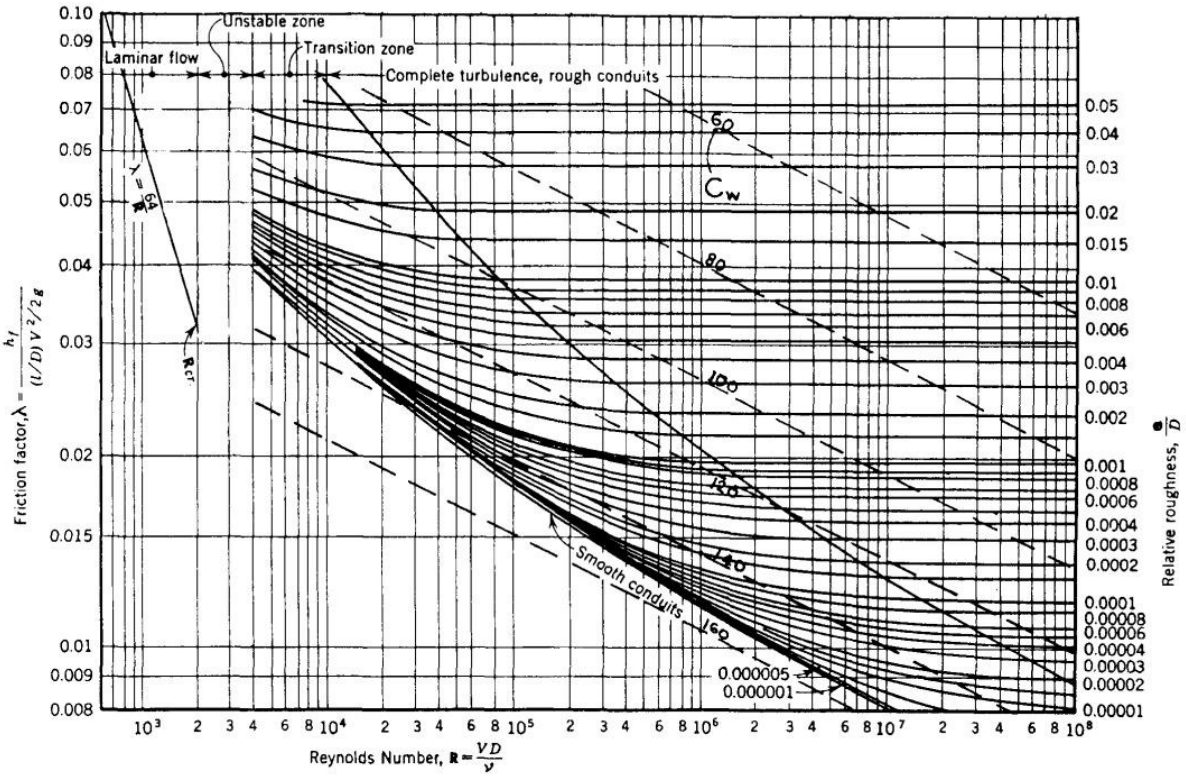

Figure 19: Modified Moody diagram to include the Hazen-Williams coefficients (after Stephenson, 1989).

This diagram illustrates how the Hazen-Williams equation misses the curvature on the diagram as compared to properly utilizing relative roughness. This effect is more apparent in the fully-developed turbulent zone. The Hazen-Williams equation may be stated as follows:

$$U = kC_{HW}R_h^{0.63}S_f^{0.54} \tag{31}$$

Or

Metric:

$$h_f = \frac{6.84LU^{1.85}}{C_{HW}^{1.85}D_p^{1.165}} \tag{32}$$

$$U < 3\frac{m}{s}$$

$$D_p > 0.05\ m$$

Where:

$k = 0.849$ for SI units, 1.318 for Imperial units $(-)$,

C_{HW} = The Hazen-Williams coefficient of hydraulic conductivity $(-)$,

R_h = Hydraulic radius of flow area (L), and

S_f = Slope of the energy gradient $\left(\frac{L}{L}\right)$.

The Halifax Water (2022) requests that the Hazen-Williams equation be utilized to account for friction loss for forcemain designs, within their design guidelines. It is also suggested within the guidelines that the Hazen-Williams coefficient be determined by field tests where possible. The Hazen-Williams equation has received broad scrutiny for its lack of generality and applicability (Jain, 1978; Liou,1998). Jain (1978) suggested that without careful consideration, errors of up to 39% could occur in the estimation of the losses with the Hazen-Williams equation. Jain also pointed out that the proper corrective factor should be selected with respect to the hydraulic radius and friction slope. The value of the coefficient for the Hazen-Williams equation does not account for the Reynolds number (an indicator of turbulence) nor the change in the efficiency of the energy cascade. Liou (1998) points out that various textbooks, references, and software manuals utilize tabulated Hazen-Williams coefficient values without indicating applicable Reynolds numbers and pipe size ranges, which will lead to significant errors. Chistensen (2000) has presented a small window associated with accurate usage of the Hazen-Williams equation (see Appendix D).

3.6 Valves, Actuators, Fittings and Bends

Valves and actuators are essential to the lift-stations in sewerage systems. However, they are often neglected in estimating hydraulic losses. Valves and actuators allow for proper control and safer operation. Valves, fittings, bends, and changes in pipe sections contribute to energy losses. Tullis (1989) has outlined the types of valves and associated (typical) utilizations (see Table 4).

Table 4: Categories of valves and their uses (after Tullis, 1989).

Valve Type	Functionality
Control Valves	
Energy dissipation flow and cavitation control	Control flow or dissipate energy while controlling cavitation
Isolation and sectionalizing	Isolate a pump or control valve/section of a long pipe for repairs
Free discharge	Release water from reservoirs and bypass turbines for transient control
Bypass	For recirculation at a pump start-up, filling a pipeline, and equalizing pressure across large valves/gates before being opened
Scour/Drain (Suribabu and Sivakumar, 2021)	Flush out the sediments and contaminants. Also used to drain water when repairs or maintenance are needed.
Pressure Regulation Valves	
Pressure relief	Protects pipes against excess pressure, such as water hammer
Surge-anticipating	Like a pressure relief valve but is activated by warning of transient
Pressure-reducing/sustaining	Maintain proper upstream or downstream pressure
Non-Return Valves	
Check valves	Prevents backflow
Air Control	
Air relief/vacuum breaker	Remove or admit air to a pipe during transients or filling/draining

Woolf *et al.* (2021) describes the types of valves used in chemical processing, but such are also utilized in lift-stations. Valves can also be in multiple categories. Common valves utilized within wastewater applications are described in Table 5.

Table 5: Common valve types in lift-station applications (after Woolf *et al.*, 2021)

Valve	Functionality
Ball	Utilized in constricting or stopping the flow, contains a sphere with a hole through the middle that rotates perpendicular to the flow.
Butterfly	A disk-type valve is attached to a rotating shaft and a gear system to provide some mechanical advantage. The shaft rotation occurs in the direction of flow to control flow at high capacities.
Globe	A plug-like valve consists of a moving disk-type element that sits on a ring to restrict flow. Glove valves tend to have some mechanism to retract the disk from the ring to allow flow to occur.
Plug	Cylindrical/conically tapered plug rotates inside the valve body to control flow. When the valve aligns with the pipe, it allows flow. When the valve is perpendicular to the flow, it stops the flow.
Gate	Contains a plate that moves in and out of the flow direction. The plate is attached to some mechanism to retract the disk when needed.
Check	Implements a mechanism that allows fluid flow in one direction, configurations include lift, swing, tilting disk, and diaphragm.

Peter *et al.* (2021) outlines the functionality of actuators. These apply the forces needed to operate valves. In high-pressure systems, it becomes difficult to operate valves manually. Actuators can also help with the proper timing of opening and closing valves. Actuator types include pneumatic, motion, conversion, hydraulic, and electric. Most small lift-stations do not use actuators to throttle flow, and valves are fully open or fully closed.

Minor head losses in a system occur at valves, fitting, and bends. The kinetic head is scaled by a factor related to the specific appurtenance. Minor losses are calculated as follows:

$$h_m = K\frac{U^2}{2g} \tag{33}$$

Where:

$K =$ Minor loss coefficient applicable to the fitting $(-)$,

$U =$ Nominal velocity through the fitting $\left(\frac{L}{T}\right)$, and

$g =$ Gravitational acceleration $\left(\frac{L}{T^2}\right)$.

Where the value of K depends on the nature of the fitting or appurtenance (see Appendix D, Table 50).

Manufacturers of valves and fittings publish minor loss coefficient values based on the size, shape, and type of fitting (Crane, 2013). This process is often costly and intensive, leading to interpolation/extrapolations of previous experiments to estimate losses for new products. The minor loss coefficient tends to increase with decreasing fitting size, irrespective of flow velocity. A common methodology for dealing with minor losses in a forcemain is to estimate an equivalent pipe length-diameter ratio. The forcemain segment can be considered uniform by converting minor losses due to fittings to an equivalent length of pipe such that:

$$K = f\left(\frac{L}{D_p}\right) \tag{34}$$

In the context of this study, the above means that there are several possible interpretations (or combinations of misinterpretations) that can result from having unaccounted-for fittings for one (or combination) of the following:

1) The forcemain is longer than accounted than previously thought.
2) The diameter of the forcemain is smaller than previously thought.
3) The apparent Darcy-Weisbach friction factor is higher due to increased inferred roughness.

Expansion and contractions also depend on the structure of the junction. It often relies on angles and lengths of openings to determine accurately. All contractions and expansion were assumed to be sudden and dealt with as per Crane (2013) guidelines:

$$Expansion: K = \left(1 - \frac{{D_{p_1}}^2}{D_{p_2}^2}\right)^2 \quad (35)$$

$$Contraction: K = 0.5\left(1 - \frac{D_{p_1}^2}{{D_{p_2}}^2}\right) \quad (36)$$

Subscripts 1 and 2 refer to the inside diameters of the smaller and larger pipes, respectively.

Minor losses are suspected to change over time due to similar processes such as occlusion. Valve manufacturers do suggest that the head loss due to flow through a valve varies based on flow velocity, size of the valve and type of valve. However, no literature exists for how the pressure drop over a valve or fitting would change over time in wastewater application.

3.7 Flow Establishment

Additional losses are needed to be overcome within the system due to acceleration. As we consider the system unsteady, acceleration should be considered. Acceleration was incorporated based on the methodology provided by Franzini and Finnemore (1997). Acceleration head was considered by:

$$h_a = \frac{L}{g}\left(\frac{dU}{dt}\right) \quad (37)$$

The pressure output by the pump influences acceleration. As previously mentioned, the start-up and stopping phenomena could not be established for the pumps and were assumed to be

instantaneously at the head expected in operation. As mentioned previously, this often is the case for small to medium-sized pumps.

3.8 Lift-station Design Requirements

3.8.1 Wet-well Design

Various components must be considered when designing wet-wells. Halifax Water (2022) has strict guidelines for the designs of the wet-well. Some important components include gravity sewer, flowrate in and out, baffle, benching, pump on and off floats, emergency storage, and the active, dead, and total volume (Figure 20). Small duplex-type wet-well designs often utilize a cylindrical concrete cast casing. The volume is often created from pre-cast rings that lock together in-place when constructing a wet-well and must be able to fit all equipment in the well (as well as potential future upgrades). The active volume is designed to allow liquid storage under normal operations and is set by a level measuring device (*e.g.* a float). Below the active volume is a dead volume that the pump requires to ensure the net positive suction head is provided to the pump. Together, the dead volume and active volume comprise the total liquid volume capacity in the wet-well.

A wet-well must accommodate the peak wet weather flow at full capacity without exceeding the total lift-station capacity. The sizing must also account for the maximum number of starts and stops of the pump per hour as determined by the manufacturer. The bottom of the wet-well should be designed to allow for minimum deposition of solid and sludge from the wastewater. Deposition can be reasonably dealt with by benching the bottom of the wet-well to keep the wastewater material suspended. A baffle may be needed to stop highly turbulent flows from entering the wet-well. Emergency storage may be required in cases where a backup generator is not present. The emergency storage tank should be sized adequately to accommodate peak flow for a time equivalent to the average power outage for the area in the past 10 years. An emergency overflow must be present for cases where the system is completely over-capacity. The wet-well should be designed to withstand the 100-year flood. The wet-well should be optimally designed for a minimum of 50-year service life. Retention times in small lift-stations must be short enough to prevent entrained gases from escaping the liquid in any significant

manner. The American Society for Civil Engineering (1969) suggests that liquids should remain in the wet-well for between 5 to 30 minutes. Pincince (1970) stated that the designers should consider keeping the cycle longer to allow pumps to cool before restarting. However, smaller pumps tend to produce smaller amounts of heat during pumping. Due to less time required to cool down, the smaller pumps can have more cycles per hour than larger pumps. Halifax Water (2022) requires the pumps to handle at least 15 starts per hour. Other design considerations are included, such as the safety, integrity, and accessibility of the system.

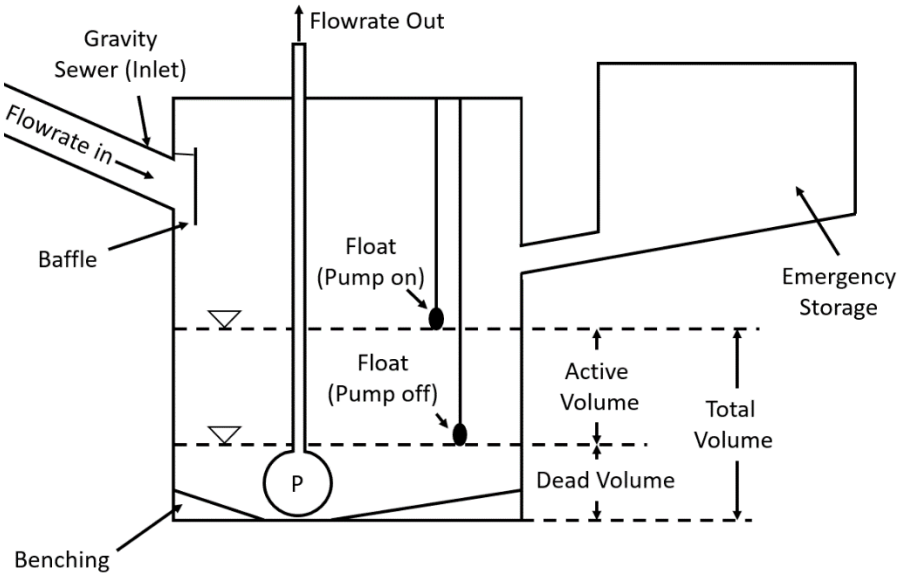

Figure 20: Simple schematic of some important concepts for wet-well design.

3.8.2 Forcemain Design

The guidelines surrounding designs for forcemains vary significantly by jurisdiction. Halifax Water (2022) suggests that forcemains should be designed to last at least 75 years. The minimum and maximum cover must be 1.6 and 2.4 metres, respectively. Small and medium-sized lift-stations must be equipped with at least two forcemains (attached to two separate pumps). The forcemain shall terminate into a benched (and sometimes baffled) manhole, where it is transitioned back into a gravity-driven sewerage system. If the future development of an

area is expected, the design must incorporate upgrades for future designs. Recently, Halifax Water (*ibid*) states that forcemain designs must also incorporate pressure and flow monitoring.

The Environmental Protection Agency (EPA) in the United States (2000) states that several aspects of design are of importance, such as the forcemain material and hydraulics (including diameter sizing, friction losses, surges, and maintenance). The recommended loss formulation for forcemains is the Hazen-Williams equation (Halifax Water, 2022; EPA, 2000). The EPA (2000) suggested that lift-station forcemains should typically be designed for velocities between 0.6 and 2.4 meters per second. Short forcemains with low head requirements may increase to 2.7 meters per second. The forcemain velocity is not recommended to be more than 3 meters per second. Halifax Water (2022) requires the velocity to be more than 0.9 meters per second. Forcemain materials are determined by wastewater quantity and quality, required pressure resistance, corrosion resistance, availability, hydraulic friction characteristics, cost, and the presence of pressure surges (EPA, 2000). The EPA (*ibid*) also states that the vertical alignment of the forcemain should allow for the forcemain to always remain full and allow for enough pressure to prevent gas release. The pipe should be pigged if the forcemain has excessive head losses due to build-up.

3.9 Lift-station Layout

The interaction between the components is driven by the design of the system. When determining the system hydraulics, it is important to consider the physical setup. The head on the intake (suction side) of the pump can either be in a head or lift position. In the head position, the fluid level on the suction side is above the pump intake. In the lift position, the fluid level is below the intake of the pump. The static total head is the difference between the liquid level on the discharge side and the liquid level on the suction side (Figure 21). If the suction side has a head, the static total head is the difference between the discharge head and the suction head. If the suction side has a lift, the static total head is the difference between the discharge head and the suction head.

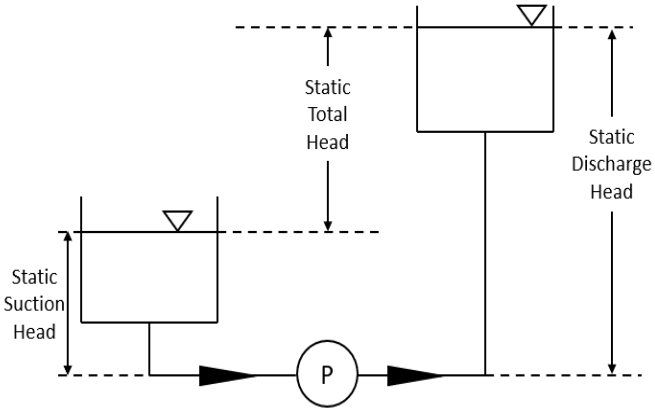

a) Head on the suction side of the pump.

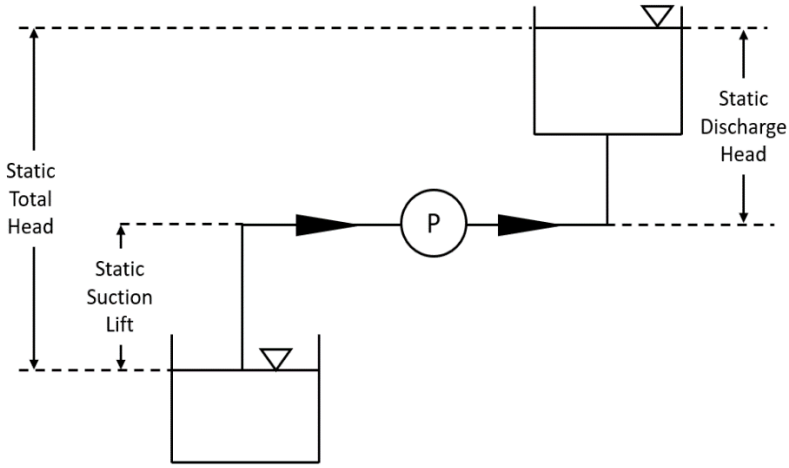

b) Lift on the suction side of the pump.

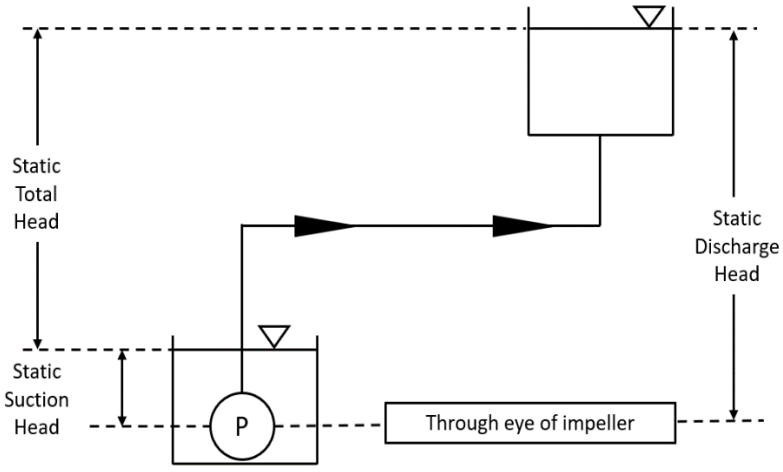

c) A submersible pump system set-up (common arrangement for head on the suction side of the pump, small duplex stations).

Figure 21: Static head definitions for three possible intake arrangements.

Halifax Water (2022) presents guidelines for lift-station layouts based on size. A small lift-station can produce less than 75 litres per second at full capacity. A typical small submersible pump system set-up expected from designs for Halifax Water (2022) is depicted in Figure 21, including important design considerations. A small lift-station has a manhole along the incoming sewer line just before the wet-well. The gravity-driven sewer empties into a wet-well. The wet-well is equipped with methods for monitoring the liquid level. Floats are usually required as a primary mechanism for level monitoring or as a backup mechanism. Pre-programmed levels for an alarm include a high level, low level, high-high level, and a low-low level. The high and low levels trigger the action of only one pump at a time. The high level will trigger one pump to turn on. The low level will trigger one pump to turn off. A high-high level triggers both pumps to begin pumping. The low-low level causes both pumps to stop. The valves, other appurtenance, and monitoring devices for the forcemains are housed in a valve chamber (see Figure 6). The forcemains pump the sewage into the outlet such as a transition manhole (see Figure 1). A lift-station is considered medium-sized when the flow capacity of the system is between 75 and 220 litres per second. Medium-sized stations should consist of two wet-well contraptions, both having at least two pumps (at least four pumps total) with guide rails for easy maintenance and removal. Medium and small-sized stations share various of the same types of components. An example of a medium-sized lift-station is presented in Appendix D as presented by Halifax Water (2022).

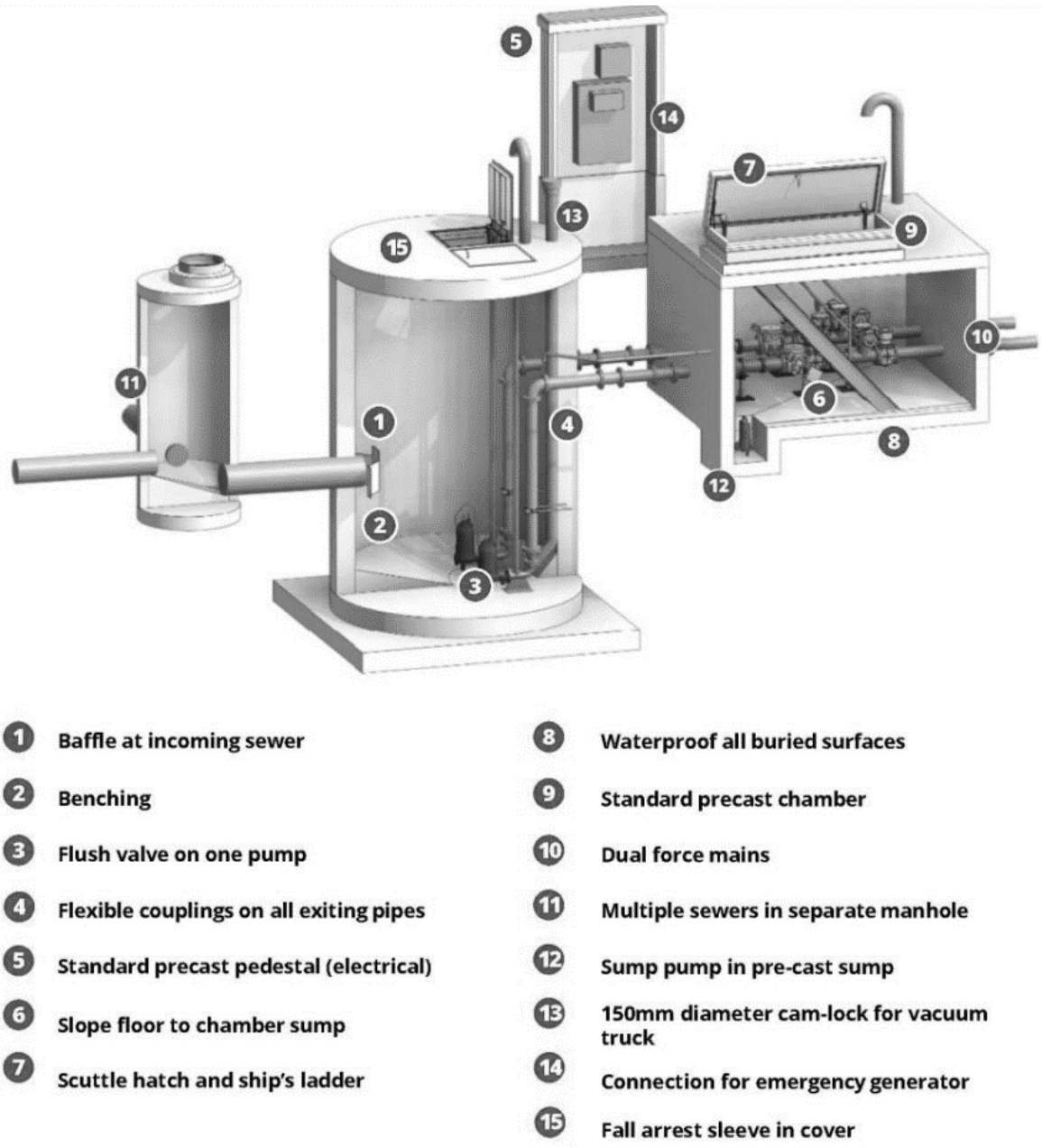

Figure 22: Example of small lift-station set-up (after Halifax Water, 2022)

3.10 Wastewater Characteristics

Water can be used for various domestic uses, such as drinking, cooking, hand washing, bathing, laundry, and toilet flushing, and outdoors for irrigation and car washing. In 2000, the United Nations found that Canada had the most per capita water consumption out of 20 countries

including developed countries like the United States and Germany (Metcalf and Eddy, 2014). Metcalf and Eddy (*ibid*) state that inflow and infiltration into the domestic systems were high during storm events. They also proclaim that the domestic wastewater flow varied throughout the day with the least inflow early in the morning, and the highest inflow around noon. The increasing size of a community diminishes this pattern, resulting in the variation becoming less signifigant throughout the day. The population associated with the sewage system can also significantly affect the total flow rate within the system. Increasing populations can cause the pump cycles to become shorter, wearing out the pump and forcemain faster.

Wastewater is often comprised of various materials, from rags to colloidal materials. Metcalf and Eddy (2014) found that the density of wastewater is the same as that of drinking water in the absence of industrial waste. Although the fluid density is temperature dependent, it also varies with total solids (suspended and dissolved) content. An increase in water temperature can also foster the growth of undesirable plants and fungi within sewerage systems and wastewater plants (Metcalf and Eddy, *ibid*). Wastewater quality indexes can also affect the service life of a forcemain. Although wastewater quality indexes differ between locations and usage, Metcalf and Eddy (*ibid*) provide guidance for reasonable values of several indexes, including pH and alkalinity. There were no publicly available wastewater indices for general use in Nova Scotia.

Several wastewater temperatures were investigated throughout the United States and select countries worldwide. It was found that the mean annual temperature of wastewater was from approximately 3 to 27 degrees Celsius in the United States (Metcalf and Eddy, 2014). Temperatures as high as 30 degrees Celsius have been reported in the Middle East and Africa. Temperatures of wastewater seem to follow a similar trend to average ambient temperatures within the provided data (Metcalf and Eddy, 2014). As a result, it follows a seasonal variation in temperature (wastewater temperatures tend to be higher during the summer and lower during the winter). There was no publicly available data for general Nova Scotia wastewater temperatures.

3.11 Monitoring of Lift-stations and Sources of Error

As monitoring devices become more wildly utilized for small and medium-sized stations, it is also important to understand the limitations of such devices. In recent years, Halifax Water

(2022) has started requiring all small and medium-sized lift-stations to be equipped with various types of monitoring, including but not limited to station voltage, pump motor currents, impeller speed, station liquid level, high and low-level alarms, pump underload and overload alarms, pumps status, flowrate, pump inlet and outlet pressure monitoring, and overflow rates. Distinguishments have been presented within the guidelines between small, medium, and large stations, but requirements for what monitoring is implemented within each size station are unclear. However, small-sized stations commissioned before the release of the Halifax Water design standards (2022) are without considerable monitoring equipment. Therefore, small, and older stations would be equipped with only float sensors to begin and stop the operation of the pump. There tends to be little to no continuous monitoring in such stations.

Pressure transmitters (or transducers) are utilized to determine the pressure on the discharge side of the pump(s). Pressure transmitters can have measurement errors. Such equipment should be calibrated. Hashemian and Jiang (2009) have suggested several aspects that should be considered when calibrating. First, consider zeroing the transmitter and considering the span/range of pressures the transmitter must endure. Various aspects can lead to degradation in the accuracy of the transmitters, such as temperature, pressure, humidity, vibration, maintenance activities, and aging in general. Hashemian and Jiang (*ibid*) provided a typical range for accuracy of 0.25% in precision sensors and around 1.25% of the span for sensors in less demanding applications. Hashemian and Jiang (*ibid*) suggested general sources of error for pressure transmitters outlined in Table 6 and a general formula to determine total error as follows:

$$Total\ Error = \sqrt{(PMA)^2 + (PEA)^2 + (SCA + SD)^2 + (SPE)^2 + (STE)^2} + Bias \qquad (38)$$

Table 6: Uncertainty sources for pressure transmitters (Hashemian and Jiang, 2009)

Uncertainty source	Description
Process measurement accuracy (PMA)	Introduced by inherent noise in the process, such as density corrections
Primary element accuracy (PEA)	Introduced by flow metering devices
Sensor calibration accuracy (SCA)	Introduced by the initial bench calibration
Sensor drift (SD)	Introduced over time as the sensor drifts from calibration settings
Sensor pressure effects (SPE)	(-)
Sensor temperature effects (STE)	(-)
Bias	(-)

Different methodologies measure liquid levels within a well such as floats, displacers, admittance probes, ultrasonic measurement, microwave, immersible head transmitters, conductance probes, air bubblers, and diaphragm boxes (Jones, 2008). The guidelines surrounding level monitoring change depending on the province, state, or country for lift-stations. Within Atlantic Canada, there is no general methodology to monitor liquid levels (Environment Canada, 2006). There is, however, mention that there needs to be a method to determine the off and on times for the pump with respect to the liquid level. Cities like Calgary (2016) are more stringent with how lift-stations are designed and implemented. Level sensors in said jurisdiction that are accepted without special approval are ultrasonic level sensors or floats.

Jones (2008) describes floats as a buoyant body that rides on the surface of the liquid. A float is suspended from a rod or a cable that mechanically links it to an elevation monitoring device. A float could also contain a magnet and slide up and down a rod containing reed switches. A tethered type of float can also be utilized in which a hollow spherical-shaped vessel contains a switch inside. When the float changes position (*e.g.* the water level is higher than the float level), a switch is activated. Floats are utilized in wastewater applications due to their wide variety of materials, low expense, and simplicity of use. The disadvantages are they are difficult

to adjust, the cables wear out fast and must be replaced every 2 to 3 years, and access to the wet-well is required for maintenance.

Ultrasonic sensors allow for liquid level monitoring by emitting sound waves and measuring the time to sense the reflection of these waves to determine the distance of the liquid level from the sensor. Where more accuracy is required, more calibration and preparation are required. In more detailed testing, the speed of sound can be affected heavily by temperature, relative humidity, change in pressure, and the concentration of carbon dioxide in the medium (Panda *et al.*, 2016). Manufacturers of products usually specify high accuracy rates within their specifications for liquid level testing. Pumping tests done by HR Wallingford in the UK (Lauchlan *et al.*, 2005) suggested that ultrasonic sensors were reasonably accurate, between 0.2 to 1.2mm depending on the depth change in the well. The depth changes within the wells studied (*ibid*) were from 0.5 to 1 meter. Monitoring dynamic level changes in sloshing environments causes variable errors, depending on the current state of the liquid being investigated (Terzic *et al.*, 2010).

Flow meters are often utilized within modern lift-stations. For wastewater purposes, the most common being the electromagnetic flow meter. Electromagnetic flow meters generate external voltages directly proportional to the fluid velocity within a pipe. IEEE Xplore (2009) states the main advantages of the electromagnetic flow meter are:

- non-invasive,
- high accuracy ($\pm$ 0.5% of flowrate or lower),
- negligible pressure loss,
- no moving parts, and
- Not sensitive to fluid viscosity/measurement scales.

However, IEEE Xplore (2009) also states disadvantages of this type of flow meter:

- high cost,
- sensitivity to electromagnetic interferences, mechanical vibrations, electrochemical voltages, and
- accurate minimal conductivity valves.

Ultrasonic flow measurements were utilized in the HR Wallingford study (Lauchlan, 2005). In wastewater applications, these flow meters tend to be placed far down a straight pipe to avoid inaccuracies. When properly utilized, ultrasonic measurements have also been found to be accurate to $\pm 1\%$ in laboratory studies (Stoker, 2011).

3.12 Pump-down Tests at Actual Lift-stations

HR Wallingford conducted a large-scale study of lift-stations in the United Kingdom (Lauchlan *et al.*, 2005). HR Wallingford was hired to investigate the hydraulic resistance of forcemains. Beyond the physical features of a given system (i.e., forcemain diameter, well geometries, valves, bends, and other appurtenances), the information obtained from the pump-down test included the fluid flow rate through the forcemain, energy gradient, and temperature of the liquid. Pipe diameters were determined by measurement if the pipe was exposed. If the pipe was not exposed, the pipe diameter was estimated by design drawing records, pipe standards/catalogues, and age. The flow rate in the tests was determined by ultrasonic pipe flow meters, in-line electromagnetic meters, or volumetrically (naively). The wet-well was monitored continuously with ultrasonic level sensors, and it was possible to infer the variation in flow using the geometry of the wet-well. The energy gradient was inferred utilizing a pressure transducer on the discharge side of the pump. The pressure was continuously recorded for both static and pressurized conditions. The HR Wallingford study focused on forcemains less than 200 millimetres for one client and between 600 to 1000 millimetre diameter pipes for another client. It was found that numerous sites did not have sufficient records to make reliable inferences about forcemain conditions.

Two key findings arose from Lauchlan *et al.* (2005). The first was that biofilm is likely to affect hydraulic resistance. As the velocity increased, the roughness decreased to a certain point. Once this point was reached, the roughness predicted was as expected, though the method of interpretation may be questioned. Hansen (2007) suggested that the biofilm in the conduit may act like that of grass in a swale, wherein increased velocity causes the vegetation to bend in the direction of the flow (Kowen and Li, 1980; Carollo *et al.*, 2005). At some point, the grass cannot bend much further and becomes as a static roughness. The second finding of the HR

Wallingford study was that the hydraulic resistance was generally found to increase with decreasing velocity. Hansen (2007) pointed out that this happens (in any case) on the Moody diagram in the partially-developed turbulent zone.

A similar study to was conducted by Michalos (2016) and found that of 415 stations, nearly half of all the associated forcemains were operating at under 1.1 meters per second. Michalos (*ibid*) also found that absolute roughness estimates were between 35 and 0.01 millimetres for the mains of interest. Like the HR Wallingford study, it was found that biofilm effects were present regardless of diameter, pipe age, or material. The analysis utilized SCADA information such as flow rate, discharge pressures, and liquid levels. Michalos (2016) and Lauchlan *et al.* (2005) found an increased cost of pumping under aged conditions compared to initial estimates. Gong *et al.* (2019) investigated the role of biofilms on hydraulic resistance in conduits by running groundwater containing iron-feeding bacteria through plastic pipes and found that increases in head loss can happen quickly. Gong *et al.* (*ibid*) attributed much of the head loss to the decreased cross-sectional area but also suggested that absolute roughness increased.

It can be inferred that the forcemains within the studies mentioned above tend to operate in the partially turbulent and transitional phases of flow. This would imply that the Darcy-Weisbach friction factor increases with decreasing flow rate for a given relative roughness. It would therefore be expected that the head loss would increase with respect to time during a given test. The aforementioned studies did not include such temporal changes and their effects. It also appears that the sensitivity of the inferred roughness to aspects such as diameter is high.

4.0 Theoretical Considerations

4.1 Pump-Down Tests

In a pump-down test, the time it takes for the system to empty a known volume is measured. The test may or may not include taking measurements associated with the pumping, such as the depth of liquid and the dynamic head with respect to time. A small and minimally instrumented lift-station (the common duplex system built in decades past) has only level signals. When these are triggered, they turn the pump on (and turn off) at the top and bottom of the active volume, respectively. Simple float switches are often used, and no continuous data is collected. The time that it takes for this active volume to be removed is the basis for the most basic type of test, referred to herein as the naive pump-down test.

It is possible to determine how long this should take, especially if all components are in like-new condition. Such a determination requires detailed knowledge of the physical system (such as fittings, conduit diameters, wet-well footprint, and characteristic curve), and in this case, a pristine forcemain as the starting point. The temporal migration of the operating point can then be simulated and at a very small-time step. It is then possible to use this modelling tool to search for the assumed forcemain roughness that causes the duration of the simulation pump-down test to match the duration of the observed pump-down test.

In the general case, the discharge through a forcemain during a pump-down test may be expected to vary in a non-linear manner, such as in Figure 23. This is because the descriptors of the governing fluid mechanics are non-linear. Not only are the relationships between flow and dynamic head inherently non-linear (characteristic curve, system curve, Darcy Weisbach friction factor) they interact during any given test. A naïve interpretation of hydraulic resistance is one step further removed from the inferential modelling search described above and is described within the next section.

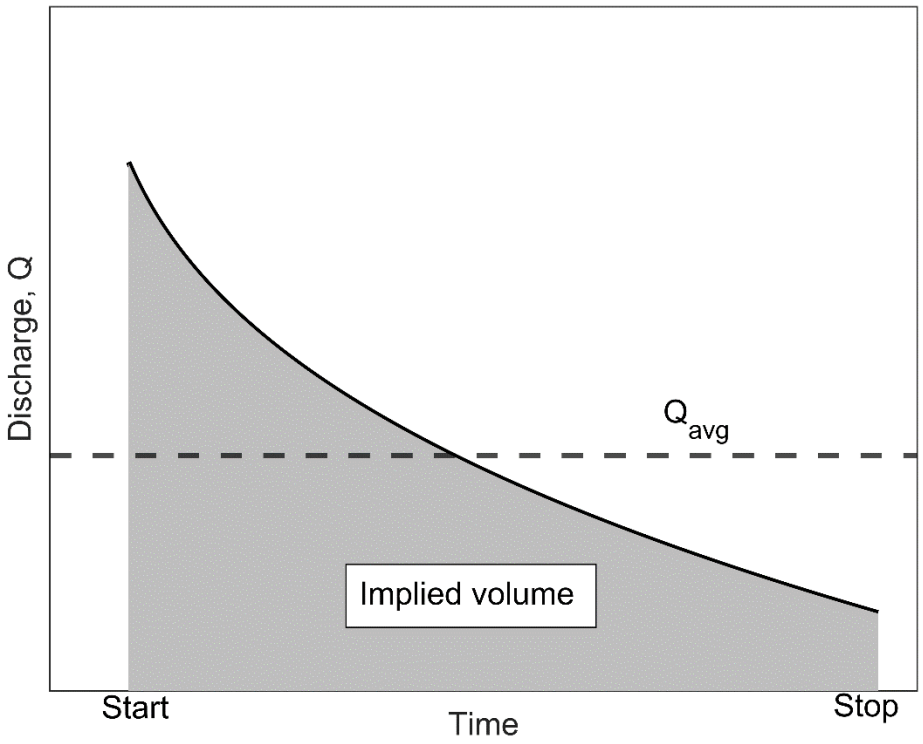

Figure 23: Decline in discharge over time during a pump-down test (not considering flow establishment).

4.2 Naïve Interpretation of Hydraulic Resistance

Additional assumptions are needed to make inferences about the hydraulic resistance of the forcemain apart from just the results of the naïve pump down test. The naïve pump-down test can be used to determine the volumetrically averaged flow rate for the wet-well. Information regarding the dynamic head provided by the pump and static head is required to infer the friction losses of the system along with the characteristics of the system. If there is inflow into the wet-well during pumping, it needs to be considered.

The average dynamic head provided by the pump is often determined with the average flow rate. The dynamic head data provided by the pump may be noisy (as read by a pressure meter). The noise may be enough to cause the average dynamic head provided by the pump to fluctuate between tests. There was no measured discharge pressure data for this study. The characteristic curve, as provided by the manufacturer, was assumed to be reliable.

The choice of the static suction head affects the inference of the total losses through the forcemain. The static suction head associated with the operating point at the true average flow rate is determined by the dynamics of the system. However, the static suction head assumed for the naïve interpretation of hydraulic resistance is the mid-point of the low and high alarm levels.

If there is a significant inflow during the pumping test, it must be considered. The naïve pump-down test provides an average flow rate in the wet-well but not the average flow rate through the forcemain (if inflow is considered). The average flow rate through the forcemain was the summation of the average flow rate in the wet-well plus the average inflow rate as determined when the pump is offline for the naïve interpretation of hydraulic resistance. These assumptions will be referred to herein as the naïve interpretation of hydraulic resistance and is summarized as follows:

$$Q_{well_{avg}} = \frac{(h_{ss_{start}} - h_{ss_{end}})A}{t_{naive}} \quad (39)$$

$$Q_{avg} = Q_{well_{avg}} + Q_{in_{avg}} \quad (40)$$

$$H_{p_{avg}} = c - aQ_{avg}^{b} \quad (41)$$

$$h_{ss_{avg}} = \frac{h_{ss_{start}} + h_{ss_{end}}}{2} \quad (42)$$

The main purpose of the naïve interpretation of hydraulic resistance is to allow industry professionals to gauge the condition of the forcemain. The naïve interpretation of hydraulic resistance alludes to a single energy grade line slope (due to single friction loss over a pipe segment). Therefore, one apparent roughness or smoothness characteristic can be inferred. If the forcemain is in bad condition due to increased hydraulic resistance, the energy loss due to friction will be larger. Industry professionals can compare the energy losses (or inferred resistance metric such as roughness) to the initial commissioning energy loss (or metric) and determine the condition of the forcemain. A forcemain in poorer condition will need to be

evaluated and addressed. Options for addressing and evaluating the forcemain include physical investigation, pigging, repairing, or replacing the forcemain. It should be noted that these processes are cost intensive. Therefore, an accurate methodology for inferring the hydraulic resistance can avoid costs associated with poor forcemain conditions.

4.3 Characteristics of Halifax Water Forcemain Systems - Digital Database versus Engineering Drawings

As previously described, lift stations have headers that contain such appurtenances as isolation valves, backflow prevention valves, bends, and cross-over 'plumbing' that may enable the flow from a given pump to be directed to a different forcemain (for a dual pump and full-length dual-forcemain arrangement). The flow and/or pressure metering chamber (if any) that is just downstream of the header, and which is also on the lift station site (same civic address), will have additional appurtenances of its own. The header and the metering chamber will therefore introduce a host of minor losses, and these occur before the beginning of the forcemain proper. The forcemain proper will usually be routed under travelled ways and paved roads. In following the prescribed route, the designer makes use of bend appurtenances (also known as elbows) to effect changes in direction (angles of 90°, 45°, 22.5°, 11.25°, and 5.625° all being generally available elbows). These bends cause minor losses along the forcemain proper but their contribution to the overall hydraulic resistance is not large. For a forcemain with an inside diameter of 100 mm that is operating with a Darcy-Weisbach friction factor of $f = 0.02$, a 45° elbow would be equivalent to only about one meter of such a forcemain.

The manner in which the Halifax-Water digital database documents the equipment, appurtenances, fittings, and forcemain proper for a given system under its jurisdiction is in a list-like manner. It may state that there are five 22.5° elbows with ID 100 mm, but without indicating where each elbow is located. Most of would probably be along the path of the 100 mm forcemain proper. In calculating the total hydraulic resistance of everything that is downstream of the pump it does not matter where such appurtenances are located, as long as resistance (head loss) is calculated using the correct kinetic head. The research on the four specific Halifax Water stations (described individually in later sections) was directed at inferring

the hydraulic resistance of the forcemain in its entirety, not just the forcemain proper. However, the database provided by the water utility did not necessarily indicate the length of the forcemain proper. It would probably be the conduit listed as having the longest single length because engineering design practice is to use just one inside diameter for the forcemain proper. There are exceptions. The forcemain under Akerley Blvd leaves the metering chamber as a dual forcemain and then passes under Windmill Road, a distance of about 52 meters. This dual conduit arrangement stops at the bottom of Akerley Blvd, at which point the flow merges into a single uphill conduit (forcemain) that is just over 630 m long. Initial use of a pair of smaller diameters may have been done to avoid coming too close to conduits running under Windmill Road, given that there are strict rules about keeping potable watermains etc. minimum distances away from pressurized sewers.

A given system will referred to as either a segmented or a non-segmented, with justifications. "Segmented" indicates that the base information came from engineering drawings, whereas "non-segmented" indicates that the information about the system came from the database of Halifax Water. Segmented does not refer to the method by which lengths of conduit were joined together. For the Monte-Carlo-based study of hypothetical systems, the idealized system consisted of a pump and a single-diameter forcemain of length L, since (in any case) an appurtenance can be computationally replaced by (effectively included as) a short length of conduit having the same diameter as the forcemain itself.

It can be said that everything that is between the discharge side of the pump itself and the outlet point will resist the efforts of the pump to move the wastewater to the higher elevation at the outlet; the header, fittings, short connections between fittings, the metering chamber (if any), its fittings and connecting lengths, and the forcemain proper, the latter with its lengths and various kinds of connections that enable changes in slope and in horizontal direction. In this study nothing that was hydraulically relevant to the amount of resistance experienced by the pump was omitted. However, the minor losses due to all fittings and appurtenances were specifically and separately assessed. This meant that the contributions of these many fittings to the overall resistance would not be attributed to conduit friction.

4.4 System Interaction

The system may be broken down into four components, the wet-well, pump, pipes, and outlet. The interactions between the components are complex. The active volume within the wet-well starts to be removed when the start signal (high alarm) is called by either float or measuring equipment. The pump stops when the level in the well reaches the set lower limit (low alarm). The static head changes as the liquid level falls due to pumping. The flow rate out of the well is much greater than entering the well, which would be ideally zero but depends on the time of day the test was conducted and the capacity of the lift-station. As the liquid level falls within the wet-well, the static head increases from the lowest static head ($H_{ST_{min}}$) to the highest static head ($H_{ST_{max}}$). This increase in static head decreases the flow rate that the pump can provide. The outflow influenced by the losses associated with the forcemain, valves, bends, and other appurtenances. As the flow rate changes, the head losses associated with the forcemain also change. The following two figures (Figure 24 and Figure 25) depict system components and some of the interactions. The energy (EGL) and hydraulic (HGL) grade lines depict a snapshot during a test.

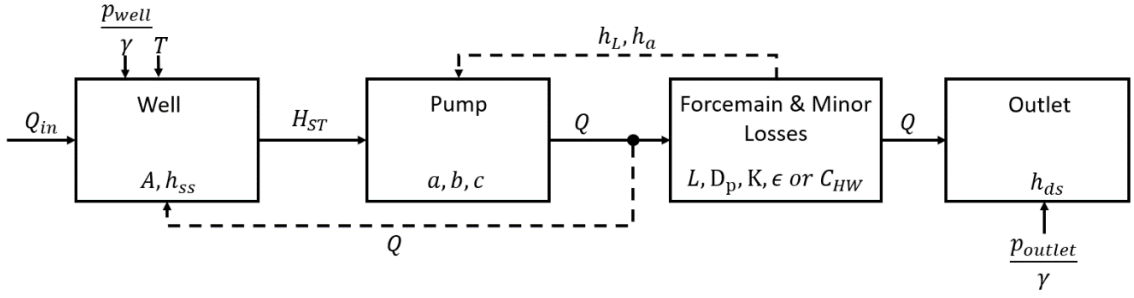

Figure 24: Schematic of lift-station as a system. Average velocity through the forcemain as determined by the flow rate. The minor loss coefficient and static discharge head can change depending on outlet configuration.

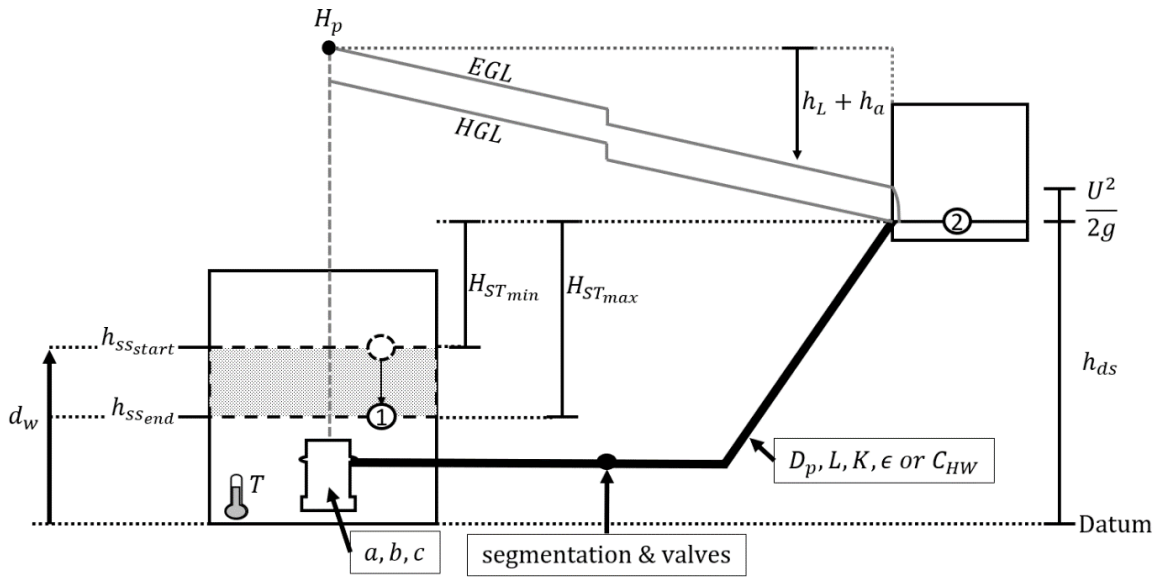

Figure 25: Schematic of lift-station with hydraulically relevant quantities (elevation view, not to scale).

The interaction between the required head by the system and the dynamic head provided by the pump at the operating point is essential. The flow and dynamic head provided by the pump interact dynamically with the system. The dynamic head required by the system and the dynamic head and flow provided by a given pump agree on a physical compromise, definable as the interaction of the system curve and the characteristic curve at a point (see Figure 26 and Figure 27). Without flow establishment consideration the characteristic curve can be determined by equations (43), (44), and (45).

$$H_{system} = H_{ST} + h_L \tag{43}$$

$$h_L = h_f + h_m \tag{44}$$

$$H_{ST} = h_{ds} - h_{ss} \tag{45}$$

Where:

H_{ST} = Static total head, a net static head (L),

h_L = Head loss due to pipe friction, valves, bends, and fittings (L).

The characteristic curve can be acquired for a given pump from its manufacturer. The characteristic curve is like that provided by equation (12). Where the characteristic and system curve intersect dictate the head and flow a given pump can provide. The intersection point of the two curves is known as the operating point. The operating point associated with the pump operating at the best efficiency point is sometimes called a duty point. An engineer would select a pump with a duty point within the operational range. The operating range would therefore be comprised of various operating points that migrate as the static head increases over a pumping test. The operating point is therefore estimated during design but not precisely so. The intersection point (and therefore operating point) is depicted in Figure 26 and determined as follows:

$$H_{system} = H_p = H_o \tag{46}$$

$$H_{ST} + h_L = c - aQ^b \tag{47}$$

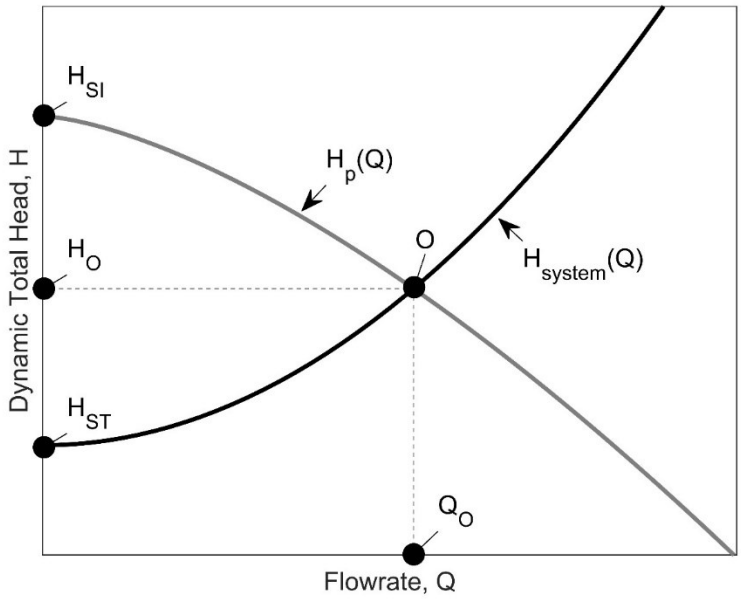

Figure 26: Operating point as dictated by the intersection of the characteristic curve and system curve. Head (H_O) and flowrate (Q_O) at the operating point (O) without flow establishment consideration.

The dynamics of pump-down tests change due to the falling liquid level within the wet-well. This causes the operating point to migrate; as the operating point migrates, additional variables of importance change within the system. One is the Darcy-Weisbach friction factor, influenced by the changing Reynolds Number (Hansen, 2007). Due to regulations imposed during design, most lift-station designs operate within the partially-developed turbulent (PDT) flow regime. Operating within the PDT flow regime implies an increase in the Darcy-Weisbach friction factor as the flow decreases. Figure 27 depicts the migration of the operating point along the characteristic and Figure 28 depicts the migration of the Darcy-Weisbach friction factor during pumping for a rougher and smoother main.

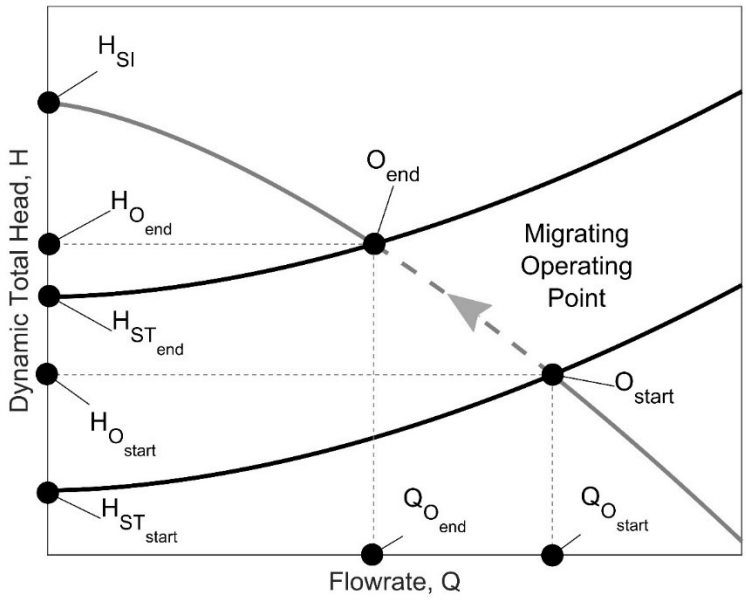

Figure 27: Migration of the operating point during a pump-down test.

4.5 Effects of Age or Deterioration on Migration of Operating Point

Literature review presented in Section 3.0 suggests that the hydraulic resistance changes with time due to the internal diameter of the forcemain and the roughness. With a decrease in effective diameter and an increase in roughness, the relative roughness increases over a

prolonged period (P.P) from the initial commissioning (I.C). With higher relative roughness, the system operates at lower Reynolds numbers and higher Darcy-Weisbach friction factors as compared to the initial commissioning. Therefore, the path of the operating point migration changes over time. The system curve for an equivalent static head will steepen with prolonged operation as depicted in Figure 29. The migration of the Darcy-Weisbach friction factor due to lowering flowrate and increases in relative roughness as depicted in Figure 28.

In addition, characteristic curves change over time as the pump becomes more worn, providing less head at an equivalent flow rate compared to the initial commissioning of the pump. Therefore, the operating point migration can change over time because of the deterioration of the pump. The system dynamics for deteriorated pumps and forcemains are intertwined. Figure 30 depicts the migration of the operating point for a single static head, assuming no maintenance, upgrades, or replacements for the pump or forcemain.

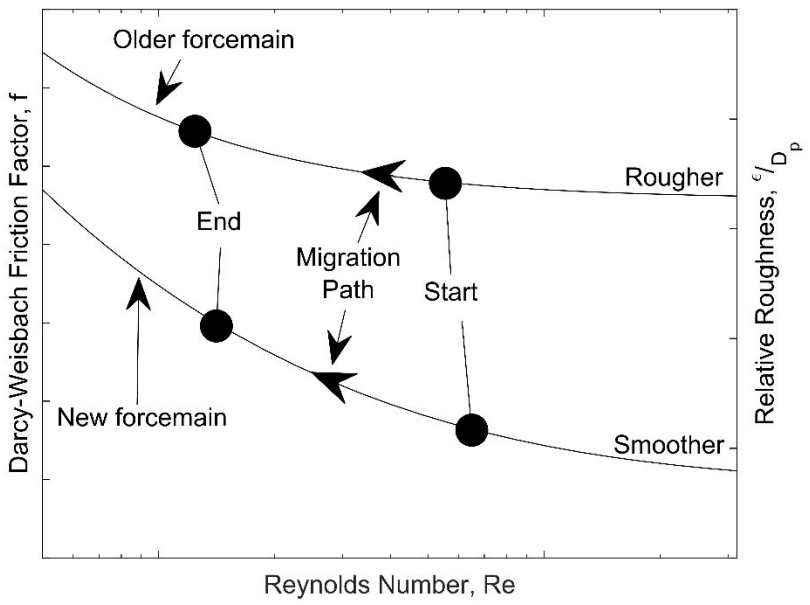

Figure 28: Relative roughness change causing a shift in migration track (no change in pump impeller).

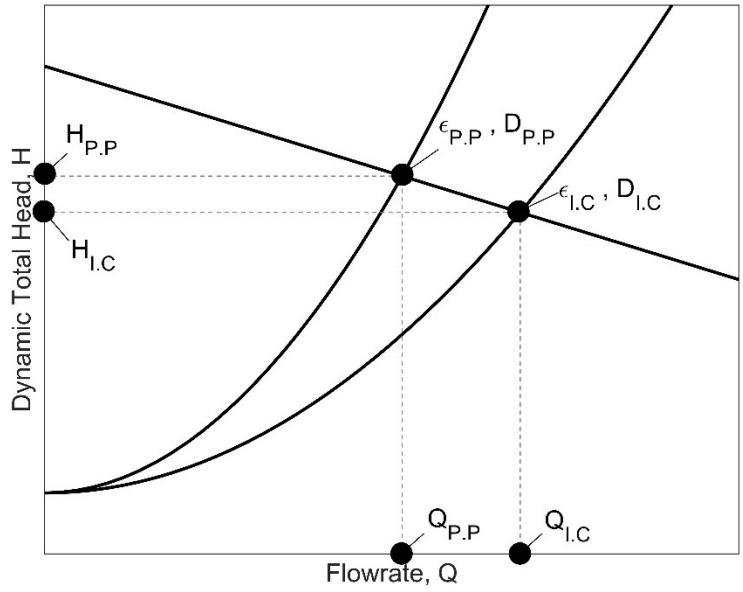

Figure 29: Single operating point change due to increased relative roughness associated with forcemain aging (single static head).

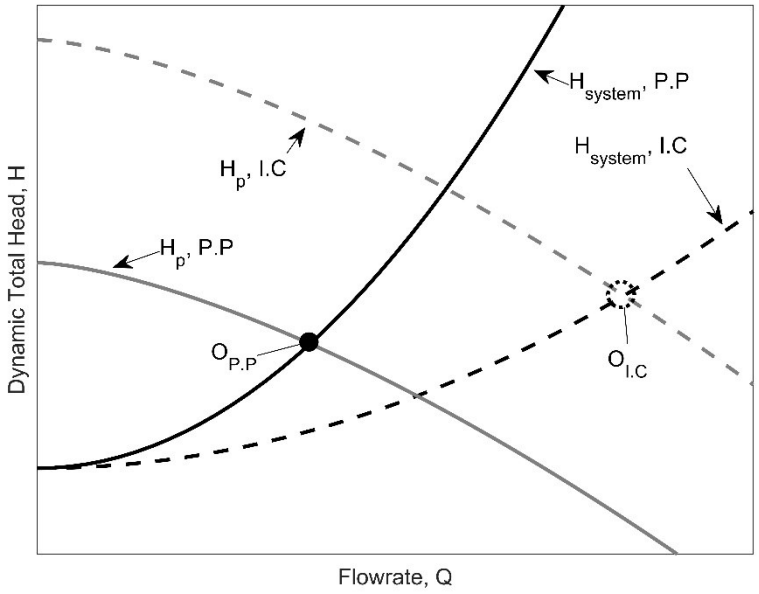

Figure 30: Single operating point change due to pump deterioration and aging forcemain (single static head) from the initial commissioning (IC) to a prolonged period (PP).

4.6 Governing Differential Equations for the Migration of the Operating Point with Flow Establishment

There is currently no literature solving the coupled non-linear equations that govern the unsteady operating point migration presented within this section. Therefore, the system of equations must be solved prior to determining hydraulic resistance through detailed modelling. It is known that no true analytical solution has been discovered due to the complexity of the system dynamics. However, in framing the dynamics of the system, there are two fundamental variables of importance for modelling the unsteady nature of the problem. The first variable that is considered is the static total head. The static head must change during a test due to the liquid being pumped from the wet-well. However, the static total head is a function of the static suction head and the static discharge head (as seen in equation (45)). Given a constant datum, the static suction head varies but static discharge head does not. Therefore, the dynamics of the system can be written in terms of the static suction head in the wet-well.

The second choice of fundamental variable is the velocity through the forcemain. However, a simplifying assumption may be imposed regarding the velocity. The velocity is assumed to be uniform throughout the cross-section (average velocity). The velocity is considered a function of the diameter of the forcemain and the flow rate through the forcemain. Therefore, the second fundamental variable for the system can be the flow rate through the forcemain. Both fundamental variables change with respect to time during pumping (as seen in Figure 24).

4.6.1 Differential Equation for Static Head

The flows in and out of the active volume change the static suction head. If the planimetric area of the wet-well is constant, the following equations can be used in creating the governing equation:

Conservation of volume:

$$\frac{dV_{well}}{dt} = \frac{dV_{in}}{dt} - \frac{dV}{dt} \quad (48)$$

Dewatering identity:

$$\frac{dh_{ss}}{dt} A = \frac{dV_{well}}{dt} \quad (49)$$

Action of the pump:

$$\frac{dV}{dt} = Q \quad (50)$$

The rate of change of head within the wet-well with respect to inflow and outflow rate is, therefore:

$$\frac{dh_{ss}}{dt} = \frac{Q_{in} - Q}{A} \quad (51)$$

4.6.2 Differential Equation for Forcemain Flow Rate

The flow rate variation through the forcemain may be coupled with the static head variation, the characteristic curve, and the overall Bernoulli energy considerations for the forcemain. A governing equation was created using equation (11) and making assumptions that fit the typical lift-station. The full derivation of the equation (52), starting at the unsteady Bernoulli energy equation, is presented in Appendix C. The points of interest in the application of the energy equation are depicted in Figure 25.

It was assumed that the pressure at the liquid surface of the wet-well and the outlet of the forcemain was atmospheric. The outlet configuration for the forcemain at the four sites was above the water surface level at the outlet. However, if the water level surface is above the outlet, the surface of the water level should be utilized as the downstream point of interest. Other assumptions were that the kinetic head at the surface of the liquid level within the well was negligible during pumping, and that the minor loss coefficient associated with different outlet configurations (i.e. non-submerged or submerged) can be accounted for by increasing or decreasing the minor loss coefficient associated with the end of the forcemain (i.e.

$K_{end-segment} = K_{end-segment} + K_{outlet-configuration}$). If the forcemain is segmented, each segment must consider the friction losses, minor losses, and acceleration head separately or find an equivalent main. Although, the mathematically equivalent main will change depending on the flowrate through the forcemain (and rate of change of flow rate) with unsteady considerations.

The flow rate variation for the system may be coupled with the head in the wet-well as per equation (51). Rearranging the energy equation (11) and solving for the rate of change in flow results in equation (52). Equation (52) can therefore utilize the Darcy-Weisbach friction factor (equation (17)) or the Hazen-Williams (equation (32)) for the friction loss terms. Also, equation (52) has the operational point migration embedded within the equation. Therefore any flow rate obtained through solving the coupled equations (equations (51) and (52)) also includes the migration of losses (friction and minor losses) and the dynamic head provided by the pump with respect to the flow rate for different static suction heads throughout the simulation. Simulations are expanded upon in later sections.

$$\frac{dQ}{dt} = \frac{H_p\{Q\} - h_{ds} + h_{ss}\{Q\{t\}\} - \sum\left(h_{f_i}\{\epsilon \text{ or } C_{HW}, Q\} + h_{m_i}\{Q\}\right)}{\sum \frac{L_i}{gA_{p_i}}} \quad (52)$$

Darcy-Weisbach types:

$$h_{f_i} = \frac{8}{g\pi^2}\left(f_i\{\epsilon, Q\}\frac{L_i}{D_{p_i}^5}\right)Q^2$$

Expand: *(17)*

Hazen-Williams (Metric):

$$h_{f_i} = \frac{6.84 L_i \left(\frac{4Q}{D_{p_i}^2 \pi}\right)^{1.85}}{C_{HW}^{1.85} D_{p_i}^{1.165}}$$

Expand: *(32)*

Swamee-Jain:

$$f_i\{\epsilon, Q\} = \frac{0.25}{\left(\log_{10}\left(\frac{\epsilon}{D_{p_i}3.71} + \frac{5.74}{\left(\frac{4Q}{\pi D_{p_i}\nu}\right)^{0.9}}\right)\right)^2}$$

Expand: *(23)*

Characteristic curve: $$H_p\{Q\} = c - aQ^b$$ Reiterate: *(12)*

Where:

i = Index referring to a specific segment of forcemain, valves or fittings $(-)$,

A_p = Internal area of the forcemain (L^2).

4.7 Relating Effects of Flow Establishment

Flow establishment (Franzini & Finnemore, 1997) is the brief period at the start of a test during which the stagnant liquid body changes from no movement up to the flow at the operating point. Due to the nature of the problem being dynamic and unsteady, flow establishment should be considered for accurate analysis. The flow rate in the forcemain is zero while the pump is off. When the pump turns on, there is a period of flow acceleration relating to two critical components of the system. The first component is the energy required to begin moving the weight of the sewage within the forcemain on the pump start-up. The forcemain remains full of liquid while the pump is offline. Another component of flow establishment, probably occurring along with the acceleration of the fluid column, is the time required for the pump to meet its operating point because it is activated by an electric motor. An electric motor is also a generator. The so-called back electromotive force (emf) from the motor toward the supply grid is zero when the rotation is zero. As the rotational rpm builds to about 1800 rpm, the back emf increases to its operational value, during which time the angular momentum builds, overcoming the rotational inertia. In the interests of introducing less stress on the closed-coupled unit and of lessening water hammer, SCADA systems are sometimes required to have a soft start, especially for medium and large lift-stations. It is common to completely neglect start-up mechanics.

Assuming the pump start-up is phenomena is negligible, the migration of the operating point is in two phases. Phase one can be understood as the flowrate and head associated with the period between starting the pump until the flow is established (see Figure 31, phase one). During this phase, the dynamic head provided by the pump may be assumed the shut-in-head at the start of

pumping. Once the flow is established, the dynamic head provided by the pump declines as the flow rate increases until the flow is at the established flow rate for the operational point. During this phase, the flowrate is increasing along the migration path while the liquid level declines in the wet-well. Phase two is considered when the migration of the operational point flips direction (see Figure 31, phase two). At this point, the flow is established and begins to decline as the level in the wet-well declines. The flow rate continues to decline throughout the test until the active volume is emptied. An example of the flow rate over time during a pump-down test, including flow establishment, is depicted in Figure 32.

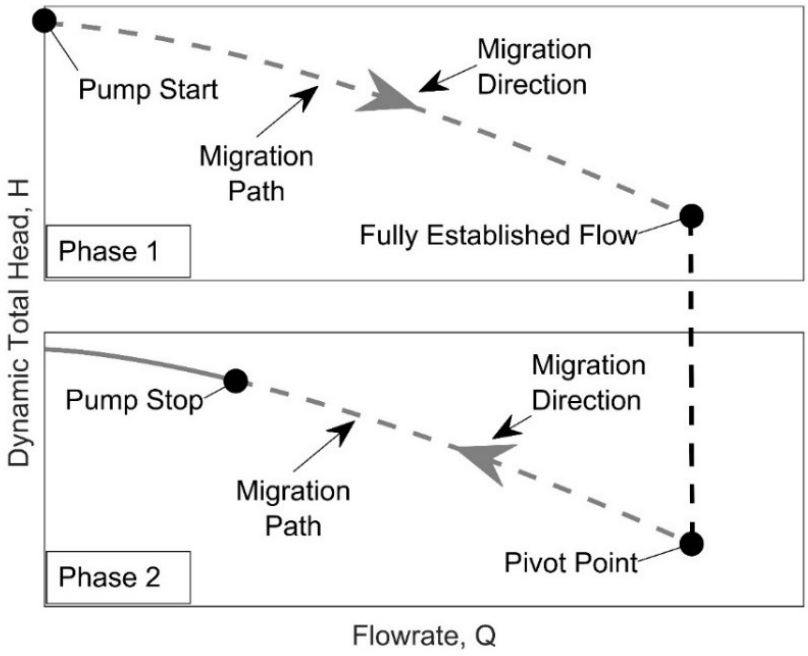

Figure 31: Migration pathway for operating point during with flow establishment (no pump start-up consideration).

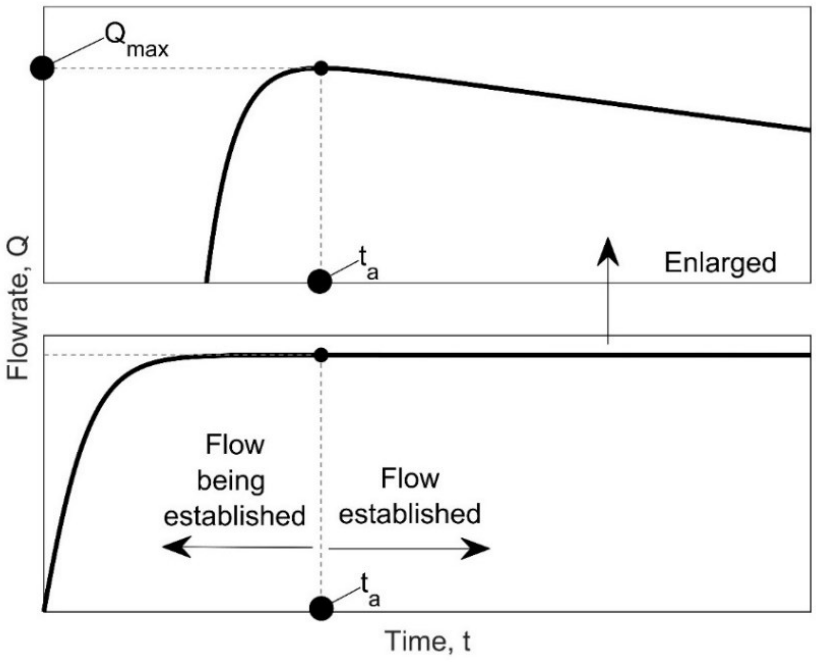

Figure 32: Example of the flow rate versus time over a pump-down test, including flow establishment.

4.8 Equivalent Solutions with Naïve Pump-down Test Information

An accurate estimate of the hydraulic resistance of a forcemain could be obtained given perfect knowledge of the dynamic head provided by the pump, the flow rate, and the liquid level in the well at any instant during pumping. A naïve interpretation is conducted as outline in Section 4.2. When considering a more detailed approach to interpreting the hydraulic resistance, there may be numerous solutions of characteristics of the lift-station and forcemain combinations that provide the same average flowrate.

If the forcemain is old and in poor condition, the volumetrically determined flow rate is noticeably lower than the flow rate that would occur through the same forcemain when initially commissioned. This is due to how much longer it takes to evacuate the same volume for a system after a prolonged period. This lower flow rate, though determined volumetrically, still has diagnostic value, especially if the migration of the operating point can be modelled in detail. It is also true that the dynamic head at the moment at which the pump was at the average flow rate is not known. The naïve pump-down test only partially bounds the inferential problem at the

starting and stopping head in the wet-well, a time dictated by the start and stop of the pump(s), and the active volume of the wet-well. Figure 33 illustrates the contrast between having a single head versus a flow point to work with, and what a pump-down test provides.

It is probable that a forcemain in poor condition would exhibit a roughness that has increased and a diameter that decreased when compared to the condition at commissioning. This means that aging tends to cause relative roughness to increase for two reasons. Therefore, it is reasonable to search for both the diameter and relative roughness of an aged forcemain, not primarily absolute roughness. If the flow does not significantly affect the relative roughness (such as the bending of biofilm due to velocity increases), any given pump-down test must migrate along a curve with a single value of relative roughness on the as depicted on the Moody Diagram (Figure 16 and Figure 28).

However, it would still be of interest to determine the absolute roughness utilizing the nominal diameter of the installed forcemain as might be found in an engineering design drawing. If the implied roughness inferred is too large, it could be granted that a reasonable explanation could be that the diameter utilized in the inference is too large and the area presently available to the flow during the test had likely been reduced via mineral and/or biological occlusion. If some sort of field measurement for the inside diameter exists, it would be of interest to find the apparent absolute roughness using the measured diameter(s) of the forcemain of interest. A complete survey of how the inside diameter varies through the entire length of a forcemain when the forcemain is still in use would be difficult. Field measurements of inside diameters are sometimes done at and near the receiving manhole (Jean, 2006).

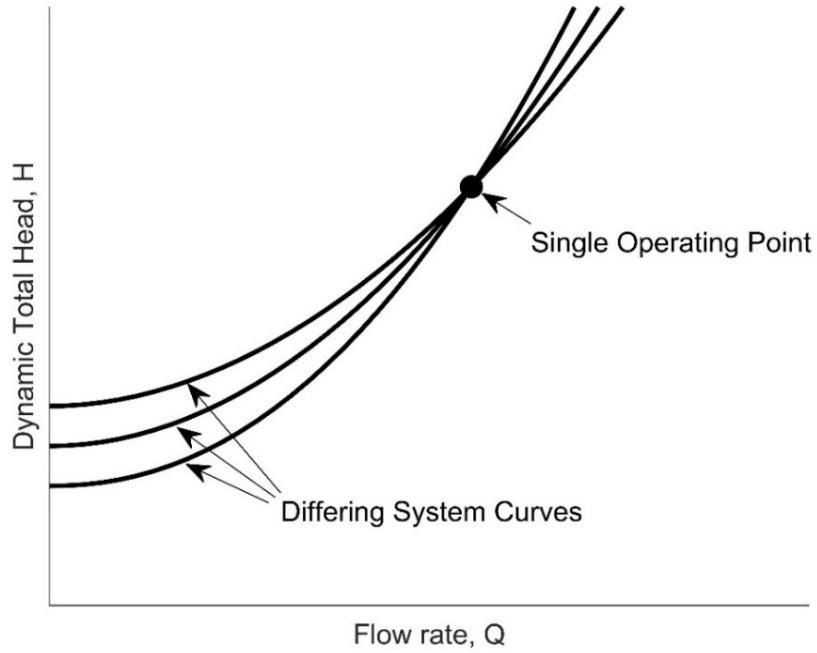

a) System curves that all go through a single value of flow rate, Q.

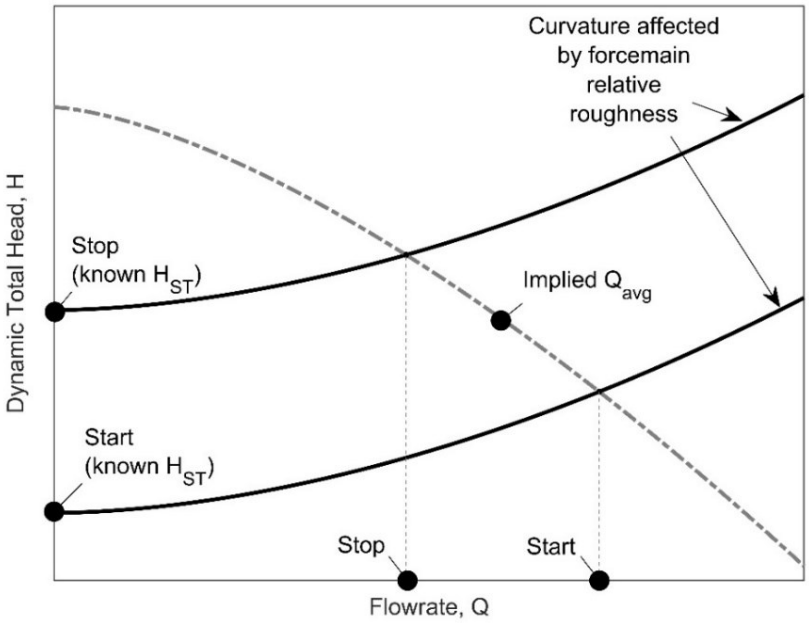

b) System curves of a pump-down test are associated with an average flow rate and imply specific amounts of curvature.

Figure 33: Contrast between implications of a single dynamic total head versus flow rate operating point and what a pump-down test provides.

In the inference of hydraulic resistance, it was not expected that the period of flow establishment would be negligible. It was expected that the duration of the initial flow establishment would be

affected by the roughness and internal diameter of the forcemain, just as roughness must affect the Darcy-Weisbach friction factor, and therefore the loss of head due to friction. Therefore, differing absolute roughness and inside diameters can produce the same volumetrically averaged flow rate during a pump-down test (see Figure 34) given that flow establishment has been considered. The differences in the relative roughness that result in a similar average flow rate can be a significant range.

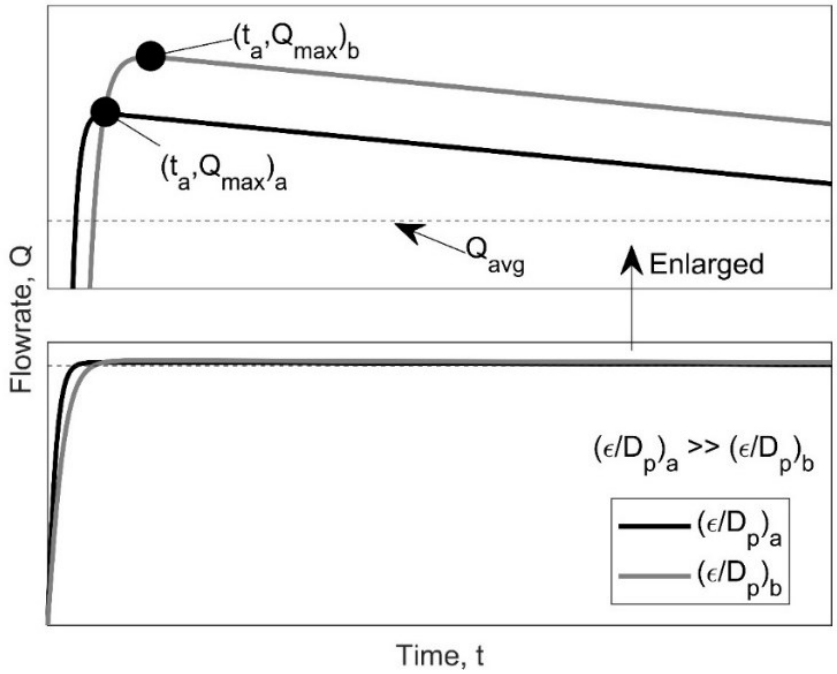

Figure 34: Flow rate over time with flow establishment of two different relative roughness (a & b) meeting the same average flow rate.

5.0 Methodologies

5.1 System Identification

System identification is an integral part of approaching a problem. Identification can assist in determining approaches to solving complex issues by relating them to similar systems that already have solutions. The definitions and guidelines summarized within this section are adapted from Mellodge (2016).

The governing equations presented in Section 4.6 are considered a dynamic system. Dynamic refers to the constantly changing energy throughout the test. A system refers to a group of parts that work together. Dynamic systems can relate to the inputs, outputs, and system characteristics that change with time. The system is considered continuous within the testing time frame and is non-linear. Non-linear systems are those in which the differentials cannot be mapped linearly with system components. Mellodge (2016) mentioned that non-linear systems are often defined by what they are not, making general results challenging to determine. The problem requires memory of previous inputs to understand present conditions, concluding the system is causal.

Commonly utilized Darcy-Weisbach friction factor estimation methods tend to be comprised of "dead zones (*e.g.* the critical/transitional region on the Moody Diagram)." Dead zones in this context refer to piecewise functions in which a section has a non-defined region or is taken to be zero. Some hard-coded limits were implemented to ensure the equilibrium points were within the ranges intended for realistic solutions.

Utilizing numerical techniques can lead to numerical instability within a solution or compound the error in a solution. It is essential to minimize numerical instability by choosing proper step sizes within the model. The time step should be small enough to ensure the model converges on the correct solution with a tolerable error and stability is maintained throughout the simulation.

5.2 Data Acquisition and Correction

5.2.1 Lift-station and Forcemain Configuration

Information about each lift-station and forcemain was collected previously by Jean (2006). Additional forcemain and lift-station characteristics were provided by Halifax Water during this study to supplement the data collected by Jean (2006). Table 7 summarizes the information collected for each lift-station.

Table 7: Station characteristics and data required for pump-down tests.

Characteristic or information	Use	Source(s)
The temperature of the liquid	Affects the kinematic viscosity of the liquid.	Station thermometer or thermistor
Pipe material(s)	Affects the rate and nature of deterioration of the forcemain. Also implies a specific commercially available inside diameter.	Field inspection and/or design drawings
Inside diameter(s) of forcemain	Affects the hydraulic capacity of the system.	Field measurement and/or design drawings
Fittings, bends, and other appurtenances	Cause localized energy losses known as minor losses. Minor losses are determined by the nature and number of fittings, bends, and other appurtenances	Design drawings and product information from manufacturers or textbooks
Pipe length(s)	Affects the energy loss due to friction and flow establishment.	Design drawings
Maximum liquid height in wet-well	Setting set through the SCADA system for a lift-station. Utilized in the determination of the lowest static head during a test.	Float switch or sensor (acoustic, laser, etc.)
Minimum liquid height in wet-well	Setting set through the SCADA system for a lift-station. Utilized in the determination of the highest static head during a test.	Float switch or sensor (acoustic, laser, etc.)
Area of well	Affects how the volume changes with depth.	Field measurement or design drawings

(**Table 7**, continued)

Characteristic curve of the pump	Describes how the dynamic head provided by the pump changes with the flow rate (pump output)—provided among other useful curves for a pump.	Pump manufacturer
Pressure and flowrate during a test	Enables a more direct interpretation of the condition of the forcemain	Pressure and flow meters (not frequently available)
Time required to pump out active volume	Utilized in determining an average flow rate for a given test utilizing elapsed time and active volume.	Timer
Forcemain condition at outlet	Submerged or unsubmerged, accounting for different energy losses at the outlet.	Field inspection and/or design drawings.

5.2.2 Supplementary Station Information

Supplementary information would not typically be known when utilizing naïve pump-down tests but collecting additional data to validate results was of interest, where available. The sites investigated in the study had some form of additional supplementary information. Although, the supplementary information was not the same for each site. Table 8 summarizes the data acquisition available for each Halifax Regional Municipality station analyzed in the study.

It was found that some data had considerable noise. Some data appeared to be missing for brief periods at the start and end of certain pump-down tests. In the general case, the noise in the data was due to turbulence in the wet-well caused by inflows, the pump, and equipment tolerances. Noise and missing data were dealt with by fitting curves to the data available and utilizing the fitted curves when necessary (also see Section 5.5.)

Table 8: Data acquisition equipment for the four stations analyzed.

	Location			
Index	**Trinity Lake**	**Akerley Boulevard**	**Ragged Lake**	**Melville Cove**
Level Trigger	Ultrasonic	Ultrasonic*	Float	Ultrasonic*
Continuous flow monitoring (forcemain)	Magnetic	Magnetic	N/A	N/A
Continuous level monitoring	Ultrasonic	Ultrasonic	Unknown**	Ultrasonic
Continuous inflow monitoring	N/A***			
Pressure Monitoring	N/A***			

*Float back-up

**Data from Jean (2006), but no methodology for collection is stated.

***Not available

5.3 Error Metrics

Error metrics were utilized to evaluate different methodologies in the study. Error metrics utilized were percentage relative errors and scalar errors. The error metrics compare an actual (or benchmark) and a predicted value associated with a variable such that:

$$E_{\Lambda_{percent}} = \left| \frac{\Lambda_{predicted} - \Lambda_{actual}}{\Lambda_{actual}} \right| * 100 \quad (53)$$

$$E_{\Lambda_{scalar}} = \frac{\Lambda_{predicted}}{\Lambda_{actual}} \quad (54)$$

Where:

$E_{\Lambda_{percent}}$ = Error associated with any variable "Λ" expressed as a percentage $(-)$,

$E_{\Lambda_{scalar}}$ = Error associated with any variable "Λ" expressed as a scalar $(-)$,

$\Lambda_{predicted}$ = Predicted value of any variable "Λ" (#), and

Λ_{actual} = Actual value of any variable "Λ" (or another benchmark value) (#).

If a directional error did not matter, a percentage error was utilized. Where directional error had to be considered, scalar errors were utilized.

5.4 Modelling Software & Algorithms

MATLAB (Mathworks, 2019) allows for the easy implementation of numerical techniques and is optimized for scientific computing while maintaining ease of use. A mathematical model was created and coded in MATLAB to assess the inference of hydraulic resistance in forcemains. Several pre-existing subroutines were utilized, as summarized in Table 9:

Table 9: MATLAB packages and functions utilized.

Modelling Package/Codes	Brief Description
Curve-fitting Toolbox (3.5.10)	Curve-fitting to data, various functions are readily available, and has some capabilities for custom fits.
fzero	Estimating roots of non-linear functions.
ODE45	An explicit Runge-Kutta fourth-order numerical integration technique with capabilities for systems of non-linear differential equations.
ksdensity	Estimated probability density utilizing kernel density estimation.
trapz	Trapezoidal method for integration.
fitctree	Constructs a classification tree, given a set of data.

5.4.1 Non-Linear Root Finding

For situations in which a root was needed for a non-linear function, the fzero (Mathworks, 2019) algorithm was utilized. The inputs required for the fzero algorithm are a function of interest with one independent variable, and an initial estimate for the root or a range to investigate. Additional options can be selected for fzero, such as what methodology to utilize in root finding or acceptable tolerances. The method is based on an algorithm created by Brent (1973).

If given an interval, the function begins by ensuring that zero is contained within the section. Zeros are ensured by having a negative and positive value at the end points of the interval. The function then computes relative logical expressions to determine which methodology should be used for determining how to take the next step. The root-finding techniques utilized within the fzero algorithm are bisection, secant, linear or inverse quadratic interpolation methods.

Bisection is a continuous determining the mid-point of the range between two points until converging on a root. Bisection is initiated by selecting an initial range such that:

$$x_a \leq x \ \leq x_b \ \mid \ fun\{x_a\} * fun\{x_b\} < 0$$

Where:

$x_{a,b}$ = Domain in which the root lies (#), and
$fun\{x\}$ = function of "x" notation (#).

Taking the mid-point between a range provided allows for a new dependent value to be established. The newly established value then updates the boundary in which the sign matches. Iterations can be repeated until a root is found.

There are limitations and advantages associated with the bisection method. The advantages are that the method is guaranteed to converge given the appropriate setup, the error can be decreased by running more iterations, and simple implementation. The limitations of bisection include that it requires knowledge of the bracketing interval, it requires a continuous function, and its speed of convergence is slower than other methods. For this study, these limitations are not significant.

The secant method allows for faster convergence, and a numerical differential is considered. The Secant method allows for faster convergence than the other methods. It requires two initial estimates for a root and utilizes those estimates to determine a numerical differentiation. The numerical differentiation creates a straight line through the two points. The root of that equation is then determined, and the dependent value is calculated. The new value then updates the furthest value from the initial point (equation (55)). A stopping criterion is implemented to determine when to stop the iterations.

$$x_{n+1} = x_n - fun\{x_n\}\left(\frac{x_n - x_{n-1}}{fun\{x_n\} - fun\{x_{n-1}\}}\right) \quad (55)$$

Where:
n = Step count $(-)$.

There are advantages and limitations to the secant method. The advantages are that convergence is faster than other methods and it does not require knowledge of the derivative of the function. The limitations of the method are that it may not converge, there is no guaranteed error bounds, and it may get stuck in local maxima or minima.

Inverse quadratic interpolation is another root-finding method, but it utilizes three initial guesses (see equation (56)). If the three initial guesses are sufficiently distant from the root of interest, the method may not converge. However, the method does converge quickly if utilized in the proper manner.

$$x_{n+1} = TERM1 + TERM2 + TERM3 \quad (56)$$

$$TERM1 = \frac{fun\{x_{n-1}\}fun\{x_n\}}{(fun\{x_{n-2}\} - fun\{x_{n-1}\})(fun\{x_{n-2}\} - fun\{x_n\})} x_{n-2}$$

$$TERM2 = \frac{fun\{x_{n-2}\}fun\{x_n\}}{(fun\{x_{n-1}\} - fun\{x_{n-2}\})(fun\{x_{n-1}\} - fun\{x_n\})} x_{n-1}$$

$$TERM3 = \frac{fun\{x_{n-2}\}fun\{x_{n-1}\}}{(fun\{x_n\} - fun\{x_{n-2}\})(fun\{x_n\} - fun\{x_{n-1}\})} x_n$$

5.4.2 Initial Value Problem

The model created has an embedded initial value problem. ODE45 (Mathworks, 2019) is a MATLAB function that implements a fourth-order Runge-Kutta methodology. The explicit Runge-Kutta fourth-order method is a popular numerical technique to integrate systems of ordinary differential equations. If the ordinary differential equations and initial conditions for the governing variables (see equations (51) and (52)) are as follows:

$$\frac{dQ}{dt} = fun\{t, Q, h_{ss}\}, \quad Q\{t = 0\} = Q_0$$

$$\frac{dh_{ss}}{dt} = fun\{t, Q\} \qquad h_{ss}\{t = 0\} = h_{ss_0}$$

A solution can then be determined for $Q\{t\}$ and $h_{ss}\{t\}$ by numerical integration with the explicit Runge-Kutta fourth-order method as follows:

$$Q_{j+1} = Q_j + \frac{1}{6}\Delta t(k_1 + 2k_2 + 2k_3 + k_4) \tag{57}$$

$$h_{ss_{j+1}} = h_{ss_j} + \frac{1}{6}\Delta t(l_1 + 2l_2 + 2l_3 + l_4) \tag{58}$$

$$t_{j+1} = t_j + \Delta t \tag{59}$$

$$k_1 = \frac{dQ}{dt}\left\{t_j, Q_j, h_{ss_j}\right\}$$

$$l_1 = \frac{h_{ss}}{dt}\{t_j, Q_j\}$$

$$k_2 = \frac{dQ}{dt}\left\{t_j + \frac{\Delta t}{2}, Q_j + \Delta \mathrm{t}\left(\frac{k_1}{2}\right), h_{ss_j} + \Delta t\left(\frac{l_1}{2}\right)\right\}$$

$$l_2 = \frac{dh_{ss}}{dt}\left\{t_j + \frac{\Delta t}{2}, Q_j + \Delta \mathrm{t}\left(\frac{k_1}{2}\right)\right\}$$

$$k_3 = \frac{dQ}{dt}\left\{t_j + \frac{\Delta \mathrm{t}}{2}, Q_j + \Delta \mathrm{t}\left(\frac{k_2}{2}\right), h_{ss_j} + \Delta t\left(\frac{l_2}{2}\right)\right\}$$

$$l_3 = \frac{dh_{ss}}{dt}\left\{t_j + \frac{\Delta \mathrm{t}}{2}, Q_j + \Delta \mathrm{t}\left(\frac{k_2}{2}\right)\right\}$$

$$k_4 = \frac{dQ}{dt}\{t_j + \Delta \mathrm{t}, Q_j + \Delta \mathrm{t} k_3, h_{ss_j} + \Delta \mathrm{t} l_3\}$$

$$l_4 = \frac{dh_{ss}}{dt}\{t_j + \Delta \mathrm{t}, Q_j + \Delta \mathrm{t} l_3\}$$

Where:
Δt = Step size (T), and
j = Step count $(-)$.

The ODE45 algorithm was influenced by Dormand and Prince (1980), where an additional two steps k_5 , l_5 and k_6, l_6 are determined for higher accuracy between steps. The additional terms are utilized to determine relative step error for the potential next step. The error terms are related to the user-defined tolerances for relative and absolute errors with the stepping scheme and are utilized in the adaptive stepping algorithm. The global error associated with the Runge-Kutta fourth-order methodology is $O(\Delta t^4)$.

There are limitations and advantages to the fourth-order Runge-Kutta methodology. The advantages of the method is that it has reliable stability characteristics and a higher accuracy as compared to lower order explicit methods. The limitation of the method is that it requires more computational effort (and therefore time) for numerical integration that some other methodologies for comparable accuracy. However, the limitations did not outweigh the advantages of the method within the study.

Numerical stability should also be considered with numerical integration techniques. Numerical instability is related to the errors introduced by a numerical technique and can relate to any sources of error affecting the resulting outputs. Common sources of error (and therefore numerical instability) include truncation (rounding errors) and relative step errors. If the problem is sufficiently stiff and the step size is too large, the stability of the method will decrease leading to more erroneous outputs. The resulting solutions in the study were stiff at the start of the simulation, requiring a smaller time step to provide accurate solutions. However, the time required to simulate a pump-down test was sufficiently short. Within the study, various time steps were considered to determine if the solution has sufficiently converged. Another potential contribution to numerical stability is the choice of initial conditions but this was not a significant issue within the study.

5.4.3 Discrete Numerical Integration

Numerical integration techniques for discrete data were required in the study. The trapz (Mathworks, 2019) algorithm was used to integrate numerically for such cases. The trapz algorithm utilizes the trapezoidal integration methodology as follows:

$$\int_{x_a}^{x_b} fun\{x\}dx \approx \frac{1}{2}\sum_{j}^{N}\left(x_{j+1}-x_j\right)\left(fun\{x_j\}+fun\{x_{j+1}\}\right) \tag{60}$$

Where:
j = Step count $(-)$, and
N = Total step count $(-)$.

The trapezoidal method has advantages and disadvantages. The advantages of the method are that it is relatively accurate compared to other methods and is easy to implement. The disadvantage is that it utilizes linear approximation between integration points, making it less accurate than methods that include curvature. The study utilizes small step sizes (more trapezoids considered), making the trapezoidal method relative accurate in the analysis. The order error for the trapezoidal method is $O(\Delta t^2)$.

5.4.4 Kernel Density

A kernel density estimation algorithm (ksdensity; Mathworks, 2019) was utilized to investigate the probability distributions associated with parameters in a Monte Carlo simulation dataset. The kernel density estimations can be determined by:

$$\widehat{fun_M}\{x\} = \frac{1}{NM}\sum_{n}^{N} Kernel\left\{\frac{(x - x_n)}{M}\right\} \tag{61}$$

Where:
N = Number of samples taken $(-)$,
M = Bandwidth $(-)$,
x_n = Random samples $(-)$, and
$Kernel$ = Kernel density function selected $(-)$.

Kernels such as a box, triangle, Gaussian, and tri-weight, can be considered. For each point found within the data set, an equal weighting is placed at the point with a specified bandwidth. These total weights are then summed together to estimate the probability density function of

interest. The densities can also be bounded by mirroring a negative version of the kernels about the boundaries.

5.4.5 Classification Tree

A classification tree was created utilizing the fitctree (Mathworks, 2019) function. Classification trees utilize recursive partitioning to divide data along maximally optimal criteria, depending on the dataset. The classification tree begins at a root node, and the decisions are imposed on the dataset to split in a binary manner. The split then grows two new branches, which again impose optimal criteria on the data at each node to divide the dataset further. The recursive partitioning continuously occurs at each node until the stopping criteria are met. Once all nodes can no longer split due to stopping criteria or the tree has fully developed, the tree is considered grown. The terminology and methodology were acquired from Izenman (2008). The proper terminology for classification tree is summarized in Table 10. A simple classification tree and terminology is depicted in Figure 35.

Table 10: Summary of background nomenclature for classification tree.

Nomenclature	Definition
Root node	The first node in the tree in which all branches are sprung.
Decision node	The node in which a decision is made to split into more nodes/leaves.
Leaf (terminal)	The last node is attached to a branch.
Parent node (non-terminal)	The node in which other nodes have sprung.
Child node	The node that directly descends from a parent node.
Branch	The subsection of a tree in which the tree is subdivided.
Splitting	Referring to the process of creating two new nodes from a decision node.
Saturation	The tree has grown to the full extent with respect to the criteria imposed.

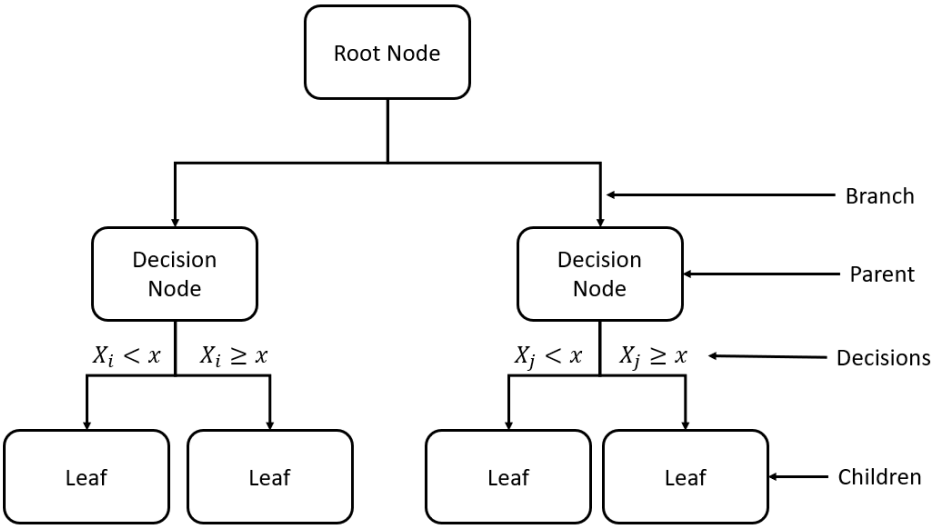

Figure 35: Simple diagram of classification tree.

Izenman (*ibid*) demonstrated that splitting at a node is determined by deciding the optimal split for the data at each node. The optimal split for any data set can be determined by goodness-of-split criteria and an impurity function. The impurity function is utilized for every parameter at every node to determine what parameter provides the optimal split. The algorithm looks to maximize the goodness-of-split function, providing mathematically optimal splitting criteria. Numerous impurity functions exist, but the impurity function utilized in the study was the Gini Index. The risk associated with each node can also be determined and utilized to predict the parameters within the tree that have the of most feature importance. The following equations were utilized within the algorithm:

$$\xi\{\tau\} = 1 - \sum_{\omega} [\Pr(\omega|\tau)]^2 \tag{62}$$

$$\Delta\xi\{s,\tau\} = \xi\{\tau\} - \Pr\left(\tau_{Left}\right)\xi\left\{\tau_{Left}\right\} - \Pr\left(\tau_{Right}\right)\xi\left\{\tau_{Right}\right\} \tag{63}$$

$$\Pr\left(\tau_{Left}\right) = \frac{N_{\tau_{Left}}}{N_{\tau}}, \Pr\left(\tau_{Right}\right) = \frac{N_{\tau_{Right}}}{N_{\tau}} \tag{64}$$

$$maximize\{\Delta\xi\{s,\tau\}\} \tag{65}$$

$$Risk\{\tau\} = \Pr\{\tau\}\,\xi\{\tau\} \tag{66}$$

$$F = \frac{Risk\{\tau\} - Risk\{\tau_{Left}\} - Risk\{\tau_{Right}\}}{N_{Branch}} \tag{67}$$

Where:

τ = Node index $(-)$,

$\xi\{\tau\}$ = Impurity as a function of τ $(-)$,

ω = Classification label (Severe, Moderate, …, etc.) $(-)$,

$\Delta\xi\{s,\tau\}$ = Goodness of Split (s) metric for node τ $(-)$,

$\tau_{Left}, \tau_{\mathrm{Right}}$ = Child nodes associated with τ, splitting left or right by imposed criteria $(-)$,

$\Pr(\tau)$ = Probability associated with τ $(-)$,

N_τ = Number of observations associated τ $(-)$,

$N_{\tau_{Left,Right}}$ = Number of observations associated τ in the left and right split, respectively $(-)$,

$Risk\{\tau\}$ = The risk associated with node τ $(-)$, and

F = Parameter importance in predicting error category $(-)$.

Additional features can be utilized within fitctree, such as weightings associated with observation misclassification costs, the maximum number of splits, and the maximum number of leaves. The tree can be visualized by plotting, such as in Figure 35, or by creating a text-style application with reference to different nodes depending on the splitting criteria. There is a trade-off between utility and accuracy when utilizing classification trees. Classification trees can increase in accuracy if the tree is allowed to grow until saturation with little or no criteria for stopping. However, letting the tree grow to saturation often leads to trees that are difficult to

interpret. In the opposite case, the prediction accuracy is low if the tree is stopped prematurely. Therefore, finding the right balance between interpretability and accuracy was essential.

5.5 Non-linear Regression Analysis for Curve-fitting

Interpolation techniques were needed to determine model aspects that were not discrete. Interpolating the data would be computationally intensive and would neglect the curvature between points. Curve-fitting techniques were utilized to resolve these issues. Aspects of the model that utilized curve-fitting techniques and the types of curve-fits utilized are presented in Table 11.

The non-linear regression analysis was conducted utilizing the Curve-fitting Toolbox (Mathworks, 2019). The toolbox has built-in fit types allowing for multiple non-linear, linear, and custom regression equations. Least squares approximation was utilized to determine equation fits for each regression equation.

Polynomial fits were defined by:

$$y = \sum_{i}^{n+1} \beta_i x^{n+1-i} \tag{68}$$

Exponential fits were determined by:

$$y = \beta_1 e^{\beta_2 x} + \beta_3 e^{\beta_4 x} \tag{69}$$

Power law fits were determined by:

$$y = \beta_1 x^{\beta_2} + \beta_3 \tag{70}$$

Therefore, regression analysis provided the best approximation estimates for the parameters of each curve-fit (i.e., β_i).

Table 11: Summary of curve-fits utilized.

Fit Type	Dependant variable	Independent variable	Use
Polynomial	Kinematic viscosity	Temperature	To determine kinematic viscosity for reasonable* temperatures.
	Specific weight	Temperature	To determine the specific weight of the fluid for reasonable* temperatures.
	Flow rate	Time	To infill and extrapolate collected continuous data.
	Wet-well depth	Time	To infill and extrapolate collected continuous data.
	Rate of change in flow rate with respect to time	Flow rate	Utilized in solving a semi-analytical solution for the time-to-reach flow establishment.
	Volume	Flow rate	Utilized in solving a semi-analytical solution for the time spent pumping.
	Pump efficiency	Flow rate	Utilized in determining energy usage and costs associated with pump-down tests.
Exponential (2)	Flow rate	Time	To infill and extrapolate collected continuous data.
	Wet-well depth	Time	To infill and extrapolate collected continuous data.
Power law	Dynamic total head (provided by a pump)	Flow rate	Utilized in the governing equations of the detailed model.

*The curve-fits were based on a range between 0 and 35 degrees Celsius to increase the accuracy of the fit.

5.6 Semi-Analytical Solutions

Exact analytical solutions are preferred to numerical solutions. Exact analytical solutions cannot be determined for the specific coupled differentials in the study. Therefore, techniques were utilized to approximate solutions such as numerical or semi-analytical methods. Using numerical techniques for solving coupled differential equations may introduce problems such as stability, relative errors between steps, and absolute errors in solutions. When numerical techniques are utilized, and exact analytical solutions cannot be determined, semi-analytical solutions are sought to confirm results.

Approximate semi-analytical solutions can be determined for this problem by employing curve-fitting with simplifying assumptions. If flow establishment is not considered, an operating point can be determined for any static head in a steady system. Equation (11) can be iteratively solved to determine the flow rate at the operating point with any static head. Therefore, solving for the operating point with respect to various static heads can reveal the relationship between flow rate and static head. Thus, the active volume in the wet-well can be related to the static suction head. The active volume can then be related to the flowrate by curve-fitting the operating points such that:

$$V = \beta_1 Q^2 + \beta_2 Q - \beta_3 \tag{71}$$

A polynomial was utilized as the curve fit due mechanistic reasoning. The curvature would be mostly determined by the loss terms within equation (11), in which flowrate is squared. The relationship was also confirmed visually for equation (71). There are two roots associated with the polynomial in equation (71). Solving for the applicable root (see Appendix C for derivation) and integrating produces an equation (72). The semi-analytical solution provides a reasonable estimate of the time required for pumping, if the time required for flow establishment is not significant.

$$t^{\#} = \beta_2 \ln\left(\left|\sqrt{4\beta_1(V+\beta_3)+\beta_2^2}-\beta_2\right|\right) + \sqrt{4\beta_1(V+\beta_3)+\beta_2^2}-\beta_2+\beta_4 \quad (72)$$

Where:

$\beta_{1,2,3}$ = Weighting coefficients for curve-fit $(-)$,

β_4 = Constant of integration (determined by initial conditions) $(-)$, and

$t^{\#}_{naive}$ = Estimated time spent pumping by analytical method (T).

A similar curve-fitting technique can provide a semi-analytical solution for the time required for the system to reach flow establishment. Equation (52) can be parameterized with the physical characteristics of the forcemain (including the roughness as determined by a naïve interpretation or a detailed model), lift-station and pump. The static head utilized in the equation can be considered the average static head (or a static head of interest). Determine the flow rate at which the rate of change of the flow rate is equal to zero (through root finding). Solve equation (52) at various flow rates between zero and the flow rate at which the rate of change of the flow rate is zero. The rate of change can then be curve-fit with respect to the flow rate. A quadratic curve-fit (equation (73)) was found to reasonably capture the relationship between the rate of change in flow rate and the flow rate. The loss terms within equation (52) will vary by the flowrate squared. The relationship was also confirmed visually for equation (73).

$$\frac{dQ}{dt} = \zeta_1 Q^2 + \zeta_2 Q + \zeta_3 \quad (73)$$

Flow establishment is complete when the rate of change in the flow rate with respect to time is zero. Therefore, the duration of flow establishment can be estimated by integrating the curve-fitted equation for flow rate with respect to time with the general formulation determined by Jeffery and Dai (2008) as follows:

$$t_a^{\#} = \frac{-2}{\sqrt{-(4\zeta_3\zeta_1 - \zeta_2^2)}} \operatorname{arctanh}\left(\frac{\zeta_2 + 2\zeta_1 Q_{Q'=0}}{\sqrt{-(4\zeta_3\zeta_1 - \zeta_2^2)}}\right) \quad \{4\zeta_3\zeta_1 - \zeta_2^2 < 0\} \tag{74}$$

$$t_a^{\#} = \frac{2}{\sqrt{(4\zeta_3\zeta_1 - \zeta_2^2)}} \arctan\left(\frac{\zeta_2 + 2\zeta_1 Q_{Q'=0}}{\sqrt{(4\zeta_3\zeta_1 - \zeta_2^2)}}\right) \quad \{4\zeta_3\zeta_1 - \zeta_2^2 > 0\} \tag{75}$$

Where:

$\zeta_{1,2,3}$ = Weighting coefficients for curve-fit $(-)$,

ζ_4 = Constant of integration $(-)$,

$Q_{Q'=0}$ = Flowrate associated with the applicable root of the differential curve-fit $\left(\frac{L^3}{T}\right)$,

$t_a^{\#}$ = Estimated duration of flow establishment (T).

The analytical solutions are created within a respective range of the independent variables presented. Therefore, any use of the equations should respect the range of the curve fits. Utilization of the equations outside of the range of the curve fit will become unstable, providing erroneous results.

5.7 Detailed Modelling

Detailed modelling refers to the inference of hydraulic resistance with a thorough modelling algorithm, as is outlined in this section. The detailed model incorporates the unsteady components of one-dimensional modelling involved in the operational point migration (including flow establishment). The model utilizes the coupled governing equations, as stated in Section 4.6. The model was solved like a parameter tuning algorithm with an embedded system of coupled non-linear differential equations, solved with an initial value problem technique.

5.7.1 Modelling Assumptions

The system can become increasingly complex as more variables are considered. The following simplifications were implemented for the detailed model:

1) The temperature of the liquid is uniform and consistent.
2) The minor loss coefficient associated with fittings, bends, and other appurtenances do not significantly change throughout the test.
3) All unaccounted-for losses associated with pumping are attributed to friction loss.
4) The design drawings are accurate and reliable enough to make inferences about system characteristics.
5) The measured data collected is error-free.
6) The curve-fits for infilling and noise reduction are accurate.
7) The pump adds fluidic energy at a point located at the beginning of the forcemain.
8) Since the characteristic curves of new pumps were used, it was assumed that the pumps were installed correctly and were well maintained.
9) That a one-dimensional, unsteady flow model accurately describes the forcemain hydraulics.
10) The time it takes for the pump to go from zero to full rotational speed is very short.
11) The physical properties of the wastewater are that of incompressible freshwater (Metcalf and Eddy, 2014).
12) Wastewater chemical properties can be estimated in a general manner (Metcalf and Eddy, 2014).

5.7.2 Modelling Algorithm

The model may be considered a parameter-tuning algorithm with an embedded initial value problem (IVP) sub-algorithm, as depicted in the flow chart in Figure 36. The detailed modeling algorithm is analogous to that of the shooting method for integration but instead of adjusting the

initial conditions, the differential equation is adjusted by changing the hydraulic resistance characteristics. Once the correct hydraulic resistance is determined, the correct boundary value is also determined. Equations (51) and (52) can be numerically integrated as a system of coupled non-linear differential equations with respect to time. These differential equations can be parameterized with the physical characteristics of a lift-station and forcemain, as outlined in Table 7. Once parameterized with known characteristics, the equations are now functions of only flowrate through the forcemain, static suction head in the wet-well, and an absolute roughness or a smoothness characteristic such that:

$$\frac{dh_{ss}}{dt} = fun\{Q\}$$

$$\frac{dQ}{dt} = fun\{\epsilon \; or \; C_{HW}, Q, h_{ss}\}$$

A value for roughness (for Darcy-Weisbach friction factor) or a smoothness characteristic (for Hazen-Williams) of the forcemain can be assumed at the start of the model. The initial guess can be the characteristics of a new pipe or a range in which to search. The initial conditions for the model were determined based on the physical reality of the pump-down test. The high alarm in the wet-well causes the SCADA system to trigger the pump to turn on. At the instant the pump turns on, there is a stagnant liquid column within the forcemain that must begin moving. The migration path for the flow rate with respect to the dynamic head provided by the pump during flow establishment is outlined in Section 4.6. The flow rate must therefore begin at zero at the instant the pump is turned on, and it takes some time for the flow to establish due to the acceleration associated with the liquid column. Therefore, the initial conditions may be stated for the initial flow rate and static suction head in the wet-well at the start of the pump-down test such that:

$$h_{ss}\{t = 0\} = h_{ss_{start}}$$

$$Q\{t = 0\} = 10^{-16} \approx 0$$

The model has various settings, including the selection of friction loss type (Darcy-Weisbach types including the Swamee-Jain and Brkić-Praks methods, or Hazen-Williams), absolute and relative error tolerances for the explicit stepping scheme, and a hard maximum step size to prevent the adaptive algorithm from taking steps too large. The settings must be stated at the start of the algorithm. The IVP begins by utilizing the initial conditions in Equations (51) and (52) to determine the rate of changes for the flow rate and static suction head at the start of the pump-down test. The explicit Runge-Kutta fourth-order scheme was utilized in determining the appropriate rate of change for the steps and is outlined in Section 5.4.2. It should be noted that the dynamic pump head, and the Darcy-Weisbach friction factor (if the option is chosen) update throughout the simulation with respect to the changing flow rates. The flow rate and static suction head associated with the end of the step are determined as follows:

$$Q_{j+1} = Q_j + Q_j^{'}\Delta t \qquad \textit{Restate: (57)}$$

$$Q_j' = \frac{1}{6}(k_1 + 2k_2 + 2k_3 + k_4)$$

$$h_{ss_{j+1}} = h_{ss_j} + h_{ss_j}^{'}\Delta t \qquad \textit{Restate: (58)}$$

$$h_{ss_j}' = \frac{1}{6}(l_1 + 2l_2 + 2l_3 + l_4)$$

The model also contains terminating events to ensure the algorithm converges on a realistic result. The terminating events utilized in the model are as follows:

$$h_{ss} \leq h_{ss_{end}}$$

$$t \geq t_{naive}$$

Once a step has been completed, the model checks the current simulation step results against the terminating conditions. If the terminating conditions are not met, the model updates the conditions associated with the start of the next step and completes another step. If the terminating conditions are met, the model collects the IVP results and determines the average flow rate for the simulation.

The model utilizes the volumetrically determined average flow rate to determine the roughness associated with the forcemain. The average flow rate determined naively must be equal to the average flow rate as determined by simulation such that:

$$Q_{avg_{sim}} = Model\{\epsilon \; or \; C_{HW}, \text{ initial conditions, system characteristics}\}$$

$$Q_{avg_{sim}}\{\epsilon \text{ or } C_{HW}\} - Q_{avg_{naive}} == 0$$

If the two average flow rates do not exactly equal, the algorithm then determines another guess at the roughness or smoothness parameter and repeats the process again. This process was considered parameter tuning. Parameter tuning was conducted by root finding algorithms stated in Section 5.4.1 and the resulting average simulation flowrate determined by the IVP. On entering the IVP sub-algorithm, the initial conditions reset to those mentioned previously. Once the two average flow rates are equivalent, the model accepts the roughness or smoothness characteristic and returns the value. It should be noted that the detailed model can be utilized with regards to a correct roughness or smoothness characteristic. The average flowrates will be equal after the first iteration of roughness or smoothness and will return the results immediately instead of continuing through to another iteration.

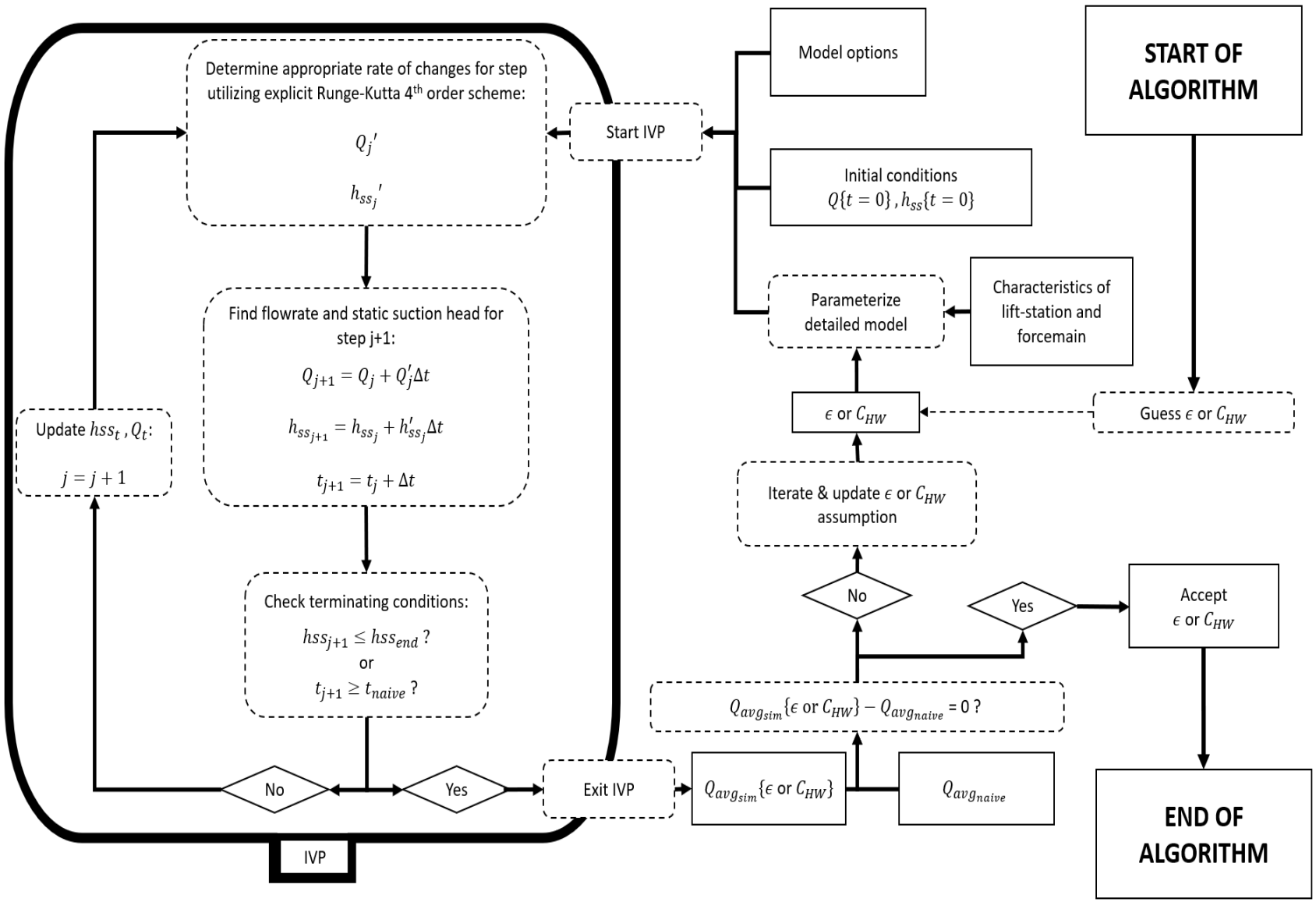

Figure 36: Flowchart of the detailed modelling algorithm for inferring roughness (ϵ) or smoothness (C_{HW}).

5.8 Techniques for Inferring Hydraulic Resistance

The inference of hydraulic resistance can differ with different friction loss methods. Eight different techniques for inferring roughness were utilized for each pump at each site (see Table 12). Three friction loss methods were utilized: Swamee-Jain (SJ), Brkić-Praks (BP), and Hazen-Williams (HW). A naïve interpretation was conducted with the three different friction loss methods (three naïve interpretations). An inference of roughness was also determined with continuous data (if provided or could be inferred) at each sampling time. Lastly, two inferences of roughness were determined through detailed modelling. The detailed modelling utilized Swamee-Jain and Hazen-William methods but not Brkić-Praks. Due to the naïve interpretation utilizing only one flowrate, one equivalent forcemain diameter was determined and utilized for analysis for the naïve interpretation. With an unsteady consideration, the equivalent forcemain diameter changes depending on the flowrate and the rate of change of flow at any time during testing. Therefore, the other methodologies utilized segmented forcemain characteristics but an equivalent forcemain could be determined at every time-step during analysis.

Table 12: Summary of inference of roughness techniques for each pump at each site.

Friction loss method	Technique
Swamee-Jain	Naïve interpretation
	Continuous data
	Detailed modelling
Hazen-William	Naïve interpretation
	Continuous data
	Detailed modelling
Brkić-Praks	Naïve interpretation
	Continuous data

5.9 Sensitivity Analysis

5.9.1 One-at-a-Time

A sensitivity analysis was conducted to test how the uncertainty of different inputs affect the resulting output of inferred roughness. The one-at-a-time (OAT) method is a common and effective methodology for sensitivity analysis. OAT refers to the perturbation of one parameter and observing the change in the resulting output. An OAT sensitivity analysis was conducted on the model by scaling the parameters by a small amount and rerunning the detailed model. The baseline of the OAT sensitivity analysis utilized non-segmented forcemain characteristics. The actual value of roughness (as needed for the equation (54)) was taken to be the inferred roughness of the detailed model using a segmented forcemain. Therefore, the scalar error associated with the baseline is different for each pump at each site.

5.9.2 Inference of Hydraulic Resistance Sensitivity due to Internal Diameter

The effective diameter was mentioned in the literature as changing and considered sensitive in the inference of hydraulic resistance (Lauchlan *et al.*, 2005; Annus *et al.*, 2018; Yousefi, 2019). The diameter of the forcemain was investigated on a theoretical basis for each site within the study. The investigation revealed how the estimation of roughness changes with a range of different diameter sizes. It should be noted that the diameter could not be assessed accurately for the entirety of the forcemain for any site. Therefore, the assumed range of forcemain diameters investigated for each site is speculative. The diameter of the forcemain was varied by a percentage of the original diameter(s) within the detailed model. The sensitivity analysis decreased the assumed forcemain diameters by a percentage of the initial commissioning sizes. Encrustation thickness was estimated to be more in a larger pipe, as a percentage loss in diameter scaled all segments. The assumed losses in diameter for the forcemain segments are depicted in Figure 37.

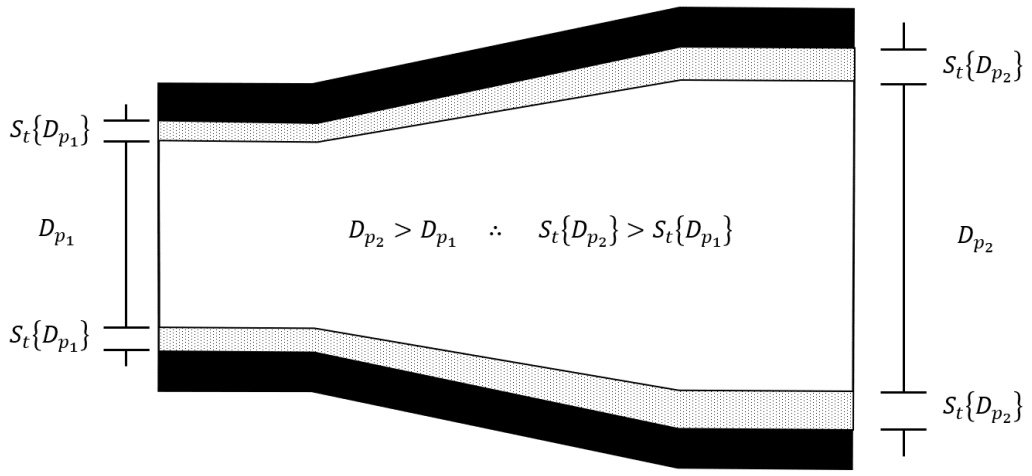

Figure 37: Loss in effective diameter(s) for theoretical roughness inference due to encrustation for the sensitivity analysis. Encrustation was considered a set percentage loss in all diameters. Larger diameters (denoted with 2) theoretically had more encrustation than smaller diameter segments (denoted with 1) in the forcemain.

5.10 Monte Carlo Simulations with Detailed Model

Understanding the effects of a single parameter on a system with numerous parameters and parameter interaction effects is difficult. A system can be perturbed with an OAT approach when it is simple. Alternatively, a small set of different combinations of parameters can be created and analyzed to investigate which parameters have the most significant effect on an outcome of a simple system. When system dynamics are non-linear, the problem becomes increasingly difficult as the state of one parameter may rely on another. The difficulty can also compound with the number of parameters in consideration. In one instance, a parameter may have negligible effects on the output of a model. In another instance, the parameter may have a significant effect when appropriately coupled with other parameters.

A Monte Carlo simulation approach is utilized to gain insight into the system dynamics. In this study, a Monte Carlo simulation approach assisted in determining which parameters are associated with an erroneous inference of hydraulic resistance. Two methods in the study utilize the results of the Monte Carlo simulations. The first method investigated the simulation results

utilizing probability density estimation techniques based on data stratification with respect to an error produced. The error associated with the simulations compares the naïve interpretation of roughness to the actual roughness utilized in the simulation. The second method utilized the simulation results by creating a classification tree with respect to the stratified data.

5.10.1 Probability Density Estimation

A Monte Carlo methodology was adopted to investigate the parameter (and parameter combination) effects on the outcome of the roughness estimation using naïve pumping tests. Figure 38 is a summary flow chart of how the Monte Carlo simulations can provide probability density estimations for parameters of interest.

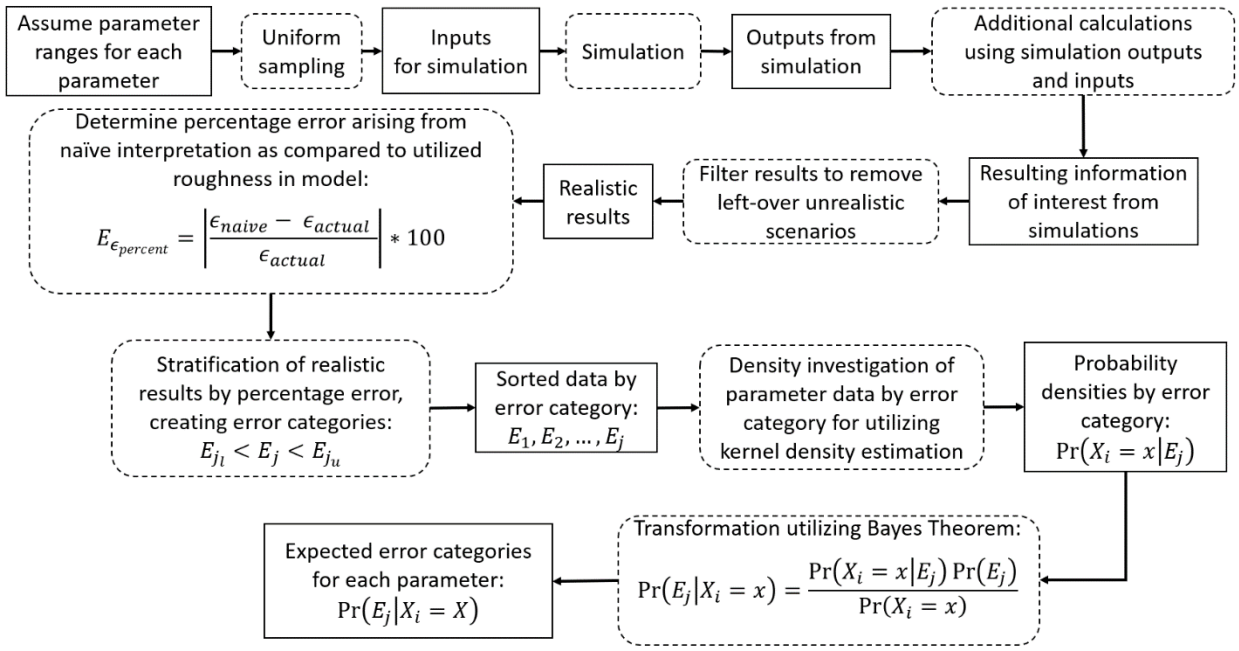

Figure 38: Summary of the process of determining probability densities utilizing Monte Carlo simulation results with respect to erroneous inferences of roughness.

Parameter ranges associated with small and medium lift-stations were assumed for the study. Simulations were conducted by randomly sampling along the parameter ranges to create

parameter sets for each simulation. Although the distribution of the parameters is unknown, a uniform distribution was utilized for sampling along the range. The simulation results were utilized in acquiring a naïve interpretation of roughness for each simulation. The percentage error associated with the naïve interpretation of roughness and the actual roughness utilized within the simulation was determined using equation (53). Figure 39 demonstrates the process of generating, simulating, and determining resulting information of interest (as per Figure 38).

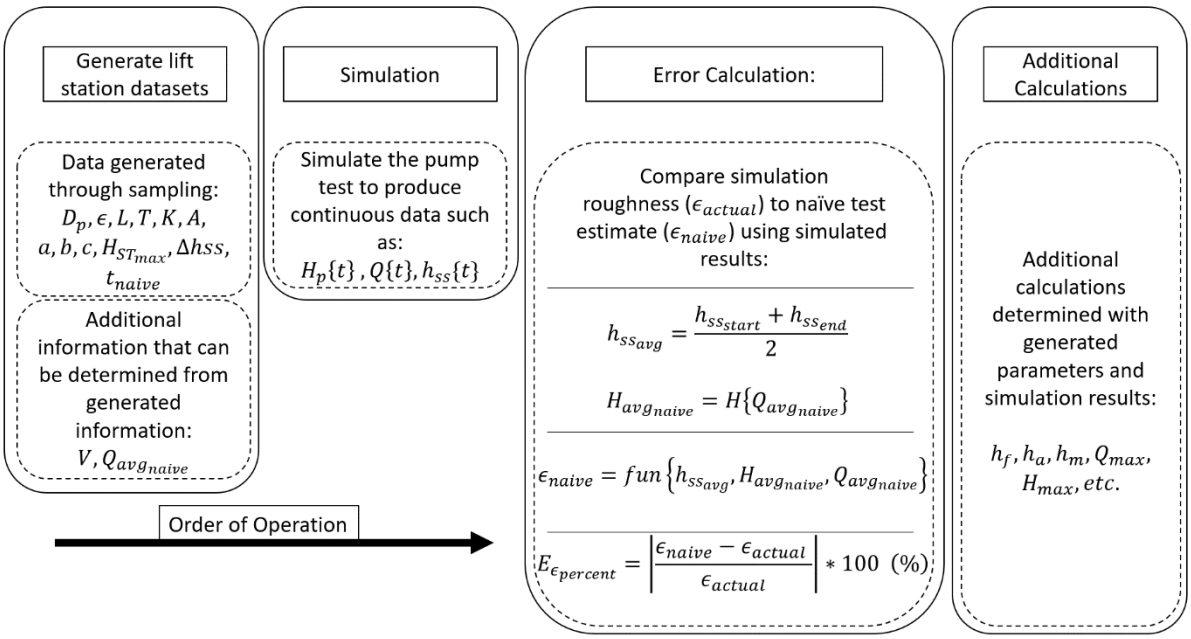

Figure 39: Determining the percentage error associated with the naïve interpretation of roughness and other outputs from the Monte Carlo simulations.

The results that are of interest from each simulation were recorded. A realistic dataset should be utilized when determining the probability density estimations. Where possible, the parameter sampling techniques would consider other parameters, if needed. For example, the static head must be between zero static head and the maximum head the pump could provide. A lift-station would not be designed to utilize a pump that could not overcome the static total head of the system.

Filters were also imposed on the results of the simulations to ensure a dataset of realistic results. Filters of interest were velocity limits through the forcemain, depth change of liquid level in the

wet-well during pumping, and equation limitations (although, naïve interpretations of roughness were often outside of equation limitations). The filters leave only the simulation results that passed all filtering criteria, discarding the unrealistic results.

The errors between the naïve interpretation of roughness and actual roughness used in each simulation were rank ordered from highest to lowest error. Error categories (E_j) were created regarding the error in the naïve interpretation of roughness. Four error categories were utilized in the study: negligible, mild, moderate, and severe. Each category has its own limits (like that of bins in a histogram). The upper and lower limit for each error category were set subjectively for the study (see the following domain limits and Figure 40). Splitting the dataset into different error categories is known here-in as stratification (of the dataset or by error category). The stratification of the dataset allowed for the investigation of the differences between the parameter sets associated with each error category.

$$E_{j_u} \leq E_j \leq E_{j_l}$$

Where:

$E_j =$ Error categories determined by error thresholds $(-)$,

$E_{j_u}, E_{j_u} =$ Error thresholds for upper and lower limits for each category $(-)$.

Once the dataset was sorted by error category, probability density estimates for each parameter in each error category (Pr $(X_i = x|E_j)$) were determined. The probability density estimations were determined by kernel density estimation techniques for each parameter. This process was also utilized in determining the probability density function of all the data for each parameter (Pr $(X_i = x)$). The probability of being in any specific error category (Pr (E_j)) was determined by the ratio of simulations that results in a specific error category to the total number of simulations in the dataset. The probability of being in a particular error category given a specific value of a parameter (Pr$\left(E_j \middle| X_i = x\right)$) was determined by Bayes theorem as follows:

$$X_i \sim \text{Uniform}\left(\text{Parameter}_{i_u}, \text{Parameter}_{i_l}\right)$$

$$\Pr\left(X_i = x \middle| E_j\right) = \Pr(X_i = x \mid E_{j_u} \leq ||X_i|| \leq E_{j_l}) \tag{76}$$

$$\Pr\left(E_j \middle| X_i = x\right) = \frac{\Pr\left(X_i = x \middle| E_j\right) \Pr\left(E_j\right)}{\Pr(X_i = x)} \tag{77}$$

Where:

$X_i =$ Random variable associated with a specific parameter (#),

$\text{Parameter}_{i_u}, \text{Parameter}_{i_l} =$ Upper and lower range limits associated with parameter (#) and,

$x =$ Specific value of a parameter (#).

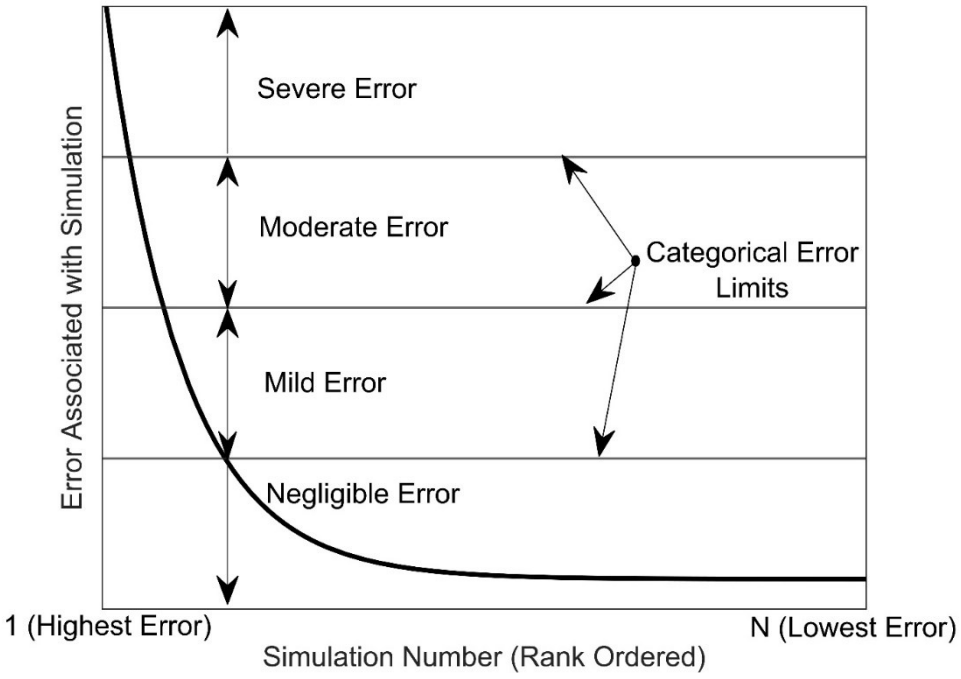

Figure 40: Stratification of simulation dataset into error categories. Error categories refer to the percentage error in the naïve interpretation of roughness and the roughness utilized in the model between imposed limits. Four categories were utilized in the study: severe, moderate, mild, and negligible.

An example of probability density estimations as determined by kernel density estimation and the subsequent transformation by Bayes theorem is depicted in Figure 41. The legend contains

utility labels to illustrate increasing severity between the categories (one being the lowest). It should be noted that the total probability of being in any of the error categories is not equal and therefore have unequal scaling during transformation.

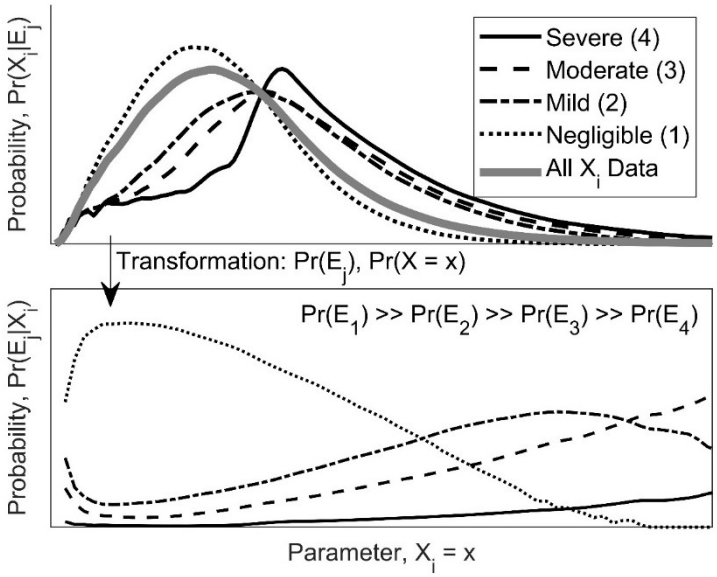

Figure 41: Example probability density estimation $Pr(X_i = x \mid E_j)$ for a parameter at a specific value ($X_i = x$) for each error category (E_j) and subsequent transformation through Bayes theorem $Pr(E_j|X_i = x)$. The total number of data points in each error category dataset is not equal. Therefore, the scaling associated with transformation is not equivalent between error categories.

5.10.2 Validity of Number of Monte Carlo Simulations for Dataset

When utilizing Monte Carlo simulations, the number of simulations are needed to have a valid assessment of the behaviour of the system is required. Kottegoda and Rosso (2008) provide guidance for ensuring the validity of the Monte Carlo simulation dataset. Kottegoda and Rosso (*ibid*) state that a multi-dimensional space utilized in a Monte Carlo simulation may lead to an error proportional to the inverse square root number of sample points drawn. Information regarding the probability that some event of interest occurs, the number of occurrences of some event within the sample size, and the estimated probability distribution are of utility.

Kottegoda & Rosso (2008) suggest the probability distribution of each parameter is often unknown before running the experiment, but it is estimated and and later validated. Assuming the probability is normally distributed, the confidence intervals can be determined (equation (78)). Knowing the desired confidence intervals on the probability distributions can also be useful in determining the number of simulations that need to be conducted (equation (79)). Determining the number of simulations (n_{needed}) to ensure the proability confidence interval is suitable to capture the range of possible probabilities (as measured by $Z_{\alpha/2}$ for normal distributions) often requires the analysis to accept a certain tolerance of error (denoted e, see denominator of equation (79)). Kottegoda & Rosso (*ibid*) state that error tolerance should be between zero and one. For instance, the number of simulations needed to ensure a suitable confidence interval can change depending on the accepted tolerance for the study. The amount of error to tolerate is generally subjective. Therefore it is essential to state all accepted error tolerances for each parameter.

The central limit theorem was utilized to obtain a normal distribution to utilize equations (78) and (79). The most probable value of the resulting distribution was utilized in the equations. It should be noted that this method of utilizing the equations (78) and (79) was done simplistically. With a more thorough method, the confidence intervals change with any particular parameter value, as outlined by Kottegoda & Rosso (*ibid*). Each parameter in each error category has an accepted error tolerance regarding the number of simulations within the error category.

$$\Pr(Entity) \approx \widehat{Pr}$$

$$\widehat{\Pr} \pm Z_{\frac{\alpha}{2}} \sqrt{\frac{\widehat{Pr}\left(1-\widehat{Pr}\right)}{\mathrm{n}}} \tag{78}$$

$$n_{needed} \geq \frac{Z_{\frac{\alpha}{2}}^{2}\left(1-\widehat{\Pr}\right)}{e^{2}\widehat{\Pr}} \tag{79}$$

$$0 \leq e \leq 1$$

Where:

$\widehat{Pr}$ = Probability estimated to be predictive of the actual sample probability $(-)$,

$Z_{\frac{\alpha}{2}}$ = Z score associated with normal distribution at probability $\left(1-\frac{\alpha}{2}\right)$ $(-)$,

α = Confidence tolerance $(-)$,

e = Acceptable error tolerance for the number of simulations needed $(-)$, and

n = Number of simulations $(-)$.

5.10.3 Classification Tree

After splitting the dataset as outlined in Section 5.10.1, a classification tree was created to generalize the results. The most erroneous outcomes from the naïve interpretation of roughness were of the most importance. The most erroneous outcomes would be allotted to the severe category within the study. Therefore, steps were taken to minimize the chances of severe category data being predicted as another category while maintaining the interpretability of the classification tree.

Misclassification costs were imposed on the classification tree to ensure the accuracy of the severe category. The misclassification costs associated with the severe category were magnitudes higher than other error categories. Accuracy in predicting categories other than severe was lowered to increase the interpretability of the classification tree. However, it is preferable to predict a negligible system to be severe than the reverse.

Simulation data is associated with the boundaries of each error category. At the categorical limits, data falls on both sides of the limit with a similar scale. For example, if an error category limit is 100 percent, data associated with 101 percent and 99 percent errors result in two separate error categories. However, the actual difference in these errors is not significant. If different values are chosen for the boundaries of each category, these data points could be in the same category. Therefore, the classification tree should only be utilized to determine when detailed modelling would be needed.

6.0 Results

Governing variables and equations were determined as outlined in Section 4.6. A detailed model was developed as outlined in Section 5.7 utilizing the governing equations. The model could determine the roughness associated with a forcemain given system characteristics and an average flowrate determined naïvely. The naive interpretation of roughness was determined as outlined in Section 4.2. The model was utilized to determine when a naïve interpretation of roughness will produce erroneous outcomes.

The following sub-sections outline the results from utilizing four real sets of data collected from sites around Halifax, and hypothetical lift-stations. The hypothetical lift-stations were determined as outline in Section 5.10. The hypothetical lift-station simulations only utilized the Swamee-Jain methodology for friction head losses and not the Hazen-Williams or Brkić and Praks. The results discussion is presented in Section 7.0. All tools and scripts utilized within the study the study will be made available through the open-source platform, GitHub (Strong, 2022).

6.1 Four Halifax Sites Considered

Eight different sets of data were investigated (four sites with two pumps per site). The Trinity Lane pump one results are presented in this section for explanation. The analysis conducted was the same for each site. Data collection was completed by Jean (2006) and utilized in this study. Information regarding model inputs and data collection can be found in Appendix A. Information regarding model results and inferential work will be presented in Appendix B.

One-at-a-time sensitivity analysis was conducted on the detailed model inputs to assess the sensitivity of the inference of roughness as outlined in Section 5.9.1 for each site. A scalar error metric $\left(E_{\epsilon_{scalar}}\right)$ was utilized to assess the sensitivity. The sensitivity analysis utilized a non-segmented forcemain.

The inference of roughness due to an assumed internal diameter of the forcemain was investigated as per Section 5.9.2. The analysis assumed that starting forcemain diameters were initial commissioning sizes. Therefore, percentage losses in diameters were assumed based on

the initial commissioning sizes. The assumed diameters for the analysis were theoretical and were not confirmed with in-field data collection.

Water quality indices were approximated from general wastewater quality information provided by Metcalf and Eddy (2014). Inferences based on water quality indices and forcemain characteristics were determined as outlined in Section 3.2. However, most of the literature estimates are not created for wastewater forcemains. Therefore, the literature estimates may not be reliable for wastewater forcemain applications and require further analysis of their validity in such cases.

The simulation results for flow rate and static suction head with respect to time for the Trinity Lane, pump one, are presented in Figure 42. The operating point migration associated with the detailed modelling utilizing the inferred roughness from the model is depicted in Figure 43. Darcy-Weisbach friction migrates during the simulation and is presented in Figure 44 for Trinity Lane pump one. The naïve interpretation of roughness, the detailed modelling inferred roughness, and the continuous data inferences are presented in Figure 45. The naïve interpretation of the Hazen-Williams coefficient, the detailed modelling inferred coefficient, and the continuous data inferences are presented in Figure 46. Theoretical percentage diameter losses were investigated, and the Trinity Lane pump one results are presented in Figure 47. One-at-a-time sensitivity analysis was conducted for each model input utilized by the detailed model (Trinity Lane pump one, Figure 48). The analysis utilized a non-segmented forcemain as would appear in a digital database of summarized station information. Lastly, for Trinity Lane pump one, the relevant literature inferences utilizing wastewater quality and forcemain characteristics are presented in Figure 49.

General summaries of the results for the four sites are also presented herein. The naïve interpretation of roughness utilizing Swamee-Jain (Table 13) and the coefficient for Hazen-Williams (Table 14) are presented and the detailed model inferred roughness for each site. Hazen-Williams coefficients inferred with data associated with key times during simulation are presented in Table 15. Ranges for Reynolds numbers and Darcy-Weisbach friction factors for the eight sites are presented in Table 16. Semi-analytical solution estimates for the time spent establishing flow and the naïve pumping time are presented in

Table 17. For comparison, the detailed model flow establishment duration and actual naïve time spent pumping are also presented. Energy expenditure estimates relating to the sites at the time of testing and initial commissioning are presented in Table 18. It was estimated that each station would run for 21900 cycles per year (2.5 cycles per hour). An energy cost of $0.156 per kilowatt-hour was assumed for the calculations. Energy metrics were utilized in determining the condition of the forcemain. Forcemain condition metrics are presented in Table 20. The condition of the forcemain for each site is presented in Table 21. Model goodness-of-fit metrics are provided, comparing the model output to continuously measured data (Table 19).

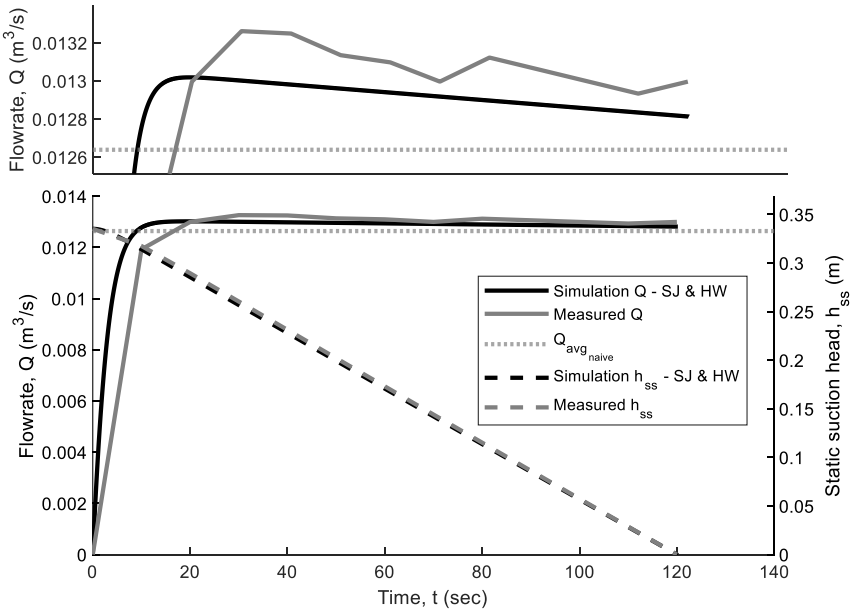

Figure 42: Trinity Lane - pump one: the detailed model simulation flow rate (left axis) through the forcemain and static suction head (right axis) in the wet-well with respect to time.

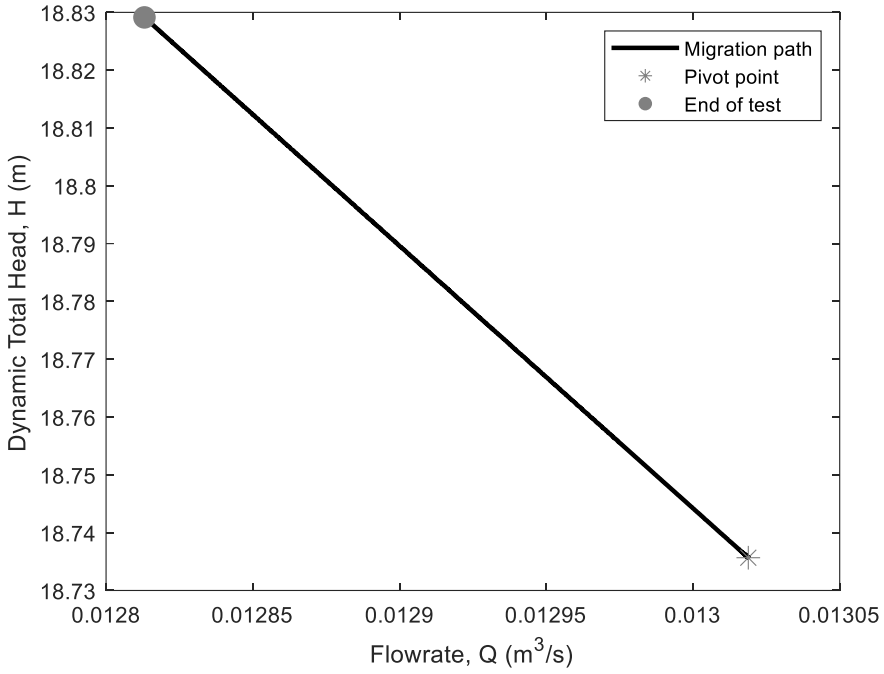

Figure 43: Trinity Lane - pump one: migration of the operating point after flow establishment for the simulation. The pivot point is the point at which flow establishment has completed.

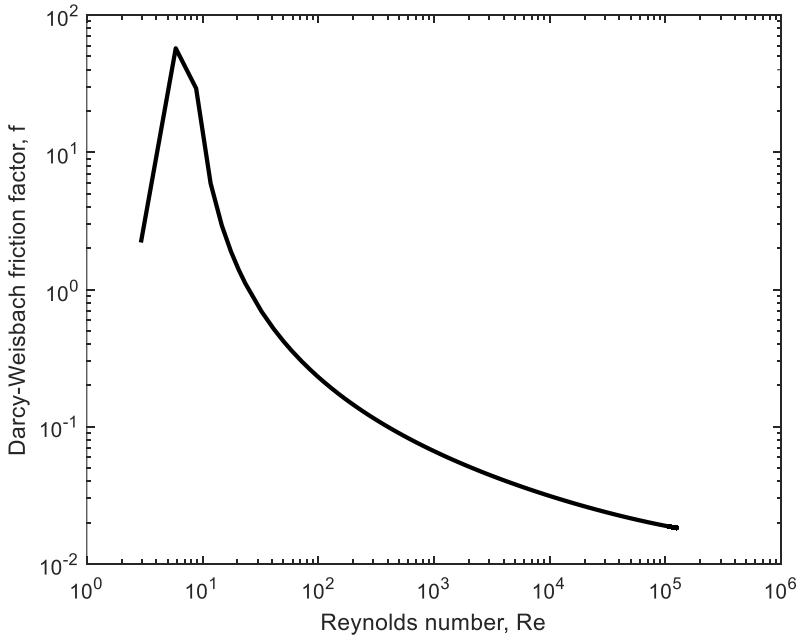

Figure 44: Trinity Lane - pump one: Darcy-Weisbach friction factor migration for the detailed model simulation (log-log scale). The friction loss method utilized is Swamee-Jain.

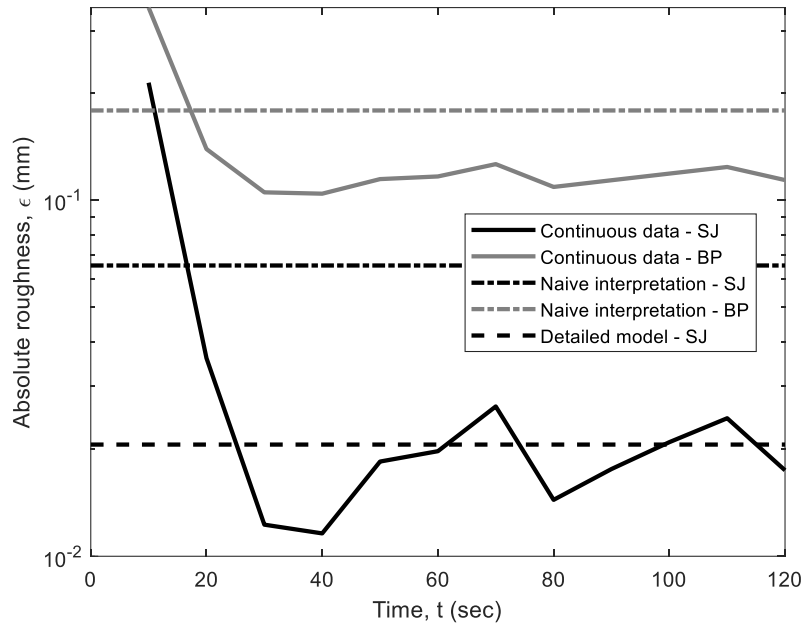

Figure 45: Trinity Lane - pump one: different techniques for inferring roughness. Two friction loss methods are present, Swamee-Jain (SJ) and Brkić-Praks (BP). Continuous data was utilized at every sampling time to infer roughness for comparison. The naïve interpretations and the detailed modelling inferences are time-invariant.

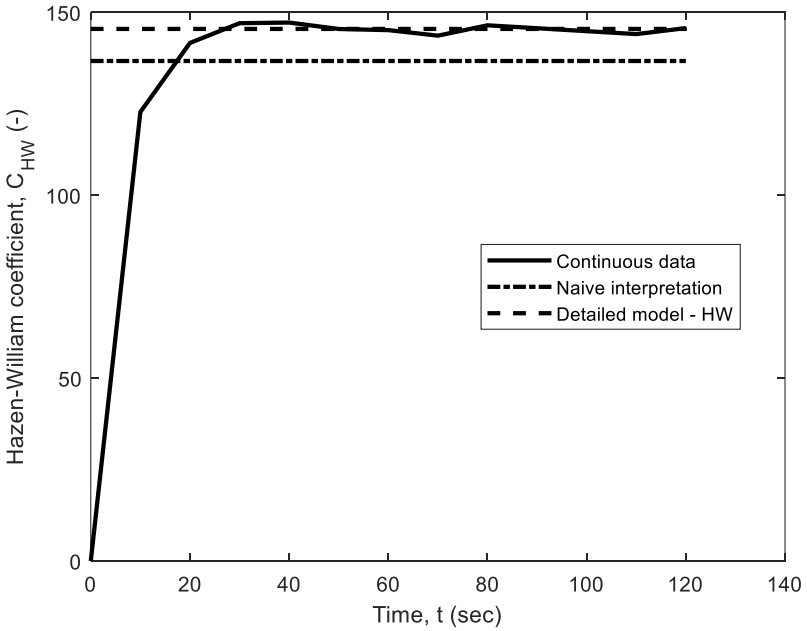

Figure 46: Trinity Lane – pump one: different techniques for inferring the Hazen-Williams coefficient. The naïve interpretation and the detailed model inferences are time-invariant. Continuous data was utilized at every sampling time to infer the coefficient for comparison.

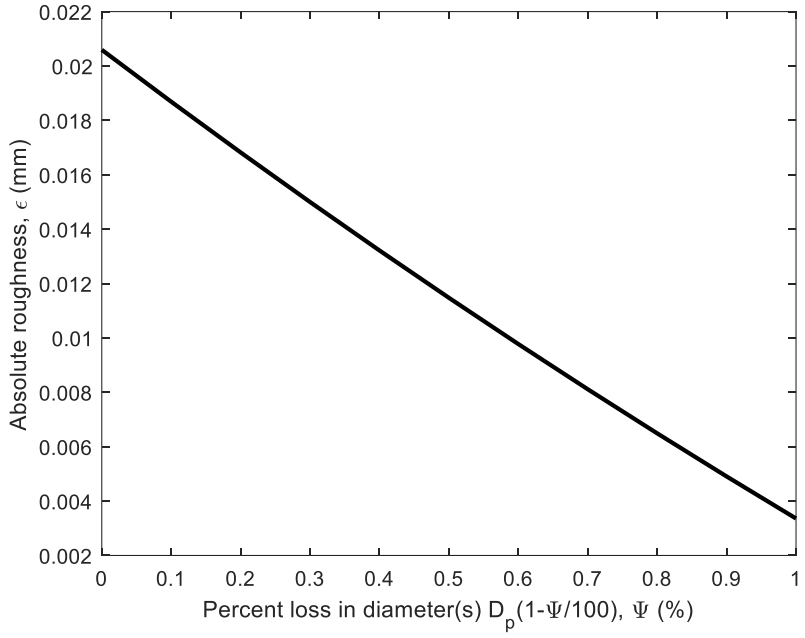

Figure 47: Trinity Lane - pump one: the effect of reducing the assumed internal diameter(s) of the forcemain on the inference of roughness with detailed modelling. Reductions were percent losses of the diameter(s) starting at the initial commissioning sizes.

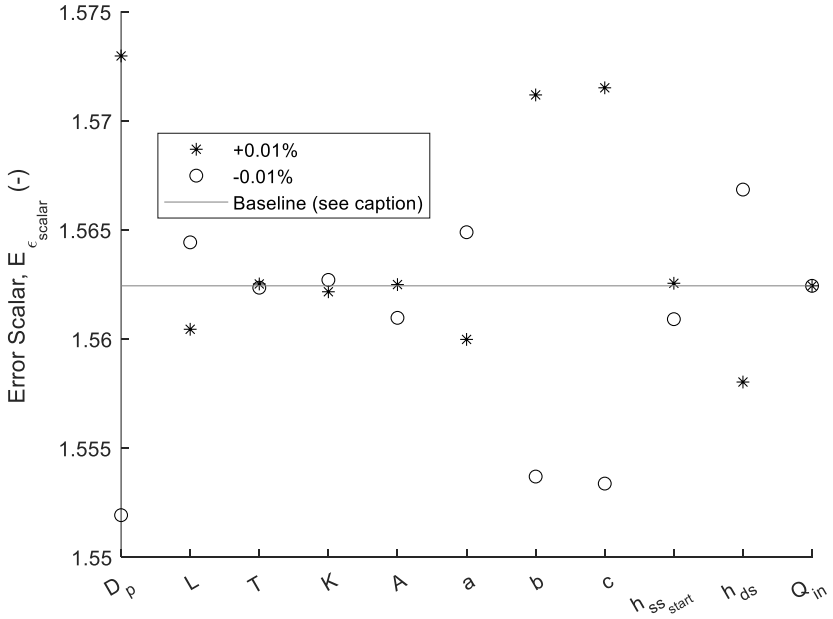

Figure 48: Trinity Lane - pump one: one-at-a-time sensitivity analysis for the inference of roughness due to perturbations of relevant parameters in the detailed model (along the abscissa). The analysis utilized a non-segmented forcemain. The baseline is the error scalar due to having a non-segmented forcemain (instead of a segmented one) in the detailed model.

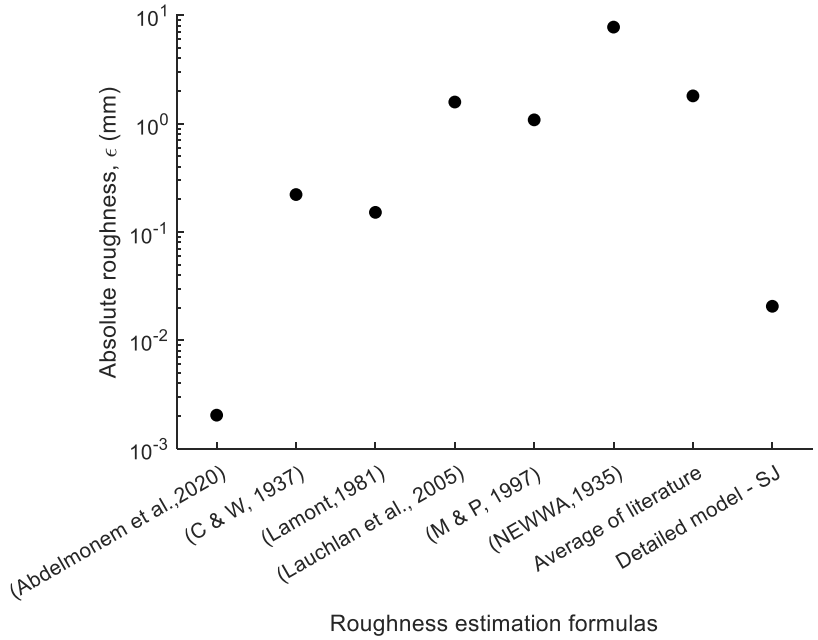

Figure 49: Trinity Lane – pump one: inference of roughness with respect to forcemain characteristics and water quality indices provided in the literature. The relevant authors cited along the abscissa.

Table 13: Absolute roughness inferences for the four sites (Swamee-Jain Methodology)

Location	**Inferred roughness (model), ϵ_{model} (mm)**	**Inferred relative roughness (model), $\frac{\epsilon_{model}}{D_{peq}}$ (-) ***	**Inferred roughness (naïve), $\epsilon_{naïve}$ (mm)**	**Error scalar, $\frac{\epsilon_{model}}{\epsilon_{naive}}$ (-)**	**Roughness at installation, ϵ_0 (mm)**
Trinity Lane – Pump 1	0.021	$1.950*10^{-4}$	0.0660	0.314	0.002
Trinity Lane – Pump 2	0.221	0.002	0.323	0.684	0.002
Ragged Lake – Pump 1	34.410	0.139	36.600	0.940	0.250
Ragged Lake – Pump 2	47.230	0.190	49.400	0.952	0.250
Akerley Boulevard – Pump 1	7.080	0.037	8.530	0.830	0.250
Akerley Boulevard – Pump 2	5.830	0.031	7.190	0.811	0.250
Melville Cove – Pump 1	260.238	1.047	267.512	0.973	0.250
Melville Cove – Pump 2	23.473	0.094	30.524	0.769	0.250

*Utilizing an equivalent diameter forcemain

Table 14: Hazen-Williams coefficient inference for the four sites.

Location	Inferred Hazen-Williams coefficient (model), $C_{HW_{model}}$	Inferred Hazen-Williams coefficient (naïve), $C_{HW_{naive}}$	Error scalar, $\frac{C_{HW_{model}}}{C_{HW_{naive}}}$ $(-)$	Hazen-Williams coefficient range during pumping test in simulation*	Hazen-Williams coefficient at installation, C_{HW_0}
Trinity Lane – Pump 1	145.502	136.739	1.064	187.283	150
Trinity Lane – Pump 2	122.953	116.996	1.051	278.059	150
Ragged Lake – Pump 1	48.915	47.761	1.024	48.6215	140
Ragged Lake – Pump 2	44.120	43.193	1.021	43.876	140
Akerley Boulevard – Pump 1	73.516	70.228	1.047	434.991	140
Akerley Boulevard – Pump 2	76.689	72.987	1.051	516.855	140
Melville Cove – Pump 1	17.844	17.587	1.015	134.718	140
Melville Cove – Pump 2	55.298	51.015	1.084	303.977	140

*Using only finite information and is significantly impacted by the step size.

Table 15: Hazen-Williams coefficients inferred with information associated with various simulation times.

Location	Hazen-Williams coefficient at the start of the test*	Hazen-Williams coefficient at the end of the test	Hazen-Williams coefficient at the pivot point associated with end of flow establishment
Trinity Lane – Pump 1	329.389	142.111	142.110
Trinity Lane – Pump 2	398.806	120.748	120.699
Ragged Lake – Pump 1 **	$1.113*10^{-10}$	48.624	48.604
Ragged Lake – Pump 2 **	$1.113*10^{-10}$	43.877	43.860
Akerley Boulevard – Pump 1	506.394	71.410	71.365
Akerley Boulevard – Pump 2	591.179	74.329	74.287
Melville Cove – Pump 1	152.336	17.622	17.613
Melville Cove – Pump 2	355.508	51.537	51.517

*First non-infinite value encountered in simulation. The inferences were conducted outside a reasonable Reynolds number range as stated by Stephenson (1989). The time required to enter the reasonable range is relatively quick.

**Instability associated start of simulation inferences for Ragged Lake.

See Figure 19 for the Stephenson (1989) overlay on the Moody Diagram for reference.

Table 16: Supplementary outputs from detailed modelling (Swamee-Jain).

Location	Average Reynolds number*, $R_{e_{avg}}$	Max Reynolds number*, $R_{e_{max}}$	Average Darcy-Weisbach friction factor, $f_{avg_{model}}$	Max Darcy-Weisbach friction factor**, $f_{max_{model}}$	Minimum Darcy-Weisbach friction factor, $f_{min_{model}}$
Trinity Lane – Pump 1	122,000	126,000	0.0185	0.0408	0.0183
Trinity Lane – Pump 2	111,000	114,000	0.0255	0.0429	0.0254
Ragged Lake – Pump 1	232,000	235,000	0.123	0.129	0.123
Ragged Lake – Pump 2	218,000	221,000	0.150	0.156	0.150
Akerley Boulevard – Pump 1	155,000	157,000	0.0630	0.0711	0.0629
Akerley Boulevard – Pump 2	159,000	162,000	0.0580	0.0666	0.0580
Melville Cove – Pump 1	147,000	148,000	0.828	0.843	0.828
Melville Cove – Pump 2	210,000	212,000	0.0985	0.105	0.0985

*Reynolds Values begin at approximately zero.

**Simulations start at approximately no flow, where the Darcy-Weisbach friction factor is large for the Swamee-Jain methodology. However, within this range flows accelerate quickly. A Reynolds Number of 4000 was adopted for each maximum Darcy-Weisbach friction factor calculation.

Table 17: Comparison of detailed model time-based estimates versus semi-analytical solutions.

Location	Time until flow establishment (model), $t_a\ (s)$	Time until flow establishment (analytical), * $t_a^{\#}\ (s)$	Error scalar, $\frac{t_a}{t_a^{\#}}\ (-)$	Time spent pumping (naïve), $t_{naive}\ (s)$	Time spent pumping (Analytical), ** $t^{\#}\ (s)$	Error scalar, $\frac{t_{naive}}{t^{\#}}\ (-)$
Trinity Lane – Pump 1	19.510	20.701	0.942	120.000	115.391	1.040
Trinity Lane – Pump 2	17.360	14.527	1.195	120.000	115.988	1.035
Ragged Lake – Pump 1	9.600	10.390	0.924	120.000	117.369	1.022
Ragged Lake – Pump 2	9.045	9.667	0.936	120.000	117.388	1.022
Akerley Boulevard – Pump 1	20.555	17.013	1.208	240.000	208.613	1.15
Akerley Boulevard – Pump 2	21.285	17.603	1.209	230.000	185.824	1.238
Melville Cove – Pump 1	2.455	2.2070	1.112	270.000	216.806	1.245
Melville Cove – Pump 2	3.860	3.941	0.979	240.000	207.907	1.154

*Inferred by utilizing equation (74)

**Inferred by utilizing equation (72)

Table 18: Energy usage and costs, current versus new installation.

Location	Current energy usage per cycle (kW-hr)	Initial energy usage per cycle (kW-hr)	Current energy cost ($/year)	Energy cost at installation ($/year)	Scalar energy cost increase (–)
Trinity Lane – Pump 1*	0.153	0.150	521.767	512.357	1.018
Trinity Lane – Pump 2*	0.151	0.136	516.462	466.043	1.108
Ragged Lake – Pump 1	1.242	0.914	4242.552	3123.795	1.358
Ragged Lake – Pump 2	1.233	0.862	4212.246	2944.369	1.431
Akerley Boulevard – Pump 1*	0.772	0.605	2636.436	2067.096	1.275
Akerley Boulevard – Pump 2*	0.746	0.584	2548.64	1997.015	1.276
Melville Cove – Pump 1	2.667	1.706	9111.844	5828.878	1.563
Melville Cove – Pump 2	2.459	2.297	8403.617	7849.940	1.071

*Efficiency data is no longer available for the pump model version. It is estimated from a similar model in series.

Table 19: Detailed model goodness-of-fit metrics utilizing continuous data for comparison.

Location	Correlation (R^2) - (−)*	Mean absolute percentage error – (%) **	RMSE – $\left(\sqrt{\frac{L}{s}}\right)$ **
Trinity Lane – Pump 1	0.997	1.737	0.288
Trinity Lane – Pump 2	0.827	20.039	2.163
Ragged Lake – Pump 1	N/A*	0.327	0.236
Ragged Lake – Pump 2	N/A*	0.457	0.296
Akerley Boulevard – Pump 1	1.000	1.164	0.308
Akerley Boulevard – Pump 2	0.873	8.712	3.01
Melville Cove – Pump 1	N/A*	3.474	1.505
Melville Cove – Pump 2	N/A*	8.004	4.757

Model outputs for models utilizing Swamee-Jain and Hazen-William are very similar; therefore, the metrics are similar for both detailed models.
*Correlation only for sites with continuous data collection through flow meters. The metric works poorly on the inferred flow rates through other methods.
**Where continuous data was inferred from liquid level monitoring, periods including flow establishment were not considered in calculation of the metric.

Table 20: Conditions for forcemains based on assumed current energy costs as compared to initial commissioning costs.

Condition	Lower limit on energy cost increase (%)*	Upper limit on energy cost increase (%)*
Like new	0	10%
Acceptable	10%	20%
Tolerable	20%	30%
Poor	30%	40%
Needs attention	40%	∞

*Based on a percentage increase in energy costs per year from the initial commissioning of the site.

Table 21: Assumed condition of the forcemain based on energy costs.

Location	Assumed increase in energy cost per year (%)	Assumed condition*
Trinity Lane – Pump 1	1.84	Like new
Trinity Lane – Pump 2	10.82	Acceptable
Ragged Lake – Pump 1	35.81	Poor
Ragged Lake – Pump 2	43.06	Needs attention
Akerley Boulevard – Pump 1	27.54	Tolerable
Akerley Boulevard – Pump 2	27.62	Tolerable
Melville Cove – Pump 1	56.32	Needs attention
Melville Cove – Pump 2	7.05	Acceptable

*Based on condition assessment presented in Table 20.

6.2 Hypothetical Lift-Stations

A million sets of unique model inputs were determined for the hypothetical lift-stations. The inputs were determined by uniform random sampling along a defined range. Table 24 summarizes the parameter ranges for the model inputs. Table 23 states the filtering criteria imposed on the simulation dataset to ensure realistic results. After filtering, 767,761 sets of simulation data remained. The results from each simulation were recorded and utilized to obtain additional parameters of interest. Error categories were developed to assess the erroneous inferences of roughness from a naïve interpretation. The imposed error category and their respective limits are stated in Table 22. The utility labels within the table refer to an increasing order of severity in error (as suggested by the average error within the category). Error tolerances were determined for each parameter in each category to ensure a suitable sample size for the simulation dataset. The error tolerances for each parameter were based on a confidence interval of 90% (Figure 135 within Appendix C). The 29 parameters of interest are summarized

with descriptions in Table 49 within Appendix C.

Table 22: Error thresholds for each error category.

Error category	Utility label	Minimum error in category	Maximum error in category	Sample size (percent of total)	Average error in category (%)
Negligible	1	0	10	67.8	4
Mild	2	10	25	20.4	16
Moderate	3	25	100	9.9	45
Severe	4	100	100+	1.8	294

Table 23: Filter criteria to ensure realistic simulation results.

Parameter filter on results	Description	Minimum	Maximum
Re_{avg} (-)	Reynolds number associated with the average flowrate through the forcemain.	0	10^8
t_{naive} (sec)	Time spent pumping as determined by a naïve pump-down test.	25	600
$\left(\frac{\epsilon}{D_p}\right)_{model}$ (-)	Relative roughness associated with the simulation.	10^{-6}	0.5
$U_{avg}\left(\frac{m}{s}\right)$	Average velocity through the forcemain determined with the average flowrate.	0.4	3.3
$H_{ST_{max}}(m)$	Maximum static total head during pumping test.	10^{-3}	c

Table 24: Parameter sampling ranges and filters for Monte Carlo simulations inputs.

Parameter	Description	Lower limit	Upper limit
D_p (mm)	Internal diameter of the forcemain.	100	400
ϵ_{naive} (mm)	Naïve interpretation of roughness.	0.01	50
L (m)	Length of the forcemain.	75	3600
T (°C)	Temperature of the liquid in the wet-well.	3	27
K (-)	Minor loss coefficient.	0.5	20
A (m^2)	Area of the wet-well.	2	35
a	Coefficient of the characteristic curve.	-100	-1800
b	Exponent of the characteristic curve.	0.75	3
c	Constant of the characteristic curve (shut-in head).	10	90
$H_{ST_{max}}$ (m)	Maximum static total head during pumping test.	0.01	88
Δh_{ss} (m)	Change in static suction head during pumping test.	0.003	5
$\Phi Q_{avg} = Q_{in}$, Φ (%)	Inflow rate during pumping test as a scalar of the approximated average flowrate.	0	10

6.2.1 Classification Tree

A classification tree was created with a subset of the parameters of interest (see Table 49 in Appendix C). Although numerous parameters were available to be utilized, only a subset were useful in creating the classification tree. The parameters that the algorithm determined useful in creating the tree and their relative parameter importance are stated in Table 25. Misclassification costs were imposed to ensure the severe category would be the most accurate. The costs of

misclassification used in creating the classification tree are depicted in Figure 50. Prediction accuracies for the classification tree are presented in Figure 51. The error category for the four sites considered were predicted with the classification tree as presented in Table 26. The complete classification tree is in Appendix E.

Table 25: Relative feature importance in the classification tree.

Parameter	Description	Relative feature importance (%)
t_{naive} (s)	Time spent pumping as determined by a naïve pump-down test.	61.57
$\left(\frac{\epsilon}{D_p}\right)_{naive}$	Naïve interpretation of relative roughness.	26.70
$D_p\ (mm)$	Internal diameter of the forcemain.	3.23
$f_{avg_{naive}}\ (-)$	Darcy-Weisbach friction factor determined with the average flowrate and naïve interpretation of relative roughness.	2.24
$h_{l_{naive-avg}}\ (m)$	The average losses (friction and minor) through the forcemain determined with the average flowrate and naïve interpretation of relative roughness.	2.08
$\frac{V_{pipe}}{V}\ (-)$	The ratio of the volume of liquid within a stagnant forcemain to the active volume.	1.38
$U_{avg}\ \left(\frac{m}{s}\right)$	Average velocity through the forcemain determined with the average flowrate.	1.18
$V\ (m^3)$	Active volume in the wet-well.	0.87
$h_{f_{naive-avg}}\ (m)$	Average friction losses determined by the average flowrate through the forcemain and naïve interpretation of relative roughness.	0.3
$\Delta h_{ss}\ (m)$	Change in static suction head during a pumping test.	0.27
$A\ (m^2)$	Area of the wet-well.	0.01

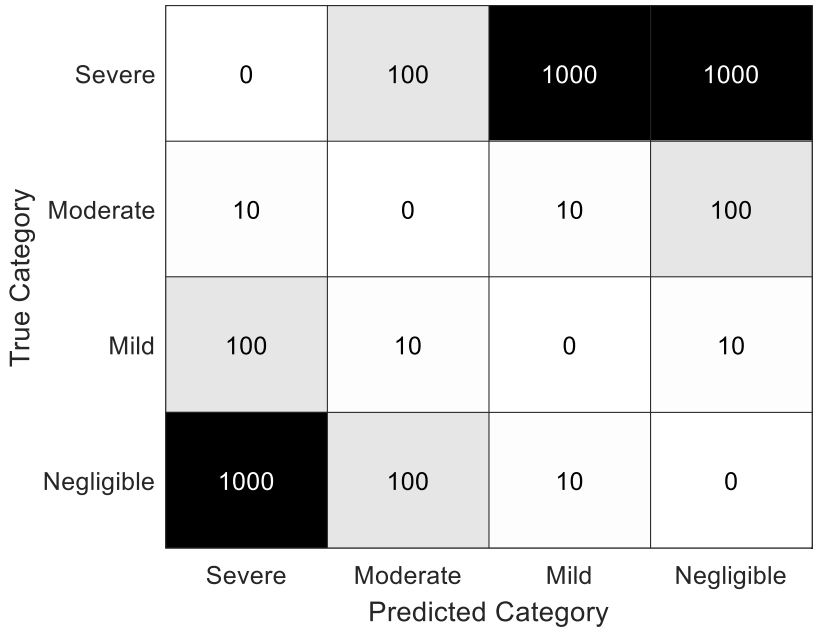

Figure 50: Costs of misclassification utilized for the classification tree concerning the error category.

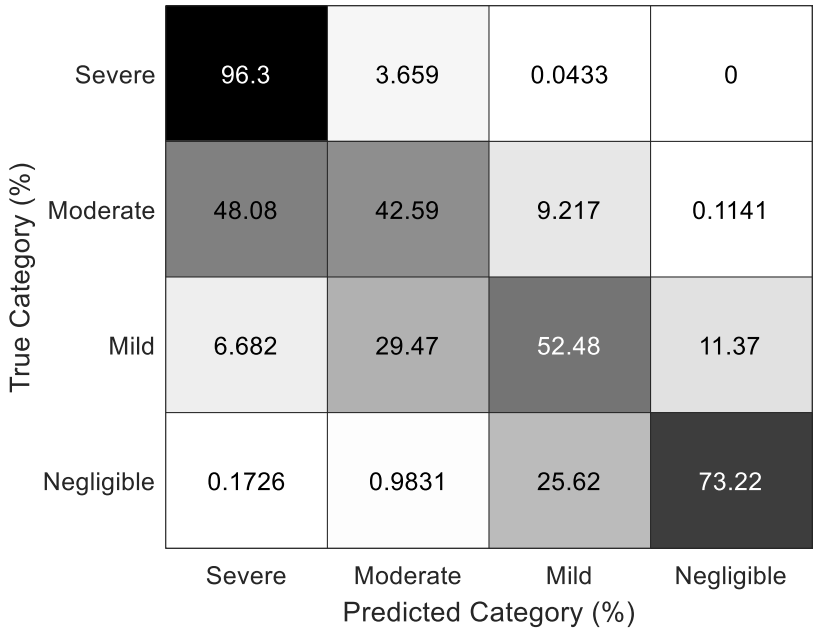

Figure 51: Classification tree accuracy based on the simulation dataset.

Table 26: Predicting error category for four sites considered with classification tree.

Location	Actual error category	Predicted error category	Correct? (Yes/No)
Trinity Lane – Pump 1	Severe	Severe	Yes
Trinity Lane – Pump 2	Severe	Moderate	No
Ragged Lake – Pump 1	Negligible	Negligible	Yes
Ragged Lake – Pump 2	Negligible	Negligible	Yes
Akerley Boulevard – Pump 1	Mild	Mild	Yes
Akerley Boulevard – Pump 2	Mild	Mild	Yes
Melville Cove – Pump 1	Negligible	Negligible	Yes
Melville Cove – Pump 2	Mild	Mild	Yes

6.2.2 Probability Density Estimation

Probability density estimates were determined with kernel density estimation techniques for all parameters of interest stated in Table 49. Figure 52 illustrates the probability density estimations for each error category given a specific parameter value for 8 of the 29 parameters. The probability density estimates for the other parameters of interest are depicted in Figure 132, Figure 133, and Figure 134 within Appendix C. Cumulative probability density estimations are presented for a specific parameter value given an error category within Appendix C.

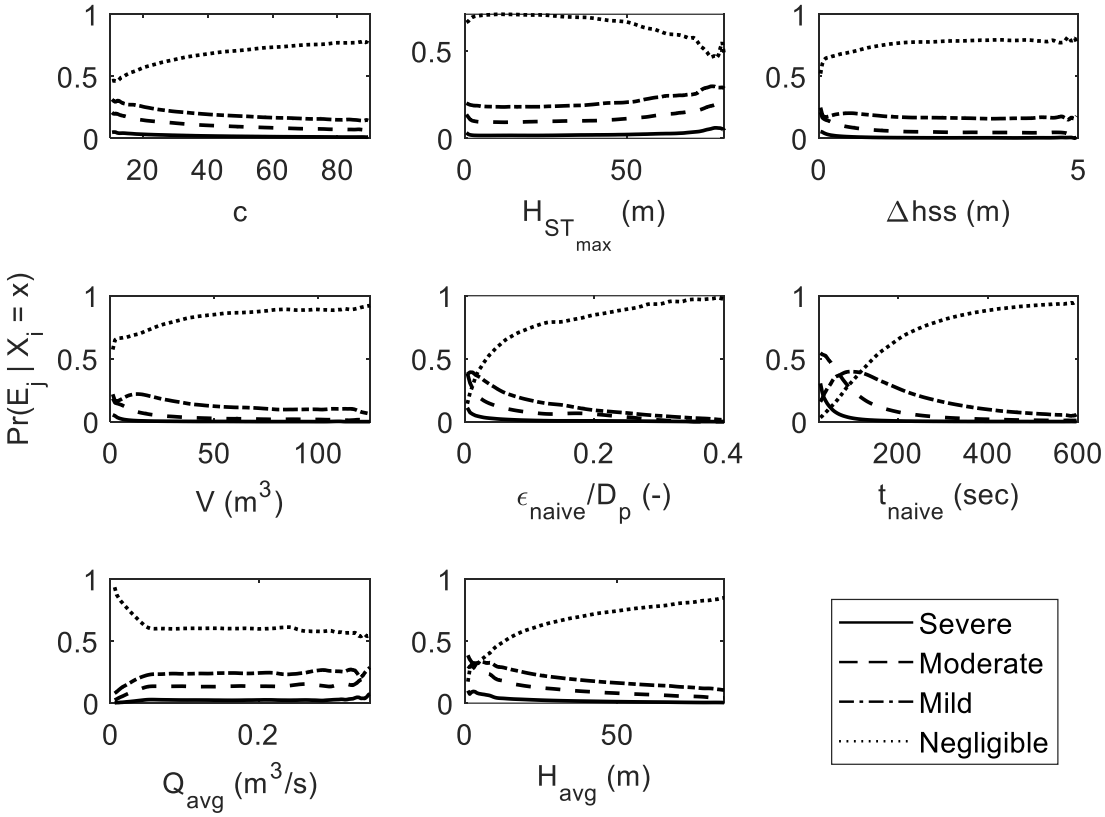

Figure 52: Part one of four - probability density estimations of an expected error category given a specific parameter value, $Pr(E_j \mid X_i = x)$.

7.0 Discussion

7.1 Four Halifax Sites Considered

Analysis was conducted on the forcemain associated with each pump at each site. However, the discussion presented within the section will be with respect to pump one for each site unless results significantly differ. A general discussion of the finding from four real sites will be presented there after.

7.1.1 Trinity Lane

Trinity Lane was the newest of the stations investigated. It is expected that the system would not have changed significantly between the initial commissioning of the site in 2004 to the date of testing in 2006. The pumping systems for the site were expected to behave in the same manner, as they are duplicates of one another (see Figure 142). However, the flow meters attached to the forcemains detected different outflow patterns for the two pumps (Figure 55 and Figure 57) where pump two had a lagged start time compared to pump one.

The inference of roughness (concerning Darcy-Weisbach derivatives) differed between the techniques. The detailed model inference of roughness was 0.02 millimetres while the naïve interpretation of roughness utilizing Swamee-Jain was 0.07 millimetres, and Brkić-Praks was 0.18 millimetres. Therefore, the naïve interpretation overestimated the roughness compared to the detailed model. The detailed model inference was most accurate compared to continuous data inferences (see Figure 45). Inferences of the Hazen-Williams coefficient were also conducted. The detailed model inference was 146, while the naïve interpretation was 137. Inferences determined by the continuous data reveal that the detailed model was more accurate than the naïve interpretation of hydraulic resistance (Figure 46). The forcemain condition metrics (see Table 21) suggest that forcemains are still in fair condition.

Utilizing the detailed model and inferred roughness, the simulated flow rate reached flow establishment and was lower at operating flow than the flow meter indicated. Pump two (Figure 74) was less accurate after flow establishment than pump one (Figure 42) when compared to

flow meter data (see Table 19 for model fit metrics). The lagged start was not considered in the detailed model and is partly responsible for lower flow rates after flow establishment. The migration of the operating point after flow establishment is depicted in Figure 43.

A one-at-a-time sensitivity analysis (see Figure 48) was conducted for the forcemain associated with pump one. The inputs were perturbed by 0.01%, and it was determined that the internal diameter of the forcemain, exponent of the characteristic curve and shut-in head were the most sensitive to the perturbation (relative to the other inputs) for the inference of roughness, as illustrated in Figure 79. The resulting scalar error was nearly 0.6% higher than the baseline for the three inputs. The forcemain length, scalar pump coefficient, and static discharge head were also affected significantly but were not as pronounced. The temperature of the liquid, minor loss coefficient, wet-well area, and wet-well inflow did not significantly change the inference of roughness due to perturbation. The baseline scalar error was 1.56 for the inference of roughness due to utilizing a non-segmented forcemain compared to a segmented forcemain in the detailed model. Therefore, it was determined that using a segmented forcemain to infer roughness was necessary for this site.

The sensitivity of the inference of roughness due to the diameter was investigated. A 1% decrease in the forcemain diameters was associated with a drop of 0.02 to 0.002-millimetre for the inference of roughness (see Figure 47). Pumps one and two for Trinity Lane were found to have minimal absolute changes due to losses in diameter with respect to the absolute roughness.

In the literature, PVC pipes were not well-researched concerning roughness growth as a function of water quality. Therefore, the literature estimations should be utilized with caution. However, Abdelmonem (2020) provided a roughness equation concerning raw sewage, and it was found to be comparable to the detailed model inference for both forcemains (see Figure 49).

7.1.2 Ragged Lake

Ragged Lake had the third oldest forcemain of the sites considered. Some change was expected in the hydraulic resistance due to probable changes in the pipe material with ordinary aging (given that initial commissioning was in 1996). The forcemains associated with each pump at

Ragged Lake combine into one header, which leads into one forcemain (see Figure 146 and Figure 147). Due to each pump utilizing the same forcemain, inferred roughness of the forcemain was expected to be similar. There was no forcemain flow rate monitoring for this site. Continuous flow rate data was estimated by monitoring the liquid level in the wet-well (see Figure 60) and relating it to the wet-well geometry.

The inference of roughness did not significantly differ between the techniques. The detailed model inference of roughness was 34.4 millimetres. The naïve interpretations of roughness were 36.6 millimetres and 36.0 millimetres for Swamee-Jain and Brkić-Praks, respectively. Therefore, the detailed model and naïve interpretation were comparable for the site. The continuously collected liquid level is illustrated in Figure 85, but the flow was not monitored by a flow meter. The inference of the Hazen-Williams coefficient also did not differ significantly for each technique. The detailed model determined a coefficient of 48.9, while the naïve interpretation inference was 47.8. The forcemain condition metrics (see Table 21) suggest that forcemains are requiring significantly more energy for pumping, increasing the operating costs.

The detailed model and inferred roughness provided a simulated flow rate and static suction head comparable to the collected data (Figure 82). The migration of the operating point after flow establishment is depicted in Figure 83. The model metrics applicable in Table 19 suggest that the detailed model is an adequate fit for the continuously collected data. However, the continuous flow rate data was assumed to be constant. Therefore, no operational point migration could be determined from the continuous data.

The one-at-a-time analysis resulted in a similar pattern of scalar error as compared to the Trinity Lane analysis. However, the inputs were perturbed by 2% for Ragged Lake. The internal diameter of the forcemain was the most sensitive to the perturbation (Figure 88) in the roughness inference, followed by the exponent of the characteristic curve and shut-in head. The segmented and non-segmented analyses are the same for Ragged Lake, as the forcemain is a uniform diameter. A potential 10% loss in diameter initial commissioning was associated with an inferred roughness drop of 34.6 millimetres to 10.5 millimetres (Figure 87) for the forcemain attached to pump one and 46.4 millimetres to 16 millimetres for the forcemain attached to pump two (Figure 95).

Literature estimates (Figure 89) for roughness associated with water quality indices determined the detailed model inference to be 2.4 times higher than the literature average. The estimate by Colebrook and White (1937) and NEWWA (1935) were comparable to the detailed model estimate. Although uninvestigated, there may be losses attributed to friction in the analysis that are not realistic such as pressure losses due to degraded pump impeller, root intrusion, differential settlement and temporary or permanent blockages in the forcemain. At the time of the pump-down test, the forcemain outlet was clean and free of buildup.

7.1.3 Akerley Boulevard

The Akerley Boulevard lift-station was updated (in 1988) decades after implementation (1968). The upgrade included new dual forcemains with different pumps attached. The newer forcemains reconnect to the original forcemain approximately 75 meters downstream of the lift-station. Therefore, the forcemain is comprised of segments of different pipe materials, ages, lengths, and diameters (see Figure 150, Figure 153, and Figure 154). In the upgrade, flow meters were added to the station. Flow meters (Figure 65) were utilized in inferring inflow (Figure 63) along with wet-well liquid level monitoring (Figure 64). The average inflow was determined and utilized for calculations. It was revealed that the flow rate provided by pump two was higher at the operational point and took longer to achieve flow establishment when compared to pump one.

The detailed model inference of roughness was 7.0 millimetres. The naïve interpretation of roughness was 8.5 millimetres for Swamee-Jain and Brkić-Praks. The inference of the Hazen-Williams coefficient with the detailed model was 73.5, and the inference with a naïve interpretation was 70.2. It was determined that the detailed model roughness (or Hazen-Williams coefficient) correlated to the continuous data after flow establishment more than the naïve interpretation for each friction loss type (see Figure 101 and Figure 102). The simulation flow rate utilizing the roughness inferred provided an accurate flow rate compared to the continuously monitored data (see Figure 98 and Table 19). Pump two had a lagged start time and introduced similar issues to that of the Trinity Lane pump two system. The forcemain

condition metrics (see Table 21) suggest that forcemains energy costs are currently within the tolerable range but will require attention soon.

The one-at-a-time sensitivity analysis (Figure 104) revealed similar patterns of system behaviour due to perturbations as Ragged Lake. The baseline scalar error for utilizing a non-segmented forcemain instead of a segmented forcemain was 1.19 on the inference of roughness. Literature estimated for the inference of roughness (Figure 113) utilizing water quality indices was comparable to that of the detailed model. Although, NEWWA (1935) was much higher (147 millimetres) than the rest of the estimates, skewing the literature average. This site has the most detailed information and data collection available of the four sites.

7.1.4 Melville Cove

Melville cove was the oldest station investigated in the study, initially commissioned in 1966. Due to the age of the station, it was expected to have at least some change or departure from initial commissioning. The station has two pumps, each with a forcemain. The forcemains were shorter than the other sites and the station had a larger static total head to overcome (see Figure 155 and Figure 158).

The station had no flow metering to collect continuous forcemain flow data. Therefore, the forcemain continuous flowrate data was inferred through continuous liquid level monitoring and relating it to the geometry of the wet-well (Figure 70). The liquid level monitoring was utilized to determine the inflow while the pump was offline (Figure 69). It was found that the average flow rate through the forcemain from pump one was almost 150% lower than that of pump two. A high discrepancy in the forcemain flow was unexpected as both pumps were of the same make, model, and were installed on the same date. The discrepancy was not corrected during the field testing. The owner verified after testing that the pump had been experiencing issues. The owner corrected the issues with pump one and confirmed that the flow rate was similar to the second pump. However, the test was not redone, with the pump in better condition. The test utilizing pump two had a larger active volume when compared to pump one. The forcemain condition metrics (see Table 21) suggest that the forcemain associated with pump one will require attention as the energy costs are significantly different than initial commissioning.

The inferences of roughness were significantly different when comparing pump one to pump two. The detailed model inferred a roughness of 260 millimetres and 23.5 millimetres for pumps one and two, respectively. Even though the forcemains and pumps are nearly identical systems, the roughness inferred for pump one was 11 times larger than for pump two. The naïve interpretation of roughness for the forcemain attached to pump one was 268 and 266 millimetres for Swamee-Jain and Brkić-Praks, respectively. The naïve interpretation of roughness for the forcemain attached to pump two was 30.5 and 30.1 millimetres for Swamee-Jain and Brkić-Praks, respectively. The inference of the Hazen-Williams coefficient was 17.8 for the detailed model and 17.6 for the naïve interpretation of the forcemain attached to pump one. The continuous data for all Darcy-Weisbach type loss methods are associated with an extensive range of inferences (from 230 mm to 310 millimetres for pump one). It should be noted that these inferences are outside of the applicable ranges of the equations utilized.

The one-at-a-time sensitivity analysis revealed that the segmented forcemain was not as important to consider for pump one, increasing the roughness inference by a scalar of 1.08 as compared to the segmented forcemain. Also, the detailed model inputs were not as sensitive as the other sites for a 2% perturbation (see Figure 120). However, pump two has a baseline scalar error of 1.39 (Figure 128). The most sensitive input was the characteristic curve for the pump two system. The exponent associated with the characteristic curve deviated to 2.53 from the baseline scalar error when perturbed (an 82% increase in scalar error). A 10% drop in the assumed diameter caused the inferred roughness to drop by 103 millimetres (see Figure 119). The one-at-a-time sensitivity analysis indicates that the diameter might not be sensitive, but the theoretical diameter reduction analysis does not affirm that hypothesis.

Literature estimation for roughness (Figure 121) indicate that the detailed model prediction was 3.35 times higher than the literature average. There was a separation in scale between the literature estimation for this site. NEWWA (1935) and Colebrook-White (1937) estimations were of comparable scale as the detailed model. The newer literature formulations predicted roughness lower than the model indicated. Like Ragged Lake, the unaccounted-for losses are assumed to be friction losses but may not be in reality. Encrustation estimates based on the Mielcarzewics and Pelka (1997) formulation indicate that the encrustation would be approximately 8.9 millimetres (see Table 51) of the radius of the non-segmented pipe. Encrustation estimates indicate that a 10% drop in internal diameter would not be improbable.

7.1.5 Four Sites – General Discussion

It was apparent that the need to include the segmentation of the forcemain was important. Significant scalar errors were present when using a non-segmented forcemain in the detailed model as compared to a segmented forcemain. Another issue was the pump start-up time, as seen in the continuously collected data. The start-up times were not considered in the detailed model. The detailed model simulated flow rate with the optimal inferred roughness underestimates the flow establishment period, partly due to the pump start-up time.

After achieving flow establishment, the detailed model underestimates the flow rate at the operational point. Table 27 illustrates the difference in the average flows after the flow establishment period between the simulation and continuously collected data. The percentage error associated with the average difference is also present. It was also determined that the difference between the simulation results for the detailed model with the Swamee-Jain or the Hazen-Williams friction loss methods were negligible.

The Hazen-Wiliams equation produced lower scalar errors than Darcy-Weisbach types regarding the inferences of hydraulic resistance. However, the magnitudes are not comparable between the two methodologies. Therefore, further research could be conducted on error metrics of comparable measure, such as energy expenditure during pumping for the different loss types. Friction loss equations were utilized outside of their applicable ranges. The interpretations of roughness at Ragged Lake and Melville cove were not within the applicable ranges of such equations. Therefore, inferences outside of the applicable ranges should be considered with caution. It should be noted that the Hazen-Williams coefficient will have to change during the pump-down test as outlined in Table 15. Therefore, a static value for the coefficient is erroneous. The Hazen-Williams equation was inferred utilizing outputs from the detailed model at three different times, the start of the test, the pivot point of the test and the end of the test (Table 15). The three inferences were found to be larger than the static value as determined by the detailed model. This finding would suggest that the migration of the Hazen-Williams coefficient during unsteady flow would need to be considered for the loss method. Also, the Hazen-Williams loss method was not well suited for the flow-establishment period.

Table 27: Comparison of the simulated detailed model flow rate and continuous flow rate for the four sites.

Location	**Average difference in flow (continuous vs model) – $\left(\frac{L}{s}\right)$**	**Max flow for scale (continuous or model) – $\left(\frac{L}{s}\right)$**	**Percentage error in average flow (continuous vs model) after flow establishment – (%)**
Trinity Lane – Pump 1	0.1560	13.262	1.174
Trinity Lane – Pump 2	1.171	12.933	9.051
Ragged Lake – Pump 1*	0.2710	59.276	0.4580
Ragged Lake – Pump 2*	-0.1520	55.734	0.2720
Akerley Boulevard – Pump 1	0.3140	26.176	1.201
Akerley Boulevard – Pump 2	1.124	29.40	3.824
Melville Cove – Pump 1*	-0.719	40.535	1.774
Melville Cove – Pump 2*	-3.263	60.784	5.368

*Sites did not contain continuous flowrate monitoring

All unaccounted-for losses are assumed to be friction for inferences of hydraulic resistance. There are numerous other causes for head losses that are not friction related and were not and could not be accounted for in the analysis such as root intrusion, grease build-up, and several types of forcemain damage. However, literature studies (Lauchlan *et al*., 2005; Michalos, 2016) have also not considered these losses in analysis. As revealed with Melville Cove, these un-accounted for losses can be significant. Therefore, inferences of hydraulic resistance should be conducted with vigilance in general.

The study suggests that some of the sites require attention. The energy increases stated in Table 18 varied for each pump at each site. It was found that pump one at Ragged Lake and Melville Cove required attention (see Table 21) as determined by the assumed condition criteria stated in Table 20. There were also differences in the pumps conditions at each site as illustrated with pump two at Melville cove, which was in acceptable condition.

The one-at-a-time sensitivity analysis conducted on each pump provides similar patterns in scalar error. It was determined that the assumed diameter of the forcemain and characteristic curve were the most sensitive to perturbation. The diameter of the forcemain becomes occluded, rougher, and degraded over time. The pump will require maintenance, repairs, and replacement with time. Therefore, an inference of hydraulic resistance becomes increasing difficult without more sophisticated data collection techniques such as pressure and flow rate monitoring and a method to evaluate the internal diameter of the forcemain.

A true test of hydraulic resistance would need to be able to differentiate between both aspects of the relative roughness. Such analysis would require extensive assessment such as laboratory testing of a segment of forcemain. Numerous relative roughness solutions theoretically exist that produce the average flow rate determined by the naïve pump-down test. The range of theoretical relative roughness was found to be significant. Therefore, loss of effective cross section must be considered in any analysis of hydraulic resistance, along with the absolute roughness.

Most literature formulations to determine roughness did not apply wastewater forcemains directly. However, due to a lack of literature on the inference of roughness for wastewater forcemains, the equations outlined in Section 3.2 were utilized. The literature inferences were highly variable for all four sites, which was in partially anticipated. The formulations were based on regression techniques to specific conditions, characteristics, and small datasets. Each literature estimation required different water quality indices or flow characteristics. There was no available information on the water quality indices for the four stations. Metcalf & Eddy (2014) provide general information regarding water quality, but the range in the indices is significant and vary depending on geographic location. Therefore, the literature formulations should be utilized with wariness for inferences associated with wastewater forcemains.

The semi-analytical solution estimations (Table 17) of both the naïve pump-down test time and the duration of flow establishment were within reasonable accuracy for the four sites. The naïve

pump-down test semi-analytical estimation was always lower than the actual time spent pumping and produced the most erroneous results for Ragged Lake. The duration of flow establishment semi-analytical estimate was within at least 4 seconds of the modelled duration for all sites. However, the semi-analytical solution requires a moderate amount of set-up prior to use. Therefore, future research could be conducted on more readily useable formulations.

7.2 Hypothetical Lift-Stations

It was essential to determine the generalizability of erroneous inferences associated with the naïve interpretation of roughness. Monte Carlo simulations were utilized to investigate erroneous naïve interpretations of hydraulic resistance, in a general manner. The simulation inputs were parameterized by uniform sampling of the parameter ranges as stated in Table 24. The simulation results were filtered to remove stations that would be considered unrealistic based on available knowledge. There were no regulations within design guidelines limiting the pumping time. However, pumps turning on and off too frequently causes excess wear on the components and is commonly avoided. Pumping that takes too long should also be avoided. Therefore, time limits for pumping were imposed on the simulations to stay within a reasonable time frame. The percentage of small to medium-sized lift-stations (if any) that would have pumping times less than 25 seconds are negligible. However, the lower limit was estimated by information provided within the literature review but there was no set lower limit provided. The upper limit was imposed by a general cycle time for the wet-well. Where regulations are in place for lift-station retention times in North America, there tends to be a maximum limit. An upper limit was set at 10 minutes. The Swamee-Jain methodology also has limitations on the range of applicability as outlined in Section 3.5. Literature (Lauchlan *et al.*, 2005; Michalos, 2016) suggest inferences outside of the applicable ranges were needed. Therefore, the range of applicability was widened for the simulations. However, the general usefulness of such inferences is in question and should be researched further. The flow velocity through the forcemain was also limited. Forcemain design regulations often impose a maximum and minimum criterion for forcemain velocities (see EPA, 2000). The lower sampling boundary for static total head was determined by the maximum shut-in head, as determined by the sampled

characteristic curve. A design would not be implemented for a system in which the pump could not overcome the static total head. Assuming approximately 25% error in the naïve interpretation of roughness to the actual roughness of the forcemain (mild or negligible category) is acceptable, about 12% of all simulation results would be an issue (2% severe, and 10% moderate error categories).

Two different methodologies were implemented to investigate the generalizability of erroneous outcomes of the naïve interpretation of roughness. Parameters associated with the naïve interpretation of roughness were collected or determined such as forcemain and lift-station characteristics, naïve interpretation results and detailed modelling results. These parameters were utilized in two different methodologies for determining the general erroneous inferences. The first method was a categorical classification tree, and the second method was probability density estimations utilizing kernel density estimation techniques. The important results of each method are discussed within this section.

7.2.1 Probability Density Estimation

After applying Bayes theorem to transform the probability distributions, round-off errors associated with the start and end of the distributions were present. The round-off error was addressed by truncating the tails of the distribution where the round-off error began. The confidence intervals selected for the parameters was 90%. It was determined that some parameter error tolerances (see denominator of equation (79)) needed to ensure a suitable simulation dataset size were significant in the severe error category. The largest error tolerances needed were volume of the wet-well (26%) and the change in static suction head in the wet-well (16%). The average error tolerance required for the parameters in the severe category was 8.5%. However, the error tolerance for all parameters within the negligible, mild, and moderate categories was under 4%.

After the probability densities are determined, the visual difference between the distributions for each error category data with respect to each parameter was investigated. Parameters with the most significant differences in probability density with respect to the error category were but are not limited to:

- the ratio of time spent establishing flow to the total time spent pumping $\left(\frac{t_{a_{model}}}{t_{naive}}\right)$,
- the ratio of average flowrate to maximum flow rate $\left(\frac{Q_{avg}}{Q_{max}}\right)$,
- the ratio of the volume of the pipe to active wet-well volume $\left(\frac{V_{pipe}}{V}\right)$, and
- Darcy-Weisbach friction factor estimated naively $\left(f_{naive_{avg}}\right)$.

Table 28 presents the range associated with a severe or moderate error category for multiple parameters of interest as determined in the study.

Several parameters were revealed to show negligible indication of differences between error categories. These parameters revealed negligible changes to the probability distributions when choosing a specific value of a parameter, these parameters include:

- the temperature of the liquid in the wet well (T),
- the minor loss coefficient (K),
- the area of the wet-well (A),
- the characteristic curve exponent and coefficient (b, a), and
- the ratio of the average inflow to the average flow through the forcemain $\left(\frac{Q_{in}}{Q_{avg}}\right)$.

Table 28: Parameters ranges with the most probable error category being moderate or severe.

Parameter	Minimum	Maximum
t_{naive} (s)	25	71.00
$U_{(wetwell)_{avg}}\left(\frac{m}{s}\right)$	0.03	0.05
$t_{a_{model}}(s)$	67.73	100.00
$\frac{h_{a_{max}}}{h_{l_{naive-avg}}}(-)$	4.63	10
$\frac{c - H_{max}}{c}(-)$	0.97	1.00
$\frac{t_{a_{model}}}{t_{naive}}(-)$	0.34	1.00
$\frac{Q_{avg}}{Q_{max}}(-)$	0.75	0.86
$\frac{V_{pipe}}{V}(-)$	46.00	250.00
$f_{naive-avg}(-)$	0.017	0.028

7.2.2 Classification Tree

The Monte Carlo simulation datasets were downscaled for the classification tree to allow the severe error category data to have more influence. The downscaling was conducted by randomly sampling the data from each error category. The severe category dataset was left unchanged. The number of samples to take from the other error categories was determined by the number of samples within the severe error category. Therefore, there was equal sized datasets for each of the error categories after downscaling (13858 sets of simulation data in each error category, totaling 55432). The difference in the probability distributions in each category were negligible after downscaling.

The classification tree had 46 leaves in which 11 were labeled as severe, 17 were labeled as moderate, 16 labeled mild, and 2 labeled negligible. The classification tree only utilized parameters that can be determined for a naïve interpretation of roughness (as outline in Table 49 in Appendix C). The parameter determined to be the best root split was the time spent pumping (as would be determined by the naïve pump-down test). This parameter accounted for 67.5% of the relative feature importance. The root split was determined to be 156 seconds for the time spent pumping, the most severe cases under this limit. The next most important parameter was the naïve interpretation of relative roughness with 26.7% of the relative parameter importance. Therefore, time spent pumping and the naïve interpretation of relative roughness accounted for 94.2% of the relative parameter importance. However, other parameters account for key roles in determining decision node splitting criteria such as the internal diameter of the forcemain, the naïve interpretation of the Darcy-Weisbach friction factor and friction head loss, and average forcemain velocity.

The classification tree achieved 96% accuracy for the severe category, the negligible category achieved 73% accuracy, while the mild (52.48%) and moderate (42.59%) categories achieved lower accuracy rates (see Figure 51). Lower accuracies were caused by the misclassification costs selected (Figure 50) and maximum leaf limit imposed on the algorithm. Both the misclassification costs and leaf limit were chosen through iteration but resulting values were determined subjectively for the study. The severe category was determined to be the most important to classify correctly. Therefore, the misclassification costs were selected as to be conservative of the severe error category and to maintain interpretability of the classification tree. There are multiple branches leading to a severe error category. Three separate branches leading to a severe error category are presented in Table 29. The full text-style classification tree is presented in the Appendix E.

Table 29: Three branches leading to a severe error category utilizing naïve interpretation information.

Node in Branch	Branch 1	Branch 2	Branch 3
Node 1 (root split)	$t_{naive} < 156\ (s)$	$t_{naive} \geq 156\ (s)$	$t_{naive} \geq 156\ (s)$
Node 2	$t_{naive} \geq 92\ (s)$	$\frac{\epsilon_{naive}}{D_p} < 0.01\ (-)$	$\frac{\epsilon_{naive}}{D_p} \geq 0.01\ (-)$
Node 3	$\frac{\epsilon_{naive}}{D_p} < 0.05\ (-)$	$h_{L_{avg}} < 20.3\ (m)$	$h_{L_{avg}} < 5\ (m)$
Node 4	$h_{f_{avg}} \geq 21\ (m)$	$\frac{\epsilon_{naive}}{D_p} < 0.007\ (-)$	$f < 0.06$
Node 5	$f_{naive\ avg} < 0.04$	$U_{avg} < 2\ \left(\frac{m}{s}\right)$	$t_{naive} < 226\ (s)$
Node 6 (end)	Severe		

8.0 Recommendations

The naïve interpretation of hydraulic resistance was found to have issues within the study. However, there are ways to assist in mitigating erroneous outcomes such as detailed modelling, background research, and knowledge of the site. For more accurate inferences of hydraulic resistance, the following recommendations are suggested:

1. If possible, record measurements with high resolution. These measurements include flow rate, liquid level monitoring, and dynamic head provided by the pump.
2. A naïve pump-down test should be conducted after maintenance and replacement of pump parts or when a pump is newly installed.
3. Add a mid-point float within the wet-well for the naïve pump-down test, allowing one to neglect the effects of flow establishment in analysis.
4. It is necessary to consider all segments of a forcemain system for the inference of hydraulic resistance.
5. If naïve pump-down tests are conducted, consult the classification tree within Appendix E to assess what error category is likely given the information collected for a naïve interpretation of resistance.
6. The dynamics of the pump, including lagged start settings, pump start-up time, and pump stopping time should be determined.
7. When the forcemain is at the end of its service life, detailed hydraulic modelling of the forcemain should be conducted before considering replacement.

9.0 Future Research

Future research opportunities were revealed during the study. The topic of study or adjacent fields could be expanded upon in various ways. Therefore, the following list are suggestions for potential future research:

1. Pipe deterioration mechanisms regarding wastewater forcemains can be further investigated. The research could be conducted regarding wastewater composition on differing pipe materials and the hydraulics associated with the system.
2. The minor loss coefficients can be investigated regarding the consideration of unsteady flow and how the minor loss coefficients change over time in wastewater application.
3. The effects of varying inflow during pumping and evaluate the effects on the inference of roughness can be investigated.
4. A quantitative investigation of how a pump will likely deteriorate in wastewater application can be conducted, allowing for better understanding of how the pump characteristic curves migrate over time.
5. Error margins associated with flow-metering devices, level sensors, and pressure sensors/transmitters in wastewater applications can be investigated.
6. The pump start-up phenomena can be determined (from offline to fully established flow).
7. Potential tweaks to lift-stations may allow systems to operate in the most efficient range for a pump over time, such as changing level sensors for start and stop positions and maintenance effects on head loss over time.
8. Field investigations of forcemains just prior to the end of service life. Therefore, allowing laboratory testing of old forcemains to confirm results of future research.
9. A significant dataset of lift-station characteristics can be assembled to estimate probability distributions of parameters more accurately.
10. More parameters can be obtained and analyzed for a better indication of the scenarios in which a naïve interpretation of hydraulic resistance is erroneous.
11. Methods that allow for different pipe segments to have a different inferred roughness in each segment could be investigated as would happen in reality.

12. Methods for incorporating non-linear cross-sectional areas within the wet-well could be investigated.
13. A similar study can be conducted but can focus on the resulting error in energy usage. The error in energy usage may be a better indicator of when to avoid the naïve interpretation of hydraulic resistance.
14. Low cost and effort methods for inferring hydraulic resistance through physical inspection can be determined.
15. Deciphering between roughness and encrustation within a forcemain.
16. Readily useable analytical or semi-analytical solutions for inferring an accurate hydraulic resistance as compared to a naïve interpretation can be determined.

10.0 Conclusions

The naïve interpretation of hydraulic resistance was expected to be associated with certain physical systems and testing protocols tending to yield clearly erroneous outcomes. Governing variables and equations were identified for the operating point migration. It was determined that the operating point migrates in a non-linear manner during a pump-down test. This is not considered a naïve pump-down test. A detailed model was created to infer the hydraulic resistance of a wastewater forcemain and allow the generation of results from naïve pump-down tests. The model was parameterized by lift-station and forcemain characteristics and was utilized to determine when a naïve interpretation of roughness would be erroneous. Hypothetical lift-station set-ups were determined by Monte Carlo techniques. The Monte Carlo simulation dataset was investigated with probability density estimates and a classification tree. The study also utilized field data from four sites within Halifax, Nova Scotia.

Semi-analytical solutions were created and utilized within the study. The first semi-analytical solution was utilized to infer the approximate time spent pumping from a hypothetical active volume and flowrate relationship. The second solution was utilized to infer the approximate flow establishment duration from the governing differential flowrate equation. The semi-analytical solutions were found to be reasonably accurate as compared to the actual time spent pumping and duration of flow establishment, as determined by the detailed model.

Analysis of the four sites revealed several key sources of error associated with naïve interpretations of hydraulic resistance. The methodologies for inferring friction losses were found to often be utilized outside of the limitations of a given equation. Therefore, it was difficult to determine if the inferences were meaningful. The pump start-up phenomena and flow establishment could not be appropriately assessed with a naïve pump-down test. Possible unaccounted-for head losses include forcemain damage, encrustation, grease build-up, and degradation of the impellor of the pump.

Some system characteristics were determined to be important but may be neglected in the inference of hydraulic resistance. The header and subsequent main head losses prior to the main segment of the forcemain can sometimes be neglected or improperly accounted for. However, the losses associated with this segment of pipe can be significant. Sensitivity analyses revealed

that the assumed diameter of the forcemain and assumed characteristic curve for the pump can significantly impact the inferred hydraulic resistance.

The Hazen-Williams equation should not be used to assess hydraulic resistance. It is theoretically inferior to the Darcy-Weisbach loss formulation. Furthermore, the Hazen-Williams coefficient at the end of any given test will not be the same as the apparent coefficient at the beginning of a test suggesting a static value is erroneous.

The conditions of the forcemain were evaluated for the four sites based on assumed energy consumption as determined through simulation. The forcemains associated with the study sites have changed from the initial commissioning. It was determined that the forcemains associated with Ragged Lake and Melville Cove require attention (possible replacement). Akerley Boulevard is still in reasonably good condition. The forcemain at Trinity Lane is in like-new condition.

Monte Carlo simulation results were partitioned into multiple groups based on the error in the naïve interpretation of roughness compared to the simulation roughness utilized in the model, referred to as error categories. Hypothetical lift-station and forcemain characteristics were determined by uniformly sampling a parameter range for each characteristic. The error categories utilized were severe, moderate, mild, and negligible. The naïve interpretations of roughness with the highest error percentage were allotted to the severe error category. It was revealed that only 2% of the total simulations were within the severe error category, while 67% were in the negligible error category.

A classification tree with the Monte Carlo simulation datasets revealed patterns associated with the severe category in the simulation dataset. Out of the numerous features investigated, those of most importance within the tree were time spent pumping as determined by a naïve test and the relative roughness as determined by a naïve interpretation. Both parameters accounted for 94.2% of the feature importance for the classification tree. The parameter associated with the root node of the tree was the time spent pumping. The splitting value for the root was 156 seconds. Most severe error category simulations are times lower than the root split. The relative roughness splits, along with the other branch criteria, suggest that the most erroneous outcomes of roughness are within the partially developed turbulent zone.

The Monte Carlo simulation datasets were also investigated utilizing kernel density estimation techniques. Prominent parameters that were predictors of being in the moderate or severe error category include: the ratio of the duration of time spent establishing flow to the time spent pumping being greater than 0.34, the ratio of the volume in the forcemain to the volume of the wet-well is greater than 46, the ratio of the average flow rate to the maximum flow rate was less than 0.83, or the Darcy-Weisbach friction factor determined naively is between 0.017 and 0.028. Several parameters did not offer any indication of influencing the error category. These parameters include the minor loss coefficient, the temperature of the liquid, and the ratio of the inflow rate to the average flow rate through the forcemain.

It was determined that the naïve interpretation of hydraulic resistance was not suitable for certain physical systems and testing protocols. Consideration of the four datasets analyzed and modelled revealed that various important considerations are neglected when utilizing a naïve interpretation of roughness. Hypothetical stations investigated suggest that there are key characteristics that can be indicative of an erroneous result. It is recommended to utilize a more detailed modelling approach to infer hydraulic resistance in wastewater forcemains based on these findings.

References

Abdelmonem, Y., Ead, S., & Shabayek, S. (2020). Effect of Time on Pipe Roughness. *17th Canadian Hydrotechnical Conference.*

American Society of Civil Engineers (ASCE). (1969). *Design and Construction of Sanitary and Storm Sewers.* ASCE.

Balekelayi, N., & Tesfamariam, S. (2019). *Advanced Deterioration Models for Wastewater Inspection Prioritization.* University of British Columbia. Retrieved from https://open.library.ubc.ca/cIRcle/collections/ubctheses/24/items/1.0379341

Bloch, H. P., & Budris, A. R. (2013). *Pumping User's Handbook – Life Extension Fourth Edition.* The Fairmont Press, Inc.

Brent, R. (1973). *Algorithms for Minimization without Derivatives.* Prentice-Hall.

Brkić, D. (2011). Review of explicit approximations to the Colebrook relation for flow friction. *Journal of Petroleum Science and Engineering, 77*(1), 34-48. doi:10.1016/j.petrol.2011.02.006 . hal-01586547

Brkic, D., & Praks, P. (2018). Unified Friction Formulation from Laminar to Fully Rough Turbulent Flow. *Journal of Applied Sciences*.

Broward County Water & Wastewater Services Technical Standards. (2012). *WWS Lift Station Wet Well Sizing Requirements.* Broward County - Department of Public Works & Transportation + Water & Wastewater Services.

Butler, D., Digman, C., Makropoulos, C., & Davies, J. (2018). *Urban Drainage.* (4, Ed.) CRC Press.

Carollo, F. G., Ferro, V., & Termini, D. (2005). Flow Resistance Law in Channels with Flexible Submerged Vegetation. *Journal of Hydraulic Engineering, 131*(7), 554-564.

Christensen, B. A. (2000). Discussion: Limitations and Proper Use of The Hazen-Williams Equation. *Journal of Hydraulic Engineering*, 167-170.

City of Calgary. (2016). *Wastewater Lift Station Design Guidelines.* Calgary: City of Calgary. Retrieved from https://www.calgary.ca/content/dam/www/pda/pd/documents/urban-development/publications/wastewater-lift-station-design-guidelines.pdf

City of Calgary. (2016). *Wastewater Lift Station Design Guidelines.* Retrieved from https://www.calgary.ca/content/dam/www/pda/pd/documents/urban-development/publications/wastewater-lift-station-design-guidelines.pdf

Colebrook, C. F. (1939). Turbulent Flows with Particular Reference to the Transition Region Between the Smooth and Rough Pipe Laws. *Journal of the Institution of Civil Engineers, 11*.

Colebrook, C. F., & White, C. M. (1937). Experiments with Fluid Friction in Roughened Pipes. *Royal Society Proceedings*.

Colebrook, F. C., & White, M. C. (1937). The Reduction of Carrying Capacity of Pipes with Age. *Journal of the Institution of Civil Engineers, 7*, 99-118.

Crane Co. (2013). *Flow of Fluids – Through Valves, Fittings and Pipe - Technical Paper No. 410.*

Darcy, H. (1854). Sur des recherches experimentales relatives au mouvement des eaux dan les tuyaux [On experimental research relating to the movement of water in pipes]. *Comptes rendus Des Seances De L'Academie Des Sciences [Reports of the Sessions of the Academy of Sciences]., 38*, 1109-1121.

Dormand, J. R., & Prince, P. J. (1980). *A family of embedded Runge-Kutta formulae.* Journal of Computational and Applied Mathematics. doi:10.1016/0771-050X(80)90013-3

Eaton, A. A., & Ahmed, H. M. (2018). On the performance of Degradation of Centrifugal Pumps. 2018. *Proceedings of the 5th International Conference of Fluid Flow, Heat and Mass Transfer.* Avestia. doi:10.11159/ffhmt18.158

Engineers Edge. (N/A). *Moody Chart*. Retrieved from Engineers Edge: https://www.engineersedge.com/fluid_flow/pressure_drop/moody_chart.htm

Environment Canada. (2006). *Atlantic Canada Wastewater Guidelines Manual – for Collection, Treatment, and Disposal.* Nova Scotia Government. Retrieved from https://novascotia.ca/nse/wastewater/pubs.asp

Fecarotta, O., Carravetta, A., Morani, M. C., & Padulano, R. (2018). Optimal Pump Scheduling for Urban Drainage under Variable Flow Conditions. *MDPI - Resources*. doi:10.3390/resources7040073

Foray, J. (2014). Energy Efficiency Considerations in Pumps and Pump Stations. *Wastewater/Water Sustainble Energy Cohort – WSU Extension Energy Program.* Retrieved from

http://www.energy.wsu.edu/LinkClick.aspx?fileticket=t3ubiA8D8A4%3D&tabid=692&mid=1345

Franzini, J., & Finnemore, J. E. (1997). *Fluid Mechanics with engineering applications: Nineth Edition.* McGraw Hill.

Gebbie, P. (2000). Water Stability: What Does It Mean and How Do You Measure It. *Proceedings of the 63th Annual Water Industry Engineers and Operators Conference.*

Geldreich, E. E., & LeChevallier, M. (1999). *Microbiological Quality Control in Distribution System. Water Quality and Treatment, A handbook of Community Water Supplies. Ed. R.D. Letterman, 5th edition.* McGraw-Hill.

Gong, J., Erkelens, M., Lambert, M., & Forward, P. (2019). Experimental Study of Dynamic Effects of Iron Bacteria-Formed Biofilms on Pipeline Headloss and Roughness. *Journal of Water Resource Planning and Management, 145*(9). doi:04019038

Gulich, J. F. (2020). *Centrifugal Pumps – Fourth Edition.* Springer.

Gupta, R. S. (2008). *Hydrologic and Hydraulic Systems – Third Edition.* Waveland Press.

Halifax Water. (2022). *Design Specifications & Supplementary Standard Specificitions for Water, Wastewater & Stormwater Systems.* Retrieved from Halifax Water: https://halifaxwater.ca/sites/default/files/2022-05/2022_Design_Specifications.pdf

Hansen, D. (2007). Discussion: Flow Resistance of Wastewater Pumping Mains. *Proceedings of the Institution of Civil Engineers*, 51-57.

Hasemian, H. M., & Jiang, J. (2009). Pressure Transmitter Accuracy. *ISA - Transactions, 48*(4), 383-388. doi:https://doi.org/10.1016/j.isatra.2009.04.008

Hazen, A., & Williams, G. S. (1905). *Hydraulic Tables: Showing the Loss of Head due to the Friction of Water Flowing in Pipes, Aqueducts, Sewers, etc. and the Discharge Over Weirs.* John Wiley & Sons.

Hsu, A., Kaufman, R., & Glimm, J. (2022). Scaling Laws for Partially Developed Turbulence. *Frontiers in Applied Mathematics and Statistics*.

IEEE Xplore. (2009). *Flow Meters: Part 1.* IEEE Instrumentation and Measurements Magazine. doi:10.1109/MIM.2009.4762948

Izenman, A. J. (2008). *Modern Multivariate Statistical Techniques: Regression, Classification, and Manifold Learning.* Springer.

Jain, A. K., Mohan, D. M., & Khanna, P. (1978). Modified Hazen-Williams Formula. *American Society of Civil Engineers – Journal of Hydraulics Division, 102*.

Jean, G. (2006). *On Making Inferences about the Condition of Wastewater Forcemains based on Apparent Hydraulic Resistance.* Dalhousie University.

Jeffery, A., & Dai, H. H. (2008). *Handbook of Mathematical Formulas and Integrals* (4th ed.). Academic Press.

Jensen Engineered Systems. (2012). *Pump Station Design Guidelines - Second Edition.* Jensen Precast. Retrieved from https://www.jensenprecast.com/water-resources/wp-content/uploads/2020/05/Design-Guidelines-Pump-Stations-1.pdf

Jones, G. M., Bosserman, B. E., Sanks, R. L., & Tchobanoglous, G. (2008). *Pumping Station Design – Third Edition.* Butterworth-Heinemann.

Karassik, I. J., Messina, J., Cooper, P., & Heald, C. C. (2008). *The Pump Handbook – Fourth Edition.* McGraw Hill.

Kaur, K., Annus, I., Vassiljev, A., & Kandler, N. (2018). Determination of Pressure Drop and Flow Velocity in Old Rough Pipes. *MDPI, 2*(11). Retrieved from https://www.mdpi.com/2504-3900/2/11/590

Kottegoda, N. T., & Rosso, R. (2008). *Applied Statistics for Civil and Environmental Engineers.* (Second, Ed.) Blackwell Publishing.

Kouwen, N. N., & Li, R. M. (1980). Biomechanics of Vegetative Channel Linings. *Journal of Hydraulics Division*.

Kuznetz, M. (2019). *Hydraulic Design of WW Lift Stations – Course Number: CH-02-508.* Retrieved from Pdh-Pro: Continuing Education for Engineers: https://www.pdh-pro.com/wp-content/uploads/2019/03/CH-02-508.pdf

Lamont, P. A. (1981). Common Pipe Flow Formulas Compared with the Theory of Roughness. *American Water Works Association, 73* .

Lauchlan, C., May, F., & May, R. (2005). Flow Resistance of Wastewater Pumping Mains. *Water Management*(158).

Liou, C. P. (1998). Limitations and Proper Use of the Hazen-Williams Equation. *Journal of Hydraulic Engineering, 124* , 951-954.

MathWorks. (2019). *Get Started with Curve Fitting Toolbox.* Retrieved from https://www.mathworks.com/help/curvefit/getting-started-with-curve-fitting-toolbox.html?s_tid=CRUX_lftnav

Mellodge, P. (2016). *A Practical Approach to Dynamic Systems for Engineers.* Woodhead Publishing.

Metcalf & Eddy Inc. (2014). *Wastewater Engineering: Treatment and Resource Recovery - Fifth Edition.* McGraw-Hill Education.

Michalos, C. (2016). *Hydraulic Effects of Biofilms on the Design and Operation of Wastewater Forcemains.* Colorado State University.

Michalos, C. (2020). Consequences of Under-Estimating Friction Losses in Wastewater Forcemains. *Pipelines*.

Mielcarzewicz, E. W., & Pelka, H. K. (1997). HYDRAULIC CHARACTERIZATION. *Environmental Protection Engineering, 23*.

Moody, L. F. (1944). Friction Factors for Pipe Flow. *American Society for Mechanical Engineers, 66*, 671.

New England Water Works Association, NEWWA. (1935). *Committee on Pipeline Friction Coefficients - Summary of Report.* Journal NEWWA.

Nikuradse, J. (1932). Gesetzmassigkeiten der turbulenten Str ¨ omung in glatten ¨ Rohren. Forschungsarbeiten auf dem Gebiete des Ingenieurwesens.

Nikuradse, J. (1933). Stromungsgesetze in rauhen Rohren. ¨ Forschungsarbeiten auf dem Gebiete des Ingenieurwesens.

Ounsakul, T., Sirirattanachatchawan, T., Pattarachupong, W., Yokrat, Y., & Ekkawong, P. (2019). Artificial Lift Selection Using Machine Learning. *International Petroleum Technology Conference.* Retrieved from https://onepetro.org/IPTCONF/proceedings-abstract/19IPTC/2-19IPTC/D021S042R003/154328

Panda, K. G., Agrawal, D., Nshimiyimana, A., & Hossain, A. (2016). Effects of environment on accuracy of ultrasonic sensor operates in millimetre range. *Perspectives in Science, 8*, 574-576.

Papa, F., Raduji, D., Karney, B., & Robertson, M. (2014). Pump Energy Efficiency Field Testing and Benchmarking in Canada. *Journal of Water Supply: Research and Technology – AQUA, 63.7*, 570-577.

Pincince, A. (1970). Wet-Well Volume for Fixed-Speed Pumps. *Journal of Water Pollution Control Federation, 42*(1), 126-130.

Plascencia, G., Diaz-Damacillo, L., & Robles-Agudo, M. (2020). On the Estimation of the Friction Factor: a Review of Recent Approaches. *SN Applied Sciences*. doi:https://doi.org/10.1007/s42452-020-1938-6

Prandtl, L. (1935). The Mechanics of Viscous Fluids. *Aerodynamics Theory*.

Purvis, Zachary G;Kimley-Horn and Associates, Inc;. (N/A). A New Spin on Pump Station Testing and Analysis: What You Wish You Knew About Your Pump Station. *North Carolina Section of the American Water Works Association (NC AWWA).* Retrieved from https://cdn.ymaws.com/www.ncsafewater.org/resource/collection/3ADA6C44-DC80-47A8-88B5-8067A9589589/CD_Mon_PM_01.20_Purvis.pdf

Romtec Utilities, Inc. (N/A). *The Advantages of Valve Vaults in Wastewater Lift Stations*. Retrieved from Romtec Utilities: http://romtecutilities.com/the-advantages-of-valve-vaults-in-wastewater-lift-stations/

Romtec Utilities, Inc. (N/A). *Understanding Pipe Sizing for Forcemains* . Retrieved from Romtec Utilities: http://romtecutilities.com/understanding-pipe-sizing-for-force-mains

Romtec Utilities, Inc. (N/A). *Components that Should and Should Not Go in a Wetwell*. Retrieved from Romtec Utilities: http://romtecutilities.com/components-that-should-and-should-not-go-in-a-wet-well/

Shahzad, A., & James, W. (2002). Loss in Carrying Capacity of Watermains due to Encrustation and Biofouling, and Application to Walkerton, Ontario. University of Guelph: Chi Journal – Journal of Water management Modelling.

Sreenivas, J. (2011). Bends, Flow and Pressure Drop in. *Thermopedia*. doi:10.1615/AtoZ.b.bends_flow_and_pressure_drop_in

Stephenson, D. (1989). *Pipeline Design For Water Engineers* (3 ed.). Johannesburg, South Africa: Elsevier.

Stoker, D. M. (2011). *Ultrasonic Flow Measurement for Pipe Installations with Non-Ideal Conditions.* Utah State University.

Strong, R. (2022). Supplementary Information: Use of Pump-down Tests to Infer Hydraulic Rsistance of Wastwater Forcemains. Retrieved from https://github.com/ronaldbstrong/UseOfPumpDownTest-HydraulicInference

Suribabu, C. R., & Sivakumar, P. (2021). Simulating flow through scour valv in the water distribution network. *ISH Journal of Hydraulic Engineering, 28*(3), 264-270. doi:10.1080/09715010.2021.1881921

Swamee, P. K., & Jain, A. K. (1976). Explicit equations for pipe-flow problems. *Journal of the Hydraulic Division, 102*(5), 657-664.

Swamme, P. K. (2001). Optimal Design of Pumping Mains. *Journal of Transportation Engineering, 127*, 264-267.

Tekle, T. T. (2014). *Ultrasonic Stream Bridge Sensors (USBS) Error in Water Level Estimation.* University of Iowa.

Terzic, J., Nagarajah, C. R., & Alamgir, M. (2010). Fluid Level Measurement in Dynamic Environments Using a Single Ultrasonic Sensor and Support Vector Machine (SVM). *Sensors and Actuators A: Physical, 161*, 278-287.

Thorley, A. D. (1991). *Fluid Transients in Pipeline Systems.* D. & L. George Ltd.

Tullis, J. P. (1989). *Hydraulics of Pipelines – Pumps, Valves, Cavitation and Transients.* John Wilet & Sons, Inc.

United States Environmental Protection Agency. (2000). *Wastewater Technology Fact Sheet – Sewers, Forcemain: EPA 832-F-00-071.* Office of Washington, D.C.

Vladeanu, G. J. (2018). *Wastewater Pipe Condition and Deterioration Modelling for Risk-Based Decision Making.* Louisiana Tech University. Retrieved from https://digitalcommons.latech.edu/cgi/viewcontent.cgi?article=1021&context=dissertations

von Kármán, T. (1930). Mechanishe aehnlichkeit and turbulenz ["Mechanical similarity and turbulence"]. *Nachr. Ges. Wiss. Gottingen*.

Wagner, T. B., & Jennifer, S. (2014). What's in the Numbers? A Review and Analysis of More than 400 Miles of Force Main Inspection and Condition Assessment Data. *WED Collection Systems 2014: Collections on the Chesapeake.*

Woolf , P. (2020). *Chemical Process Dynamics and Controls.* Opensource: Engineering – LibreTexts. Retrieved from https://eng.libretexts.org/Bookshelves/Industrial_and_Systems_Engineering/Book%3A_Chemical_Process_Dynamics_and_Controls_(Woolf).

Xylem Inc. (2015). Pump Cavitation and How to Avoid it: Best Practices in Pump System Design. Retrieved from https://www.xylem.com/siteassets/support/case-studies/case-studies-pdf/cavitation-white-paper_final-2.pdf

Xylem Inc. (N/A). *Xylem Water Solutions & Water Technology*. Retrieved from https://www.xylem.com/en-ca/

Yousefi, A. (2019). *Head loss increase in service lines with time – With examples from Asker municipality.* Norwegian University of life science.

Appendix A - Model Inputs and Data Collection

Summary of Model inputs

Table 30: Summary of model inputs for pump one of each site.

Location	Test date	Inside diameter	Pipe material	Pipe age	Minor losses
	(DD/MM/YYYY)	(mm)	(-)	(years)	(-)
Trinity Lane	25/10/2006	106	PVC	<2	6.396
Ragged Lake	25/10/2006	248	Ductile iron	10	10.908
Akerley Boulevard	31/10/2006	191	Ductile iron	38/18*	9.255
Melville Cove	26/10/2006	252	Ductile iron	40	6.851

Location	Pipe length	Water temperature	Wet-well area	Highest static head	Lowest static head
	(m)	(°C)	(m^2)	(m)	(m)
Trinity Lane	289	11.8	4.524	12.629	12.325
Ragged Lake	472	10.4	11.150	14.741	14.119
Akerley Boulevard	696	16.4	13.690	17.385	16.949
Melville Cove	77	10	23.600	32.221	31.859

Location	Pump time	Average inflow	Characteristic curve (OLS)
	(seconds)	(m^3/s)	$c + aQ^b$
Trinity Lane	120	-	$25.9782 - 249.4735Q^{0.8152}$
Ragged Lake	120	$5.973*10^{-4}$	$51.1428 - 637.4323Q^{1.2603}$
Akerley Boulevard	240	$2.476*10^{-3}$	$36.6670 - 240.6767Q^{0.9003}$
Melville Cove	270	$6.500*10^{-3}$	$51.1428 - 637.4320Q^{1.2604}$

*Station upgraded after installation.

**All data summarized above is for the first pump of each station. Detailed data is provided in the appropriate Appendix.

***Inside diameters presented in the table are from the longest pipe segments, lengths are full lengths of forcemain, and all minor loss coefficients for systems. Although in the model, these are segmented.

Table 31: Summary of pump options & well control/monitoring for sites considered.

	Location			
Index	**Trinity Lake**	**Akerley Boulevard**	**Ragged Lake**	**Melville Cove**
Pump				
Pump type	Centrifugal	Centrifugal	Centrifugal	Centrifugal
Application	Submersible	Submersible	Submersible	Dry
Make	Flygt	Flygt	Flygt	Flygt
Impeller style	N/A	454	452	452
Impeller diameter	N/A	100	N/A	N/A
Speed (RPM)	N/A	1760	1755	1755
Rated power (kW)	N/A	14.9	35	35
Drive type	N/A	Closed coupled direct	Closed coupled direct	Closed coupled direct
Volts	N/A	600	600	600
Full amp loads	N/A	21	43	43
Start option	N/A	Soft	Soft	Soft
Wet-well control & monitoring				
Level trigger	Ultrasonic	Ultrasonic/float	Float	Ultrasonic/float
Flow meter	Magnetic	Magnetic	N/A	N/A
Level monitor	Ultrasonic	Ultrasonic	Unknown**	Ultrasonic

*N/A – Not available

**Data from Jean (2006), but no methodology is stated for how collection was conducted.

Data Collection

Trinity Lane

NO INFLOW DATA

Summary Information

Table 32: Trinity Lake site information, part one of two.

Site: Trinity Lake	
Test date (DD/MM/YYYY)	25/10/2006
Pipe material	PVC
Pipe age (years)	2
Water temperature (°C)	11.8
Wet-well area (m^2)	4.524
Average inflow (m^3/s)	0
Characteristic curve – head (m) / flowrate (m^3/s)	$25.97826 - 249.4735Q^{0.815269}$

Table 33: Trinity Lake site information, part two of two.

Site: Trinity Lake			
	Parameter	**Pump 1**	**Pump 2**
	Lowest static head (m)	12.296	12.325
	Highest static head (m)	12.632	12.629
	Pumping time (sec)	120	120
Segment 1	Diameter (mm)	100	100
	Minor losses (-)	3.500	3.500
	Length (m)	11.524	11.524
Segment 2	Diameter (mm)	106	106
	Minor losses (-)	2.896	2.896
	Length (m)	270.633	270.633

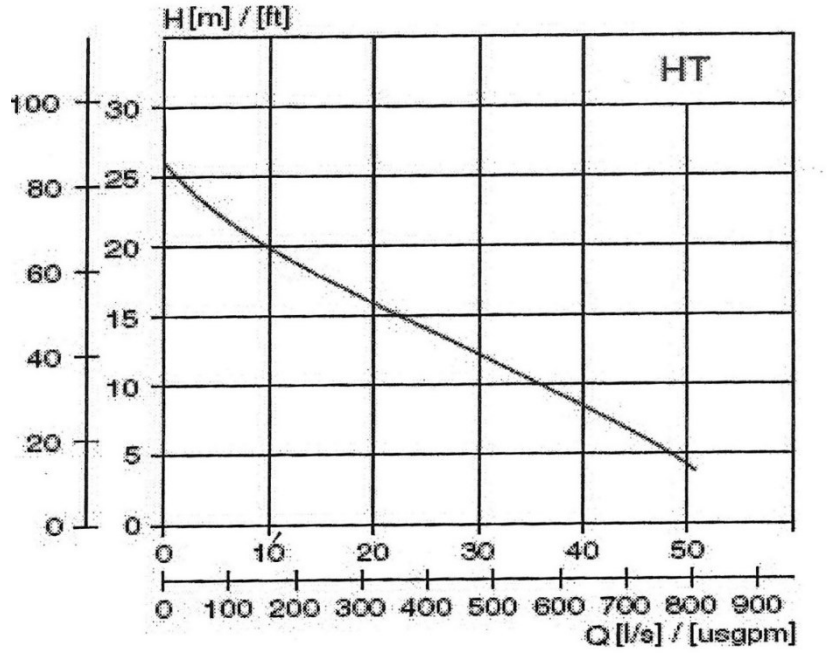

Figure 53: Characteristic curve for pumps at Trinity Lane as provided by manufacturer (Xylem Inc., undated).

Trinity Lane – Pump 1

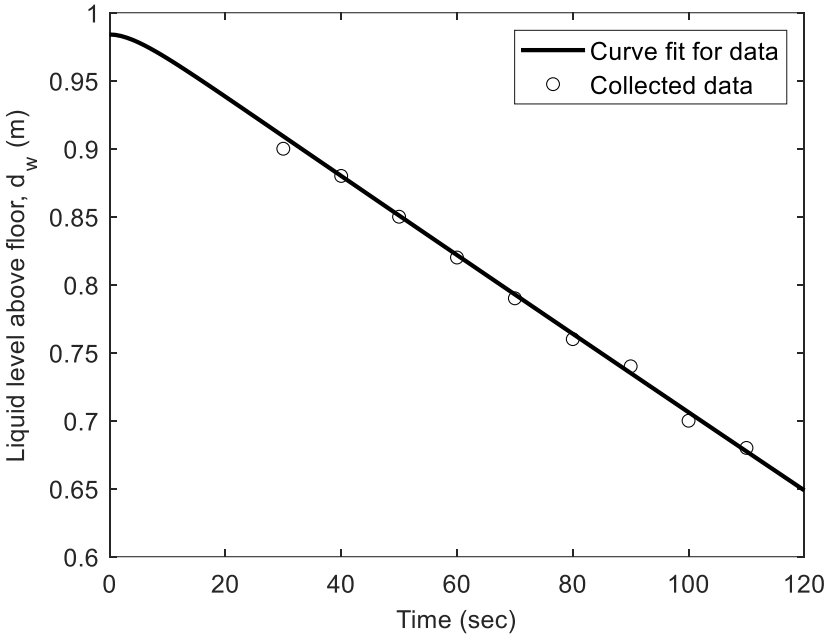

Figure 54: Trinity Lane - pump one: liquid level in the wet-well during pumping.

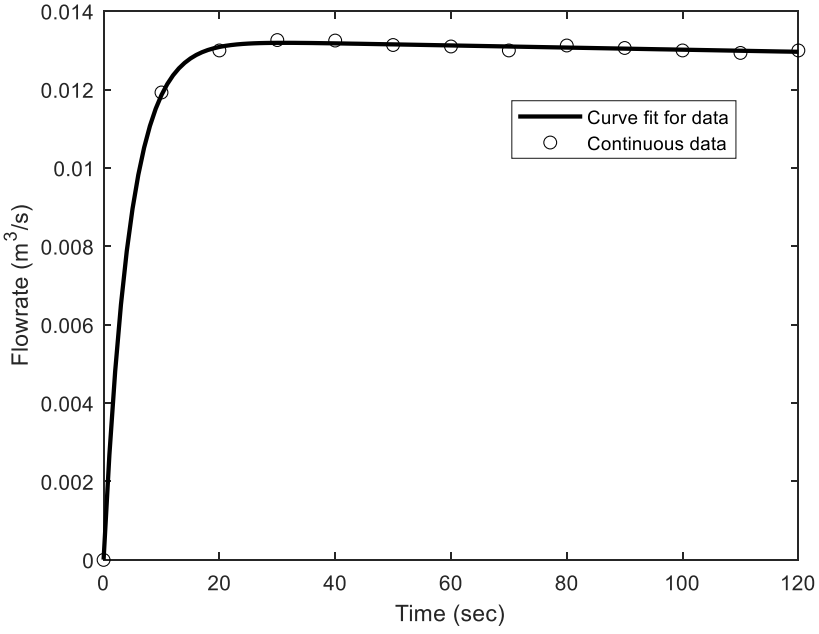

Figure 55: Trinity Lane - pump one: flow meter data for flow rate through the forcemain.

Trinity Lane – Pump 2

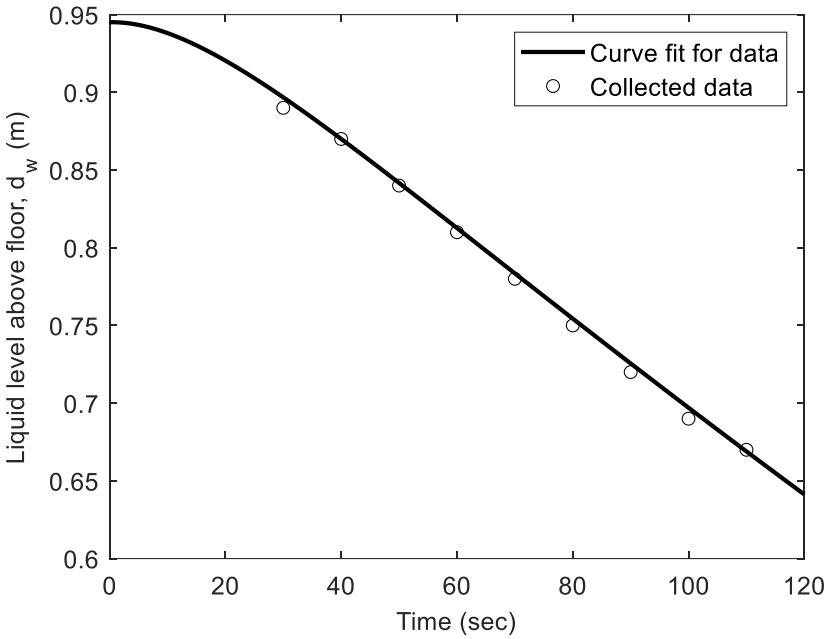

Figure 56: Trinity Lane - pump two: liquid level in the wet-well during pumping.

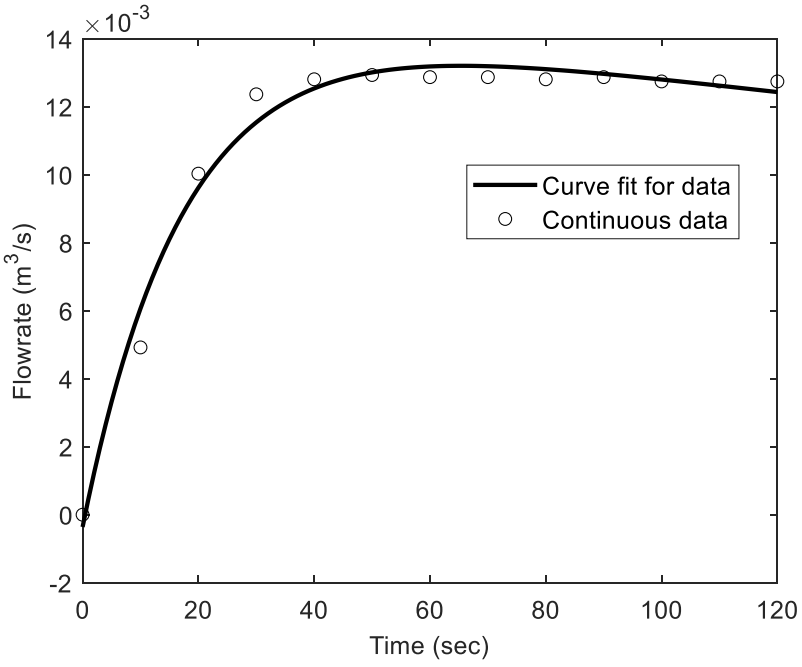

Figure 57: Trinity Lane - pump two: flow meter data for flow rate through the forcemain.

Ragged Lake

Summary Information

Table 34: Ragged Lake site information, part one of one.

Site: Ragged Lake	
Test date (DD/MM/YYYY)	25/10/2006
Pipe material	Ductile iron
Pipe age (years)	10
Water temperature (°C)	10.4
Wet-well area (m^2)	11.15
Average inflow (m^3/s)	$5.973*10^{-4}$
Characteristic curve – head (m) / flowrate (m^3/s)	$51.1428-637.4324*Q^{1.2604}$

Table 35: Ragged Lake Site Information, part two of two.

Site: Ragged Lake			
	Parameter	**Pump 1**	**Pump 2**
	Lowest static head (m)	14.119	14.149
	Highest static head (m)	14.741	14.734
	Pumping time (sec)	120	120
Segment 1	Diameter (mm)	248	248
	Minor losses (-)	10.908	10.908
	Length (m)	470	472

*Pumps start with individual forcemains, merge into a header.

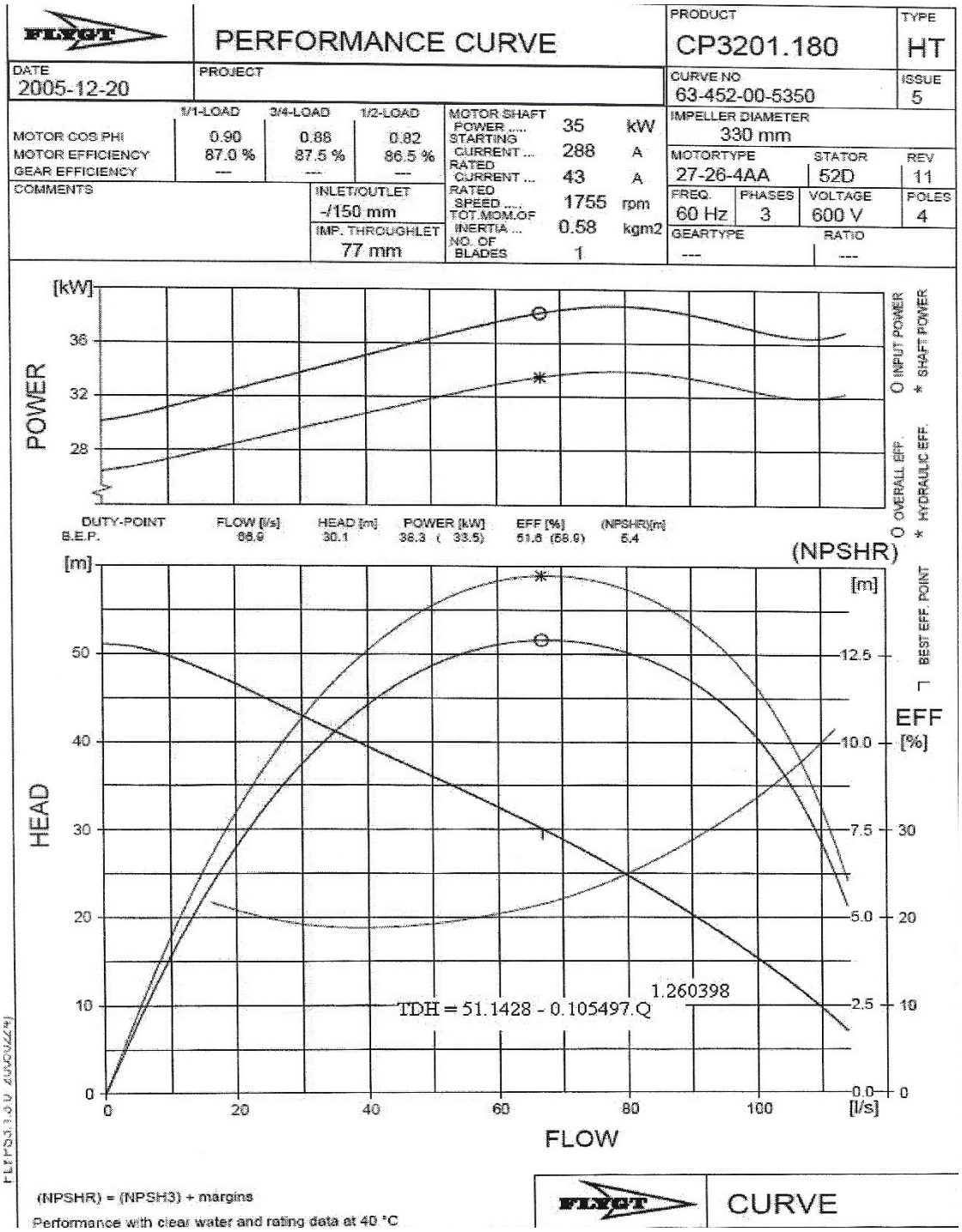

Figure 58: Characteristic curves for the pumps at Ragged Lake as provided by the manufacturer (Xylem Inc., undated).

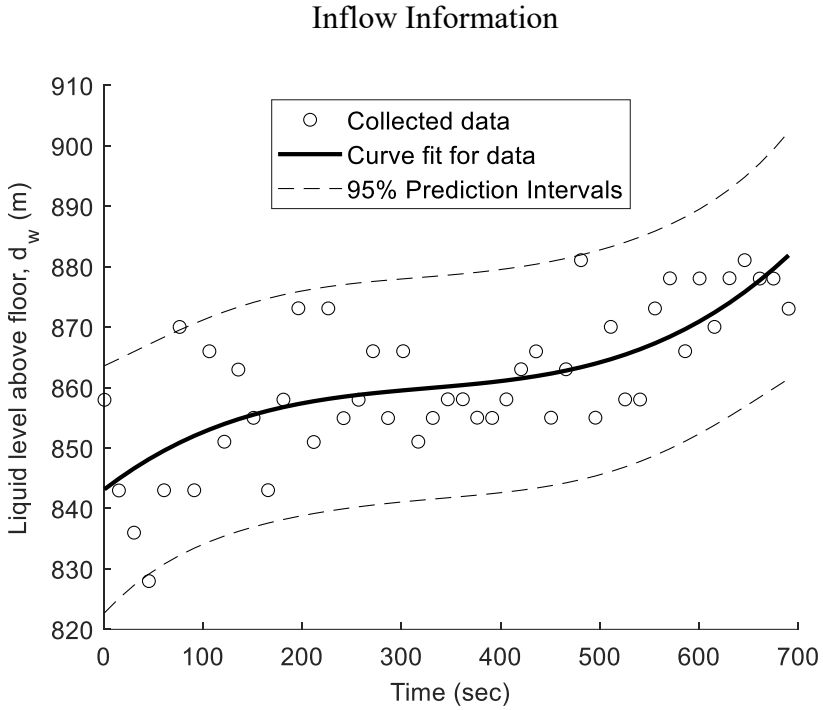

Figure 59: Ragged Lake - pump one: liquid level in the wet-well during while the pump is offline.

Ragged Lake – Pump 1

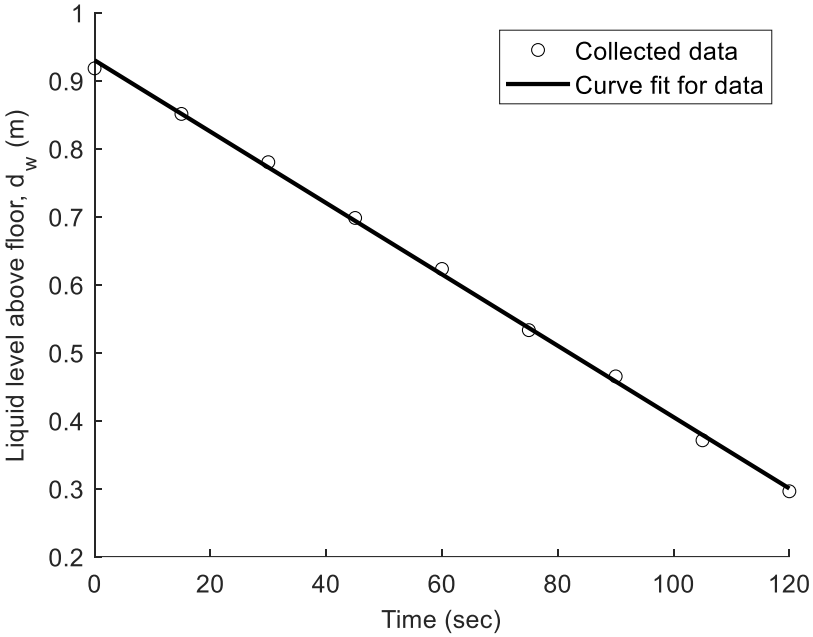

Figure 60: Ragged Lake - pump one: liquid level in the wet-well during pumping.

Ragged Lake – Pump 2

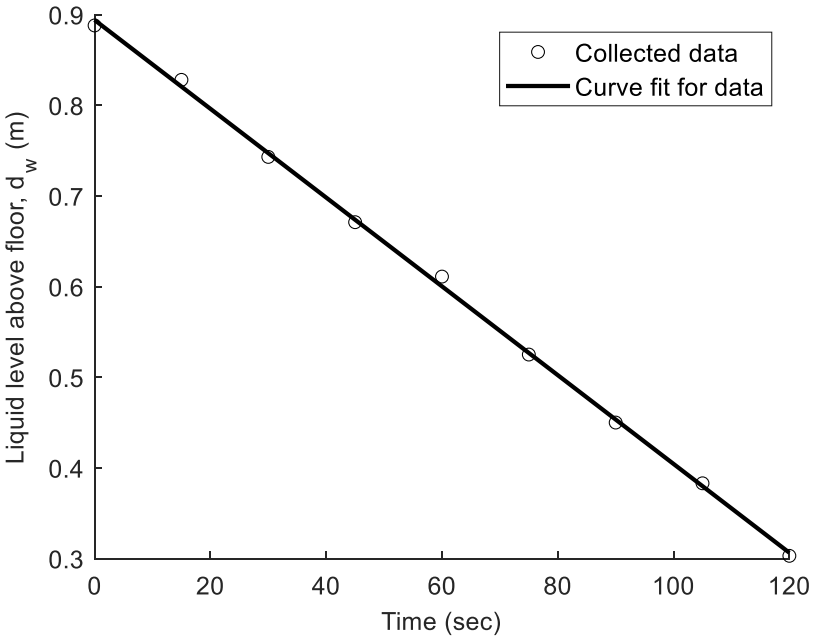

Figure 61: Ragged Lake - pump two: liquid level in the wet-well during pumping.

Akerley Boulevard

Summary Information

Table 36: Akerley Boulevard site information, part one of two.

Site: Akerley Boulevard	
Test date (DD/MM/YYYY)	31/10/2006
Pipe material	Ductile iron, PVC, stainless steel
Pipe age (years)	38/18*
Water temperature (°C)	16.4
Wet-well area (m^2)	13.69
Average inflow (m^3/s)	$2.476*10^{-3}$
Characteristic curve – head (m) / flowrate (m^3/s)	$36.6670-240.6767*Q^{0.9003}$

*Station upgraded after initial installation

Table 37: Akerley Boulevard site information, part two of two.

Site: Akerley Boulevard			
	Parameter	**Pump 1**	**Pump 2**
	Lowest static head (m)	16.949	16.937
	Highest static head (m)	17.385	17.364
	Pumping time (sec)	240	230
Segment 1	Diameter (mm)	150	150
	Minor losses (-)	6.643	6.643
	Length (m)	11.845	11.845
Segment 2	Diameter (mm)	200	200
	Minor losses (-)	1.612	1.612
	Length (m)	51.883	51.883
Segment 3	Diameter (mm)	191	191
	Minor losses (-)	1.000	1.000
	Length (m)	632.272	632.272

*Forcemains leave station attached to pumps separately until approximately 75 meters, recombining into existing single forcemain.

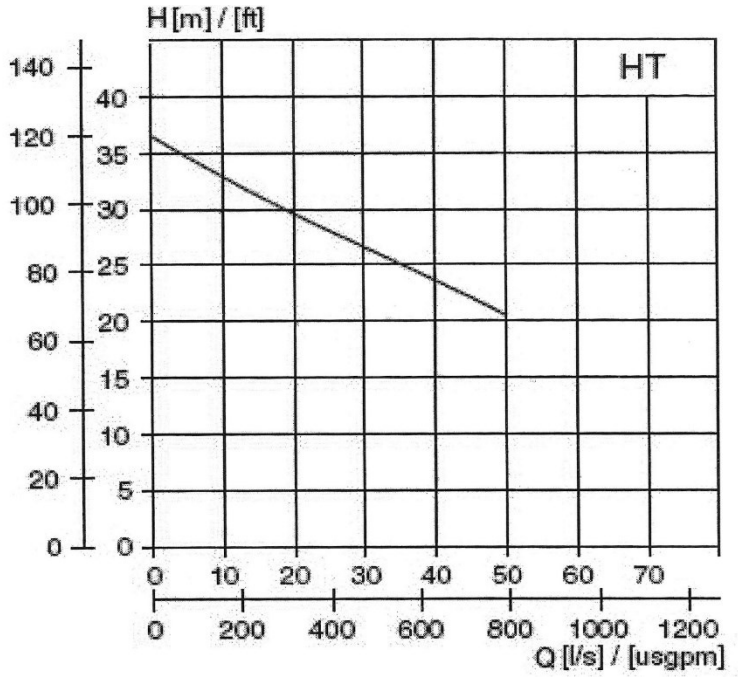

Figure 62: Characteristic curve for the pumps at Akerley Boulevard as provided by manufacturer (Xylem Inc., undated).

Inflow Information

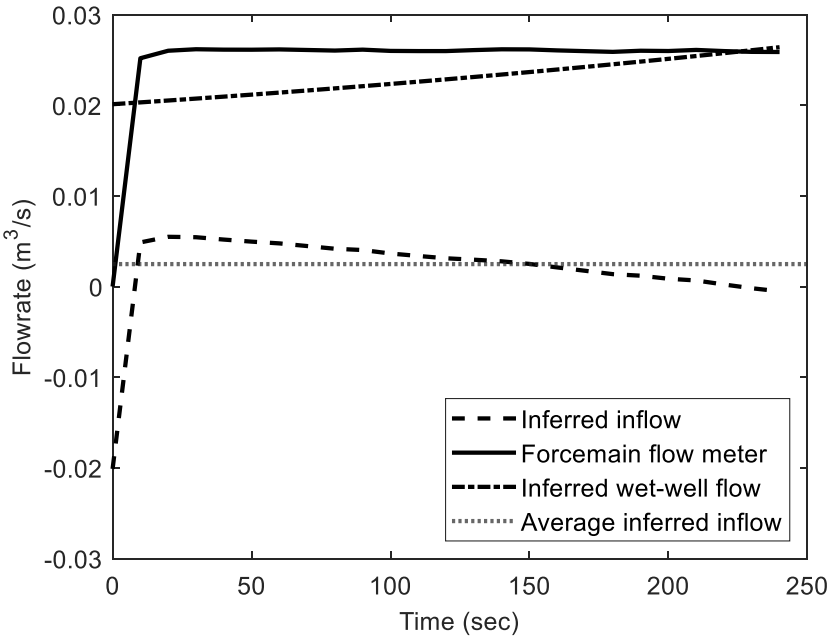

Figure 63: Akerley Boulevard: inference of inflow rate utilizing flow meter and liquid level monitoring.

Akerley Boulevard – Pump 1

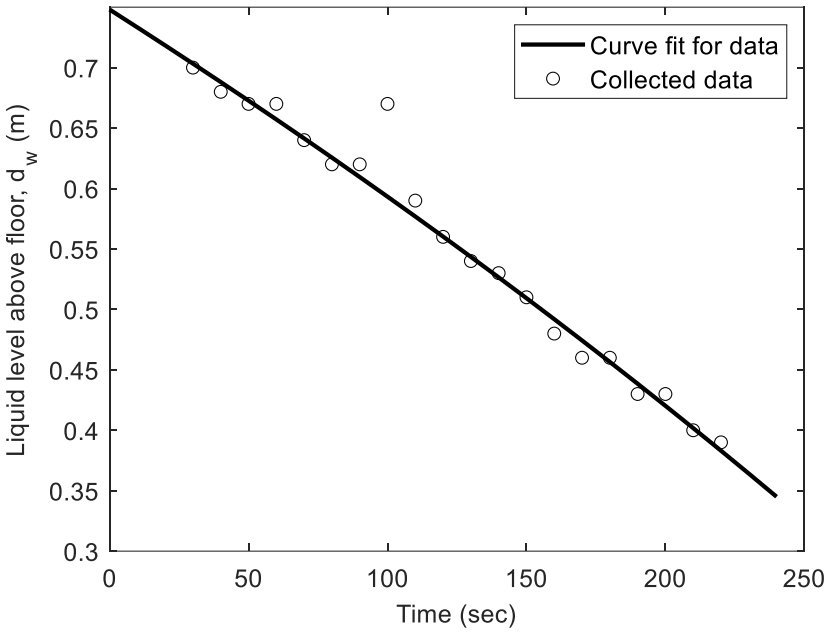

Figure 64: Akerley Boulevard - pump one: liquid level in the wet-well during pumping.

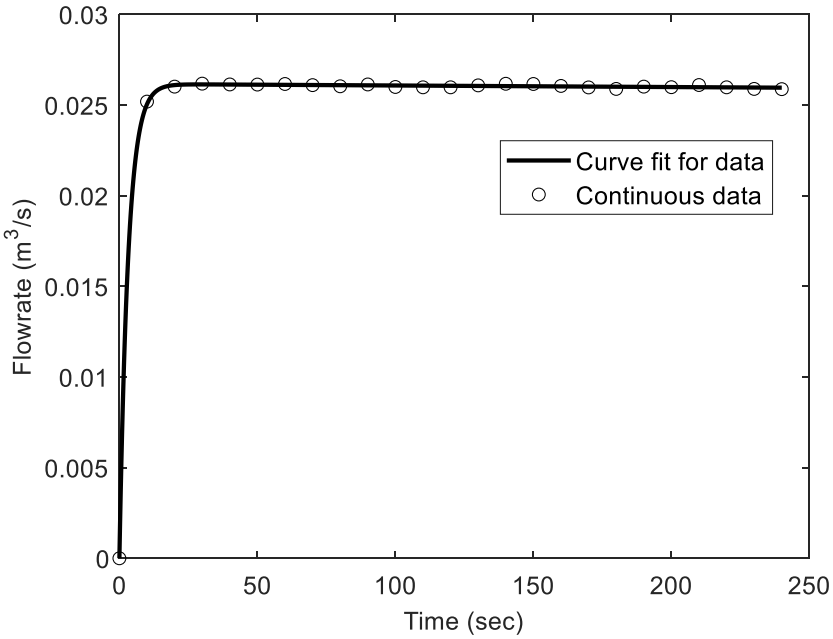

Figure 65: Akerley Boulevard - pump two: flow meter data for flow rate through the forcemain.

Akerley Boulevard – Pump 2

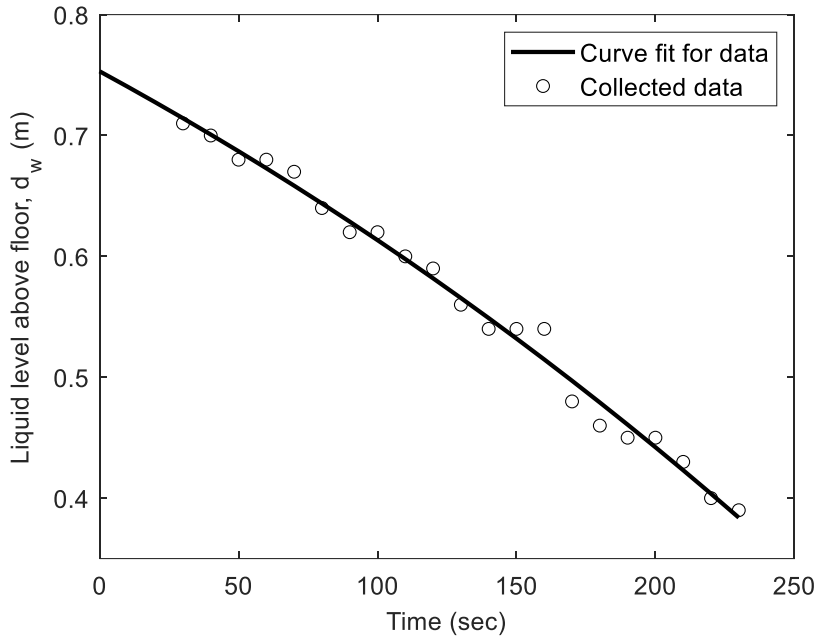

Figure 66: Akerley Boulevard - pump two: liquid level in the wet-well during pumping.

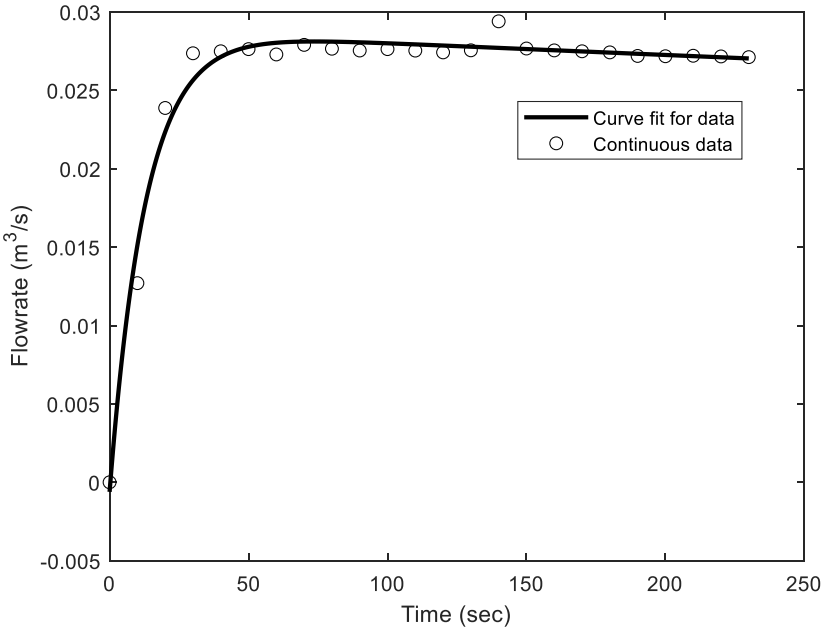

Figure 67: Akerley Boulevard - pump two: flow meter data for flow rate through the forcemain.

Melville Cove

Summary Information

Table 38: Melville Cove site information, part one of two.

Site: Melville Cove	
Test Date (DD/MM/YYYY)	26/10/2006
Pipe Material	Ductile Iron
Pipe Age (Years)	40
Water Temperature (°C)	10
Wet-well Area (m^2)	23.6
Average Inflow (m^3/s)	$6.5*10^{-3}$
Characteristic curve – Head (m) / Flowrate (m^3/s)	$51.1428-637.4320*Q^{1.2604}$

Table 39: Melville Cove site information, part two of two.

Site: Melville Cove			
	Parameter	**Pump 1**	**Pump 2**
	Lowest static head (m)	31.859	31.723
	Highest static head (m)	32.221	32.212
	Pumping time (sec)	270	240
Segment 1	Diameter (mm)	203	203
	Minor losses (-)	3.459	2.927
	Length (m)	2.825	2.825
Segment 2	Diameter (mm)	252	252
	Minor losses (-)	3.392	4.43
	Length (m)	74.22	80.72

*Inside diameter of the last segment could not be measured due to the outlet not being accessible. Assumed installation inside diameter noted in drawings.

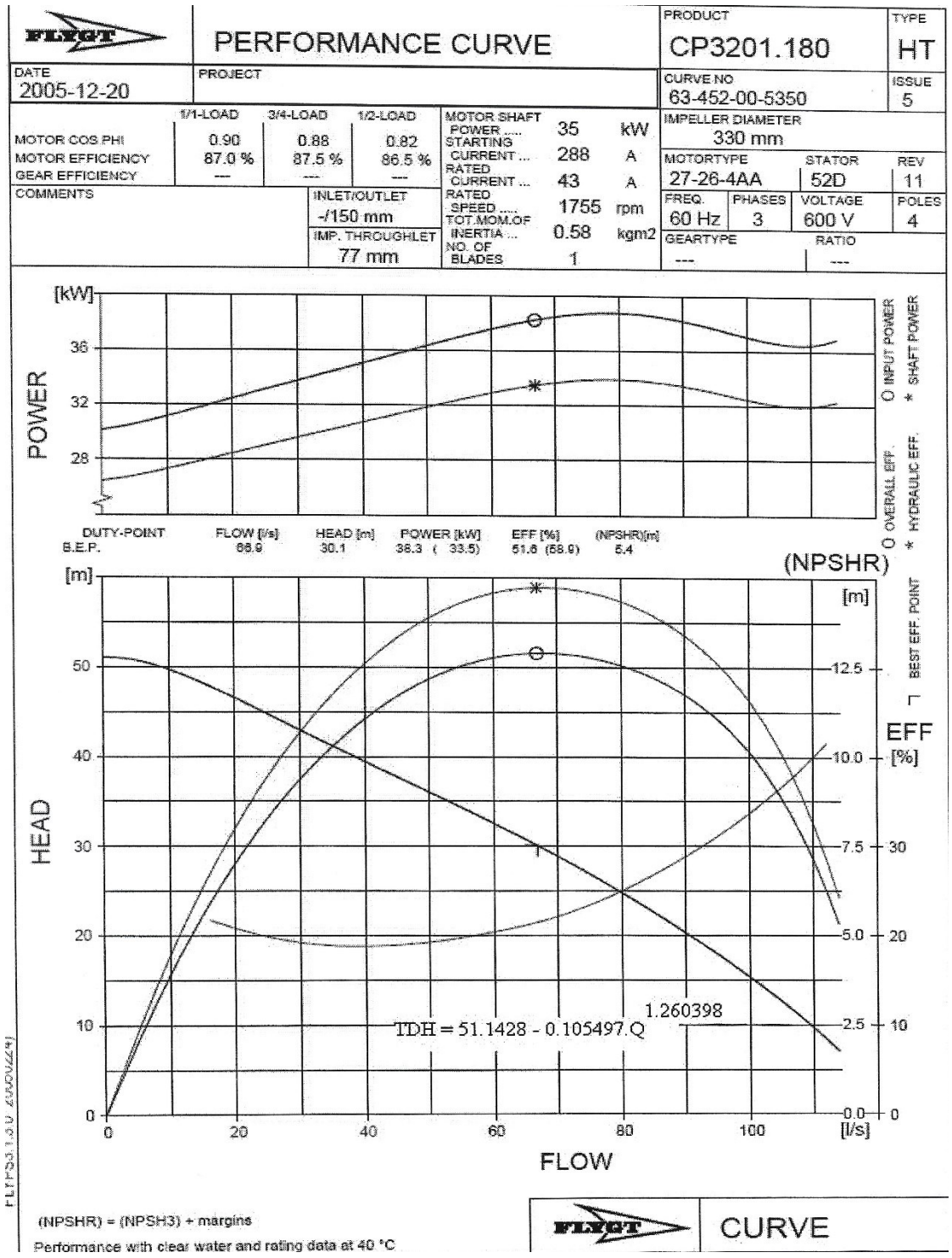

Figure 68: Characteristic curves for the pumps at Melville Cove as provided by manufacturer (Xylem Inc., undated).

Inflow Information

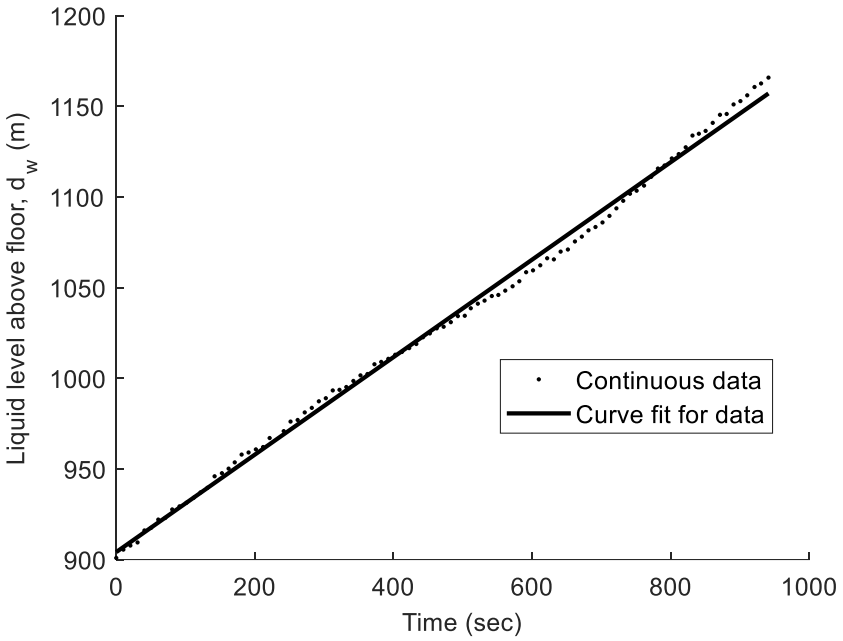

Figure 69: Melville Cove - pump one: liquid level in the wet-well during while the pump is offline.

Melville Cove – Pump 1

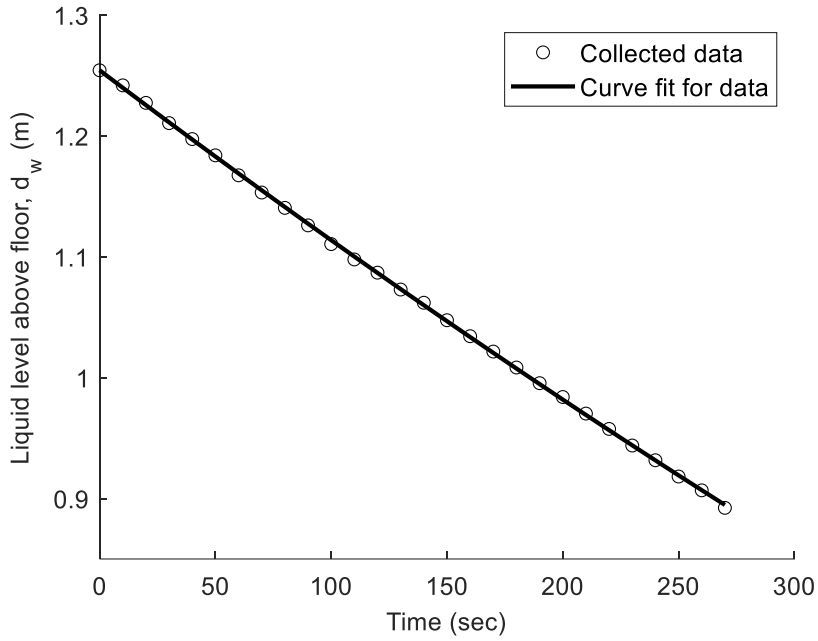

Figure 70: Melville Cove - pump one: liquid level in the wet-well during pumping.

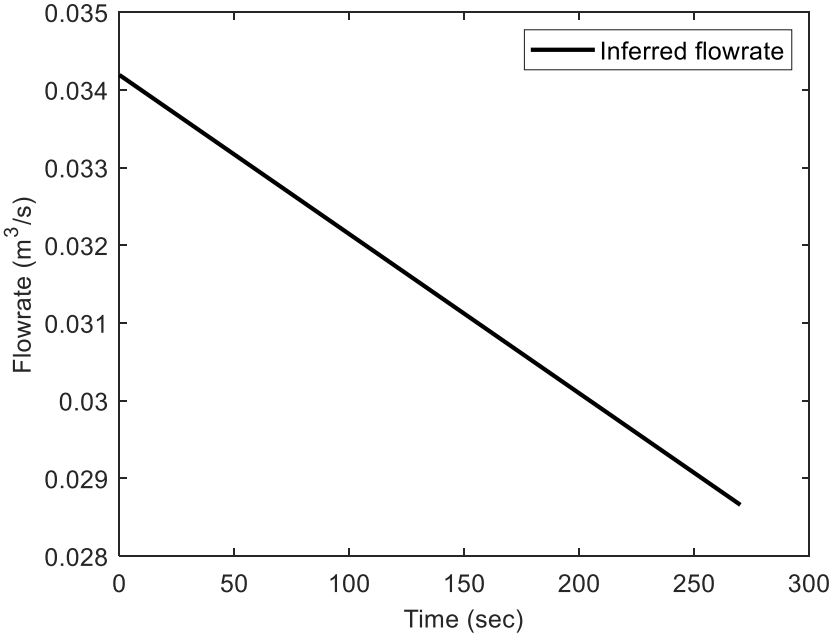

Figure 71: Melville Cove - pump one: inferred forcemain flowrate as determined by liquid level monitoring and wet-well geometry.

Melville Cove – Pump 2

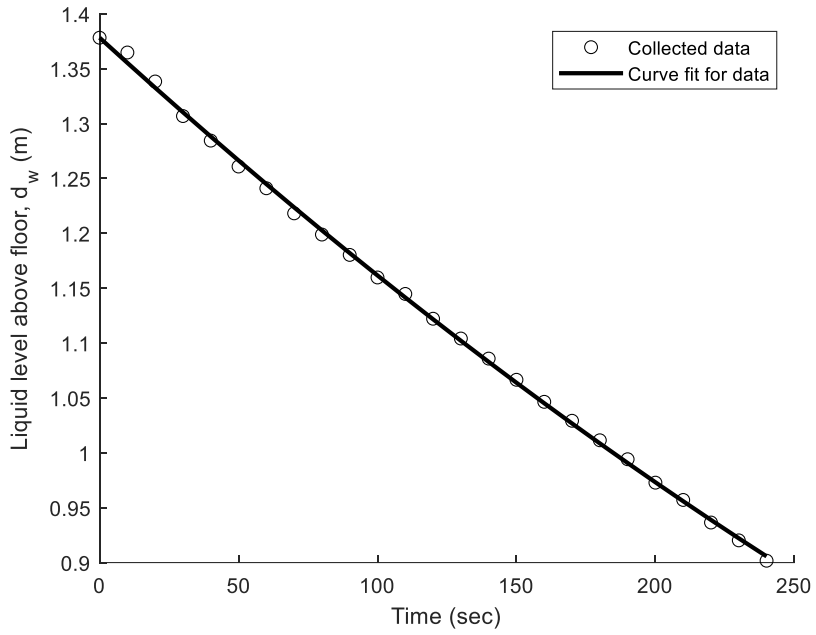

Figure 72: Melville Cove – pump two: liquid level in the wet-well during pumping.

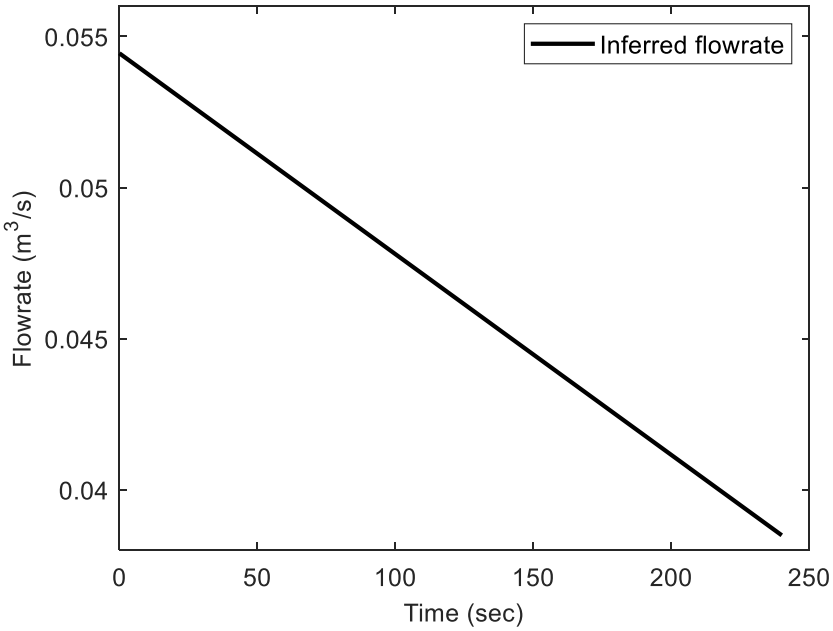

Figure 73: Melville Cove - pump two: inferred forcemain flowrate as determined by liquid level monitoring and wet-well geometry.

Appendix B - Four Sites Considered - Simulations, and Inferential Work

Table 40: Example calculations for the naïve interpretation of hydraulic resistance utilizing Trinity Lane pump one information.

Variable	Calculation* **
$Q_{well_{avg}}\left(\frac{m^3}{s}\right)$	Let the working datum be at the bottom of the active volume and the static total head be controlled by the static suction head such that: $Q_{well_{avg}} = \frac{(h_{ss_{start}} - h_{ss_{end}})A}{t_{naive}}$ $Q_{well_{avg}} = \frac{\left((H_{ST_{max}} - H_{ST_{min}}) - 0\right)A}{t_{naive}}$ $Q_{well_{avg}} = \frac{((12.632 - 12.296) - 0)4.524}{120}$ $Q_{well_{avg}} = 0.01267\frac{m^3}{s}$
$Q_{avg}\left(\frac{m^3}{s}\right)$	$Q_{avg} = Q_{well_{avg}} + Q_{in_{avg}}$ $Q_{avg} = 0.01267 + 0$ $Q_{avg} = 0.01267\frac{m^3}{s}$
$H_{avg}\ (m)$	$H_{p_{avg}} = c - aQ_{avg}^{b}$ $H_{p_{avg}} = 25.978 - 249.4735(0.01267)^{0.815269}$ $H_{p_{avg}} = 18.909\ m$

$h_{ss_{avg}}\ (m)$	Let the working datum be at the bottom of the active volume and the static total head be controlled by the static suction head such that: $$h_{ss_{avg}} = \frac{h_{ss_{start}} + h_{ss_{end}}}{2}$$ $$h_{ss_{avg}} = \frac{\left(H_{ST_{max}} - H_{ST_{min}}\right) + 0}{2}$$ $$h_{ss_{avg}} = \frac{(12.632 - 12.296) + 0}{2}$$ $$h_{ss_{avg}} = \ 0.1678\ m$$
$D_{p_{eq}}\ (m)$	Assume $f_{eq}\ \approx f_1 \approx f_2$: $$\therefore \frac{L_{eq}}{D_{p_{eq}}^5} = \sum_i^I \frac{L_i}{D_{p_i}^5}$$ $$\left(\frac{L_{eq}}{\sum_i^I \frac{L_i}{D_{p_i}^5}}\right)^{\frac{1}{5}} = D_{p_{eq}}$$ $$\left(\frac{289}{\frac{11.524}{0.1^5} + \frac{270.633}{0.106^5}}\right)^{\frac{1}{5}} = D_{p_{eq}}$$ $$D_{p_{eq}} = 0.1057\ m$$
$A_{p_{eq}}\ (m^2)$	$$A_{p_{eq}} = \pi\left(\frac{D_{p_{eq}}}{2}\right)^2$$ $$A_{p_{eq}} = \pi\left(\frac{0.1057}{2}\right)^2$$ $$A_{p_{eq}} = \ 0.00878\ m^2$$

$h_{l_{avg}}\,(m)$	Let the working datum be at the bottom of the active volume and the static total head be controlled by the static suction head such that: $h_{l_{avg}} = H_{p_{avg}} - H_{ST_{avg}}$ $h_{l_{avg}} = H_{p_{avg}} - (h_{ds} - h_{ss_{avg}})$ $h_{l_{avg}} = H_{p_{avg}} - (H_{ST_{max}} - h_{ss_{avg}})$ $h_{l_{avg}} = H_{p_{avg}} - (H_{ST_{max}} - h_{ss_{avg}})$ $h_{l_{avg}} = 18.909 - (12.632 - 0.1678)$ $h_{l_{avg}} = 6.444\ m$
$h_{v_{avg}}\,(m)$	$h_{v_{avg}} = \frac{U_{avg}^2}{2g}$ $h_{v_{avg}} = \frac{1.4401^2}{2g}$ $h_{v_{avg}} = 0.1057\ m$
$h_{m_{avg}}\,(m)$	$h_{m_{avg}} = K h_v$ $h_{m_{avg}} = (6.396)(0.1057)$ $h_{m_{avg}} = 0.6761\ m$
$h_{f_{avg}}\,(m)$	$h_{f_{avg}} = h_{l_{avg}} - h_{m_{avg}}$ $h_{f_{avg}} = 6.444 - 0.6761$ $h_{f_{avg}} = 5.768\ m$

$C_{HW\,naive}\ (-)$	$$C_{HW\,naive} = \frac{(8)\left(2^{\frac{13}{50}}\right)Q_{avg}}{D_{p_{eq}}^{\frac{263}{100}}(0.849)(\pi)\left(\frac{h_{f_{avg}}}{L_{eq}}\right)^{\frac{27}{50}}}$$ $$C_{HW\,naive} = \frac{8 * 2^{\frac{13}{50}}(0.01267)}{\left(0.1057^{\frac{263}{100}}\right)(0.849)(\pi)\left(\frac{5.768}{289}\right)^{\frac{27}{50}}}$$ $$C_{HW_{naive}} = 136.739\ (-)$$
$f_{avg_{naive}}\ (-)$	Utilizing Swamee-Jain: $$f_{naive_{avg}} = \frac{h_{f_{avg}}}{\frac{L_{eq}}{D_{p_{eq}}}h_{v_{avg}}}$$ $$f_{naive_{avg}} = \frac{5.768}{\frac{289}{0.1057}(0.1057)}$$ $$f_{naive_{avg}} = 0.01996\ (-)$$
Re_{avg}	$$Re_{avg} = \frac{U_{avg}D_{p_{eq}}}{\nu}$$ $$Re_{avg} = \frac{(1.4401)(0.1057)}{1.243 * 10^{-6}}$$ $$Re_{avg} = 122460.6\ (-)$$

$(\epsilon_{SJ})_{naive}\ (mm)$	Utilizing Swamee-Jain: $$f = \frac{0.25}{\log10\left(\frac{\frac{\varepsilon_{SJ_{naive}}}{D_{p_{eq}}}}{3.71} + \frac{5.74}{Re_{avg}^{0.9}}\right)^2}$$ $$f_{naive_{avg}} = \frac{0.25}{\log10\left(\frac{\frac{\varepsilon_{SJ_{naive}}}{D_{p_{eq}}}}{3.71} + \frac{5.74}{Re_{avg}^{0.9}}\right)^2}$$ $$0.01996 = \frac{0.25}{\log10\left(\frac{\frac{\varepsilon_{SJ_{naive}}}{0.1057}}{3.71} + \frac{5.74}{122460.6^{0.9}}\right)^2}$$ $$\varepsilon_{SJ_{naive}} = 0.0656\ \text{mm}$$

*All values shown are truncated but calculations were done with values of 10^{-16} floating point accuracy.

** Information required for calculations is presented for each site and pump. For calculations shown, information can be found in Table 30, Table 32, and Table 33. The calculations are the same for each pump at each site.

Trinity Lane

Trinity Lane – Pump 1

Table 41: Supplementary outputs for Trinity Lane pump one.

Output of interest	Value
$(\epsilon_{SJ})_{naive}\ (mm)$	0.0656
$(\epsilon_{DB})_{naive}\ (mm)$	0.179
$(\epsilon_{SJ})_{model}\ (mm)$	0.0206
$\frac{(\epsilon_{SJ})_{model}}{(\epsilon_{SJ})_{naive}}\ (-)$	0.314
$\epsilon_0\ (mm)$	0.0015
$\frac{(\epsilon_{SJ})_{model}}{D_p}\ (-)$	0.000195
$\frac{(\epsilon_{SJ})_{naive}}{D_p}\ (-)$	0.000621
$f_{avg_{naive}}\ (-)$	0.0204
$f_{avg_{model}}\ (-)$	0.0185
$f_{max_{model}}(-)$	0.0408
$f_{min_{model}}\ (-)$	0.0183
$Re_{avg_{model}}\ (-)$	122000
$Re_{max_{model}}\ (-)$	126000
$C_{HW\,model}(-)$	146
$C_{HW\,naive}\ (-)$	137

Output of interest	Value
$\frac{C_{HW_{model}}}{C_{HW_{naive}}}\ (-)$	1.06
$C_{HW_0}\ (-)$	150
$t_a\ , SJ\ model\ (s)$	19.5
$t_a^{\#}, analytical\ (s)$	20.7
Energy Usage – Time of Test $(kWhr)$	0.153
Energy Usage – Initial Implementation $(kWhr)$	0.15
Cost – Time of Test $\left(\frac{\$}{year}\right)$	522
Cost – Initial Implementation $\left(\frac{\$}{year}\right)$	512
Cost Ratio	1.02
$Q_{avg}\ \left(\frac{m^3}{s}\right)$	0.0126
$U_{avg}\ \left(\frac{m}{s}\right)$	1.44
$h_{v_{avg}}\ (m)$	0.106
$h_{f_{avg}}\ (m)$	5.77
$h_{m_{avg}}\ (m)$	0.676
$h_{ss_{avg}}\ (m)$	0.168
$H_{avg}\ (m)$	18.9
$h_{a_{max}}\ (m)$	13.7
$\frac{V_{pipe}}{V}\ (-)$	1.63

The calculations for the naïve interpretation results can be determined as stated in Table 40.

Trinity Lane – Pump 2

Table 42: Supplementary outputs for Trinity Lane pump two.

Output of interest	Value
$\left(\epsilon_{SJ}\right)_{naive}\ (mm)$	0.323
$(\epsilon_{DB})_{naive}\ (mm)$	0.464
$\left(\epsilon_{SJ}\right)_{model}\ (mm)$	0.221
$\frac{\left(\epsilon_{SJ}\right)_{model}}{\left(\epsilon_{SJ}\right)_{naive}}\ (-)$	0.684
$\epsilon_0\ (mm)$	0.0015
$\frac{\left(\epsilon_{SJ}\right)_{model}}{D_p}\ (-)$	0.00209
$\frac{\left(\epsilon_{SJ}\right)_{naive}}{D_p}\ (-)$	0.00306
$f_{avg_{naive}}\ (-)$	0.0277
$f_{avg_{model}}\ (-)$	0.0255
$f_{max_{model}}(-)$	0.0429
$f_{min_{model}}\ (-)$	0.0254
$Re_{avg_{model}}\ (-)$	111000
$Re_{max_{model}}\ (-)$	114000
$C_{HW\,model}(-)$	123
$C_{HW\,naive}\ (-)$	117
$\frac{C_{HW\,model}}{C_{HW\,naive}}\ (-)$	1.05

Output of interest	Value
$C_{HW_0}\ (-)$	150
$t_a\ , SJ\ model\ (s)$	17.4
$t_a, analytical\ (s)$	14.5
Energy Usage – Time of Test $(kWhr)$	0.151
Energy Usage – Initial Implementation $(kWhr)$	0.136
Cost – Time of Test $\left(\frac{\$}{year}\right)$	516
Cost – Initial Implementation $\left(\frac{\$}{year}\right)$	466
Cost Ratio	1.11
$Q_{avg}\ \left(\frac{m^3}{s}\right)$	0.0115
$U_{avg}\ \left(\frac{m}{s}\right)$	1.31
$h_{v_{avg}}\ (m)$	0.0868
$h_{f_{avg}}\ (m)$	6.42
$h_{m_{avg}}\ (m)$	0.555
$h_{ss_{avg}}\ (m)$	0.152
$H_{avg}\ (m)$	19.5
$h_{a_{max}}\ (m)$	13.7
$\frac{V_{pipe}}{V}\ (-)$	1.8

The calculations for the naïve interpretation results can be determined as stated in Table 40.

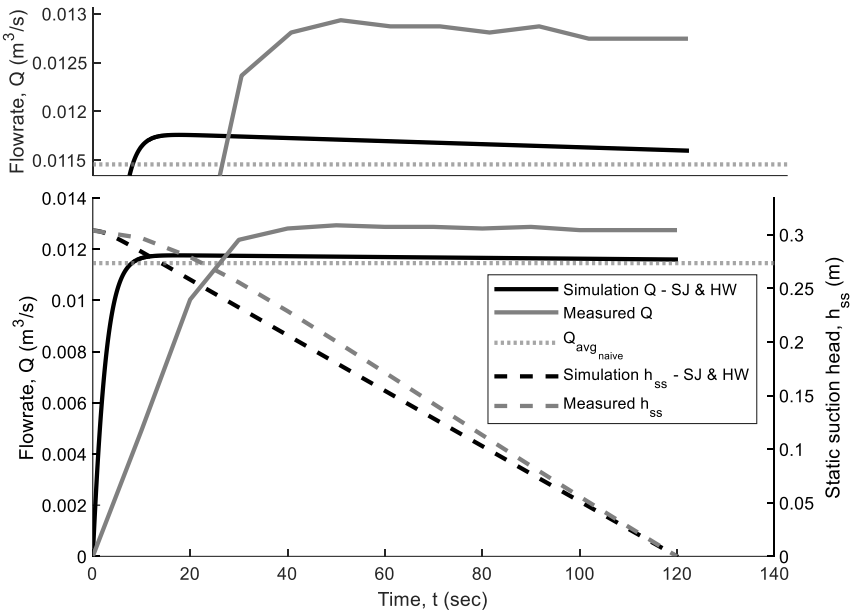

Figure 74: Trinity Lane - pump two: the detailed model simulation flow rate (left axis) through the forcemain and static suction head (right axis) in the wet-well with respect to time. Continuously collected data and the naïvely determined flow rate are also presented.

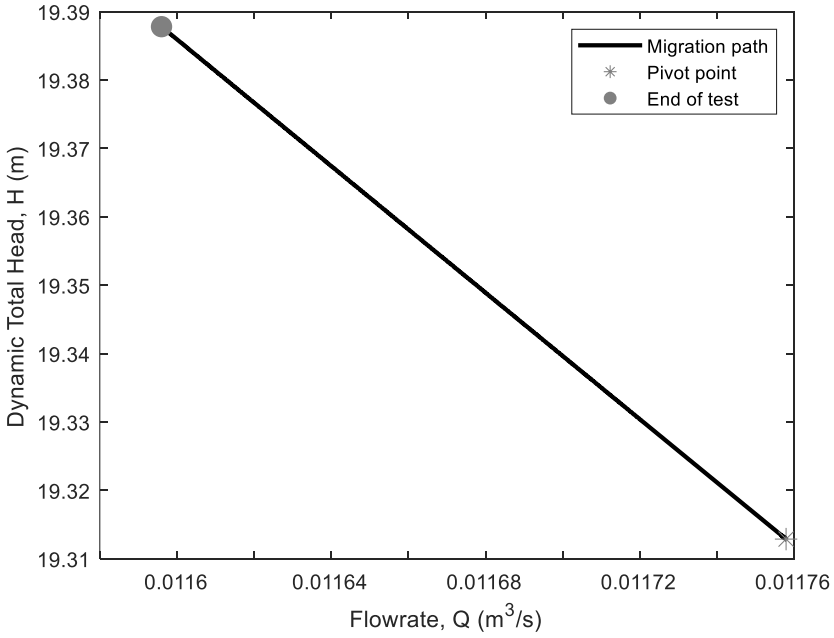

Figure 75: Trinity Lane - pump two: migration of the operating point after flow establishment for the simulation. The pivot point is the point at which flow establishment has completed.

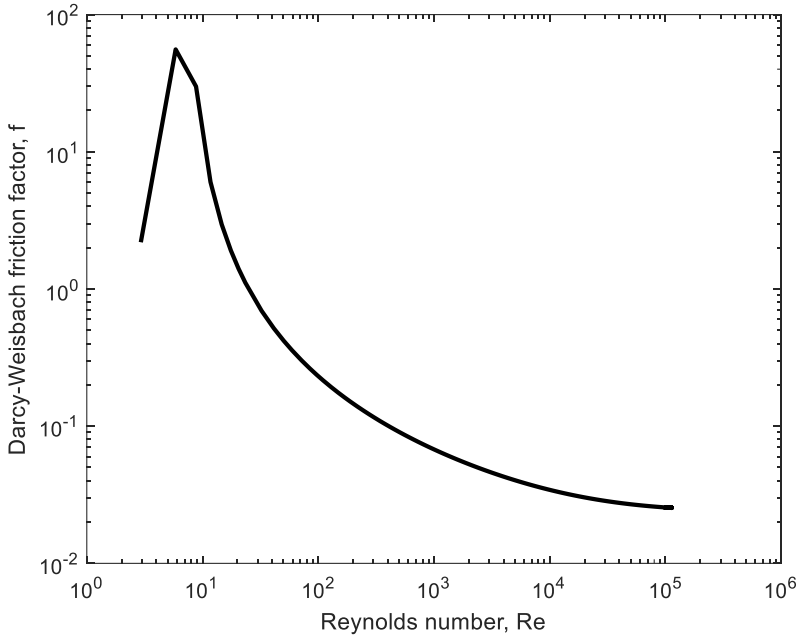

Figure 76: Trinity Lane - pump two: Darcy-Weisbach friction factor migration for the detailed model simulation (log-log scale). The friction loss method utilized is Swamee-Jain.

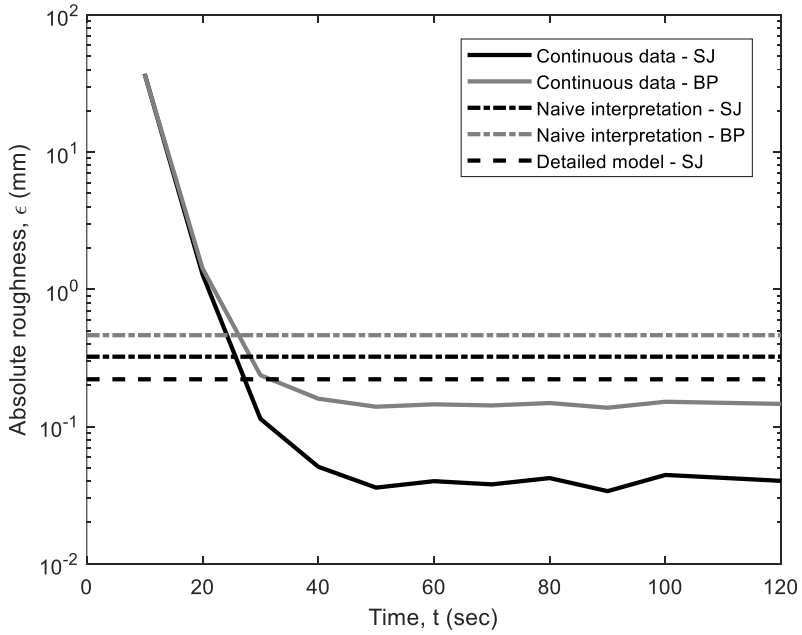

Figure 77: Trinity Lane - pump two: different techniques for inferring roughness. Two friction loss methods are present, Swamee-Jain (SJ) and Brkić-Praks (BP). Continuous data was utilized at every sampling time to infer roughness for comparison. The naïve interpretations and the detailed modelling inferences are time-invariant.

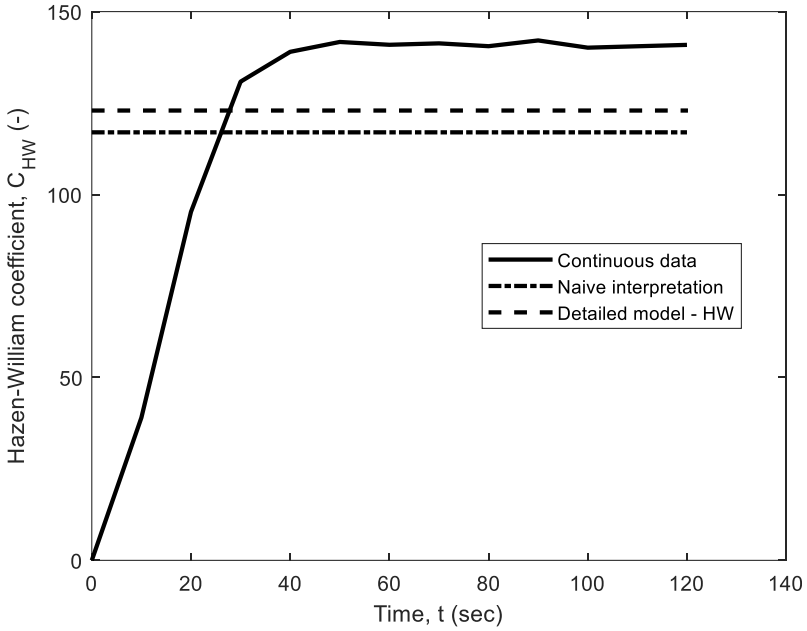

Figure 78: Trinity Lane – pump two: different techniques for inferring the Hazen-Williams coefficient. The naïve interpretation and the detailed model inferences are time-invariant. Continuous data was utilized at every sampling time to infer the coefficient for comparison.

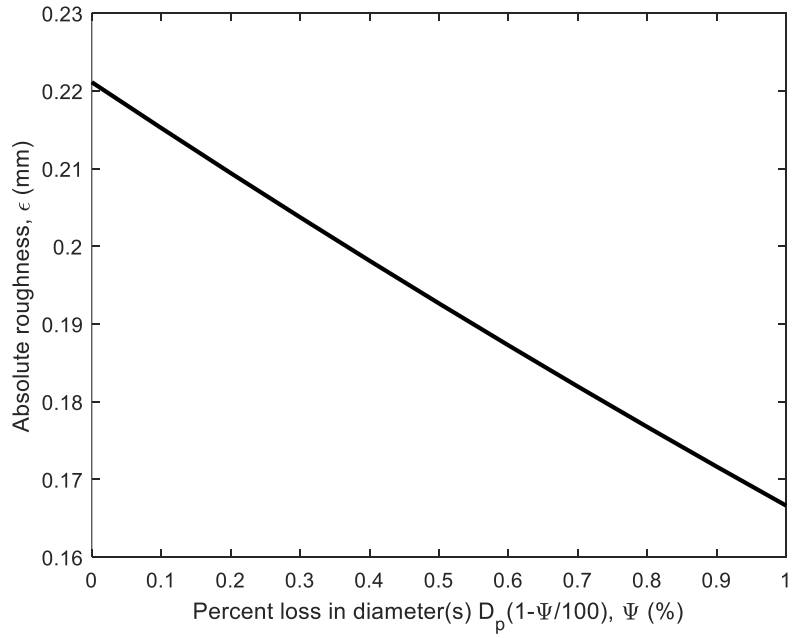

Figure 79: Trinity Lane - pump two: the effect of reducing the assumed internal diameter(s) of the forcemain on the inference of roughness with detailed modelling. Reductions were percent losses of the diameter(s) starting at the initial commissioning sizes.

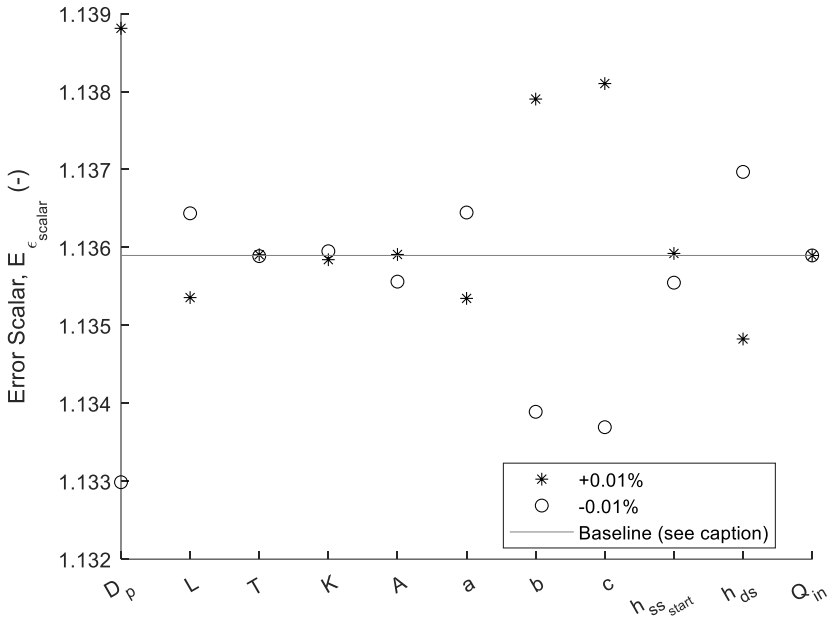

Figure 80: Trinity Lane - pump two: one-at-a-time sensitivity analysis for the inference of roughness due to perturbations of relevant parameters in the detailed model (along the abscissa). The analysis utilized a non-segmented forcemain. The baseline is the error scalar due to having a non-segmented forcemain (instead of a segmented one) in the detailed model.

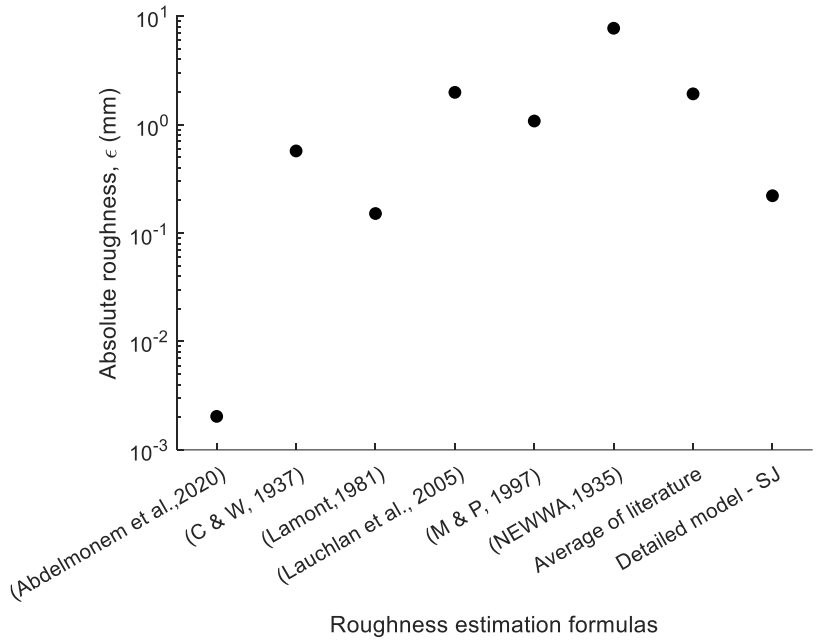

Figure 81: Trinity Lane – pump two: inference of roughness with respect to forcemain characteristics and water quality indices provided in the literature. The relevant authors cited along the abscissa.

Ragged Lake

Ragged Lake – Pump 1

Table 43: Supplementary outputs for Ragged Lake pump one.

Output of interest	Value
$\left(\epsilon_{SJ}\right)_{naive}\ (mm)$	36.6
$(\epsilon_{DB})_{naive}\ (mm)$	36
$\left(\epsilon_{SJ}\right)_{model}\ (mm)$	34.4
$\frac{\left(\epsilon_{SJ}\right)_{model}}{\left(\epsilon_{SJ}\right)_{naive}}\ (-)$	0.94
$\epsilon_0\ (mm)$	0.25
$\frac{\left(\epsilon_{SJ}\right)_{model}}{D_p}\ (-)$	0.139
$\frac{\left(\epsilon_{SJ}\right)_{naive}}{D_p}\ (-)$	0.148
$f_{avg_{naive}}\ (-)$	0.128
$f_{avg_{model}}\ (-)$	0.123
$f_{max_{model}}(-)$	0.129
$f_{min_{model}}\ (-)$	0.123
$Re_{avg_{model}}\ (-)$	232000
$Re_{max_{model}}\ (-)$	235000
$C_{HW\,model}(-)$	48.9

Output of interest	Value
$C_{HW_{naive}}\ (-)$	47.8
$\frac{C_{HW_{model}}}{C_{HW_{naive}}}\ (-)$	1.02
$C_{HW_0}\ (-)$	140
$t_a\ , SJ\ model\ (s)$	9.6
$t_a, analytical\ (s)$	10.4
Energy Usage – Time of Test $(kWhr)$	1.24
Energy Usage – Initial Implementation $(kWhr)$	0.914
Cost – Time of Test $\left(\frac{\$}{year}\right)$	4250
Cost – Initial Implementation $\left(\frac{\$}{year}\right)$	3120
Cost Ratio	1.36
$Q_{avg}\ \left(\frac{m^3}{s}\right)$	0.0584
$U_{avg}\ \left(\frac{m}{s}\right)$	1.21
$h_{v_{avg}}\ (m)$	0.0745
$h_{f_{avg}}\ (m)$	18.1
$h_{m_{avg}}\ (m)$	0.813
$h_{ss_{avg}}\ (m)$	0.311
$H_{avg}\ (m)$	33.4
$h_{a_{max}}\ (m)$	37
$\frac{V_{pipe}}{V}\ (-)$	3.29

The calculations for the naïve interpretation results can be determined as stated in Table 40.

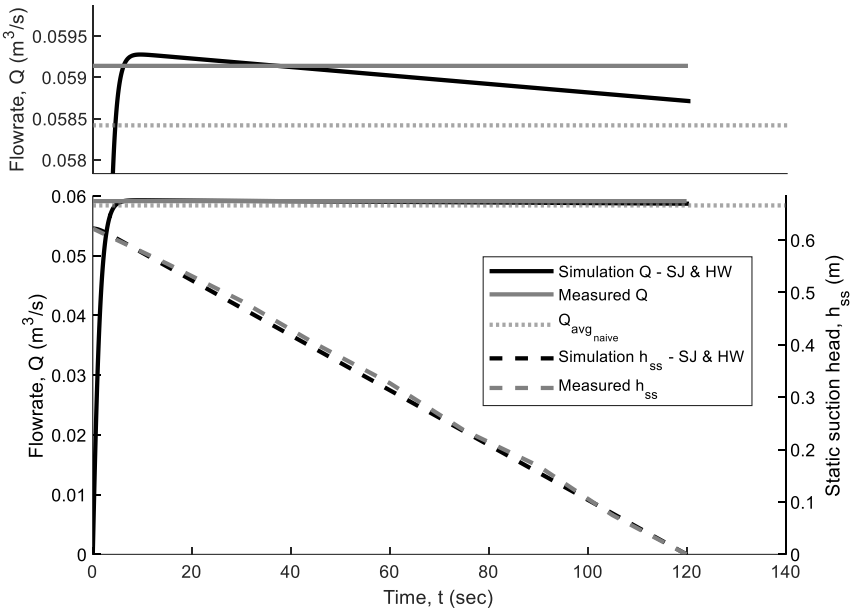

Figure 82: Ragged Lake - pump one: the detailed model simulation flow rate (left axis) through the forcemain and static suction head (right axis) in the wet-well with respect to time. Continuously collected data and the naïvely determined flow rate are also presented.

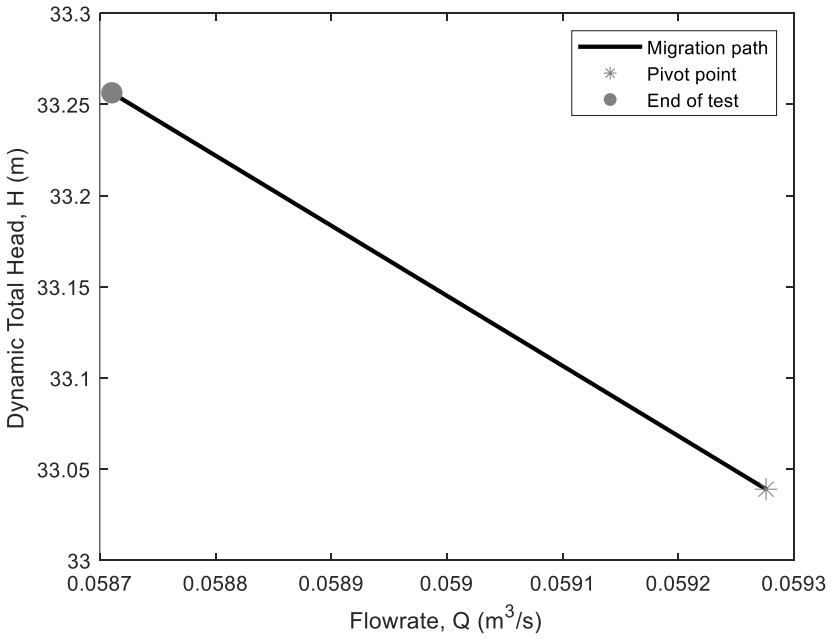

Figure 83: Ragged Lake - pump one: migration of the operating point after flow establishment for the simulation. The pivot point is the point at which flow establishment has completed.

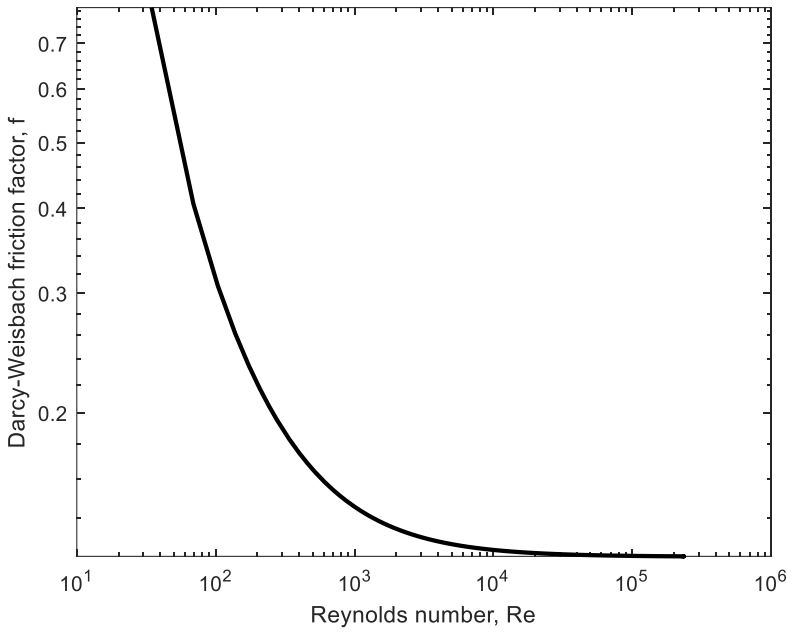

Figure 84: Ragged Lake - pump one: Darcy-Weisbach friction factor migration for the detailed model simulation (log-log scale). The friction loss method utilized is Swamee-Jain.

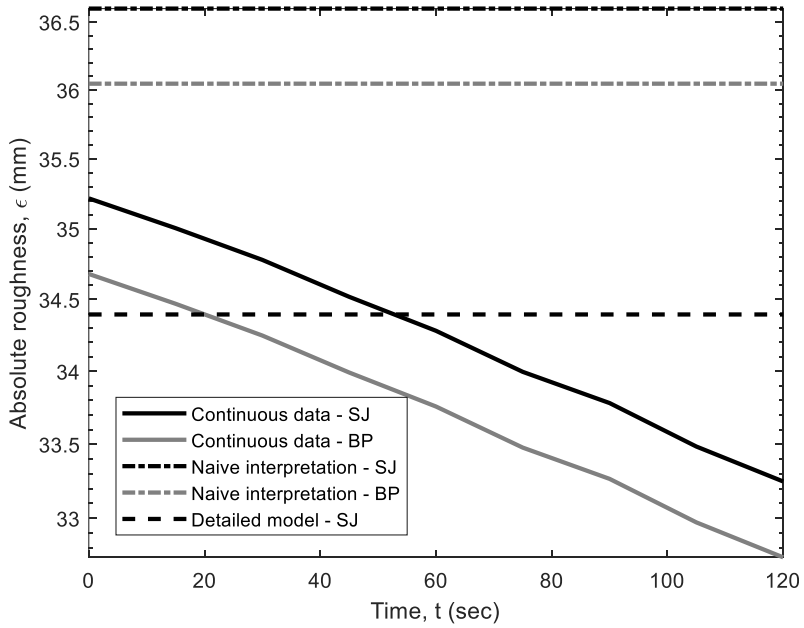

Figure 85: Ragged Lake - pump one: different techniques for inferring roughness. Two friction loss methods are present, Swamee-Jain (SJ) and Brkić-Praks (BP). Continuous data was utilized at every sampling time to infer roughness for comparison. The naïve interpretations and the detailed modelling inferences are time-invariant.

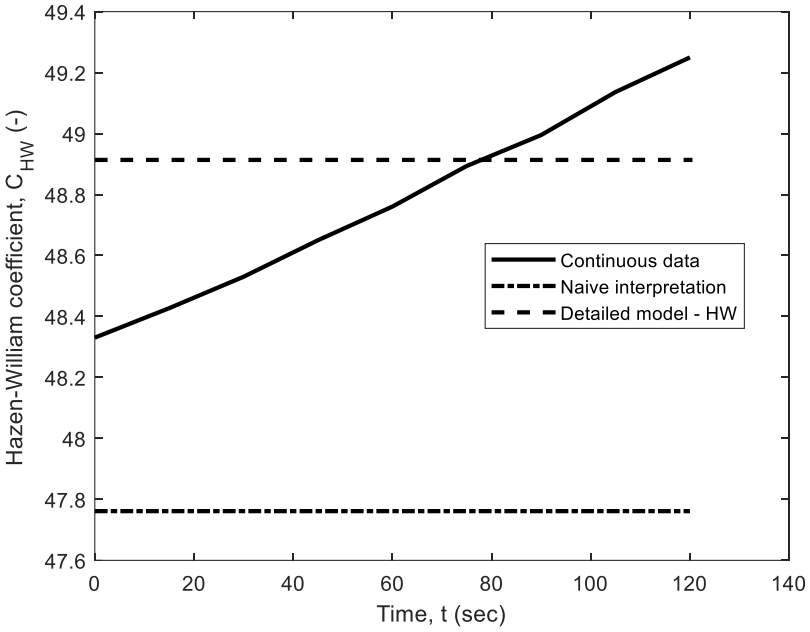

Figure 86: Ragged Lake – pump one: different techniques for inferring the Hazen-Williams coefficient. The naïve interpretation and the detailed model inferences are time-invariant. Continuous data was utilized at every sampling time to infer the coefficient for comparison.

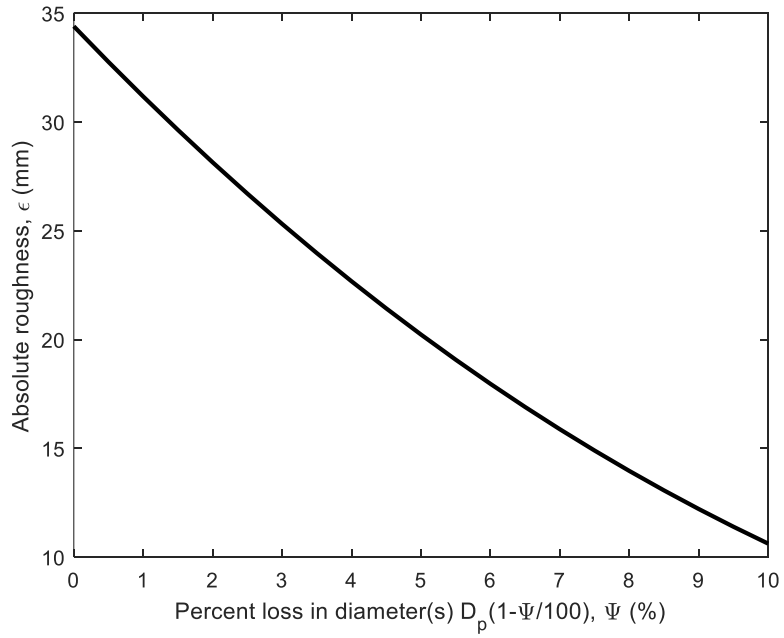

Figure 87: Ragged Lake - pump one: the effect of reducing the assumed internal diameter(s) of the forcemain on the inference of roughness with detailed modelling. Reductions were percent losses of the diameter(s) starting at the initial commissioning sizes.

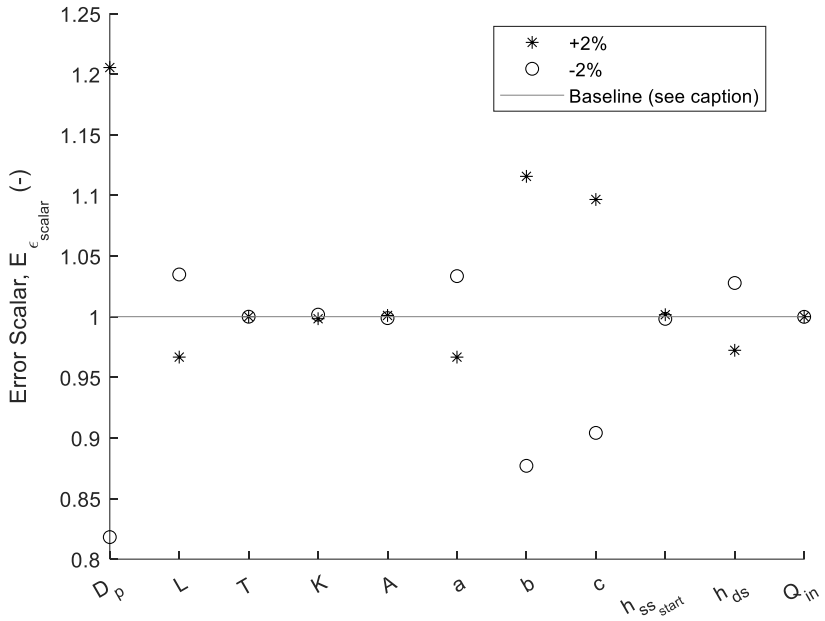

Figure 88: Ragged Lake - pump one: one-at-a-time sensitivity analysis for the inference of roughness due to perturbations of relevant parameters in the detailed model (along the abscissa). The analysis utilized a non-segmented forcemain. The baseline is the error scalar due to having a non-segmented forcemain (instead of a segmented one) in the detailed model.

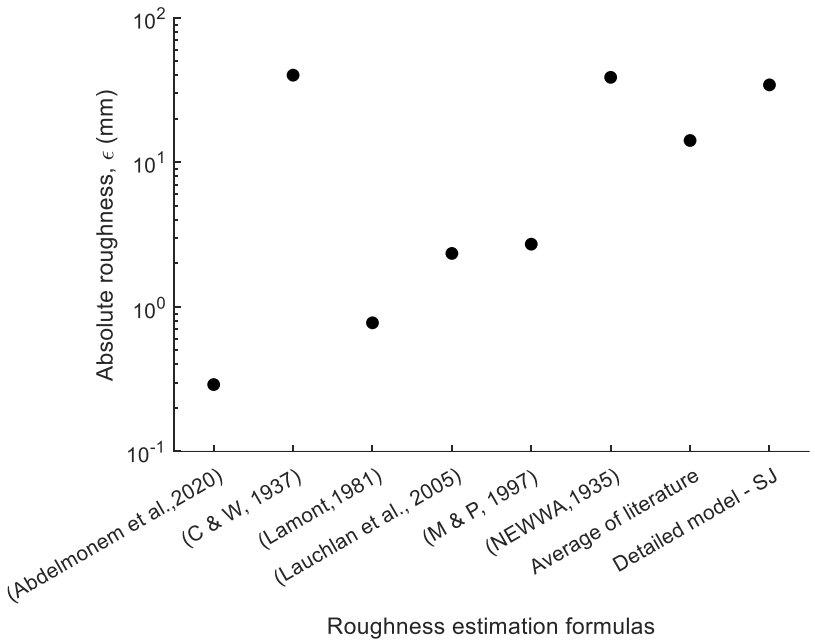

Figure 89: Ragged Lake – pump one: inference of roughness with respect to forcemain characteristics and water quality indices provided in the literature. The relevant authors cited along the abscissa.

Ragged Lake – Pump 2

Table 44: Supplementary outputs for Ragged Lake pump two.

Output of interest	Value
$(\epsilon_{SJ})_{naive}\ (mm)$	49.4
$(\epsilon_{DB})_{naive}\ (mm)$	48.7
$(\epsilon_{SJ})_{model}\ (mm)$	47
$\frac{(\epsilon_{SJ})_{model}}{(\epsilon_{SJ})_{naive}}\ (-)$	0.952
$\epsilon_0\ (mm)$	0.25
$\frac{(\epsilon_{SJ})_{model}}{D_p}\ (-)$	0.19
$\frac{(\epsilon_{SJ})_{naive}}{D_p}\ (-)$	0.199
$f_{avg_{naive}}\ (-)$	0.155
$f_{avg_{model}}\ (-)$	0.15
$f_{max_{model}}(-)$	0.156
$f_{min_{model}}\ (-)$	0.15
$Re_{avg_{model}}\ (-)$	218000
$Re_{max_{model}}\ (-)$	221000
$C_{HW\,model}(-)$	44.1
$C_{HW\,naive}\ (-)$	43.2
$\frac{C_{HW\,model}}{C_{HW\,naive}}\ (-)$	1.02

Output of interest	Value
$C_{HW_0}\ (-)$	140
$t_a\ , SJ\ model\ (s)$	9.05
$t_a, analytical\ (s)$	9.67
Energy Usage – Time of Test $(kWhr)$	1.24
Energy Usage – Initial Implementation $(kWhr)$	0.865
Cost – Time of Test $\left(\frac{\$}{year}\right)$	4220
Cost – Initial Implementation $\left(\frac{\$}{year}\right)$	2960
Cost Ratio	1.43
$Q_{avg}\ \left(\frac{m^3}{s}\right)$	0.055
$U_{avg}\ \left(\frac{m}{s}\right)$	1.14
$h_{v_{avg}}\ (m)$	0.066
$h_{f_{avg}}\ (m)$	19.5
$h_{m_{avg}}\ (m)$	0.72
$h_{ss_{avg}}\ (m)$	0.293
$H_{avg}\ (m)$	34.7
$h_{a_{max}}\ (m)$	37
$\frac{V_{pipe}}{V}\ (-)$	3.5

The calculations for the naïve interpretation results can be determined as stated in Table 40.

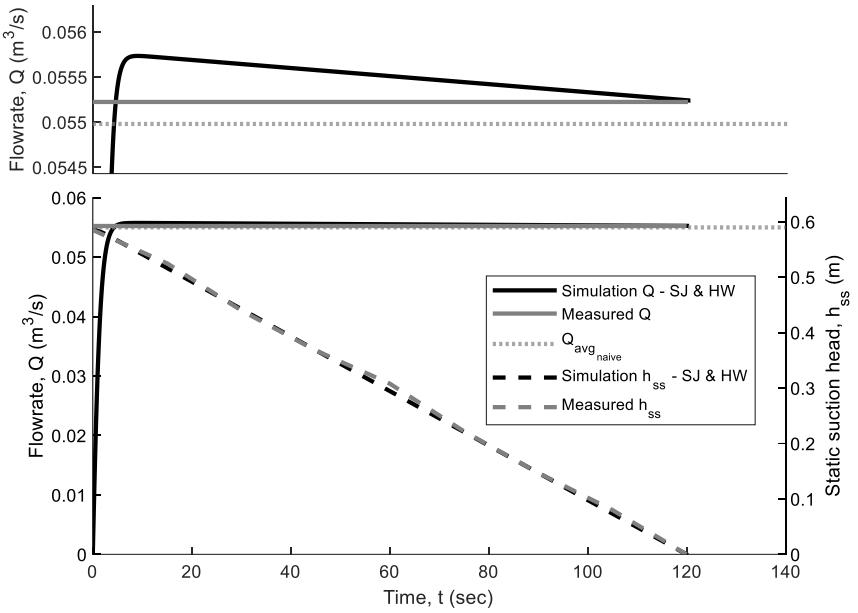

Figure 90: Ragged Lake - pump two: the detailed model simulation flow rate (left axis) through the forcemain and static suction head (right axis) in the wet-well with respect to time. Continuously collected data and the naïvely determined flow rate are also presented.

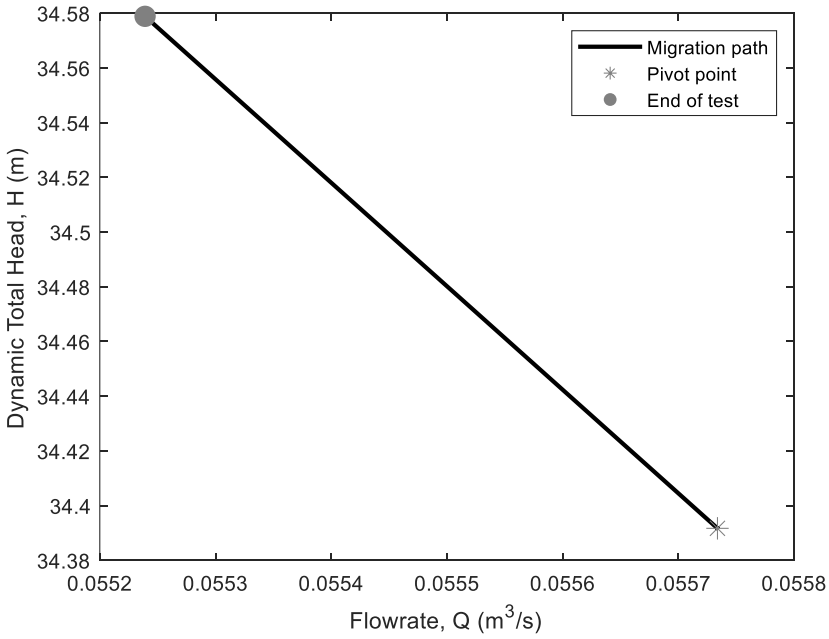

Figure 91: Ragged Lake- pump two: migration of the operating point after flow establishment for the simulation. The pivot point is the point at which flow establishment has completed.

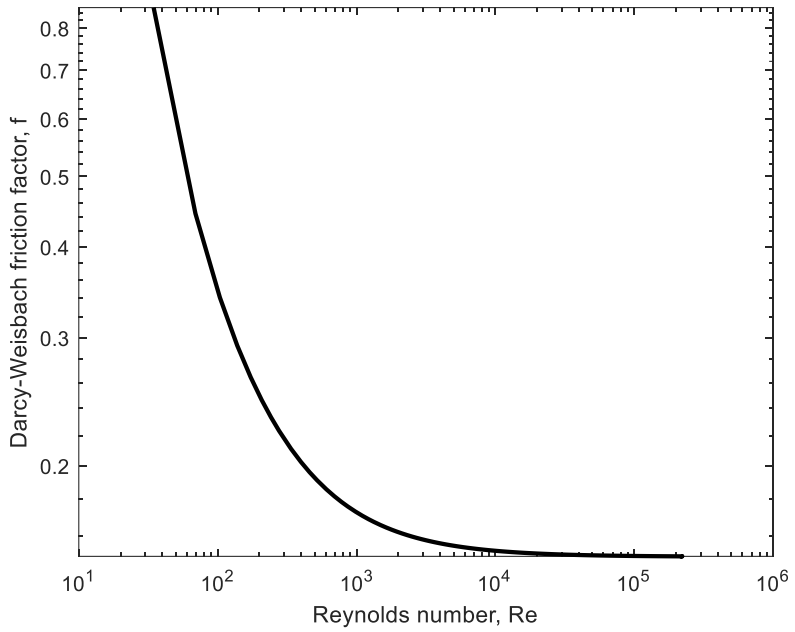

Figure 92: Ragged Lake - pump two: Darcy-Weisbach friction factor migration for the detailed model simulation (log-log scale). The friction loss method utilized is Swamee-Jain.

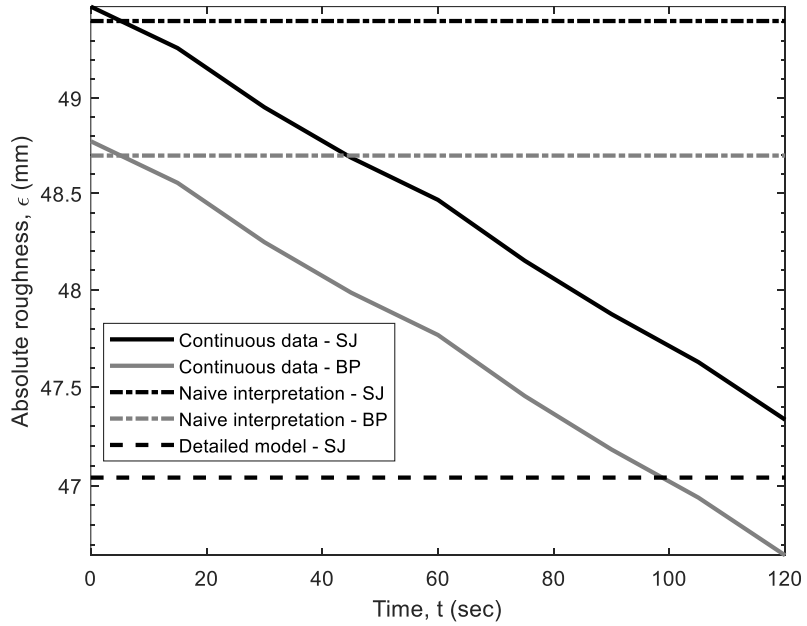

Figure 93: Ragged Lake – pump two: different techniques for inferring roughness. Two friction loss methods are present, Swamee-Jain (SJ) and Brkić-Praks (BP). Continuous data was utilized at every sampling time to infer roughness for comparison. The naïve interpretations and the detailed modelling inferences are time-invariant.

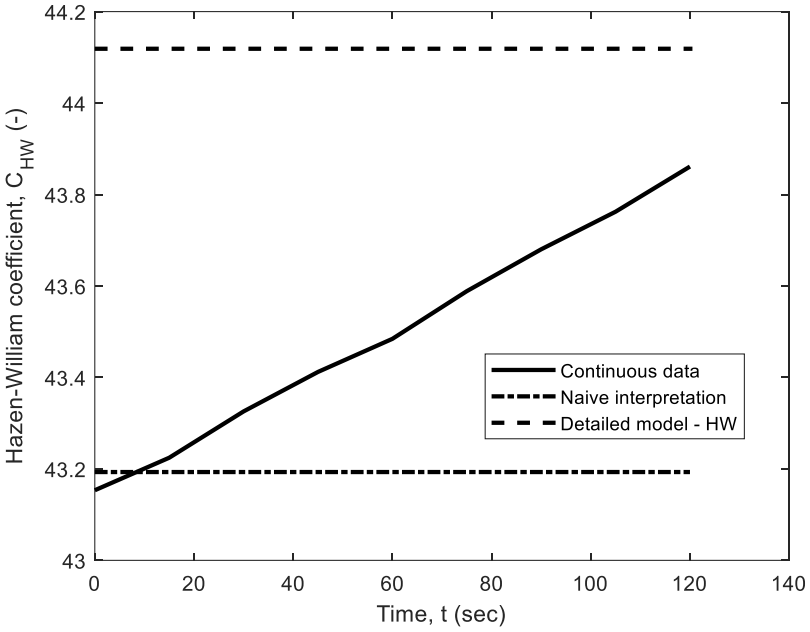

Figure 94: Ragged Lake – pump two: different techniques for inferring the Hazen-Williams coefficient. The naïve interpretation and the detailed model inferences are time-invariant. Continuous data was utilized at every sampling time to infer the coefficient for comparison.

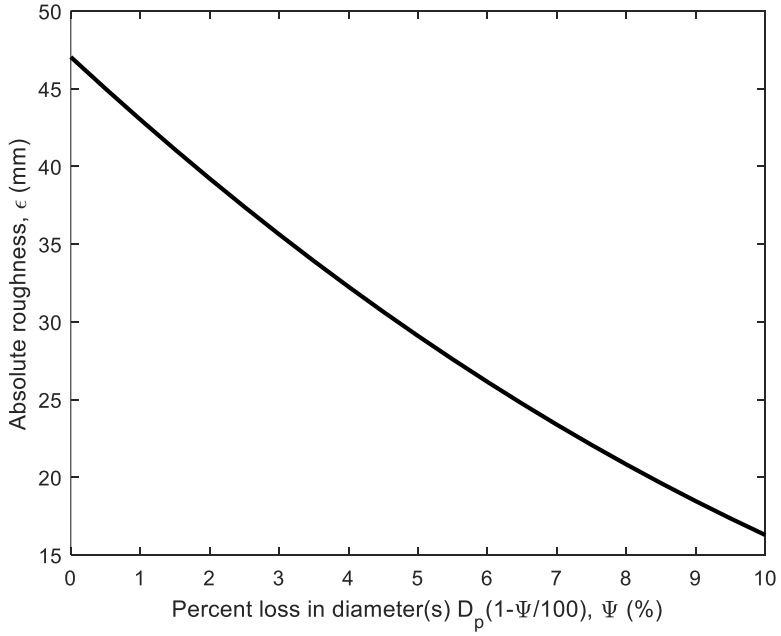

Figure 95: Ragged Lake - pump two: the effect of reducing the assumed internal diameter(s) of the forcemain on the inference of roughness with detailed modelling. Reductions were percent losses of the diameter(s) starting at the initial commissioning sizes.

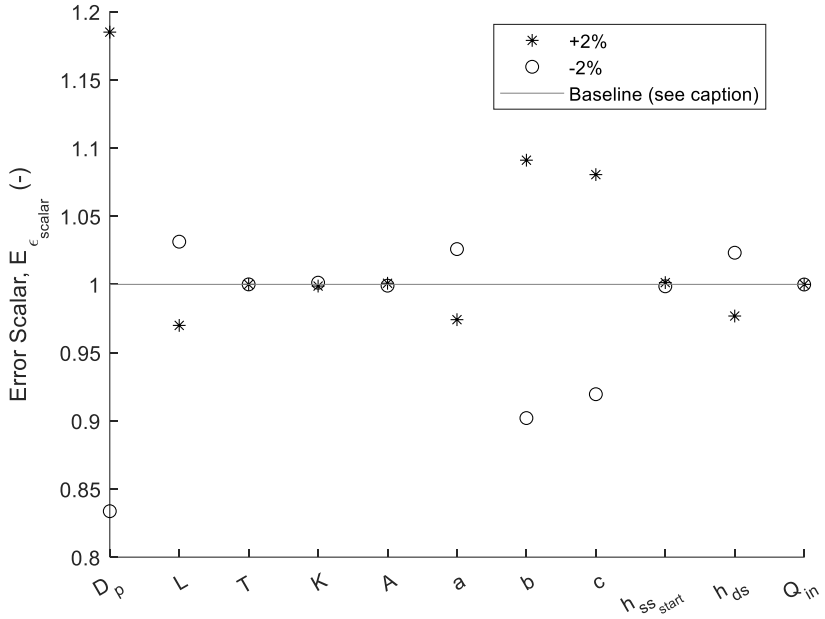

Figure 96: Ragged Lake – pump two: one-at-a-time sensitivity analysis for the inference of roughness due to perturbations of relevant parameters in the detailed model (along the abscissa). The analysis utilized a non-segmented forcemain. The baseline is the error scalar due to having a non-segmented forcemain (instead of a segmented one) in the detailed model.

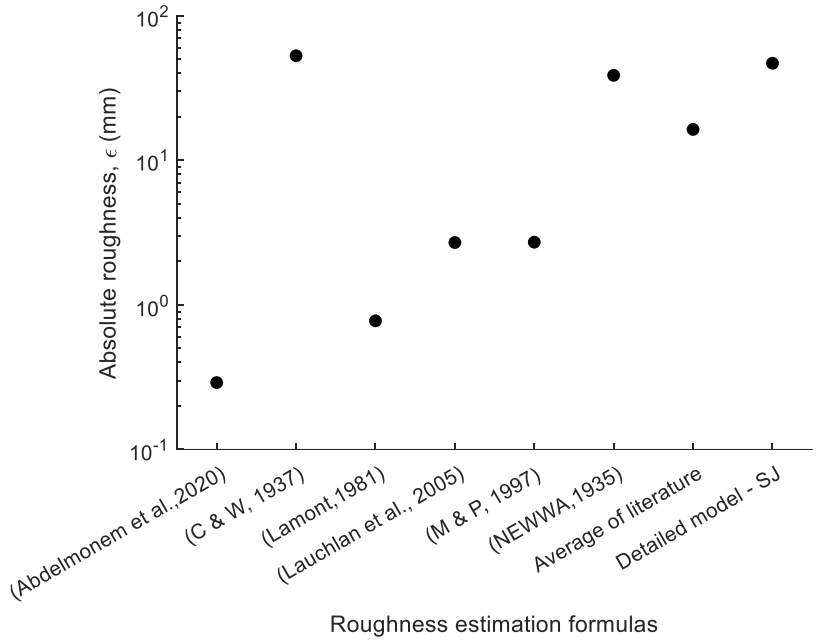

Figure 97: Ragged Lake – pump two: inference of roughness with respect to forcemain characteristics and water quality indices provided in the literature. The relevant authors cited along the abscissa.

Akerley Boulevard

Akerley Boulevard – Pump 1

Table 45: Supplementary outputs for Akerley Boulevard pump one.

Output of interest	Value
$\left(\epsilon_{SJ}\right)_{naive}\ (mm)$	8.53
$(\epsilon_{DB})_{naive}\ (mm)$	8.49
$\left(\epsilon_{SJ}\right)_{model}\ (mm)$	7.08
$\frac{\left(\epsilon_{SJ}\right)_{model}}{\left(\epsilon_{SJ}\right)_{naive}}\ (-)$	0.83
$\epsilon_0\ (mm)$	0.25
$\frac{\left(\epsilon_{SJ}\right)_{model}}{D_p}\ (-)$	0.0373
$\frac{\left(\epsilon_{SJ}\right)_{naive}}{D_p}\ (-)$	0.0449
$f_{avg_{naive}}\ (-)$	0.0683
$f_{avg_{model}}\ (-)$	0.0638
$f_{max_{model}}(-)$	0.0711
$f_{min_{model}}\ (-)$	0.0629
$Re_{avg_{model}}\ (-)$	155000
$Re_{max_{model}}\ (-)$	157000
$C_{HW\,model}(-)$	73.5
$C_{HW\,naive}\ (-)$	70.2

Output of interest	Value
$\frac{C_{HW_{model}}}{C_{HW_{naive}}}\ (-)$	1.05
$C_{HW_0}\ (-)$	140
$t_a\ , SJ\ model\ (s)$	20.6
$t_a, analytical\ (s)$	17
Energy Usage – Time of Test $(kWhr)$	0.773
Energy Usage – Initial Implementation $(kWhr)$	0.605
Cost – Time of Test $\left(\frac{\$}{year}\right)$	2640
Cost – Initial Implementation $\left(\frac{\$}{year}\right)$	2070
Cost Ratio	1.28
$Q_{avg}\ \left(\frac{m^3}{s}\right)$	0.0255
$U_{avg}\ \left(\frac{m}{s}\right)$	0.897
$h_{v_{avg}}\ (m)$	0.0411
$h_{f_{avg}}\ (m)$	10.3
$h_{m_{avg}}\ (m)$	0.38
$h_{ss_{avg}}\ (m)$	0.202
$H_{avg}\ (m)$	27.8
$h_{a_{max}}\ (m)$	19.8
$\frac{V_{pipe}}{V}\ (-)$	3.58

The calculations for the naïve interpretation results can be determined as stated in Table 40.

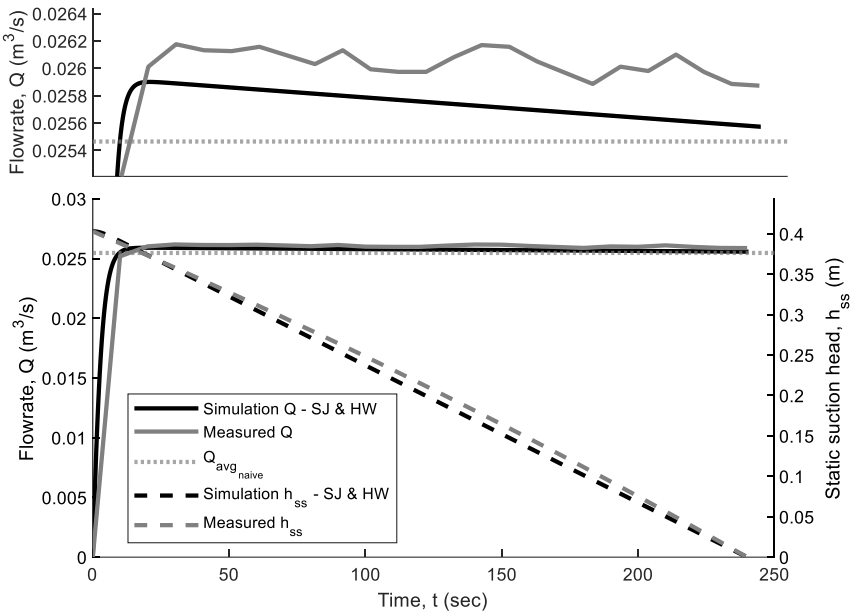

Figure 98: Akerley Boulevard - pump one: the detailed model simulation flow rate (left axis) through the forcemain and static suction head (right axis) in the wet-well with respect to time. Continuously collected data and the naïvely determined flow rate are also presented.

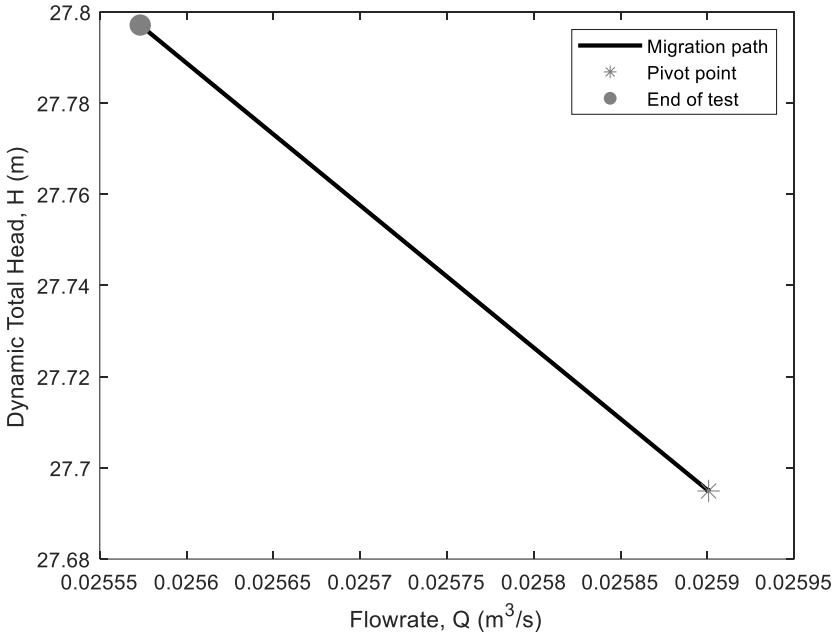

Figure 99: Akerley Boulevard - pump one: migration of the operating point after flow establishment for the simulation. The pivot point is the point at which flow establishment has completed.

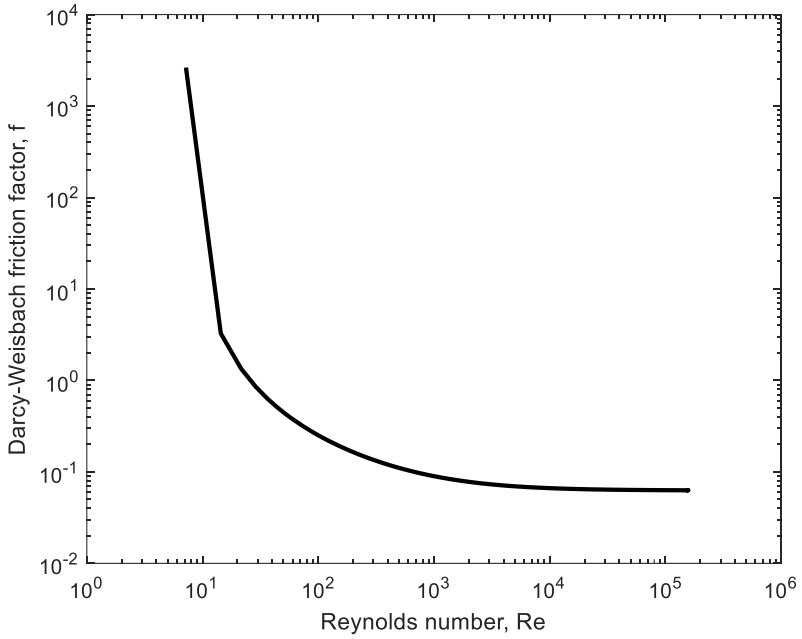

Figure 100: Akerley Boulevard - pump one: Darcy-Weisbach friction factor migration for the detailed model simulation (log-log scale). The friction loss method utilized is Swamee-Jain.

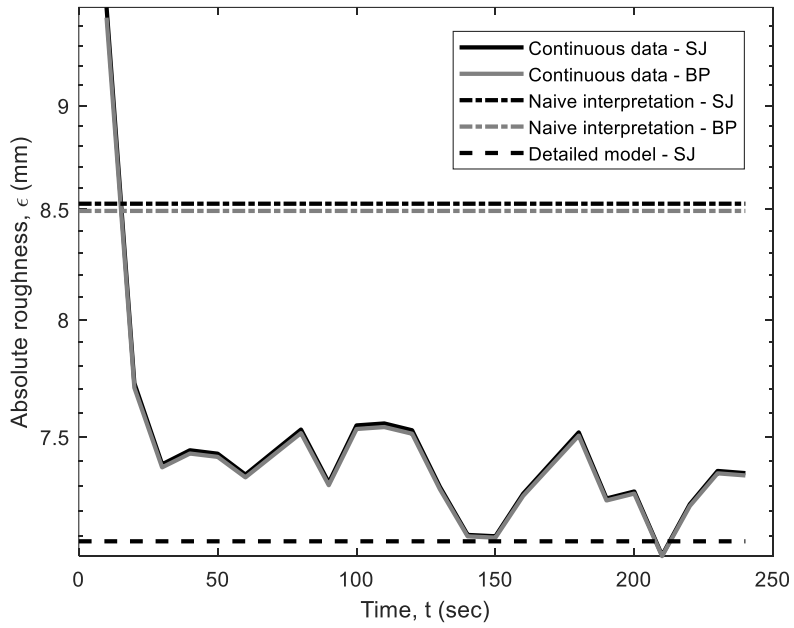

Figure 101: Akerley Boulevard - pump one: different techniques for inferring roughness. Two friction loss methods are present, Swamee-Jain (SJ) and Brkić-Praks (BP). Continuous data was utilized at every sampling time to infer roughness for comparison. The naïve interpretations and the detailed modelling inferences are time-invariant.

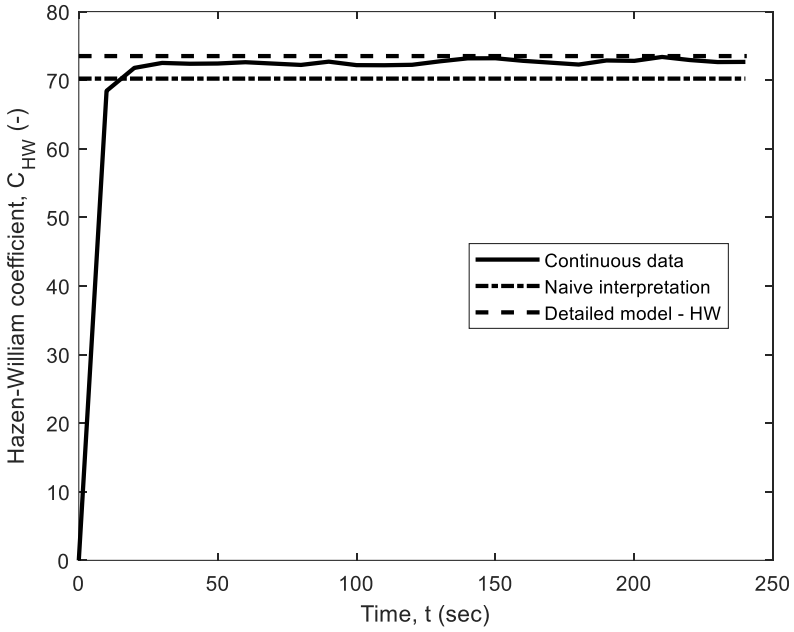

Figure 102: Akerley Boulevard - pump one: different techniques for inferring the Hazen-Williams coefficient. The naïve interpretation and the detailed model inferences are time-invariant. Continuous data was utilized at every sampling time to infer the coefficient for comparison.

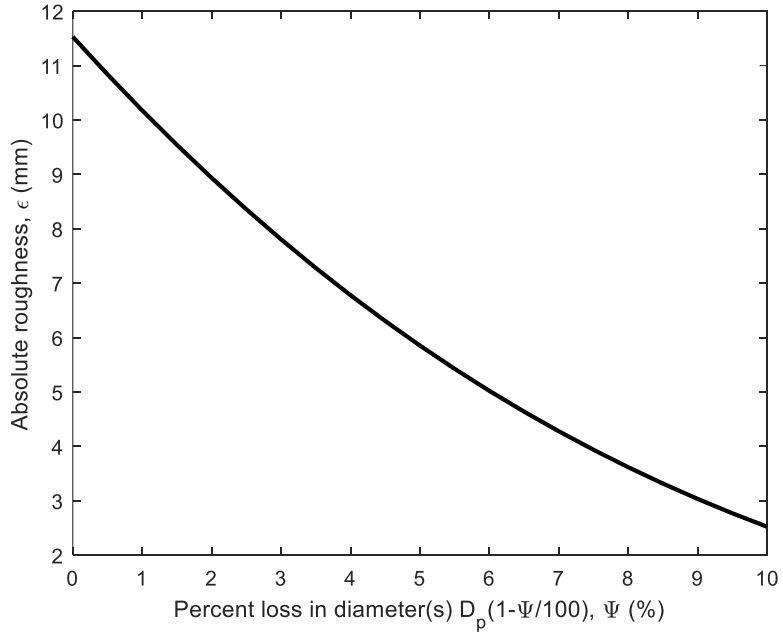

Figure 103: Akerley Boulevard - pump one: the effect of reducing the assumed internal diameter(s) of the forcemain on the inference of roughness with detailed modelling. Reductions were percent losses of the diameter(s) starting at the initial commissioning sizes.

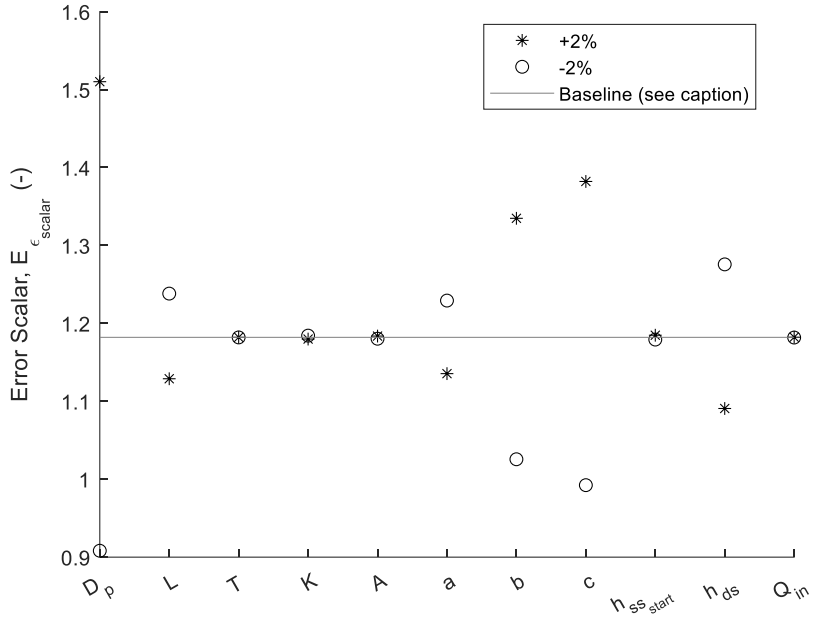

Figure 104: Akerley Boulevard - pump one: one-at-a-time sensitivity analysis for the inference of roughness due to perturbations of relevant parameters in the detailed model (along the abscissa). The analysis utilized a non-segmented forcemain. The baseline is the error scalar due to having a non-segmented forcemain (instead of a segmented one) in the detailed model.

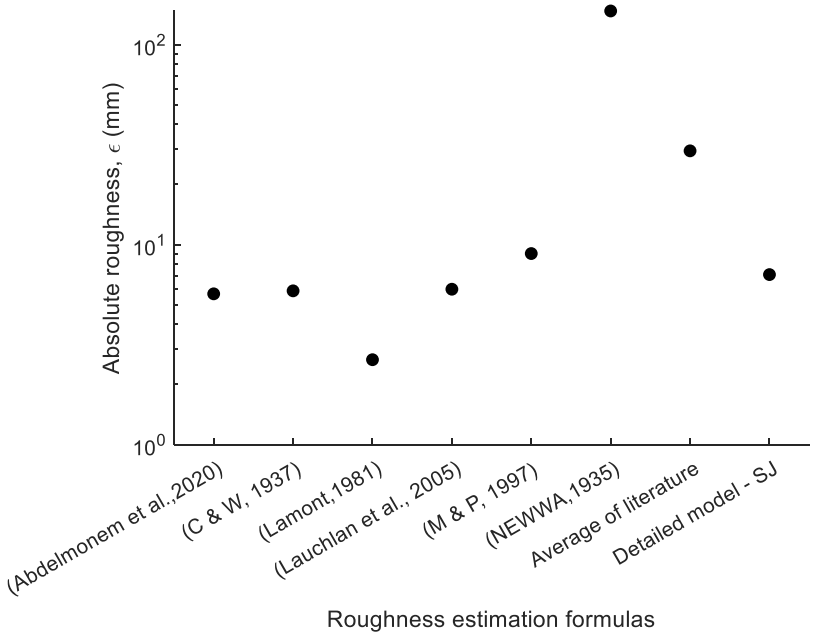

Figure 105: Akerley Boulevard - pump one: inference of roughness with respect to forcemain characteristics and water quality indices provided in the literature. The relevant authors cited along the abscissa.

Akerley Boulevard – Pump 2

Table 46: Supplementary outputs for Akerley Boulevard pump two.

Output of interest	Value
$\left(\epsilon_{SJ}\right)_{naive}\ (mm)$	7.19
$(\epsilon_{DB})_{naive}\ (mm)$	7.18
$\left(\epsilon_{SJ}\right)_{model}\ (mm)$	5.83
$\frac{\left(\epsilon_{SJ}\right)_{model}}{\left(\epsilon_{SJ}\right)_{naive}}\ (-)$	0.811
$\epsilon_0\ (mm)$	0.25
$\frac{\left(\epsilon_{SJ}\right)_{model}}{D_p}\ (-)$	0.0307
$\frac{\left(\epsilon_{SJ}\right)_{naive}}{D_p}\ (-)$	0.0378
$f_{avg_{naive}}\ (-)$	0.0633
$f_{avg_{model}}\ (-)$	0.0588
$f_{max_{model}}(-)$	0.0666
$f_{min_{model}}\ (-)$	0.058
$Re_{avg_{model}}\ (-)$	159000
$Re_{max_{model}}\ (-)$	162000
$C_{HW\,model}(-)$	76.7
$C_{HW\,naive}\ (-)$	73
$\frac{C_{HW\,model}}{C_{HW\,naive}}\ (-)$	1.05

Output of interest	Value
$C_{HW_0}\ (-)$	140
$t_a\ , SJ\ model\ (s)$	21.3
$t_a, analytical\ (s)$	17.6
Energy Usage – Time of Test $(kWhr)$	0.747
Energy Usage – Initial Implementation $(kWhr)$	0.585
Cost – Time of Test $\left(\frac{\$}{year}\right)$	2550
Cost – Initial Implementation $\left(\frac{\$}{year}\right)$	2000
Cost Ratio	1.28
$Q_{avg}\ \left(\frac{m^3}{s}\right)$	0.0261
$U_{avg}\ \left(\frac{m}{s}\right)$	0.921
$h_{v_{avg}}\ (m)$	0.0433
$h_{f_{avg}}\ (m)$	10
$h_{m_{avg}}\ (m)$	0.401
$h_{ss_{avg}}\ (m)$	0.185
$H_{avg}\ (m)$	27.6
$h_{a_{max}}\ (m)$	19.8
$\frac{V_{pipe}}{V}\ (-)$	3.91

The calculations for the naïve interpretation results can be determined as stated in Table 40.

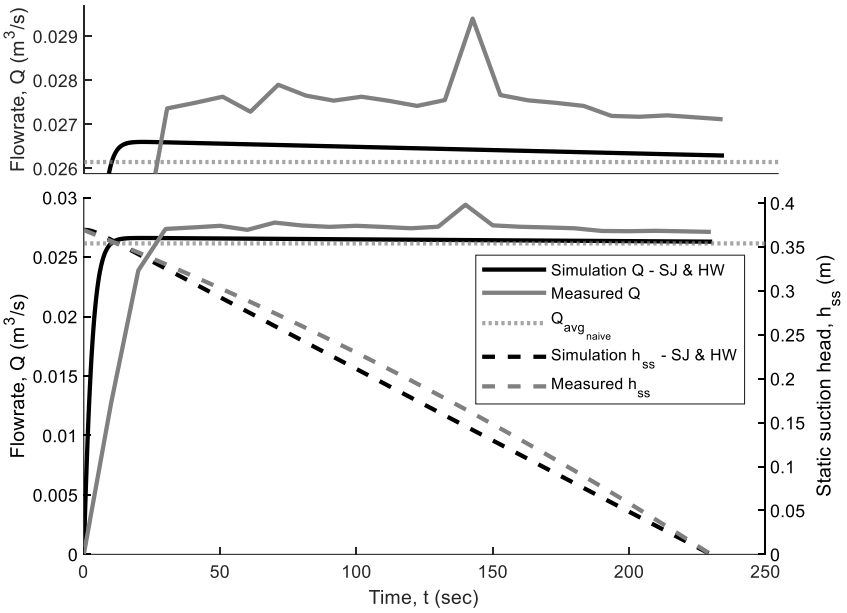

Figure 106: Akerley Boulevard - pump two: the detailed model simulation flow rate (left axis) through the forcemain and static suction head (right axis) in the wet-well with respect to time. Continuously collected data and the naïvely determined flow rate are also presented.

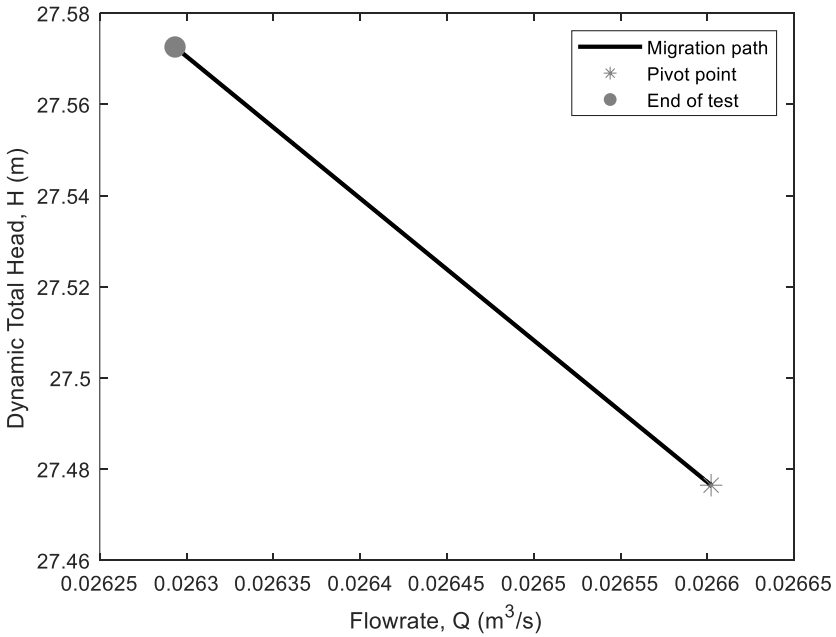

Figure 107: Akerley Boulevard - pump two: migration of the operating point after flow establishment for the simulation. The pivot point is the point at which flow establishment has completed.

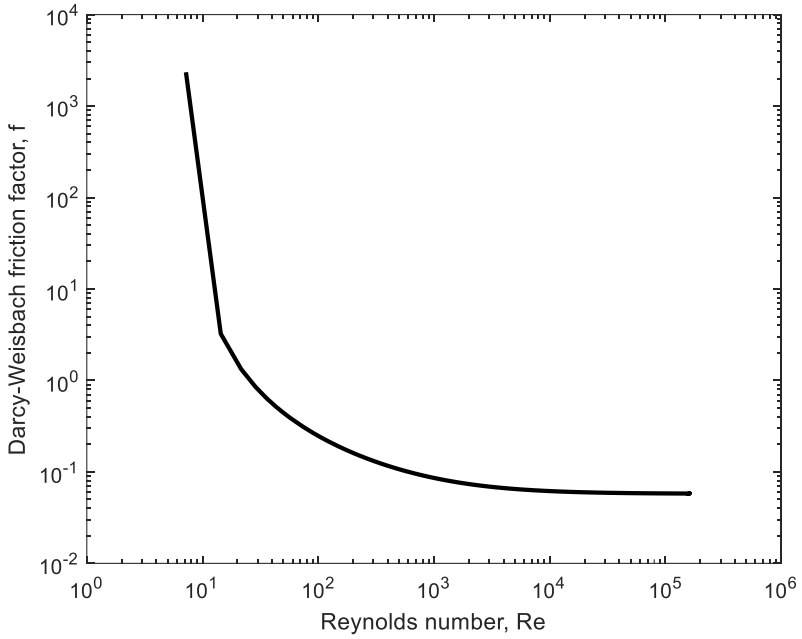

Figure 108: Akerley Boulevard - pump two: Darcy-Weisbach friction factor migration for the detailed model simulation (log-log scale). The friction loss method utilized is Swamee-Jain.

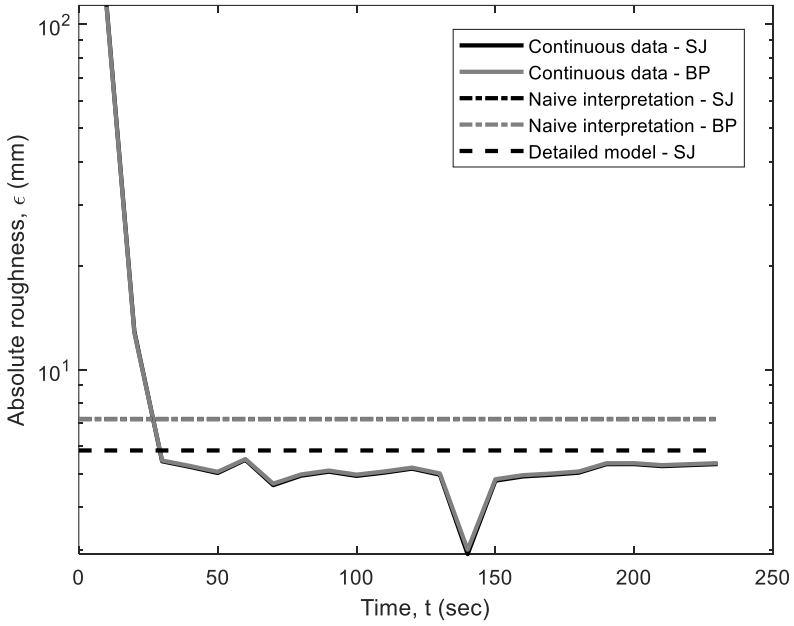

Figure 109: Akerley Boulevard - pump two: different techniques for inferring roughness. Two friction loss methods are present, Swamee-Jain (SJ) and Brkić-Praks (BP). Continuous data was utilized at every sampling time to infer roughness for comparison. The naïve interpretations and the detailed modelling inferences are time-invariant.

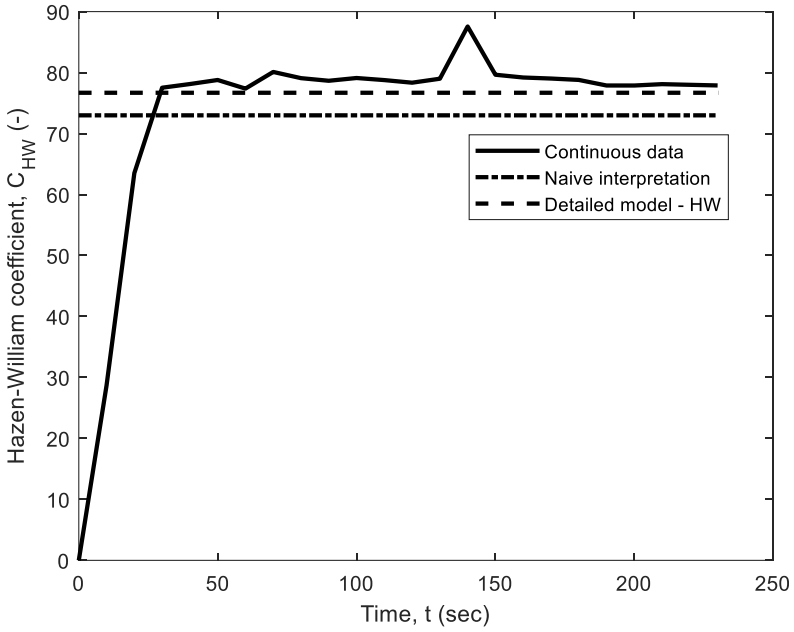

Figure 110: Akerley Boulevard - pump two: different techniques for inferring the Hazen-Williams coefficient. The naïve interpretation and the detailed model inferences are time-invariant. Continuous data was utilized at every sampling time to infer the coefficient for comparison.

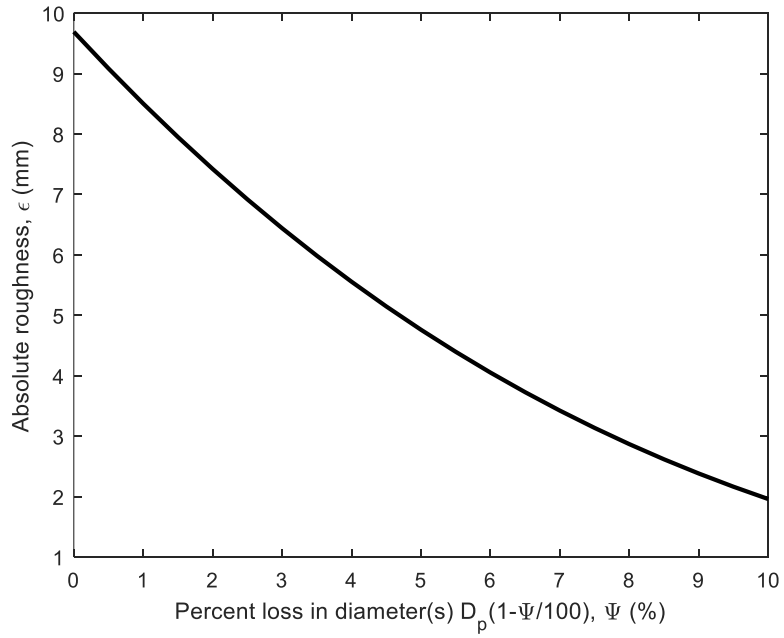

Figure 111: Akerley Boulevard - pump two: the effect of reducing the assumed internal diameter(s) of the forcemain on the inference of roughness with detailed modelling. Reductions were percent losses of the diameter(s) starting at the initial commissioning sizes.

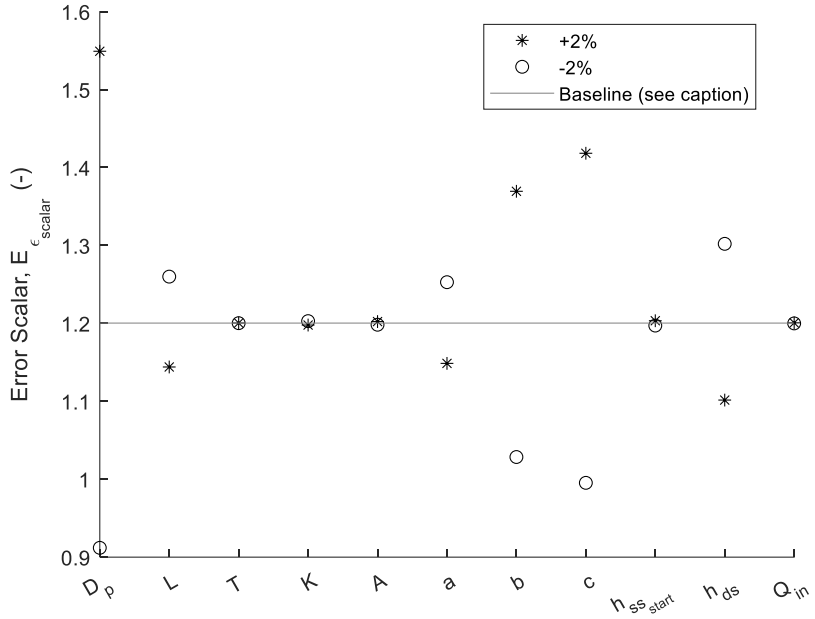

Figure 112: Akerley Boulevard - pump two: one-at-a-time sensitivity analysis for the inference of roughness due to perturbations of relevant parameters in the detailed model (along the abscissa). The analysis utilized a non-segmented forcemain. The baseline is the error scalar due to having a non-segmented forcemain (instead of a segmented one) in the detailed model.

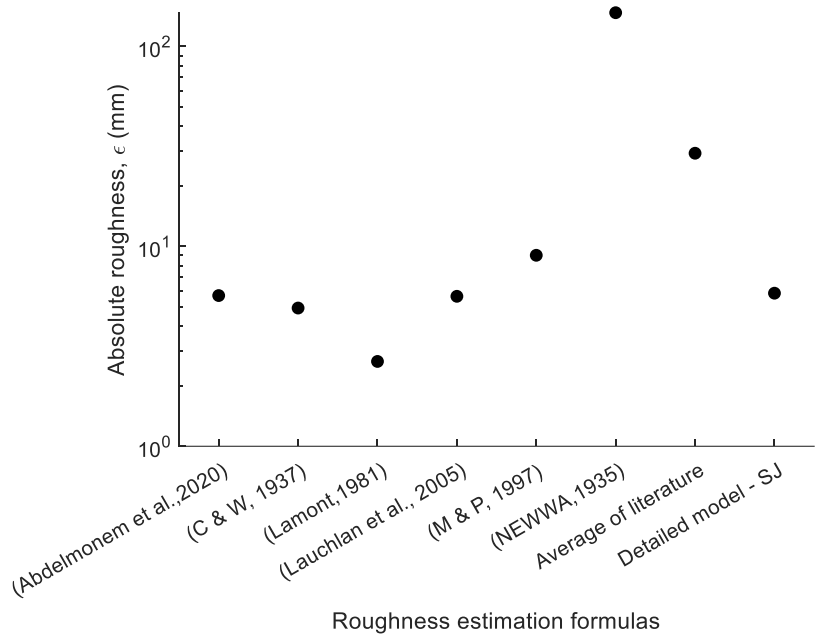

Figure 113: Akerley Boulevard - pump two: inference of roughness with respect to forcemain characteristics and water quality indices provided in the literature. The relevant authors cited along the abscissa.

Melville Cove

Melville Cove – Pump 1

Table 47: Supplementary outputs for Melville Cove pump one.

Output of interest	Value
$(\epsilon_{SJ})_{naive}\ (mm)$	268
$(\epsilon_{DB})_{naive}\ (mm)$	266
$(\epsilon_{SJ})_{model}\ (mm)$	260
$\frac{(\epsilon_{SJ})_{model}}{(\epsilon_{SJ})_{naive}}\ (-)$	0.973
$\epsilon_0\ (mm)$	0.25
$\frac{(\epsilon_{SJ})_{model}}{D_p}\ (-)$	1.05
$\frac{(\epsilon_{SJ})_{naive}}{D_p}\ (-)$	1.08
$f_{avg_{naive}}\ (-)$	0.866
$f_{avg_{model}}\ (-)$	0.828
$f_{max_{model}}(-)$	0.843
$f_{min_{model}}\ (-)$	0.828
$Re_{avg_{model}}\ (-)$	147000
$Re_{max_{model}}\ (-)$	148000
$C_{HW\,model}(-)$	17.8
$C_{HW\,naive}\ (-)$	17.6

Output of interest	Value
$\frac{C_{HW_{model}}}{C_{HW_{naive}}}\ (-)$	1.01
$C_{HW_0}\ (-)$	140
$t_a\ , SJ\ model\ (s)$	2.45
$t_a, analytical\ (s)$	2.21
Energy Usage – Time of Test $(kWhr)$	2.67
Energy Usage – Initial Implementation $(kWhr)$	1.71
Cost – Time of Test $\left(\frac{\$}{year}\right)$	9110
Cost – Initial Implementation $\left(\frac{\$}{year}\right)$	5840
Cost Ratio	1.56
$Q_{avg}\ \left(\frac{m^3}{s}\right)$	0.038
$U_{avg}\ \left(\frac{m}{s}\right)$	0.782
$h_{v_{avg}}\ (m)$	0.0312
$h_{f_{avg}}\ (m)$	8.56
$h_{m_{avg}}\ (m)$	0.214
$h_{ss_{avg}}\ (m)$	0.181
$H_{avg}\ (m)$	40.8
$h_{a_{max}}\ (m)$	19.4
$\frac{V_{pipe}}{V}\ (-)$	0.448

The calculations for the naïve interpretation results can be determined as stated in Table 40.

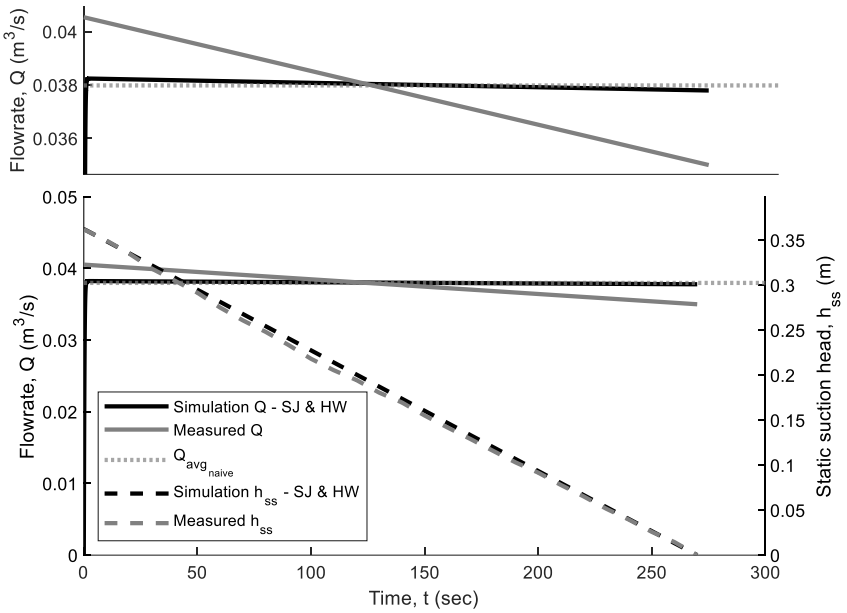

Figure 114: Melville Cove - pump one: the detailed model simulation flow rate (left axis) through the forcemain and static suction head (right axis) in the wet-well with respect to time. Continuously collected data and the naïvely determined flow rate are also presented.

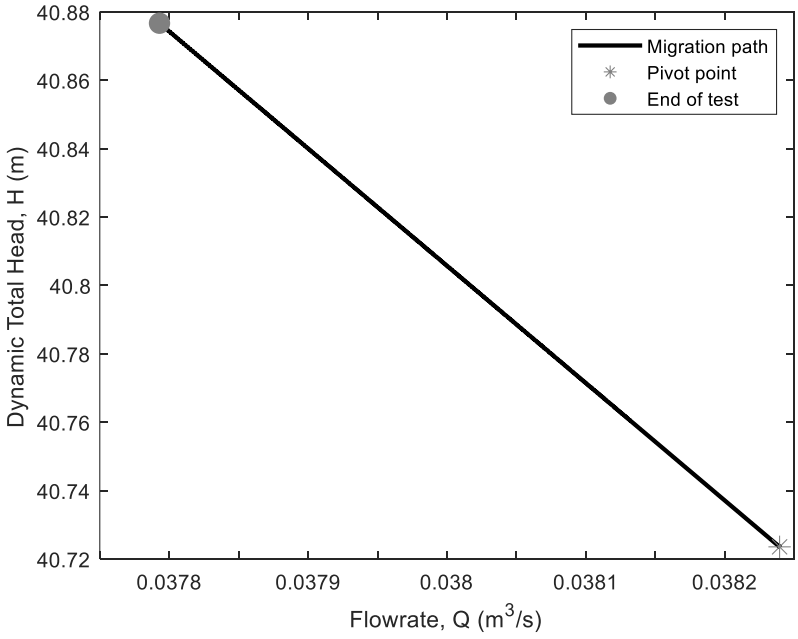

Figure 115: Melville Cove - pump one: migration of the operating point after flow establishment for the simulation. The pivot point is the point at which flow establishment has completed.

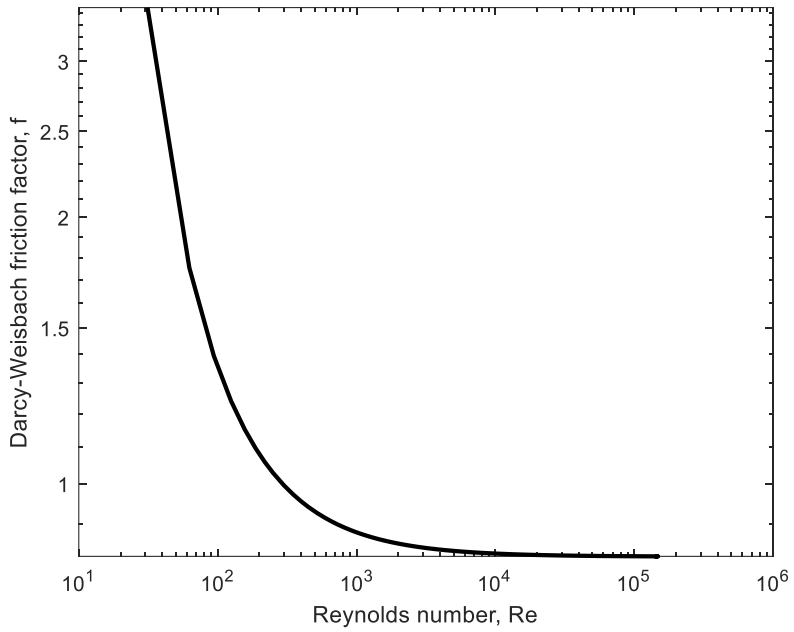

Figure 116: Melville Cove - pump one: Darcy-Weisbach friction factor migration for the detailed model simulation (log-log scale). The friction loss method utilized is Swamee-Jain.

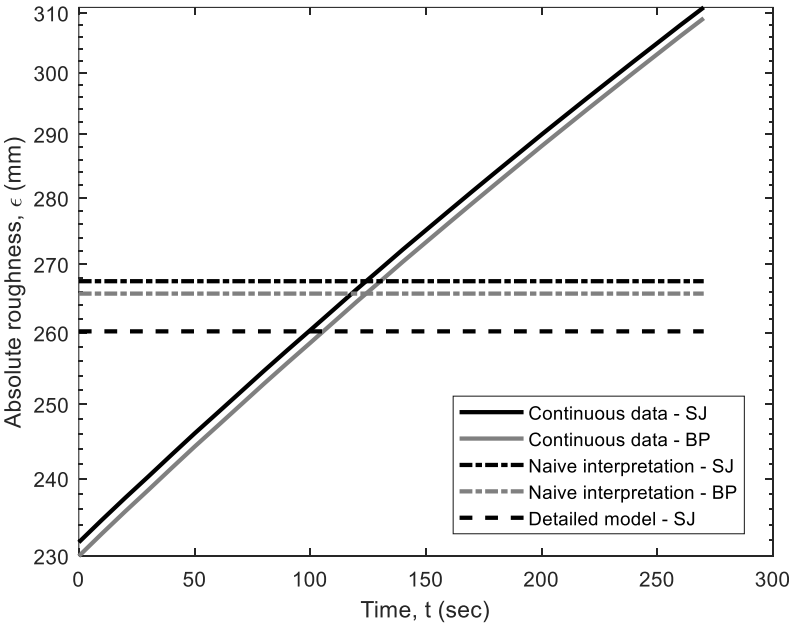

Figure 117: Melville Cove - pump one: different techniques for inferring roughness. Two friction loss methods are present, Swamee-Jain (SJ) and Brkić-Praks (BP). Continuous data was utilized at every sampling time to infer roughness for comparison. The naïve interpretations and the detailed modelling inferences are time-invariant.

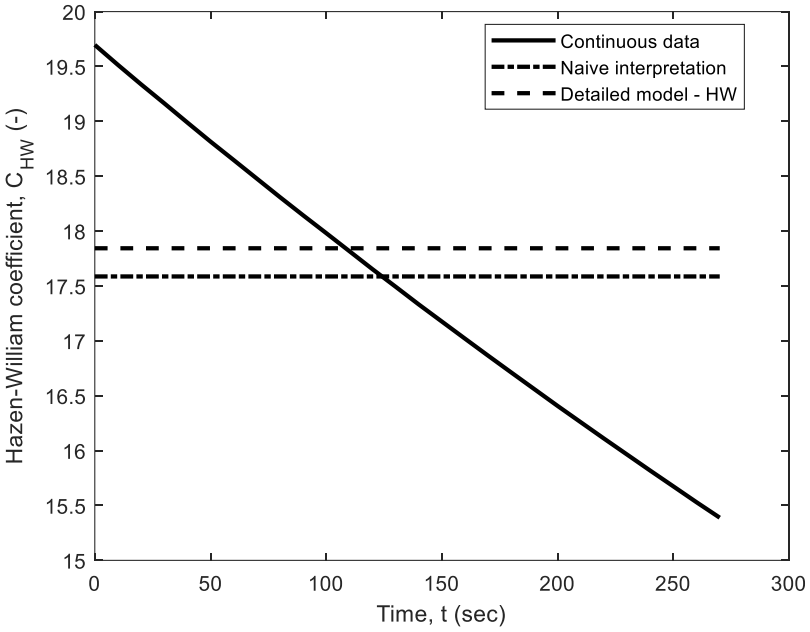

Figure 118: Melville Cove - pump one: different techniques for inferring the Hazen-Williams coefficient. The naïve interpretation and the detailed model inferences are time-invariant. Continuous data was utilized at every sampling time to infer the coefficient for comparison.

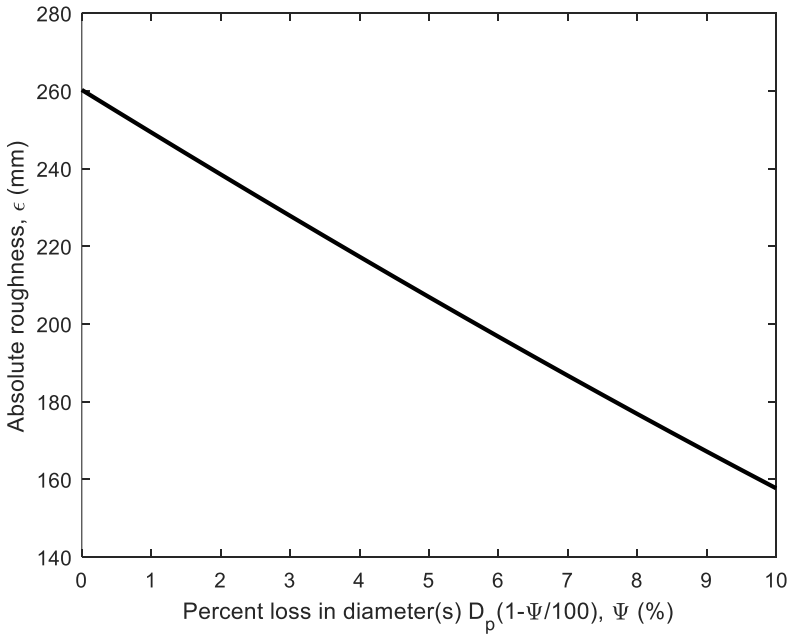

Figure 119: Melville Cove - pump one: the effect of reducing the assumed internal diameter(s) of the forcemain on the inference of roughness with detailed modelling. Reductions were percent losses of the diameter(s) starting at the initial commissioning sizes.

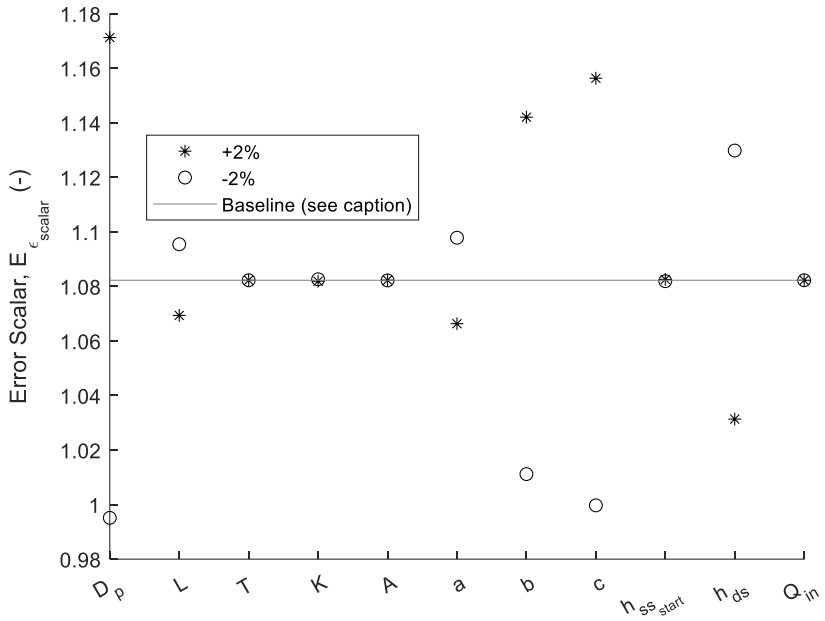

Figure 120: Melville Cove - pump one: one-at-a-time sensitivity analysis for the inference of roughness due to perturbations of relevant parameters in the detailed model (along the abscissa). The analysis utilized a non-segmented forcemain. The baseline is the error scalar due to having a non-segmented forcemain (instead of a segmented one) in the detailed model.

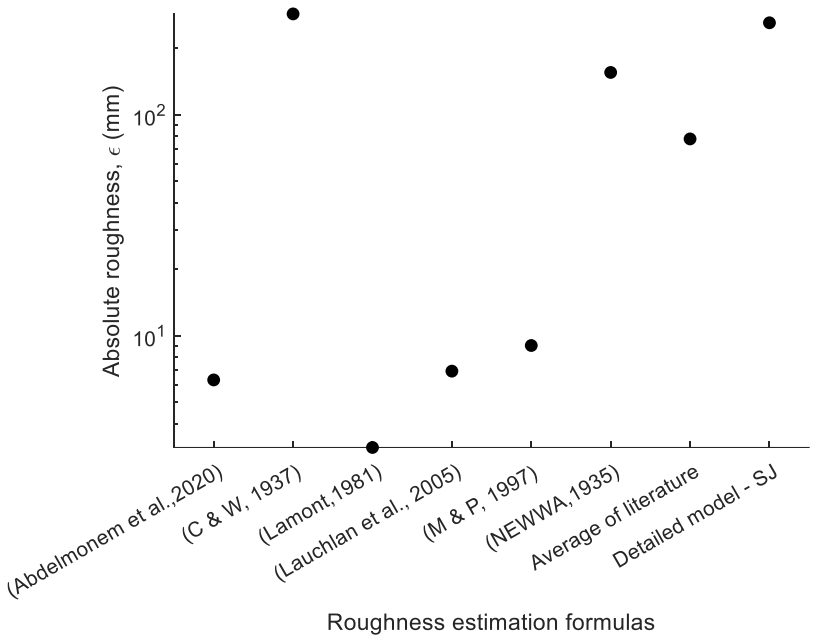

Figure 121: Melville Cove - pump one: inference of roughness with respect to forcemain characteristics and water quality indices provided in the literature. The relevant authors cited along the abscissa.

Melville Cove – Pump 2

Table 48: Supplementary outputs for Melville Cove pump two.

Output of interest	Value
$\left(\epsilon_{SJ}\right)_{naive}\ (mm)$	30.5
$(\epsilon_{DB})_{naive}\ (mm)$	30.1
$\left(\epsilon_{SJ}\right)_{model}\ (mm)$	23.5
$\frac{\left(\epsilon_{SJ}\right)_{model}}{\left(\epsilon_{SJ}\right)_{naive}}\ (-)$	0.769
$\epsilon_0\ (mm)$	0.25
$\frac{\left(\epsilon_{SJ}\right)_{model}}{D_p}\ (-)$	0.0943
$\frac{\left(\epsilon_{SJ}\right)_{naive}}{D_p}\ (-)$	0.123
$f_{avg_{naive}}\ (-)$	0.114
$f_{avg_{model}}\ (-)$	0.0985
$f_{max_{model}}(-)$	0.105
$f_{min_{model}}\ (-)$	0.0985
$Re_{avg_{model}}\ (-)$	210000
$Re_{max_{model}}\ (-)$	212000
$C_{HW\,model}(-)$	55.3
$C_{HW\,naive}\ (-)$	51
$\frac{C_{HW\,model}}{C_{HW\,naive}}\ (-)$	1.08
$C_{HW_0}\ (-)$	140

Output of interest	Value
t_a , $SJ\ model\ (s)$	3.86
$t_a, analytical\ (s)$	3.94
Energy Usage – Time of Test $(kWhr)$	2.46
Energy Usage – Initial Implementation $(kWhr)$	2.3
Cost – Time of Test $\left(\frac{\$}{year}\right)$	8400
Cost – Initial Implementation $\left(\frac{\$}{year}\right)$	7850
Cost Ratio	1.07
$Q_{avg}\ \left(\frac{m^3}{s}\right)$	0.0544
$U_{avg}\ \left(\frac{m}{s}\right)$	1.12
$h_{v_{avg}}\ (m)$	0.0639
$h_{f_{avg}}\ (m)$	2.45
$h_{m_{avg}}\ (m)$	0.47
$h_{ss_{avg}}\ (m)$	0.244
$H_{avg}\ (m)$	34.9
$h_{a_{max}}\ (m)$	19.6
$\frac{V_{pipe}}{V}\ (-)$	0.352

The calculations for the naïve interpretation results can be determined as stated in Table 40.

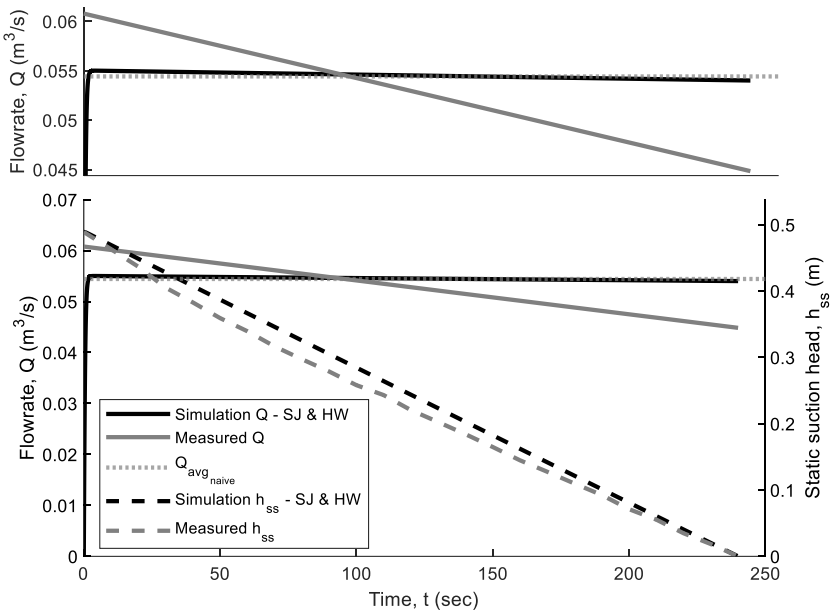

Figure 122: Melville Cove - pump two: the detailed model simulation flow rate (left axis) through the forcemain and static suction head (right axis) in the wet-well with respect to time. Continuously collected data and the naïvely determined flow rate are also presented.

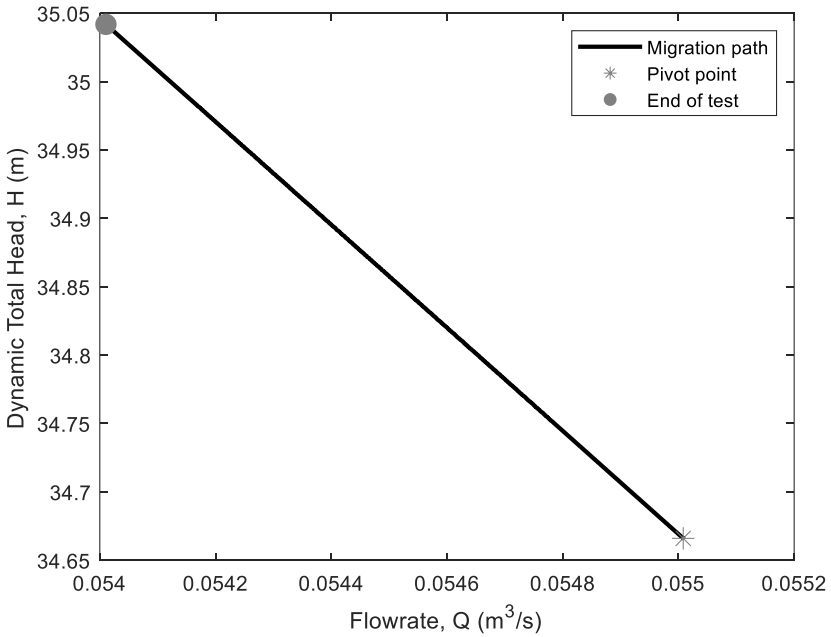

Figure 123: Melville Cove - pump two: migration of the operating point after flow establishment for the simulation. The pivot point is the point at which flow establishment has completed.

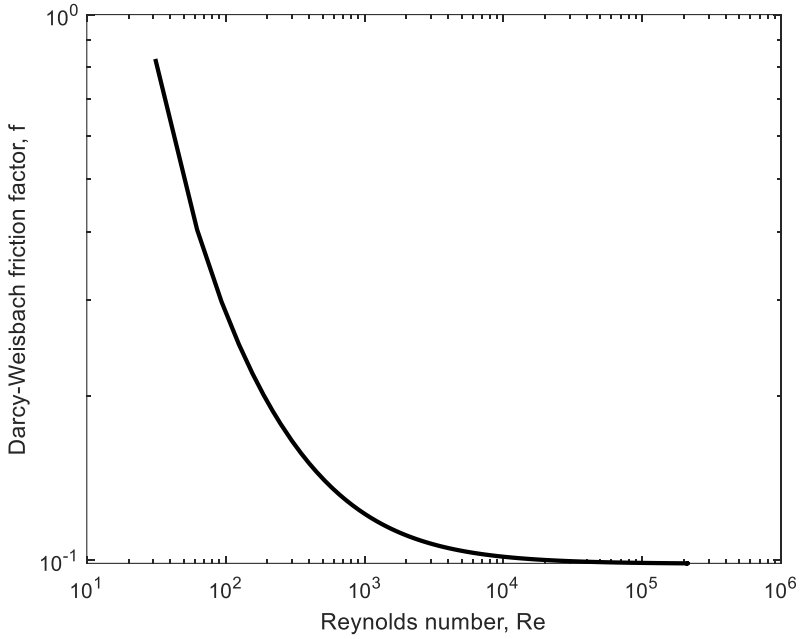

Figure 124: Melville Cove - pump two: Darcy-Weisbach friction factor migration for the detailed model simulation (log-log scale). The friction loss method utilized is Swamee-Jain.

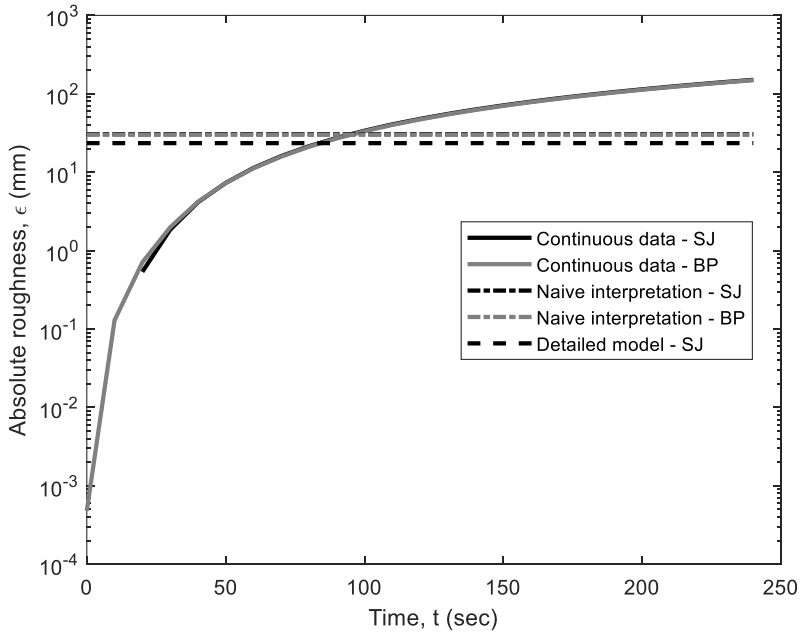

Figure 125: Melville Cove - pump two: different techniques for inferring roughness. Two friction loss methods are present, Swamee-Jain (SJ) and Brkić-Praks (BP). Continuous data was utilized at every sampling time to infer roughness for comparison. The naïve interpretations and the detailed modelling inferences are time-invariant.

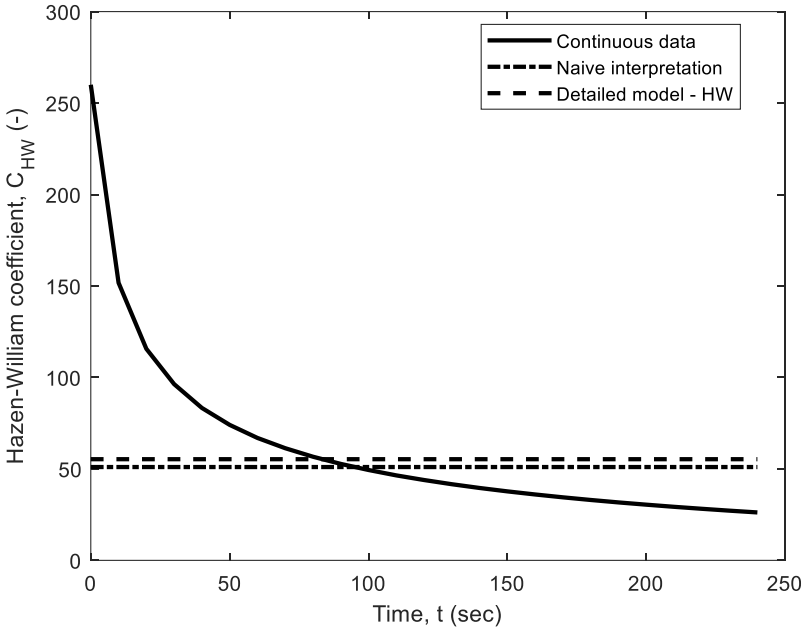

Figure 126: Melville Cove - pump two: different techniques for inferring the Hazen-Williams coefficient. The naïve interpretation and the detailed model inferences are time-invariant. Continuous data was utilized at every sampling time to infer the coefficient for comparison.

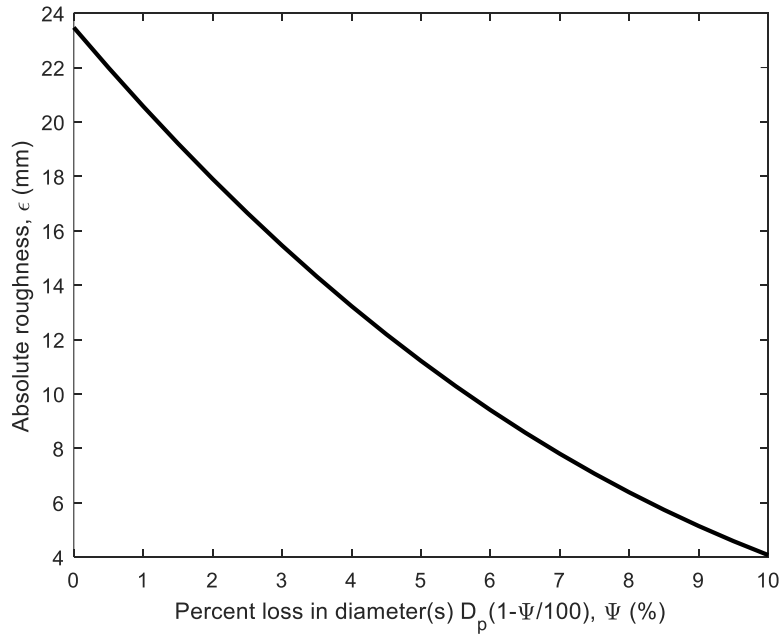

Figure 127: Melville Cove - pump two: the effect of reducing the assumed internal diameter(s) of the forcemain on the inference of roughness with detailed modelling. Reductions were percent losses of the diameter(s) starting at the initial commissioning sizes.

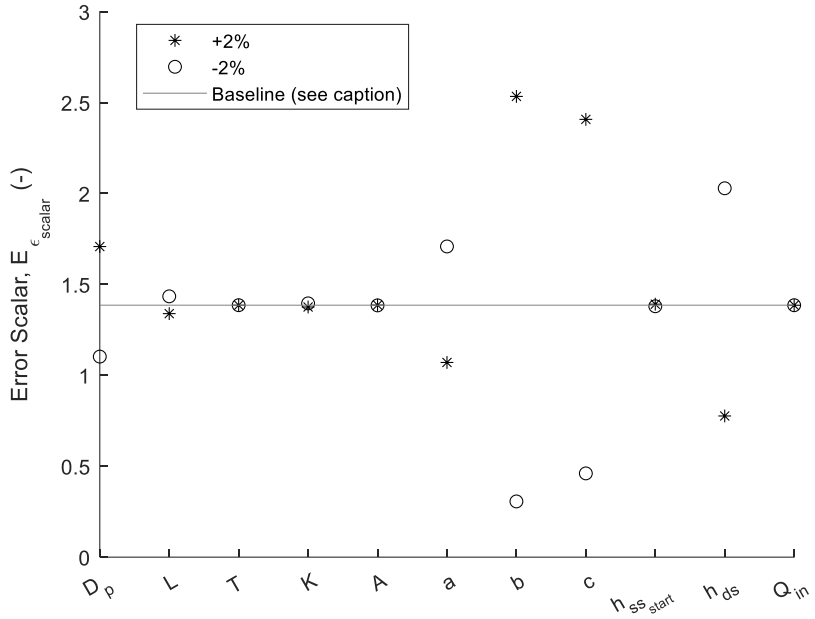

Figure 128: Melville Cove - pump two: one-at-a-time sensitivity analysis for the inference of roughness due to perturbations of relevant parameters in the detailed model (along the abscissa). The analysis utilized a non-segmented forcemain. The baseline is the error scalar due to having a non-segmented forcemain (instead of a segmented one) in the detailed model.

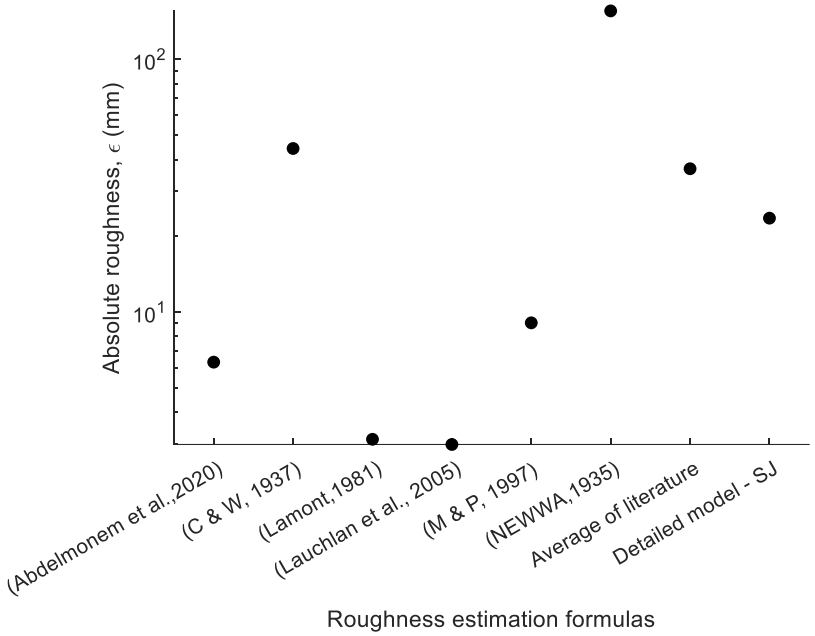

Figure 129: Melville Cove - pump two: inference of roughness with respect to forcemain characteristics and water quality indices provided in the literature. The relevant authors cited along the abscissa.

Appendix C – Monte Carlo Simulation Results

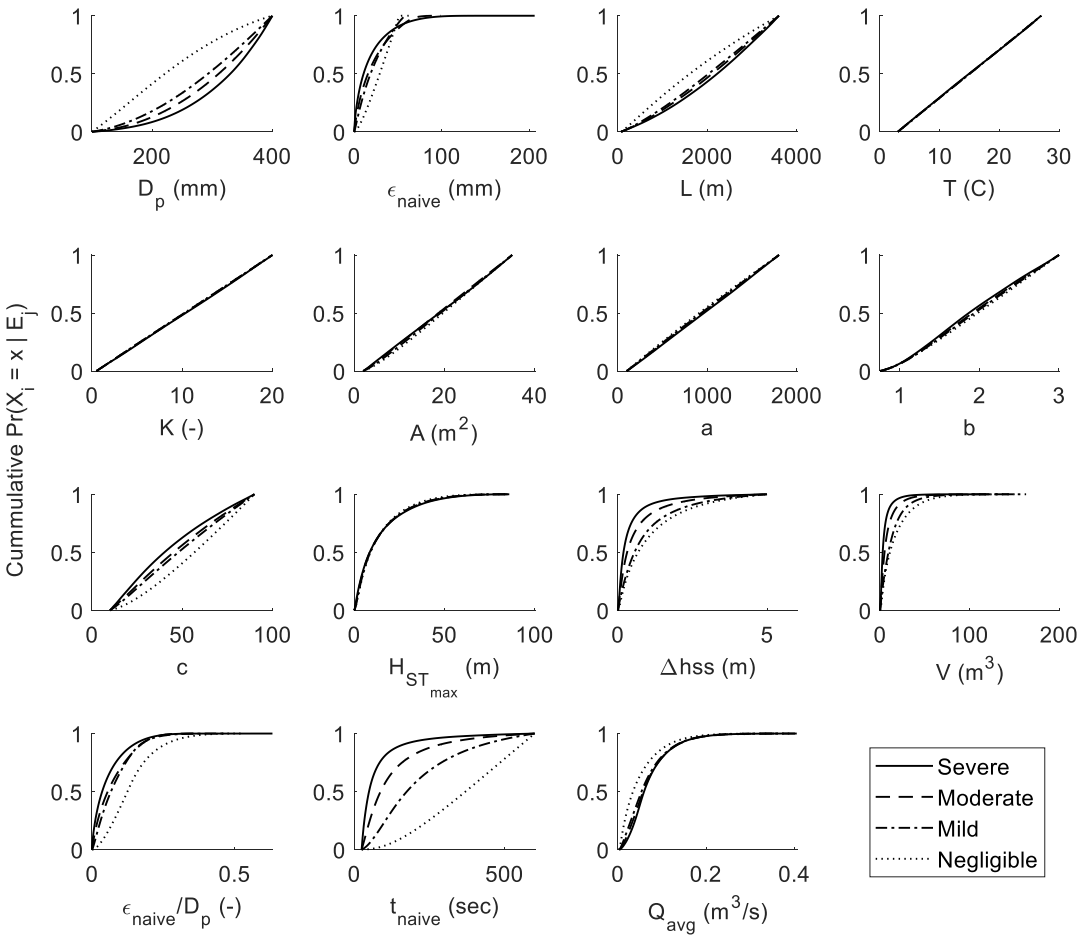

Figure 130: Part one of two: cumulative probability density for parameters by error category.

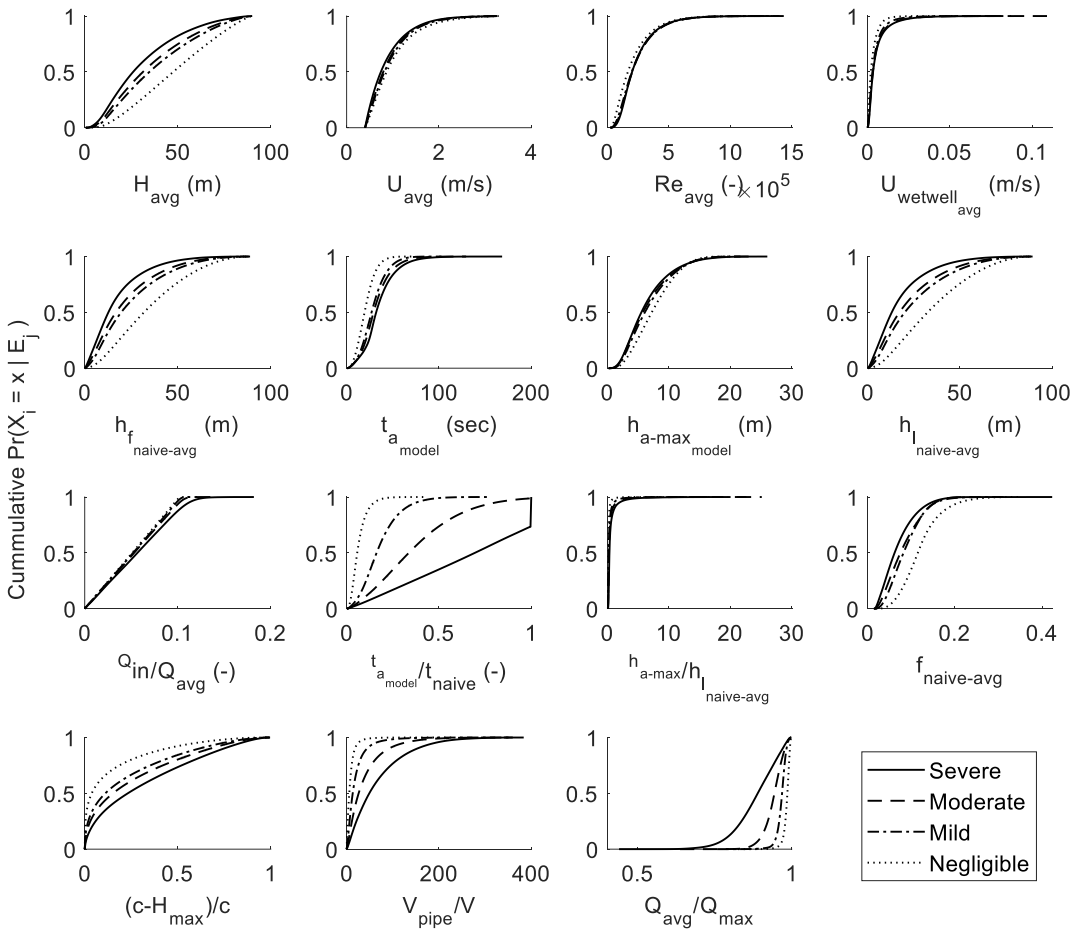

Figure 131: Part two of two: cumulative probability density for parameters by error category.

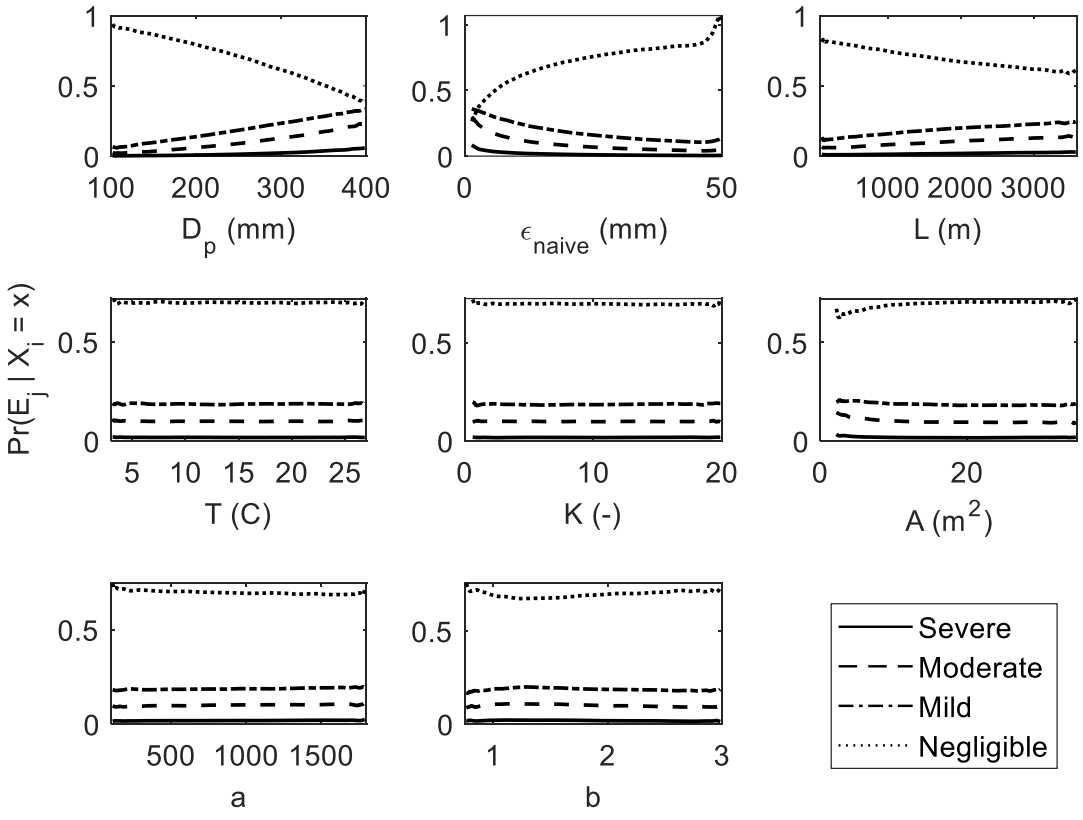

Figure 132: Part two of four - probability density estimations of an expected error category given a specific parameter value ($Pr(E_j \mid X_i = x)$).

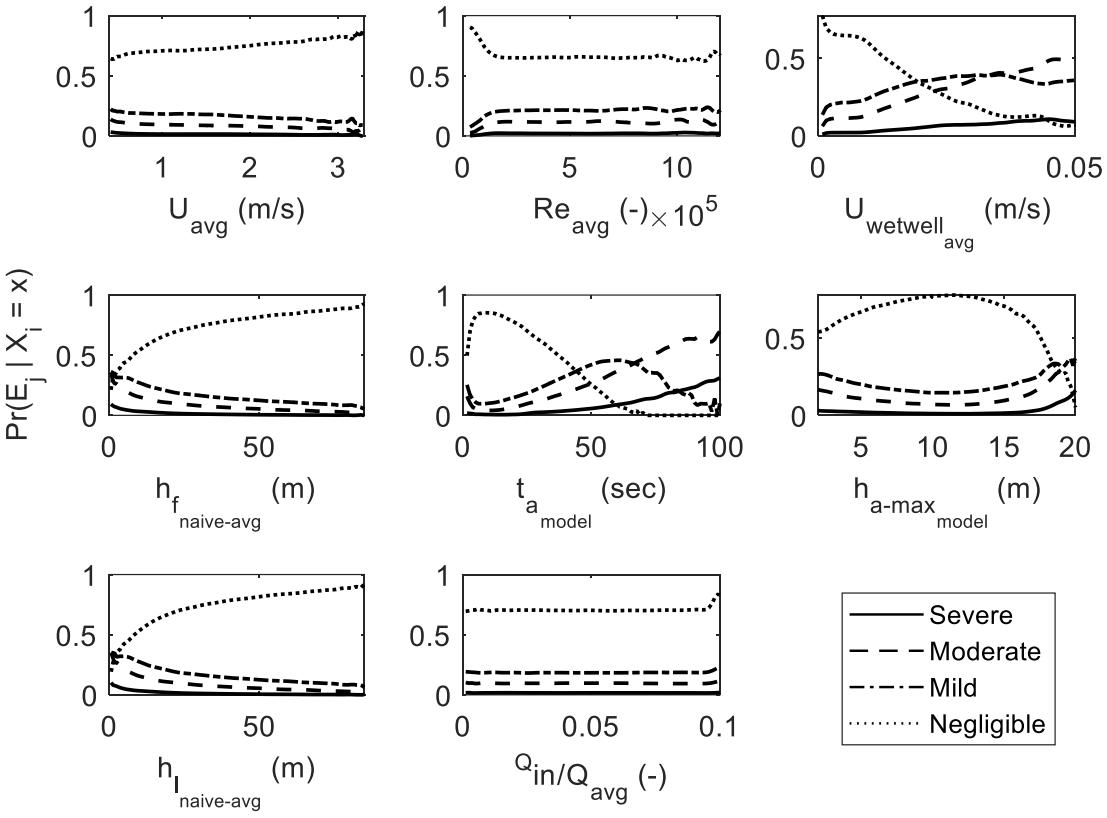

Figure 133: Part three of four - probability density estimations of an expected error category given a specific parameter value ($Pr(E_j \mid X_i = x)$).

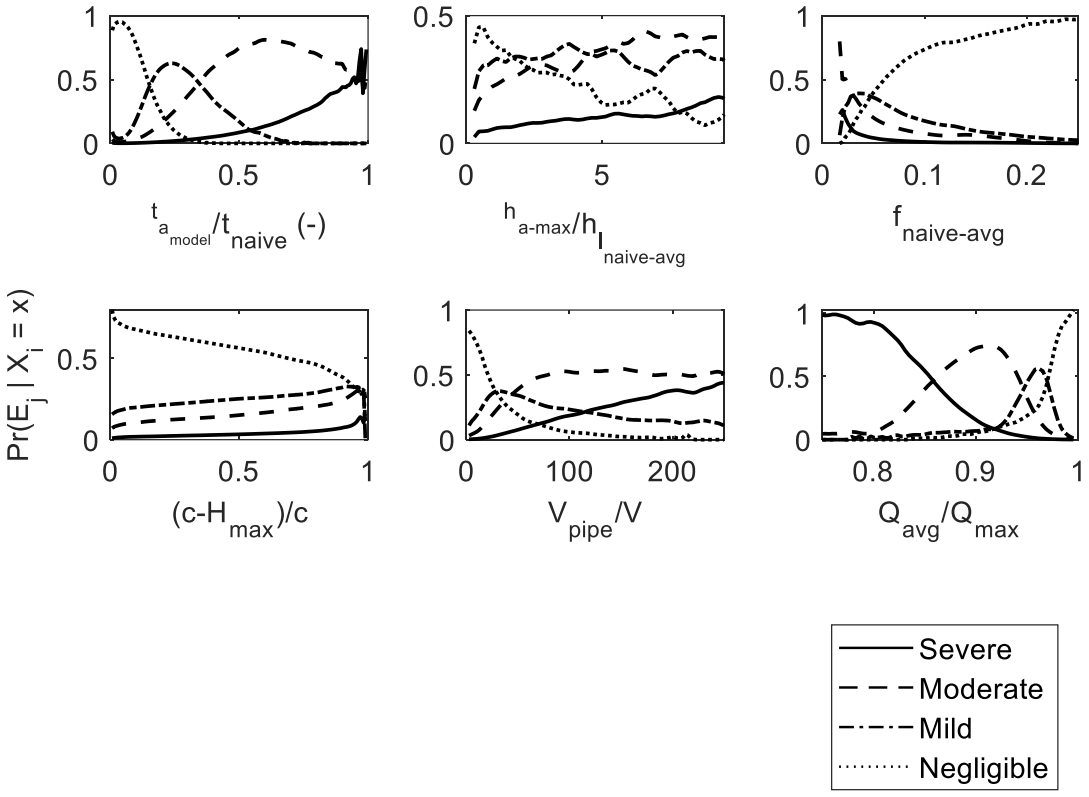

Figure 134: Part four of four - probability density estimations of an expected error category given a specific parameter value ($Pr(E_j \mid X_i = x)$).

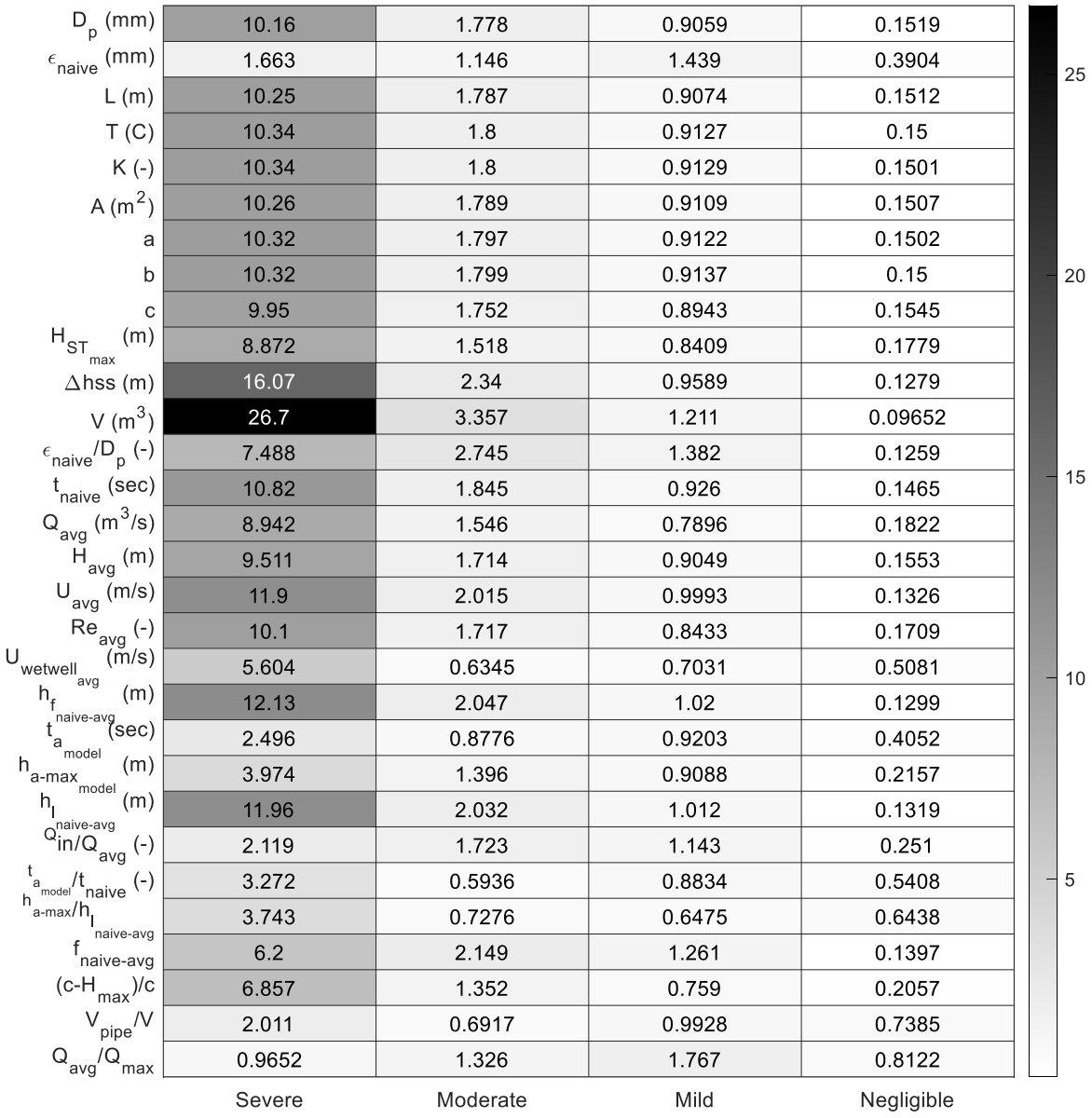

Figure 135: Error tolerance (as a percentage) to ensure a suitable sample size for each parameter in each error category

Table 49: All parameters investigated for the hypothetical lift stations - created by Monte Carlo simulations.

Parameter	Description
Available for the creation of the classification tree.	
$D_p\ (mm)$	The internal diameter of the forcemain.
$L\ (m)$	The length of the forcemain.
$T\ (°C)$	The temperature of the liquid in the wet-well.
$K\ (-)$	The minor loss coefficient.
$A\ (m^2)$	The area of the wet-well.
$a\ (-)$	The coefficient of the characteristic curve.
$b\ (-)$	The exponent of the characteristic curve.
$c\ (-)$	The constant of the characteristic curve (shut-in head).
$H_{ST_{max}}\ (m)$	The maximum static total head during a pumping test.
$\Delta h_{ss}\ (m)$	The change in static suction head during a pumping test.
$V\ (m^3)$	The active volume in the wet-well.
t_{naive} (s)	The time spent pumping as determined by a naïve pump-down test.
$Q_{avg}\ \left(\frac{m^3}{s}\right)$	The average flowrate through the forcemain as obtained for a naïve interpretation of hydraulic resistance.
$U_{avg}\ \left(\frac{m}{s}\right)$	The average velocity through the forcemain determined with the average flowrate.
$R_{e_{avg}}\ (-)$	The Reynolds number associated with the average flowrate through the forcemain.

Parameter	Description
$U_{(wetwell)_{avg}}\left(\frac{m}{s}\right)$	The average velocity of the liquid level in the wet-well as determined by the average flowrate of the wet-well.
$h_{f_{naive-avg}}(m)$	The average friction losses determined with the average flowrate through the forcemain and naïve interpretation of relative roughness.
$h_{l_{naive-avg}}(m)$	The average losses (friction and minor) through the forcemain determined with the average flowrate and naïve interpretation of relative roughness.
$\frac{Q_{in}}{Q_{avg}}(-)$	The ratio of the inflow rate during pumping to the average forcemain flowrate.
$f_{avg_{naive}}(-)$	The Darcy-Weisbach friction factor determined with the average flowrate and naïve interpretation of relative roughness.
$\frac{V_{pipe}}{V}(-)$	The ratio of the volume of liquid within a stagnant forcemain to the active volume.
$\epsilon_{naive}(mm)$	The naïve interpretation of roughness.
$\left(\frac{\epsilon}{D_p}\right)_{naive}(-)$	The naïve interpretation of relative roughness.
Not available for the creation of the classification tree.	
$t_{a_{model}}$ (s)	The duration required for flow establishment as determined by the detailed model
$h_{a_{max}}(m)$	The acceleration head associated with the maximum flowrate through the forcemain from the model.
$\frac{t_{a_{model}}}{t_{naive}}(-)$	The ratio of time spent establishing flow to the naïve pump-down test time.
$\frac{h_{a_{max}}}{h_{l_{naive}}}(-)$	The ratio of the acceleration head associated with the maximum flowrate in the simulation to the average losses associated with the forcemain.
$\frac{c - H_{max}}{c}(-)$	Ratio as inferred from Gulich (2020)
$\frac{Q_{avg}}{Q_{max}}(-)$	The ratio of the average flowrate through the forcemain not the maximum flowrate through the forcemain as determined through simulation.

Appendix D - Miscellaneous

Table 50: Common minor losses utilized in calculations (after Gupta, 2008).

Item	Loss Coefficient, K
Entrance from tank to pipe	
Flush connection	0.5
Projecting connection	0.8
Exit from pipe to tank	1.0
Sudden contraction $\left(\frac{D_{p_2}}{D_{p_1}}\right)$ **	
0.2	0.48
0.4	0.42
0.6	0.32
0.8	0.2
0.9	0.05
Sudden enlargement $\left(\frac{D_{p_1}}{D_{p_2}}\right)$ **	
0.9	0.04
0.8	0.13
0.6	0.41
0.4	0.71
0.2	0.92
90° bend and *180*° return – threaded	1.5
45° bend – threaded	0.4
90° bend and *180*° return – flanged	0.3
90° bend – flanged	0.3
Tee - threaded	

Item	Loss Coefficient, K
Through flow	0.9
Branched flow	2.0
Tee – flanged	
Through flow	0.2
Branched flow	1.0
Gate valve (open)	0.19
Check valve (open)	2.0
Globe valve (open)	10.0
Angle valve (open)	2.0
Butterfly valve (open)	0.3

**1 refers to upstream, and 2 refers to downstream

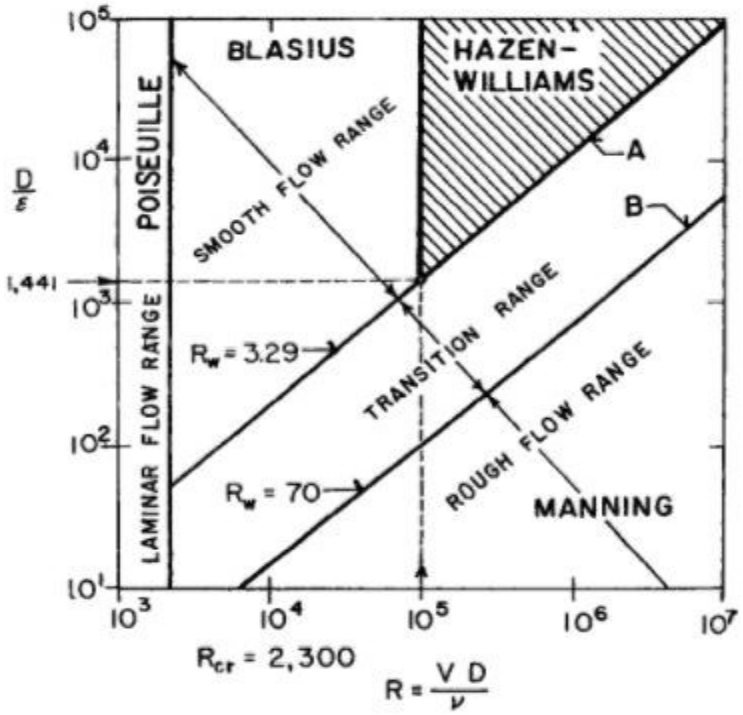

Figure 136: Small window associated with applicable range for the Hazen-Williams equation (Christensen, 2000).

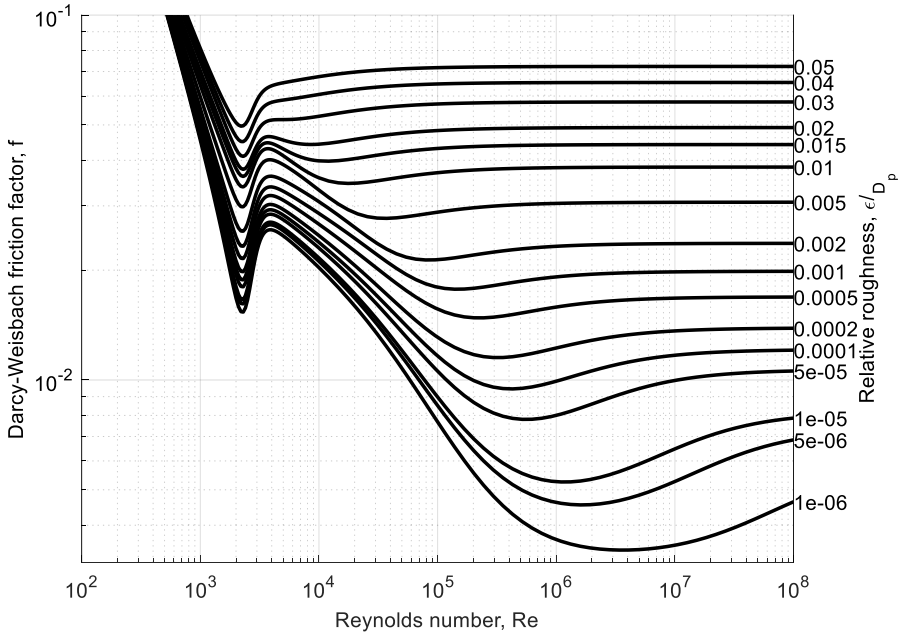

Figure 137: Brkić-Praks estimation of Darcy-Weisbach friction factor with similar information as depicted on the Moody Diagram.

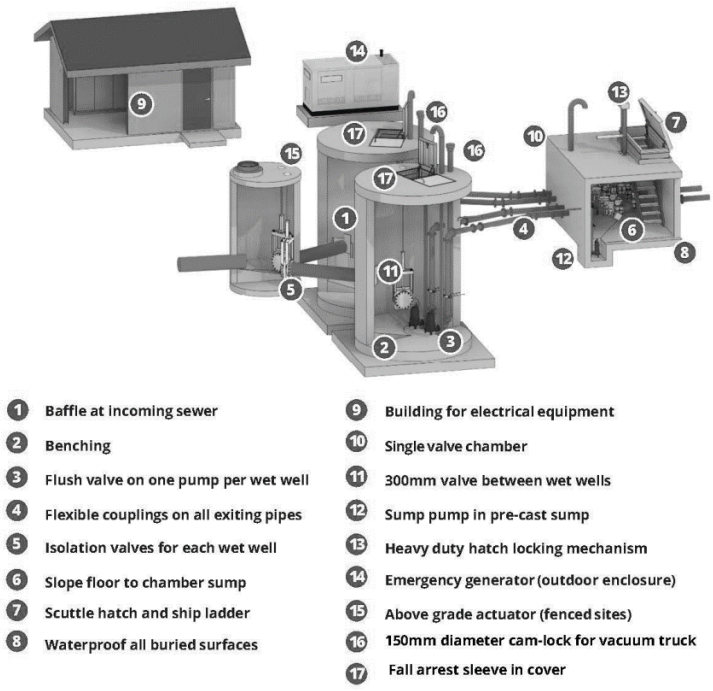

Figure 138: Example of a medium-sized lift-station set-up (after Halifax Water, 2022).

Table 51: Encrustations thickness in forcemain using Mielcarzewicz & Pelka (1997)

Location	Thickness of Encrustation (mm) – MPSt1*	Thickness of Encrustation (mm) – MPSt2*
Trinity Lane – Pump 1 & 2	1.157	0.222
Ragged Lake – Pump 1 & 2	4.793	1.549
Akerley Boulevard – Pump 1 & 2	7.188	5.322
Melville Cove – Pump 1 & 2	8.869	6.222

*MPSt refers to the Mielcarzewics and Pelka (1997) initials and encrustations thickness inference technique.

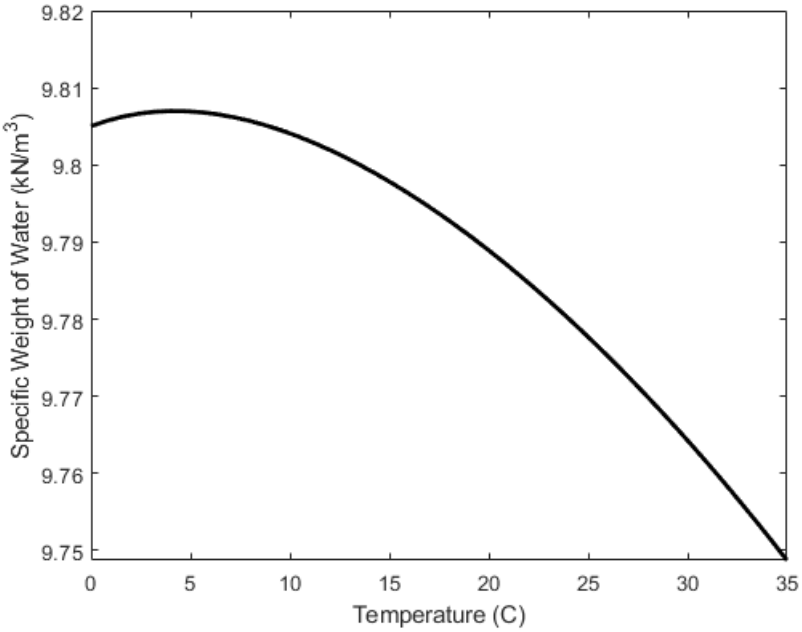

Figure 139: Specific weight of water with respect to temperature curve.

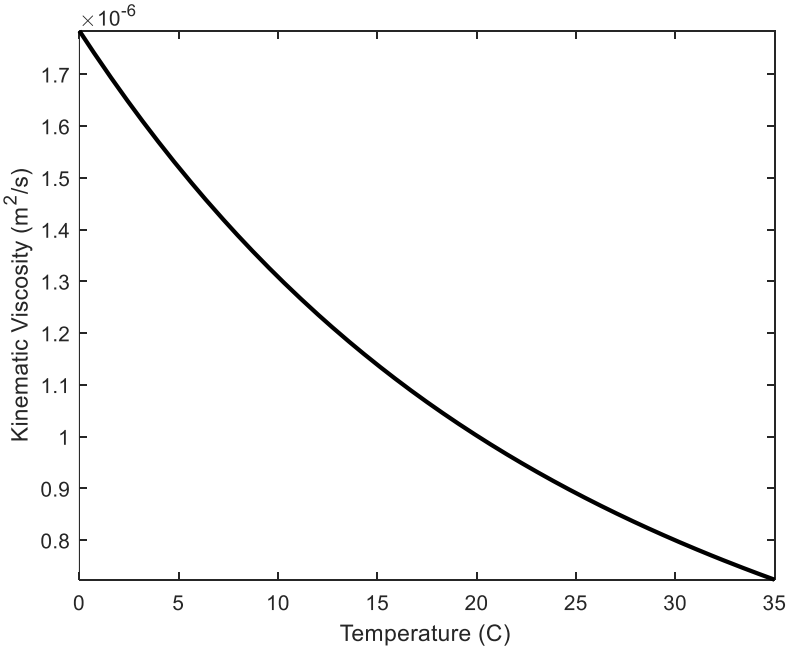

Figure 140: Kinematic viscosity with respect to temperature curve.

Governing equation for flowrate variation starting from the basic unsteady energy equation (equation (11)):

$$\frac{p_1}{\gamma} + h_{ss} + \frac{U^2}{2g} + H_p = \frac{p_2}{\gamma} + h_{ds} + \frac{U_2^2}{2g} + \sum \left(h_{f_i} + h_{m_i} + h_{a_i} \right)$$

$$Let: p_1, p_2, U_1 \approx 0$$

$Let: \frac{U_2^2}{2g}$ be lumped into minor losses ($\mathrm{K}_{\mathrm{end-segment}} = \mathrm{K}_{\mathrm{end-segment}} + \mathrm{K}_{\mathrm{outlet-configuration}}$)

$$\therefore h_{ss} + H_p = h_{ds} + \sum \left(h_{f_i} + h_{m_i} + h_{a_i} \right)$$

Where:

$$\sum h_{a_i} = \sum_i^I \left(\frac{L_i}{g A_{p_i}} \right) \frac{dQ}{dt}$$

$$A_{p_i} = \pi \left(\frac{D_{p_i}}{2} \right)^2 = \frac{\pi}{4} D_{p_i}^2$$

$$\sum h_{f_i} = \sum_i^I f_i \frac{L_i}{D_{p_i}} \frac{U^2}{2g} \; (Darcy\ Weisbach\ formulations)$$

or

$$\sum h_{f_i} = \sum_{i}^{I} \frac{6.84LU^{1.85}}{C_{HW}^{1.85} D^{1.165}} \ (Hazen - William's\ formulations)$$

$$\sum h_{m_i} = K \frac{U^2}{2g}$$

Rearranging for $\frac{dQ}{dt}$:

$$\frac{h_{ss} + H_p - h_{ds} - \sum\left(h_{f_i} + h_{m_i}\right)}{\sum \frac{L_i}{gA_{p_i}}} = \frac{dQ}{dt}$$

Where:

$$Q = \frac{U}{A_p}$$

$$Let: H_p = c + aQ^b;\ \mathrm{B} = \frac{8}{g\pi^2}; \alpha = \frac{4}{g\pi}$$

Fill and expand with respect to Darcy-Weisbach formulations:

$$\frac{h_{ss} + c + aQ^b - h_{ds} - \mathrm{B}\sum_i^I \left(f_i \frac{L_i}{D_{p_i}^5} + \frac{K_i}{D_{p_i}^4}\right) Q^2}{\alpha \sum_i^I \frac{L_i}{D_{p_i}^2}} = \frac{dQ}{dt}$$

Fill and expand with respect to the Hazen-Williams formulation:

$$\frac{h_{ss} + c + aQ^b - h_{ds} - \sum_i^I \left(\frac{6.84 L_i \left(\frac{4Q}{D_{p_i}^2 \pi} \right)^{1.85}}{C_{HW}^{1.85} D_{p_i}^{1.165}} \right) - \mathrm{B} \sum_i^I \left(\frac{K_i}{D_{p_i}^4} \right) Q^2}{\alpha \sum_i^I \frac{L_i}{D_{p_i}^2}} = \frac{dQ}{dt}$$

Analytical equation for time spent pumping utilizing operational migration (no flow establishment)

Suppose the volume in the wet-well can be adequately modelled by:

$$V = B_1 Q^2 + B_2 Q - B_3$$

Where:

$V =$ Active volume remaining in the wet-well,

Q = Flowrate provided by the pump at remaining volume.

$$0 = B_1 Q^2 + B_2 Q - (B_3 + V)$$

Applying the quadratic formula to solve for the roots:

$$Q_{1,2} = \frac{-B_2 \pm \sqrt{B_2^2 - 4B_1\left(-(B_3 + V)\right)}}{2B_1} = \frac{-B_2 \pm \sqrt{B_2^2 + 4B_1(B_3 + V)}}{2B_1}$$

The root of interest is the negative version of the quadratic formula and $Q = \frac{dV}{dt}$:

$$\frac{dV}{dt} = \frac{-B_2 - \sqrt{B_2^2 + 4B_1(B_3 + V)}}{2B_1}$$

Separate variables:

$$\frac{dV}{\frac{-B_2 - \sqrt{B_2^2 + 4B_1(B_3 + V)}}{2B_1}} = \frac{-2B_1 dV}{B_2 + \sqrt{B_2^2 + 4B_1(B_3 + V)}} = dt$$

Let:

$$x = B_2^2 + 4B_1(B_3 + V)$$

$$dx = 4B_1 dV$$

$$\frac{dx}{4B_1} = dV$$

Integration by double substitution:

$$-2B_1 \int \frac{dx}{\sqrt{x} + B_2}\left(\frac{1}{4B_1}\right) = -\frac{1}{2}\int \frac{dx}{\sqrt{x} + B_2}$$

Let:

$$w = \sqrt{x} + B_2$$

$$dw = \frac{dx}{2\sqrt{x}}$$

$$dx = dw\left(2\sqrt{x}\right)$$

Fill in:

$$-\frac{1}{2}\int \frac{2\sqrt{x}dw}{w}$$

But:

$$w = \sqrt{x} + B_2 \rightarrow x = (w - B_2)^2$$

Therefore:

$$-\frac{1}{2}\int \frac{2(w - B_2)}{w}dw = -\int \frac{(w - B_2)}{w}dw = -\int \left(1 - \frac{B_2}{w}\right)dw$$

Integrate along w:

$$-[w - B_2 \ln(|w|)] + C = B_2 \ln(|w|) + w + C = t$$

Expand w $\rightarrow x \rightarrow fun\{V\}$:

$$t = B_2 \ln\left(\left|\sqrt{4B_1(V + B_3) + B_2^2} - B_2\right|\right) + \sqrt{4B_1(V + B_3) + B_2^2} - B_2 + C$$

Appendix E - Classification Tree

The classification tree can be utilized to assess what error category a naïve interpretation of roughness will likely have given the parameters are within the limits of the tree as outlined in Table 24. The classification begins at the root node, working from left to right. If the column labeled resulting node is empty, continue with the search. For example, the first node has a decision about the time parameter at a split value of 156 seconds. Utilizing the naïve pump-down time, determine whether to proceed to node 2 (time < 156 seconds) or node 3 (time > 156 seconds). After determining what node to redirect to, continue that same sequence at the node redirected. A resulting error category can be determined at the end of the branch. The error category associated with the data that passed through the node is also presented.

Table 52: Classification tree for determining error category for naïve interpretation information determined with a naïve pumping test.

Node Index	Resulting error category	Parameter	Split value	Node redirect (<)	Node redirect (≥)	Error category at current node
1		t_{naive} (s)	156.332	2	3	Moderate
2		t_{naive} (s)	91.8292	4	5	Moderate
3		$\left(\frac{\epsilon}{D_p}\right)_{naive}$	0.0136364	6	7	Moderate
4		$\left(\frac{\epsilon}{D_p}\right)_{naive}$	0.157145	8	9	Severe
5		$\left(\frac{\epsilon}{D_p}\right)_{naive}$	0.0533768	10	11	Moderate
6		$h_{l_{naive-avg}}(m)$	20.257	12	13	Moderate
7		$h_{l_{naive-avg}}(m)$	4.75984	14	15	Mild

Node Index	Resulting error category	Parameter	Split value	Node redirect (<)	Node redirect (≥)	Error category at current node
8		$\left(\frac{\epsilon}{D_p}\right)_{naive}$	0.08405	16	17	Severe
9		$D_p\ (mm)$	225.392	18	19	Moderate
10		$h_{f_{naive-avg}}\ (m)$	21.1639	20	21	Severe
11		$D_p\ (mm)$	261.143	22	23	Mild
12		$\left(\frac{\epsilon}{D_p}\right)_{naive}$	0.00722467	24	25	Severe
13		$f_{avg_{naive}}\ (-)$	0.0238008	26	27	Moderate
14		$f_{avg_{naive}}\ (-)$	0.0647285	28	29	Moderate
15		$f_{avg_{naive}}\ (-)$	0.0716897	30	31	Mild
16		t_{naive} (s)	61.1474	32	33	Severe
17		$V\ (m^3)$	4.68487	34	35	Severe
18		$\frac{V_{pipe}}{V}\ (-)$	53.7774	36	37	Mild
19		t_{naive} (s)	53.0596	38	39	Severe
20		$f_{avg_{naive}}\ (-)$	0.0617977	40	41	Severe
21		$f_{avg_{naive}}\ (-)$	0.0409306	42	43	Moderate
22		$\left(\frac{\epsilon}{D_p}\right)_{naive}$	0.119395	44	45	Mild
23		$U_{avg}\ \left(\frac{m}{s}\right)$	1.0445	46	47	Mild
24		$U_{avg}\ \left(\frac{m}{s}\right)$	2.0369	48	49	Severe
25		$U_{avg}\ \left(\frac{m}{s}\right)$	0.744018	50	51	Moderate

Node Index	Resulting error category	Parameter	Split value	Node redirect (<)	Node redirect (≥)	Error category at current node
26		$\frac{V_{pipe}}{V}$ $(-)$	3.84249	52	53	Moderate
27		$\frac{V_{pipe}}{V}$ $(-)$	3.26166	54	55	Mild
28		t_{naive} (s)	226.062	56	57	Moderate
29		Δh_{ss} (m)	2.34701	58	59	Moderate
30		$\frac{V_{pipe}}{V}$ $(-)$	10.3243	60	61	Mild
31		$\frac{V_{pipe}}{V}$ $(-)$	17.0612	62	63	Negligible
32	Severe					
33		$h_{f_{naive-avg}}$ (m)	23.9644	64	65	Severe
34		t_{naive} (s)	64.1307	66	67	Severe
35		D_p (mm)	326.491	68	69	Mild
36	Mild					
37		D_p (mm)	158.788	70	71	Moderate
38		U_{avg} $\left(\frac{m}{s}\right)$	0.87832	72	73	Severe
39		U_{avg} $\left(\frac{m}{s}\right)$	1.11765	74	75	Mild
40	Severe					
41		U_{avg} $\left(\frac{m}{s}\right)$	0.642116	76	77	Moderate
42	Severe					
43		$\frac{V_{pipe}}{V}$ $(-)$	4.23865	78	79	Mild

Node Index	Resulting error category	Parameter	Split value	Node redirect (<)	Node redirect (≥)	Error category at current node
44	Mild					
45	Negligible					
46		$f_{avg_{naive}}\ (-)$	0.110881	80	81	Moderate
47	Mild					
48	Severe					
49	Moderate					
50		t_{naive} (s)	292.933	82	83	Moderate
51	Moderate					
52	Moderate					
53	Severe					
54	Mild					
55		t_{naive} (s)	262.221	84	85	Mild
56	Severe					
57		$A\ (m^2)$	9.48633	86	87	Moderate
58	Mild					
59		$h_{l_{naive-avg}}\ (m)$	2.2268	88	89	Moderate
60	Mild					
61		$D_p\ (mm)$	229.284	90	91	Mild
62	Negligible					
63	Mild					
64	Severe					

Node Index	Resulting error category	Parameter	Split value	Node redirect (<)	Node redirect (≥)	Error category at current node
65	Moderate					
66	Severe					
67	Moderate					
68	Mild					
69	Moderate					
70	Mild					
71	Moderate					
72	Severe					
73	Moderate					
74	Moderate					
75	Mild					
76	Severe					
77	Moderate					
78	Mild					
79	Moderate					
80	Moderate					
81	Mild					
82	Severe					
83	Moderate					
84	Moderate					
85	Mild					

Node Index	Resulting error category	Parameter	Split value	Node redirect (<)	Node redirect (≥)	Error category at current node
86	Moderate					
87	Mild					
88	Moderate					
89	Mild					
90	Mild					
91	Moderate					

Appendix F - Four Sites Considered - Physical Layouts

Trinity Lane

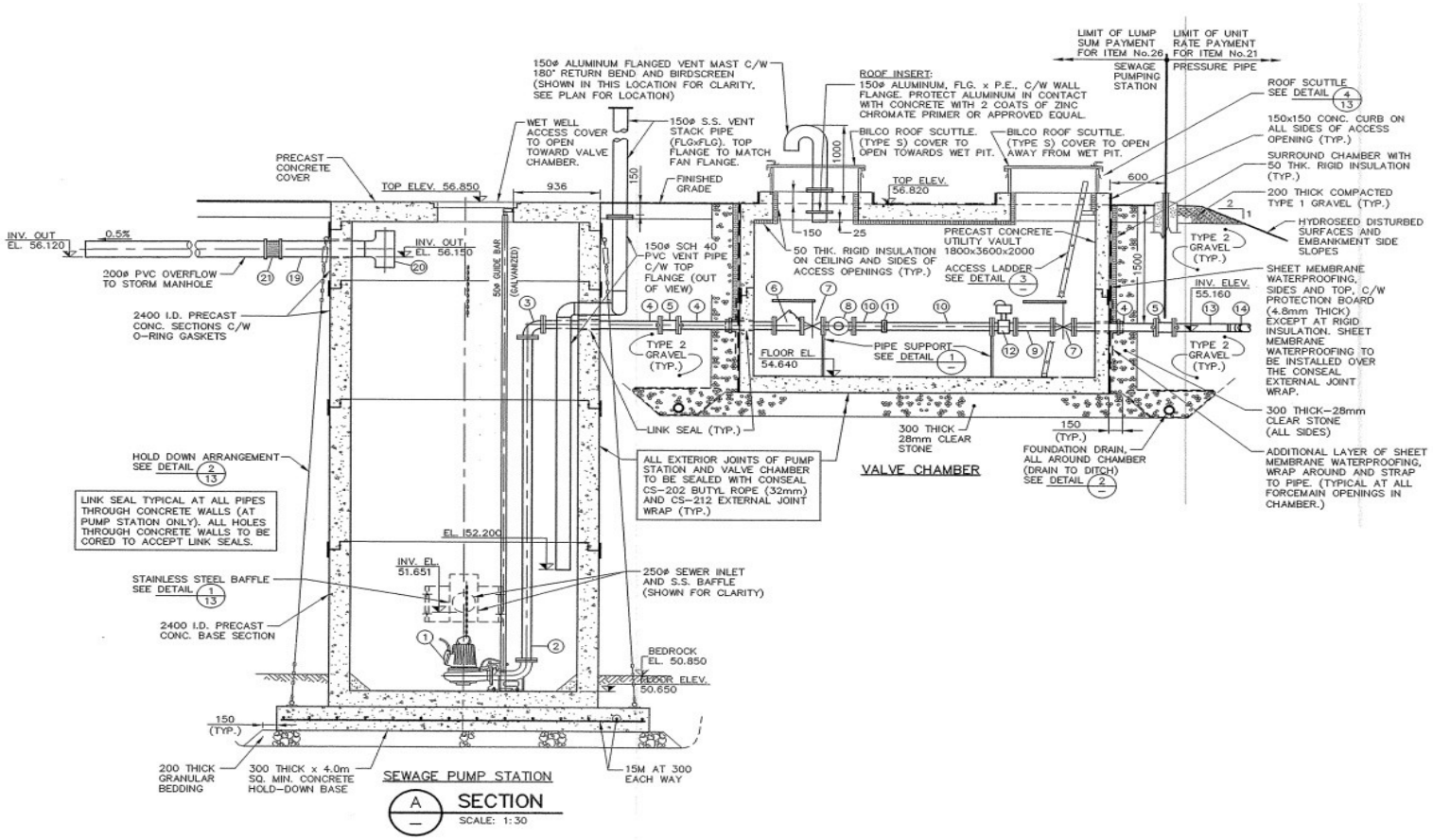

Figure 141: Trinity Lane physical layout – lift-station elevation view.

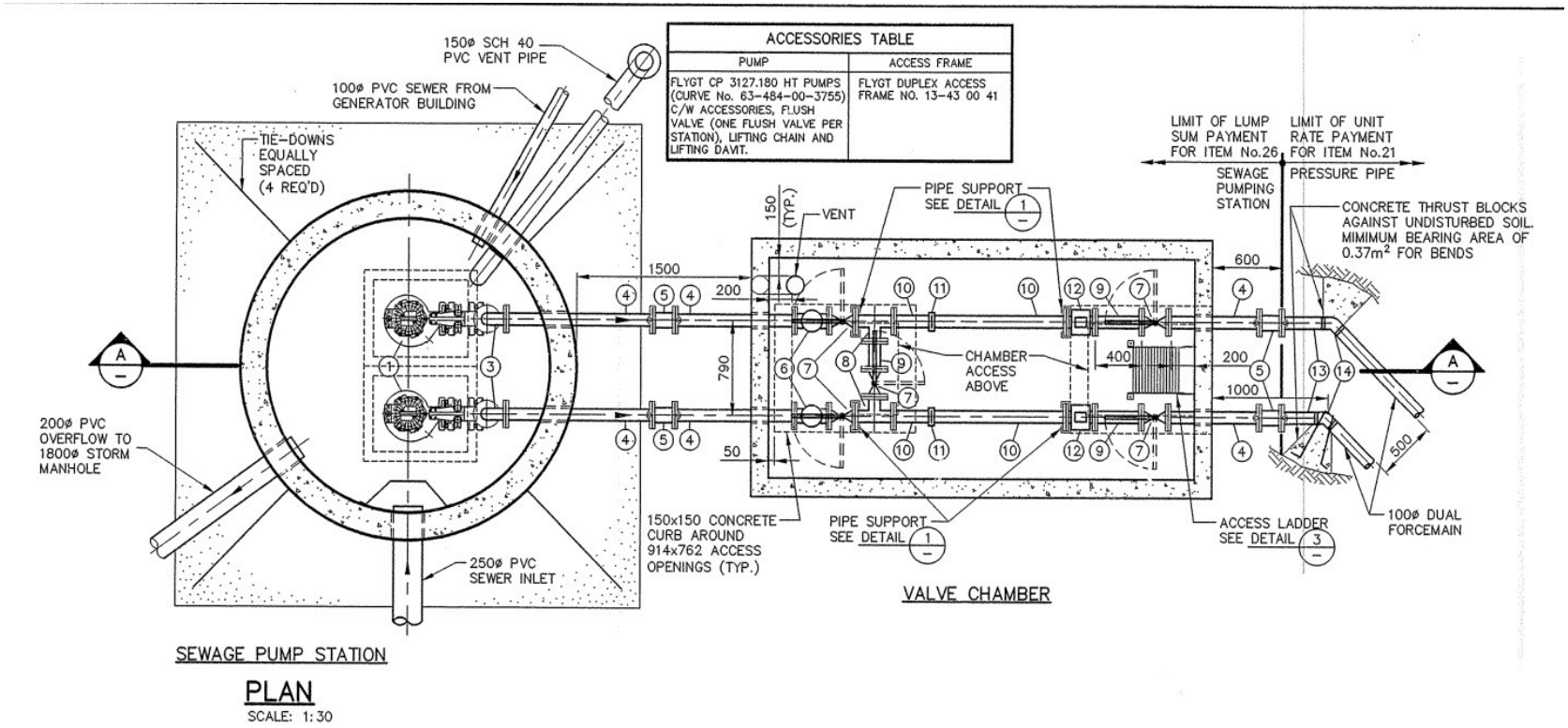

Figure 142: Trinity Lane physical layout – lift-station plan view.

LIST OF FITTINGS		
No.	QTY.	DESCRIPTION
①	2	PUMP (SEE TABLE)
②	2	100ø STAINLESS STEEL MAKE UP PIPE (FLG.)
③	2	100ø–90° STAINLESS STEEL ELBOW (FLG.)
④	6	100ø D.I. MAKE UP PIPE (FLG.–P.E.)
⑤	5	100ø D.I. M.J. SOLID SLEEVE COUPLING
⑥	2	100ø BALL CHECK VALVE (FLG.
⑦	5	100ø PLUG VALVE (FLG.)
⑧	2	100x100x100 S.S. TEE (FLG.)
⑨	1	100ø STAINLESS STEEL MAKE UP PIPE (FLG.)
⑩	4	100ø STAINLESS STEEL MAKE UP PIPE (VIC–P.E.)
⑪	2	100ø VICTAULIC COUPLING
⑫	2	100ø MAGNETIC FLOW METER (FLG.)
⑬	3	100ø PVC SERIES 160 MAKE UP PIPE.
⑭	2	100ø–45° PVC BEND
⑲	2	200ø SCH 40 MAKE UP PIPE (PE–PE) c/w LINK SEAL @ CONC. WALLS
⑳	1	200x200x200 PVC TEE (SOCKET)
㉑	1	200ø DRESSER COUPLING C/W DENSO PASTE AND TAPE

Figure 143: Trinity Lane physical layout – supplementary table for indices of engineering drawings.

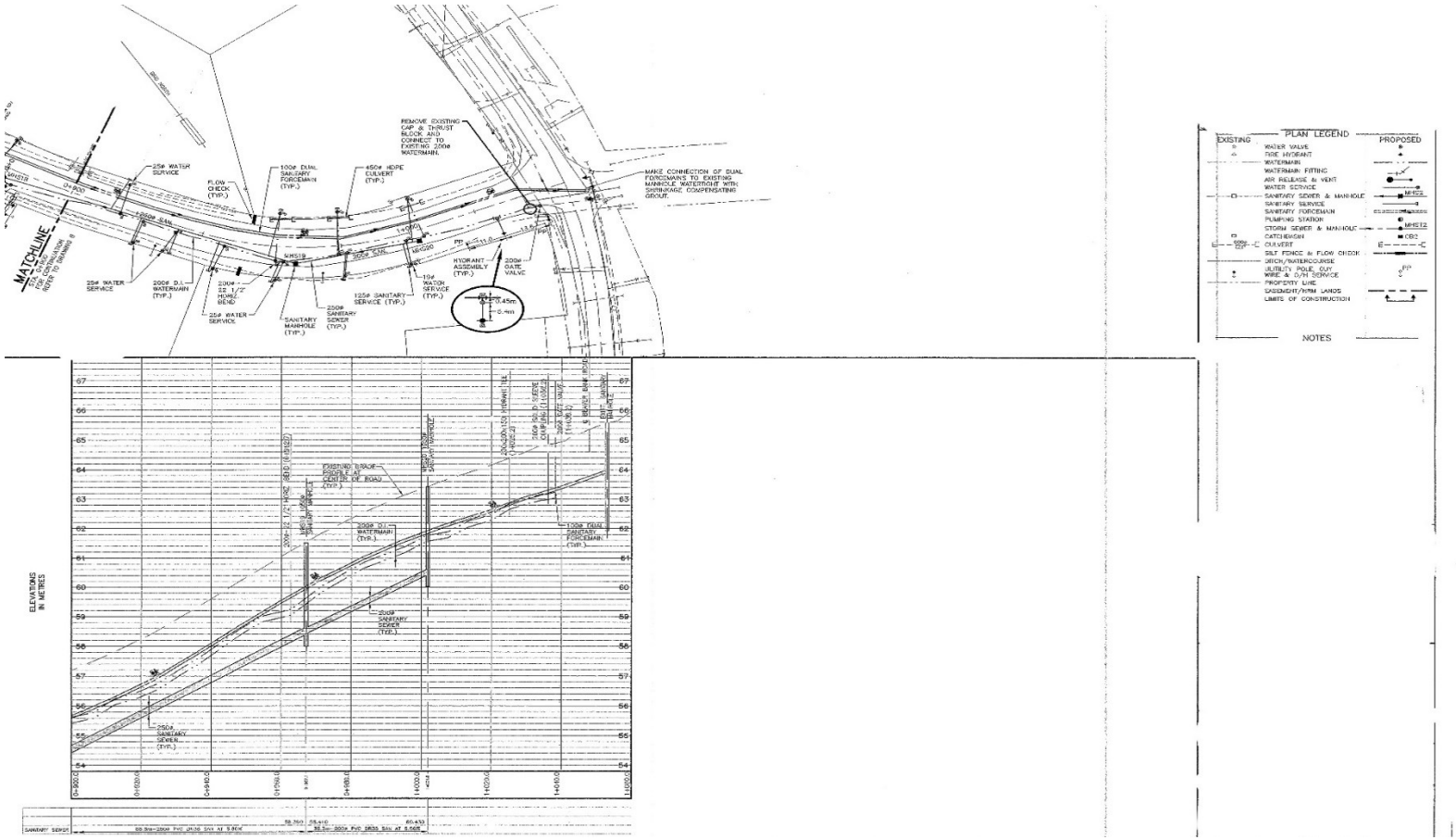

Figure 144: Trinity Lane physical layout – elevation view of forcemain part one.

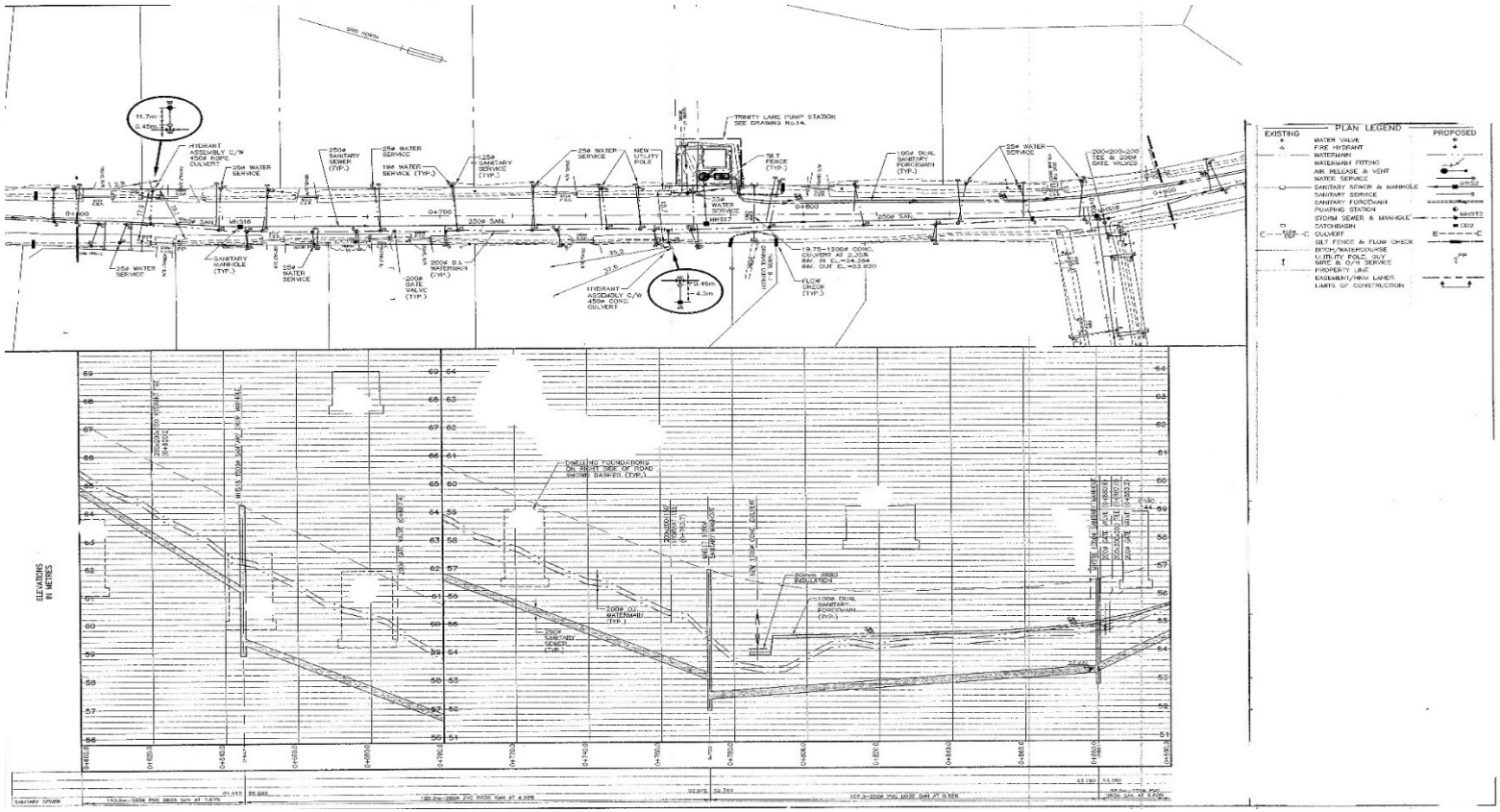

Figure 145: Trinity Lane physical layout – elevation view of forcemain part two.

Ragged Lake

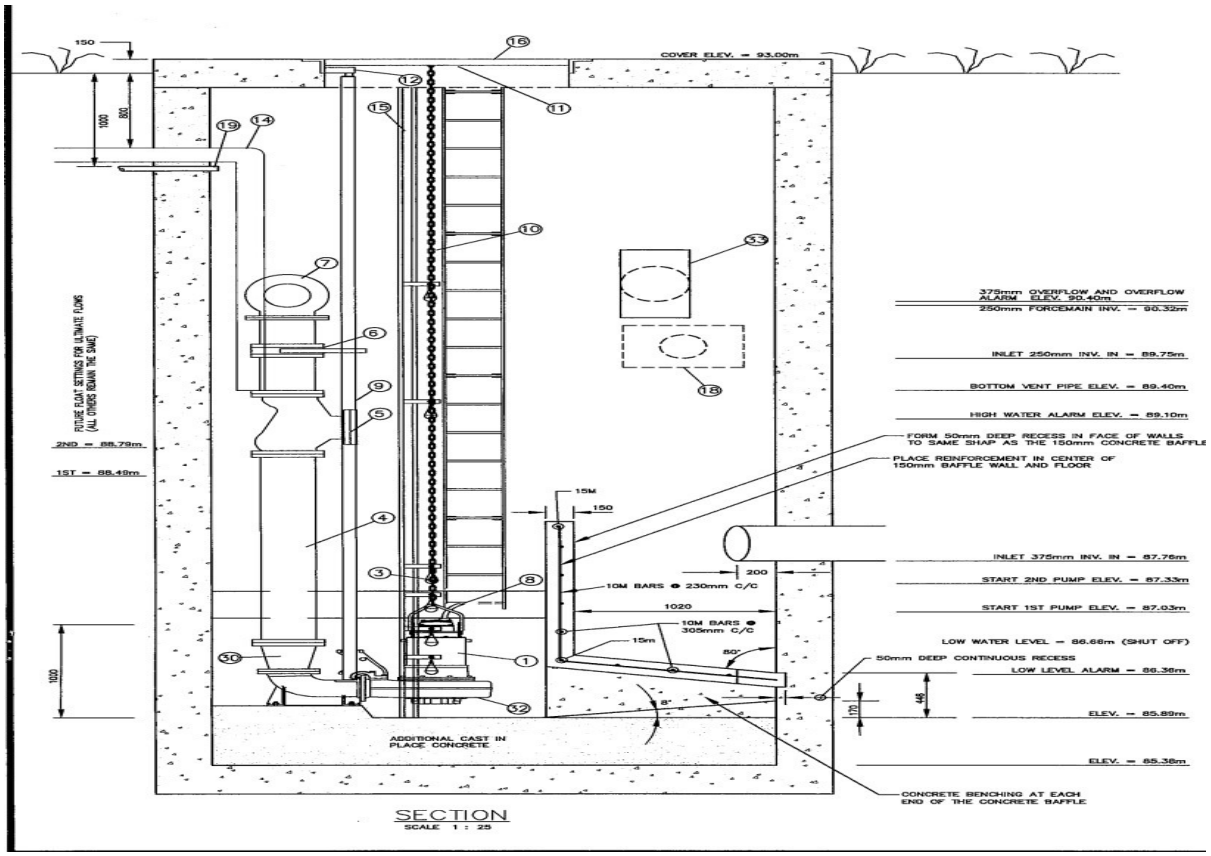

Figure 146: Ragged Lake physical layout – lift-station elevation view.

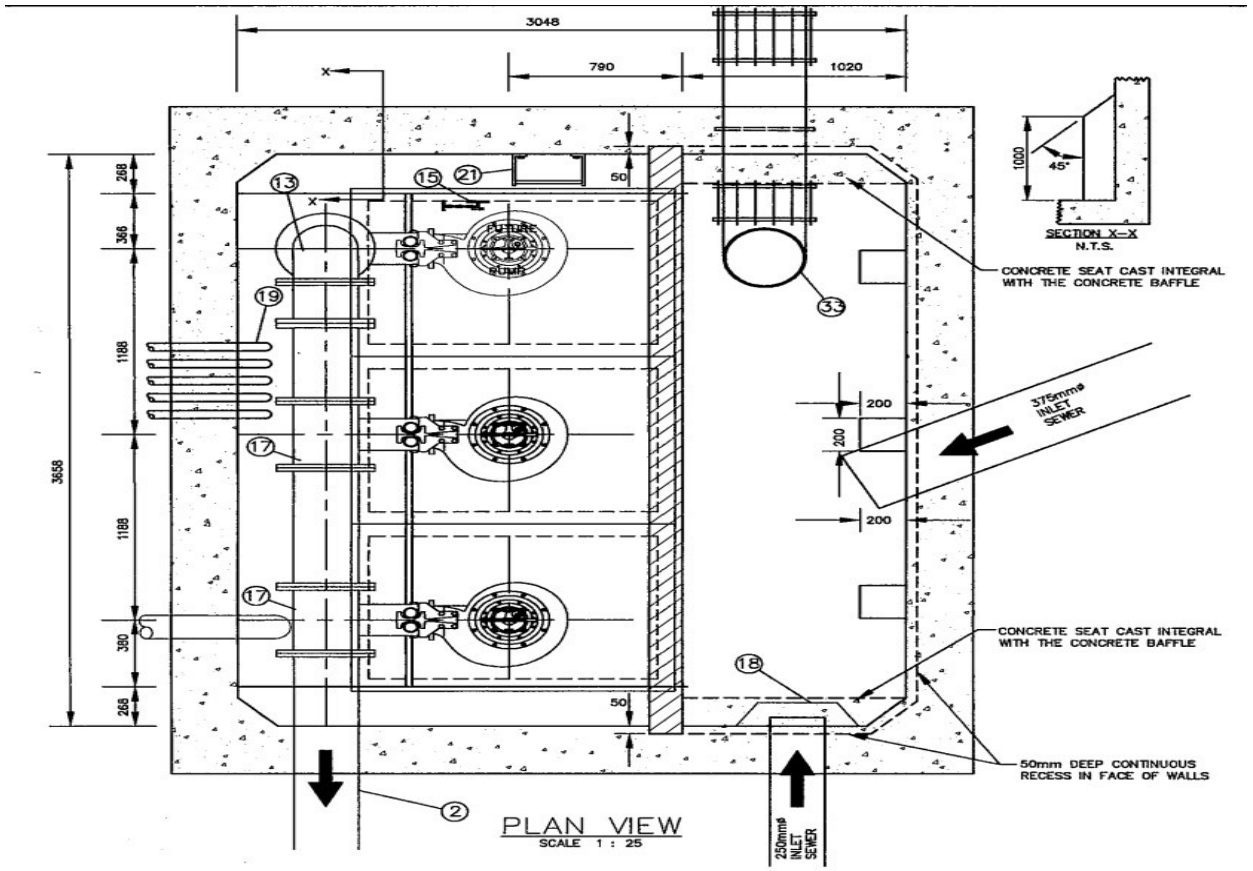

Figure 147: Ragged Lake physical layout – lift-station plan view.

MATERIAL LIST		
ITEM	QTY	DESCRIPTION
1	2	CP 3201 HT Impeller 452 47 HP 600/3/60 (OR APPROVED EQUIVALENT)
2	1	250mm DIA. DI FORCEMAIN
3	6	LEVEL REGULATOR
4	3	RISER PIPE (DUCTILE IRON) (CL54 WITH COAL TAR EPOXY LINING)
5	3	BALL CHECK VALVE (250mm)
6	3	PLUG VALVE (250mm)
7	1	FORCEMAIN PIPING (INTERNAL) (DUCTILE IRON) (CL54 WITH COAL TAR EPOXY LINING)
8	3	POWER CABLE
9	6	GUIDE BAR FOR PUMP
10	3	PUMP LIFTING CHAIN
11	3	PUMP CHAIN HOOK
12	3	PUMP UPPER GUIDE BAR HOLDER
13	3	250mm – 90° BEND
14	1	VENT PIPE (200mmø)
15	1	LEVEL REGULATOR HANGER
16	3	PUMP ACCESS HATCH (13–43 00 43)
17	2	250X250X250 TEE
18	1	BAFFLE (3mm GALVANIZED STEEL) (SEE DETAIL THIS DRAWING)
19	5	50mm ELECTRICAL CONDUIT
20	1	CONTROL PANEL (TRIPLEX MACTEC MPD 2.0) COMPLETE WITH MOTOROLA
		INTRAC 2000 MODULAR REMOTE
21	1	LADDER
22		A–LOK GASKET
23	1	VENT FAN (JOY in–line) (MODEL # 5806, 1/3 HP, 3450 RPM) (CONTINUOUS OPERATION)
24	5	RIGID CONDUIT (SEE DWG. NO. TT–51–32609)
25	3	PUMP POWER CONNECTION (SEE DWG. NO. TT–51–32609)
26	1	LEVEL REGULATOR CONNECTION (SEE DWG. NO. TT–51–32609)
27	1	STATION POWER CONNECTION (SEE DWG. NO. TT–51–32609)
28	3	PUMP SQUEEZE CONNECTOR (SEE DWG. NO. TT–51–32609)
29	3	FLOAT SQUEEZE CONNECTOR (SEE DWG. NO. TT–51–32609)
30	1	200X250 INCREASER
31		ALL JOINTS RAM–NEK GASKET
32	2	MIX FLUSH VALVE
33	1	OVERFLOW PIPE (SEE DETAIL THIS PAGE)

Figure 148: Ragged Lake physical layout – supplementary table for indices of engineering drawings.

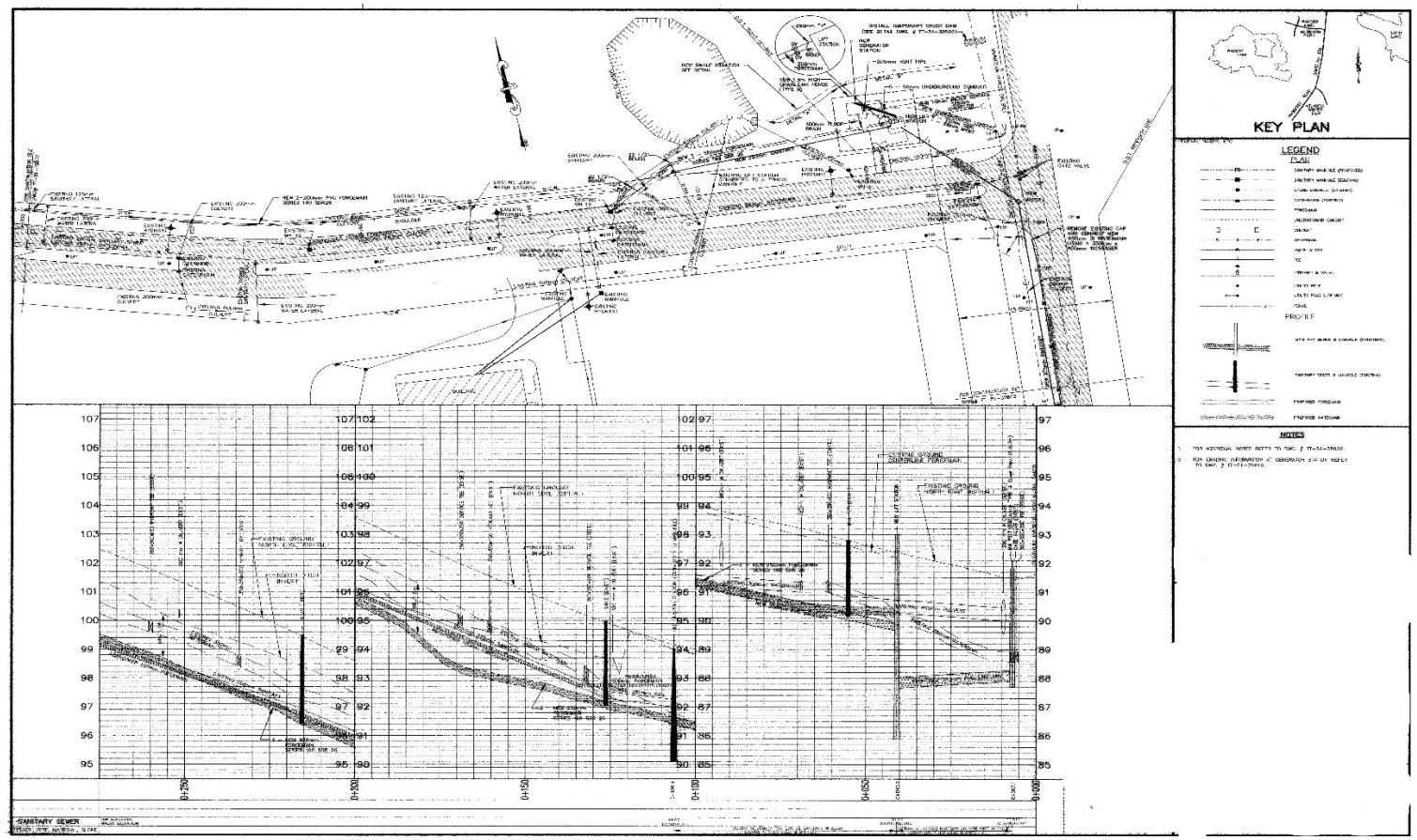

Figure 149: Ragged Lake physical layout – elevation view of forcemain.

Akerley Boulevard

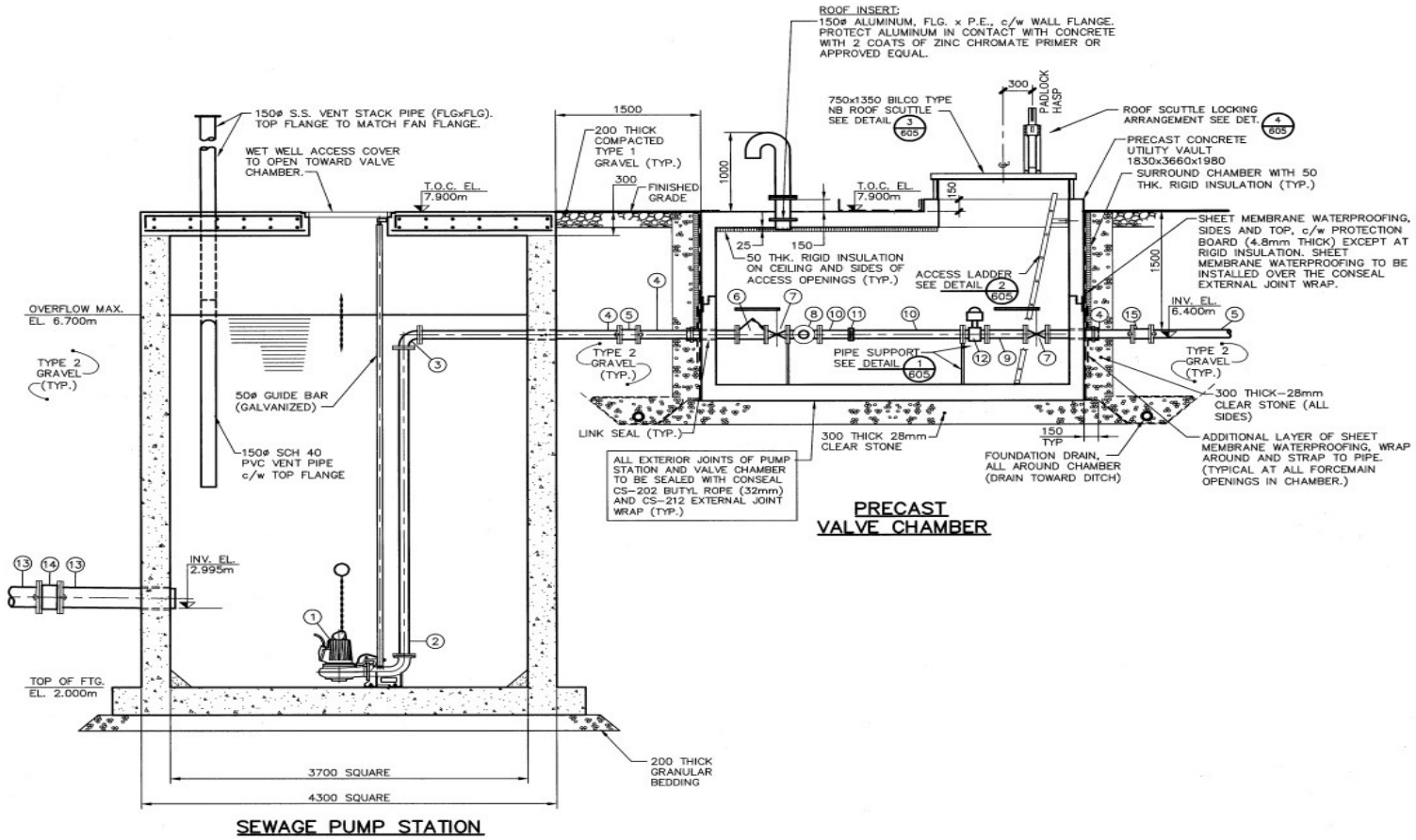

Figure 150: Akerley Boulevard physical layout – lift-station elevation view.

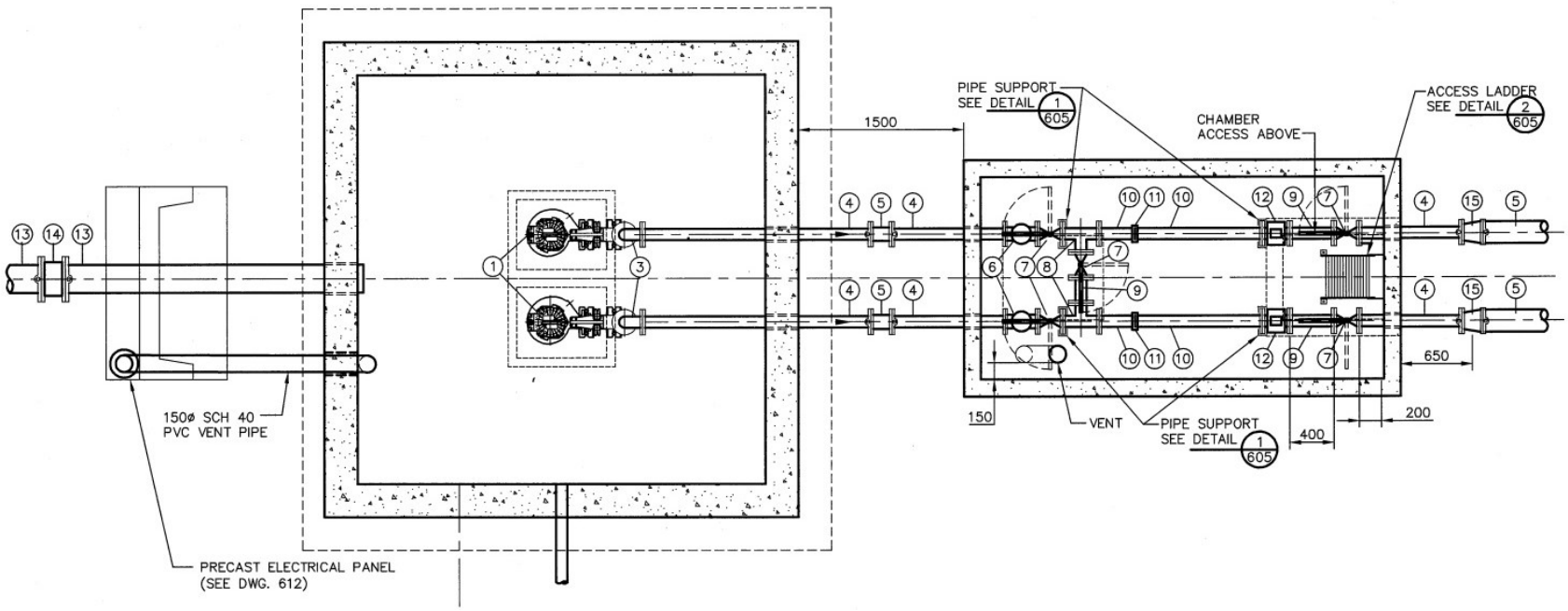

Figure 151: Akerley Boulevard physical layout – lift-station plan view.

LIST OF FITTINGS		
No.	**QTY.**	**DESCRIPTION**
①	2	PUMP (SEE TABLE)
②	2	150ø STAINLESS STEEL MAKE UP PIPE (FLG.)
③	2	150ø–90° STAINLESS STEEL ELBOW (FLG.)
④	6	150ø D.I. MAKE UP PIPE (FLG.–P.E.)
⑤	5	150ø D.I. M.J. SOLID SLEEVE COUPLING
⑥	2	150ø BALL CHECK VALVE (FLG.)
⑦	5	150ø PLUG VALVE (FLG.)
⑧	2	150x150x150 S.S. TEE (FLG.)
⑨	1	150ø STAINLESS STEEL MAKE UP PIPE (FLG.)
⑩	4	150ø STAINLESS STEEL MAKE UP PIPE (VIC–P.E.)
⑪	2	150ø VICTAULIC COUPLING
⑫	2	150ø MAGNETIC FLOW METER (FLG.)
⑬	2	250ø D.I. CL53 MAKE UP PIPE P.E. TO P.E. c/w LINK SEAL @ CONC. WALLS
⑭	1	250ø D.I. M.J. SOLID SLEEVE COUPLING
⑮	2	150ø–200ø INCREASER

Figure 152: Akerley Boulevard physical layout – supplementary table for indices of engineering drawings.

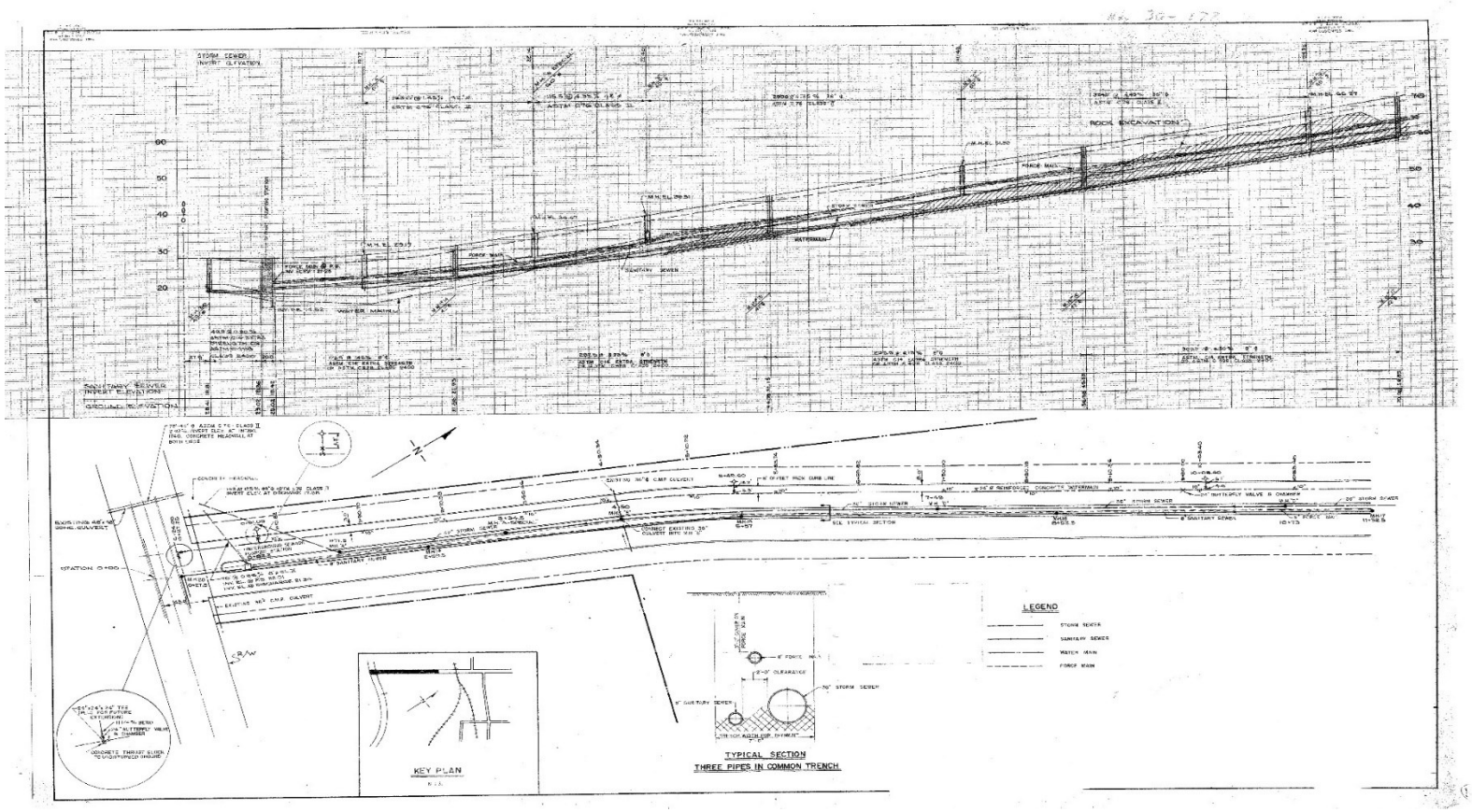

Figure 153: Akerley Boulevard physical layout – elevation view of original forcemain.

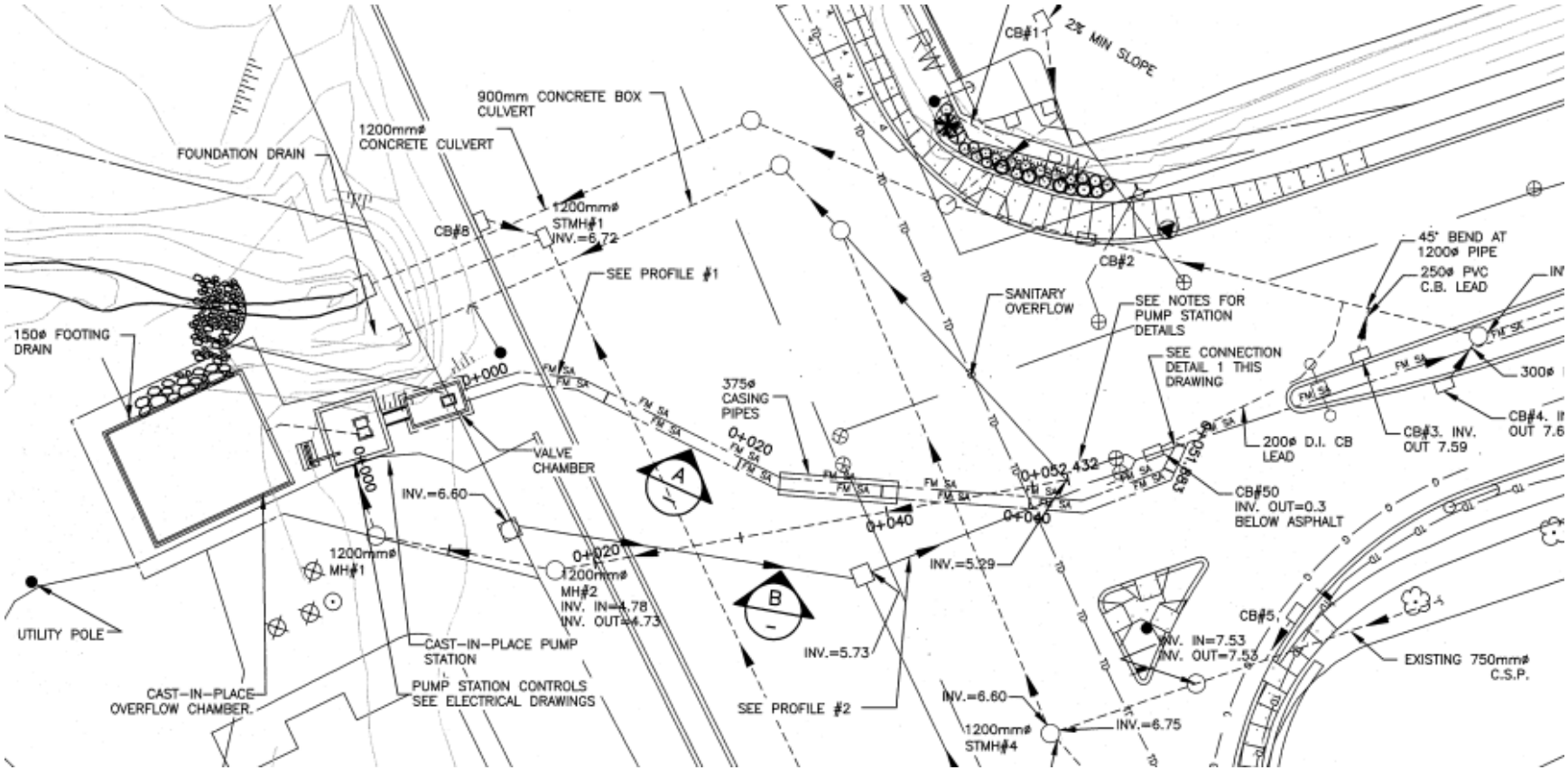

Figure 154: Akerley Boulevard physical layout – plan view of upgraded forcemain.

Melville Cove

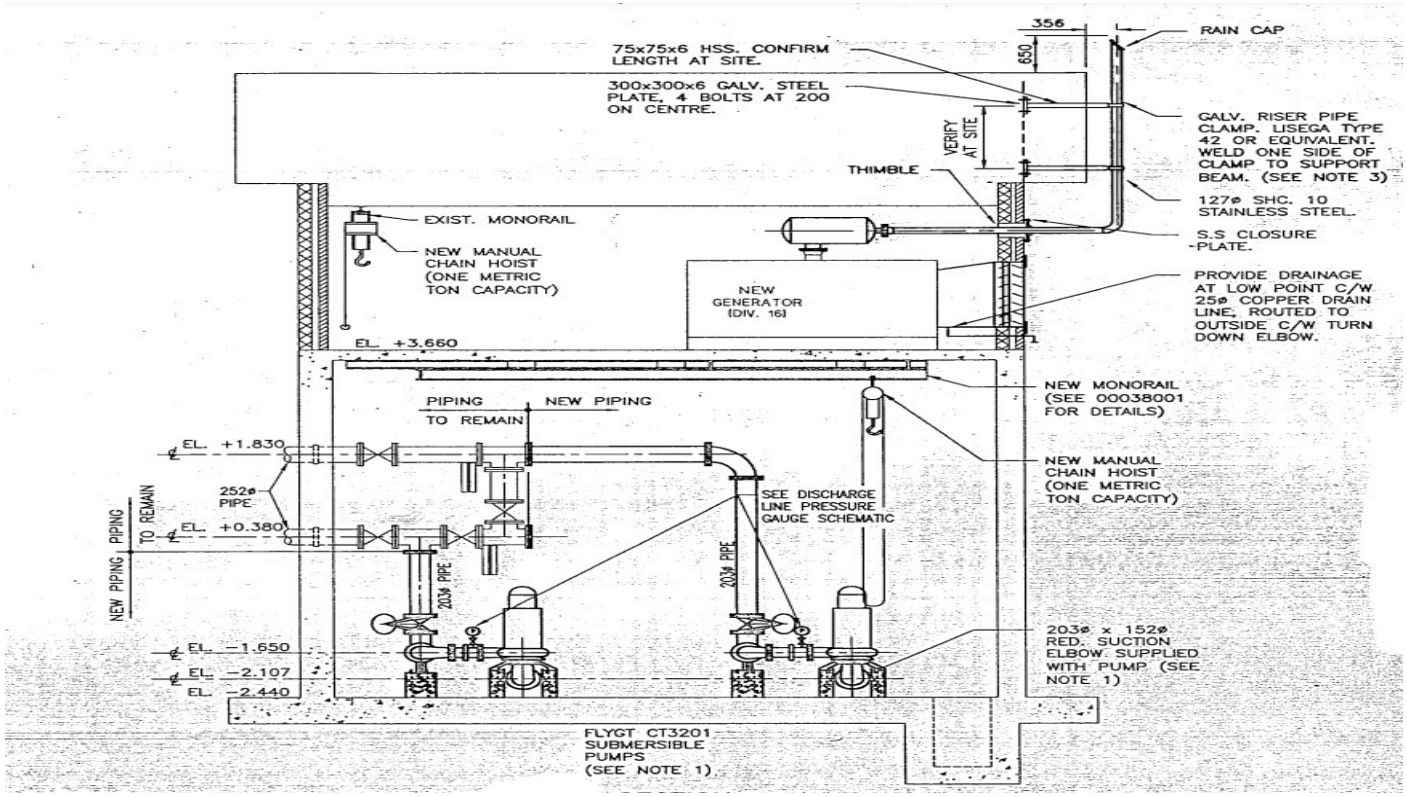

Figure 155: Melville Cove physical layout – lift-station elevation view, part one.

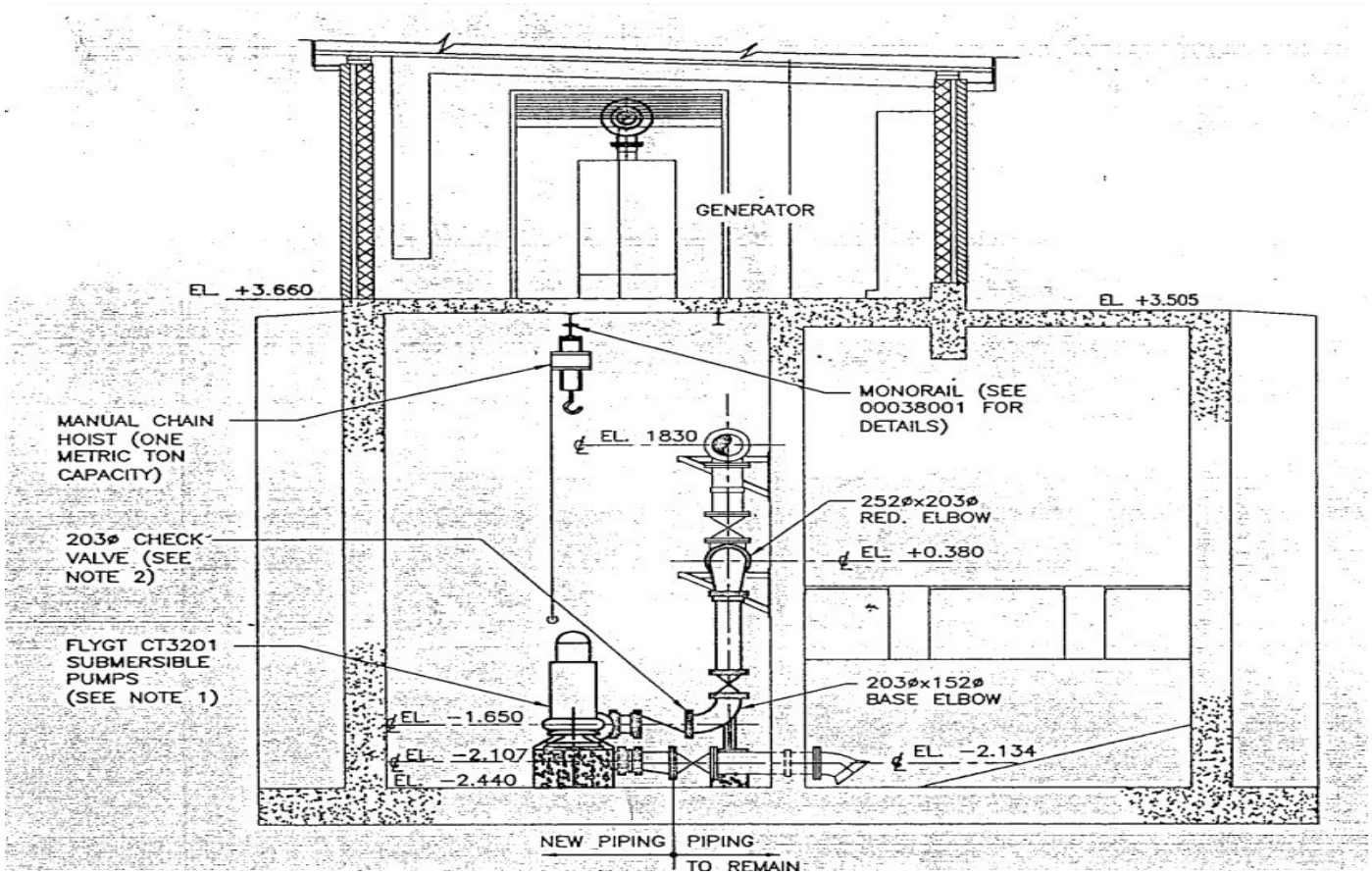

Figure 156: Melville Cove physical layout – lift-station elevation view, part two.

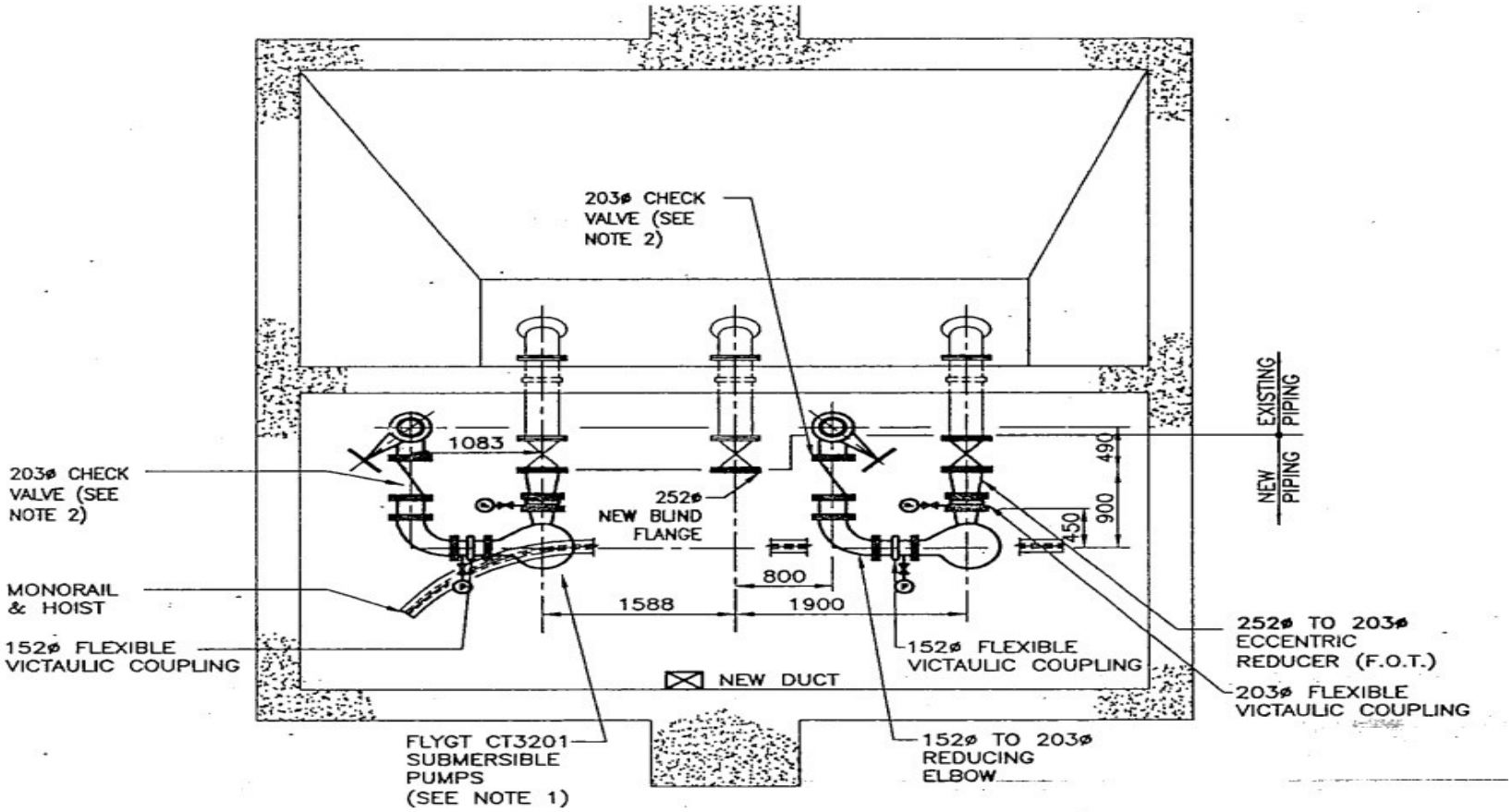

Figure 157: Melville Cove physical layout – lift-station plan view.

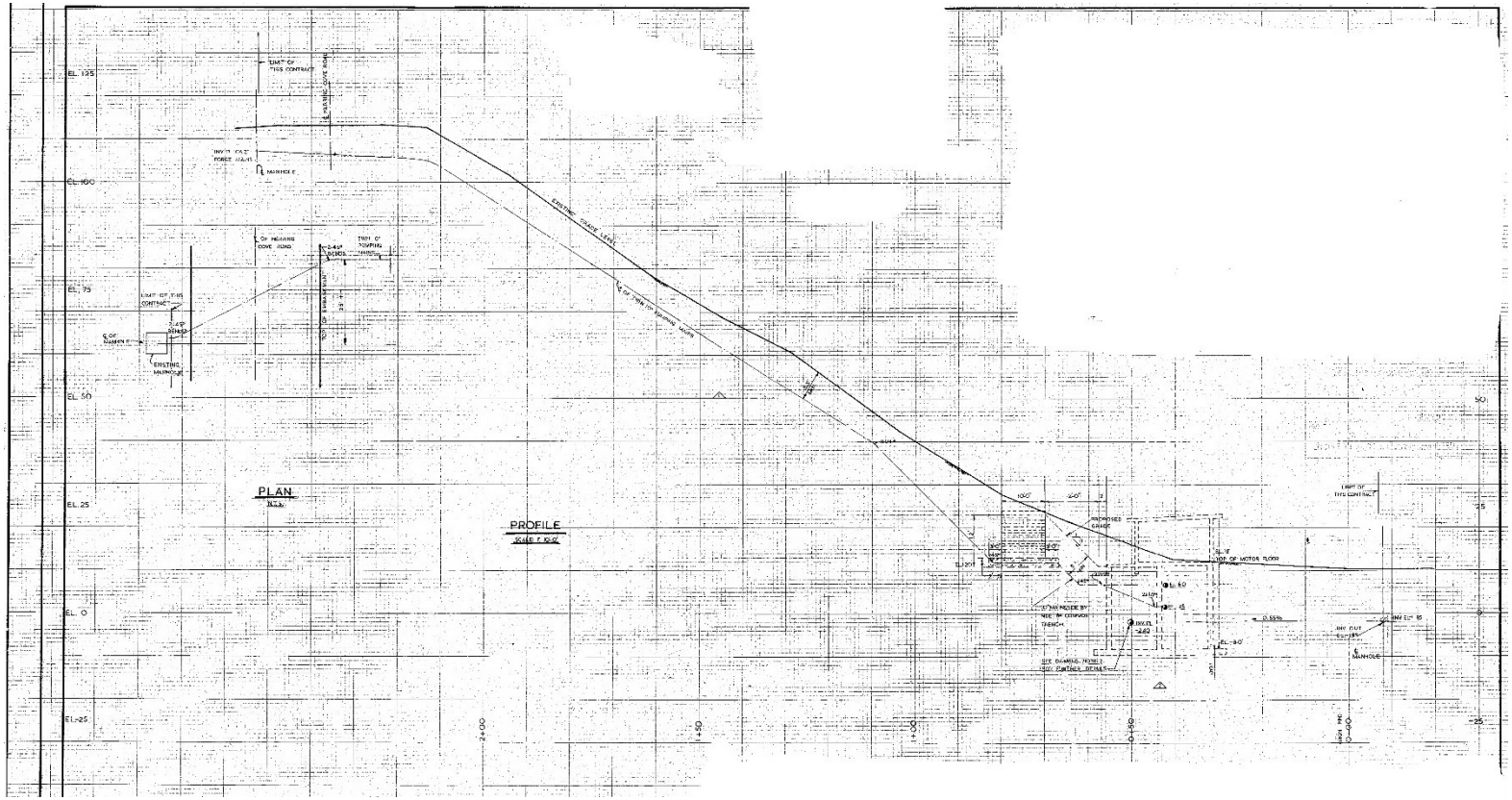

Figure 158: Melville Cove physical layout – elevation view of forcemain.